Image supplied courtesy of Cranfield University

european society for precision engineering and nanotechnology

Special Interest Group:

Thermal Issues

26th-27th February 2020

Laboratory for Machine Tools and Production Engineering (WZL) of RWTH Aachen

Aachen, Germany

euspen

Special Interest Group Meeting:
Thermal Issues
Aachen, Germany
26th – 27th February 2020

Compilation of presentations

Published by eu**spen**
ISBN: 978-0-9957751-6-9

Printed in the UK March 2020
twenty10
33 Rothersthorpe Crescent Mews
Northampton, NN4 8JD, UK

Cranfield University Campus
Building 90, College Road
Bedford MK43 0AL, UK
Tel: 0044 (0) 1234 754023
Website: www.euspen.eu

Introduction

Thermal effects are regarded as a major contributor to errors on machine tools, on measuring equipment and on workpieces. Measurement of thermal effects is becoming even more important as workpiece tolerances decrease, as thermal effects no only use a larger part of the tolerances, but also influence repeatability and long term stability of machine tools, and measuring equipment. As a consequence, several research groups and industries are working on simulation of thermal effects, in order to finally compensate thermally induces errors, or new help to develop concepts to reduce thermally induced errors.

The intensive on-going work in this area led us to bring together a further internationally coordinated meeting.

The success of this meeting which brought together leading expertise globally to an open forum for focused presentations and discussions on thermal issues in manufacturing will result in another future meeting.

Dr. Theo A.M. Ruijl
MI-Partners B.V., The Netherlands

Contents

Modelling and Model Reduction Techniques

Design Principles for Thermally Robust Production Equipment

Temperature Measurement & Control

Compensation and Correction of Thermal Effects

Poster Session

Meeting Keynote: Thermo-Energetic Design of Machine Tools – A systematic approach to solve the conflict between power efficiency, accuracy and productivity

Thermo-Energetic Design of Machine Tools – A systematic approach to solve the conflict between power efficiency, accuracy and productivity

Prof. Christian Brecher
WZL – Laboratory for Machine Tools and Production Engineering, RWTH University, Aachen, DE

Abstract

The challenge of research in the CRC/TR96 derives from the attempt to satisfy the conflicting goals of reducing energy consumption and increasing accuracy and productivity in machining. The solution approach pursued is based on measures that make it possible to guarantee process accuracy despite increasing power losses without additional energetic measures under thermal transient environmental conditions and under operating conditions characterised by individual and small series production. The scientists of the CRC/TR 96 are researching and developing effective correction and compensation solutions for the thermo-elastic machine behaviour during the course of the project, which will enable precision machining under the future conditions of energy-efficient production. In the 3rd funding phase, the CRC/TR 96 focuses on the application of the developed solutions on the entire machine under the conditions of real operation. This leads to new scientific challenges due to a multitude of uncertainties and parameter fluctuations. The models have to be further developed and new solutions for the control of variable operating conditions such as online identification have to be developed.

Biography

Professor Christian Brecher, born 25 August1969, was a research associate and senior engineer in the Machine Technology Department at the Laboratory for Machine Tools and Production Engineering (WZL) of the RWTH University in Aachen from 1995 until 2001 and earned his doctorate at the Faculty of Mechanical Engineering there. Some three years into a career in the mechanical engineering industry, he was appointed University Professor of Mechanical Engineering at the RWTH University in Aachen and Member of the Board of Directors of the WZL and IPT (Fraunhofer Institute for Production Technology). His areas of specialist expertise include machine, transmission and control systems technology. In 2012 Professor Brecher additionally became a founding member along with Professor Hopmann of the Aachen Centre for Integrative Lightweight Engineering at the RWTH University in Aachen. From 2015 to 2017 Professor Brecher became the acting Head of Institute at the Fraunhofer Institute for Production Technology IPT and in January 2018 he accepted the permanent position of Head of Institute.

Meeting Keynote: The implications of the kelvin redefinition

The implications of the kelvin redefinition

Prof. Graham Machin, FREng
National Physical Laboratory, UK

Abstract

In November 2018 the General Conference of Weights and Measures (CGPM) made history by agreeing to redefine the international system of units (the SI) in terms of a defined set of fundamental constants. The kelvin from that time on was defined in terms of a fixed value of the Boltzmann constant. Starting from the previous definition of the kelvin, based on the triple point of water, this talk will explain how the kelvin was redefined including; the wording of the redefinition, the co-ordinated effort in determining low uncertainty values of the Boltzmann constant for the redefinition, and, the extensive preparations undertaken for introducing the mise en pratique for the definition of the kelvin (MeP-K-19) which will regulate the realisation and dissemination of the kelvin from the date of its redefinition. As the international thermometry community transitions to realising and disseminating the redefined kelvin the short, medium and long-term implications that the redefinition will have for the disciple of thermometry will be discussed.

Biography

Professor Graham Machin FREng, BSc (Hons), DPhil (Oxon), DSc, CPhys, CEng, FInstP, FInstMC GM is the science leader of the NPL Temperature and Humidity Group and an NPL Fellow. He has more than 30 years' experience in thermometry research, published more than 220 technical papers and given numerous invited/keynote addresses. He is visiting Professor of Clinical Thermal Imaging (University of South Wales) and Distinguished Visiting Fellow (University of Valladolid, Spain). He represents the UK on the Consultative Committee of Thermometry (CCT) and IMEKO TC12, chairs the CCT working group for Noncontact thermometry and is an international invited expert on the CAS "very low temperature thermometry" project (2017-2022). He was President of the UK Institute of Measurement and Control (2018-2019), chair of the Euramet Technical Committee for Thermometry from (2014-2018) and served on the EPSRC Physical Sciences Strategic Advisory Team (2014-2017). GM was awarded the Institute of Measurement and Control (InstMC) Callendar medal in 2012 for "outstanding contributions to the art of temperature measurement", Honorary Scientist of the Chinese Academy of Sciences (CAS) (2019) and elected Fellow of the Royal Academy of Engineering (2019). Current research interests are primary thermometry (acoustic, radiometric and especially all aspects of realising the redefined kelvin), radiation thermometry and thermal imaging, new thermocouples, sensor self-validation methods, reliable clinical thermometry (contact, non-contact and internal), reliable temperature (and other) measurements in hostile environments (especially aerospace and nuclear decommissioning).

He is project director of the "Realising the redefined kelvin" (Sep 2019) for EURAMET, a founder member of the "Body Temperature Initiative" which aims to improve clinical thermometry throughout the NHS and leads NPL's metrology activity in nuclear decommissioning.

Measurement of Thermal Influences in Production Equipment, Process and Product

Special Interest Group Meeting on Thermal Issues
Laboratory for Machine Tools and Production Engineering (WZL) of
RWTH Aachen, Germany, February 2020
www.euspen.eu

Metrological investigation and simulation of thermo-mechanical interactions in externally driven spindles

Christian Brecher[1], Alexander Steinert[1], Stephan Neus[1], Marcel Fey[1]

[1]*Laboratory for Machine Tools and Production Engineering (WZL) of RWTH Aachen University, Germany*

A.Steinert@wzl.rwth-aachen.de

Abstract
Approaches for increasing the productivity of cutting machine tools often result in growing power densities in the main spindle and feed axis. This leads to growing heat inputs affecting the machine's accuracy. Because of its exposed position, the main spindle of a machine tool plays a key role in this context. Due to their robust and simple design and relatively low production costs, externally driven spindles can be found in many machine tools. Thus, this paper concentrates on investigating the thermo-mechanical behavior of an externally driven spindle. On the one hand, the thermo-mechanical spindle characteristics that depend on the operational conditions are focused metrologically. Therefore in this paper, an externally driven spindle is tested under varying rotational speed as well as axial and radial forces on a spindle test bench. On the other hand, a simulation model is designed to predict previously identified characteristics. A FEM-based thermic model is implemented to calculate instationary temperature fields inside the spindle and coupled to a mechanical spindle simulation.

Machine tool, spindle, thermal simulation

1. Introduction and literature survey

In modern machine tools, measures to increase productivity and approaches to improve the achievable accuracy are often in conflict with one another. Growing heat inputs and decreasing secondary times result in an elevated temperature level and thus cause a complex deviation field due to thermal deformation. One the one hand, this effect leads to tool center point (TCP) deflections. On the other hand, relative deviations inside feed axis components with roller elements like spindle bearings result in changed bearing kinematics affecting the components static and dynamic stiffness characteristics.

In this context, Gartung [1] analyzed thermal influences on the static and dynamic spindle behavior on a test rig for different bearing setups and preloads. Besides these metrological approaches, authors have developed simulation models in order to describe thermal and mechanical effects. In the field of thermal modeling, Bossmanns [2] and Gebert [3] modeled motorized spindles with the finite-difference-method (FDM) and focused on a detailed modeling of boundary condition. Furthermore, Jedrzejewski *et al.* [4] used a coupled FEM-FDM approach to calculate transient temperature distributions efficiently while Uhlmann [5] based the thermal spindle model on the finite-element-method (FEM).

The kinematic relations inside angular contact bearings have been analysed deeply in the course of time. A comprehensive documentation can be found in [6]. The integration of an analytical bearing model into FEM-based spindle models is presented in [7]. The model allows calculating mechanical properties of the spindle-bearing-system, but require an iterative calculation due to nonlinear bearing stiffness characteristics. Li developed a coupled simulation model in [8] for changed dynamic operating conditions under thermal load. In [9], Holkup *et al.* identified shifts of the first and second eigenfrequency as a function of changed thermal states with a combination of a thermal and a mechanical model. A metrological validation was not conducted.

In case of the cited simulation approaches, detailed and computationally intensive models were developed. However, the ability to run a simulation model process parallel offers great opportunities. This paper aims at developing an accurate thermo-mechanical spindle model with high resolution and short calculation times by combing a model order reduced (MOR) FE-model with live spindle data.

2. Metrological investigations

2.1. Test rig

The test object used to validate the simulation model is an externally driven spindle with two greased spindle bearings in a rigidly adjusted O-arrangement. The spindle is mounted to a massive flange that itself sits on a bed. A radial load unit is located in front of the spindle. To measure thermo-mechanical spindle characteristics, temperature sensors (thermo couples) and displacement sensors (eddy current) are integrated. Temperature information along the circumference of the first spindle bearing's outer ring and axial as well as radial displacement information of the shaft are measured. Figure 1 shows the design of the test rig.

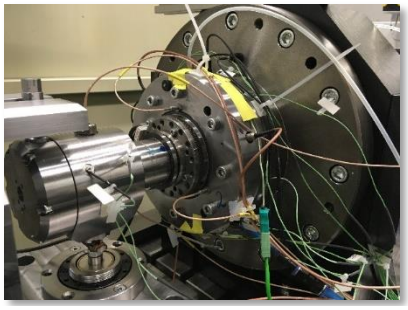

Spindle test rig
- Externally driven spindle
- Radial load unit
- Greased bearings
- Thermo couples
- Eddy current sensors

Figure 1. Spindle test rig with applied sensors.

2.2. Test execution

Different sets of mechanical boundary conditions are defined and for each combination, a long-term test is executed until steady-state temperatures of the outer ring are reached. During the tests, static stiffness and dynamic compliance are detected frequently. As a result, changed static and dynamic properties can be identified with rising temperature. Table 1 shows the considered boundary conditions.

Table 1 Sets of boundary conditions

Test number	Spindle speed/min^{-1}	Radial force/N
T1	4 000	500
T2	6 000	500

2.3. Results

Static stiffness

Figure 2 contains average outer ring temperatures of the first bearing as well as the radial stiffness of the shaft, both plotted over time. Raising the spindle speed from 4 000 to 6 000 min^{-1} at a radial force of 500 N results in higher steady-state temperatures. The time-stiffness curves show a characteristic behavior: In the beginning, static stiffness rises drastically to reach a peak after approximately 18 minutes followed by a continuous decrease. In case of test 2 (T2), the effect emerges much stronger compared to test 1 (T1). The effect can be explained with the relatively higher thermal inertia of the spindle shaft compared to the bearing rings. In the beginning, the bearing rings warm up first resulting in a rising radial pressing and stiffness on the one hand. Over time, heat flows into the spindle shaft causing an axial elongation. This, on the other hand, leads to a reduced preload in case of a spindle with bearings in O-arrangement. Since both effects have different thermal time constants, the displayed characteristic curve follows.

In case of test 2, the stiffness shows a 30% increase after 18 minutes.

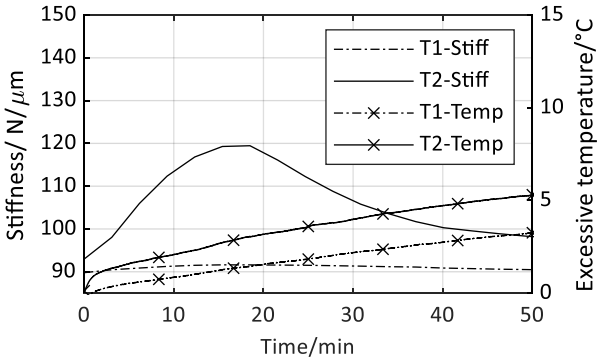

Figure 2. Static stiffness (Stiff) and average outer ring temperature (Temp) for different tests (T1 and T2).

Dynamic compliance

In figure 3, the thermal influence on the radial frequency response function (FRF) measured at the spindle shaft is plotted for test 2. The previously described behavior in the investigations of static stiffness can also be found in the dynamic compliance. As a result, both, the eigenfrequencies as well as the amplitude shift.

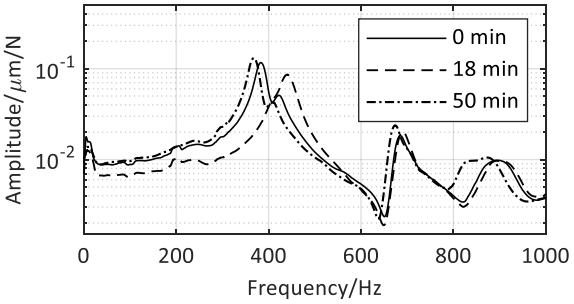

Figure 3. Dynamic compliance for different thermal states (Test 2).

3. Thermo-mechanical simulation

3.1. Approach

Besides metrological investigations, a thermo-mechanical online simulation environment is developed (Figure 4). Due to nonlinear boundary conditions and different requirements of thermal and mechanical simulations, a co-simulation is designed. For the thermal part, a model-order reduced FE-model with linear tetrahedral elements is used while the mechanical system is approximated by a Bernoulli-beam element structure with integrated analytical bearing model based on Hertzian theory. The co-simulation design allows combining simulations with different solver settings. In case of the mechanical simulation, the nonlinear bearing characteristics require an iterative calculation of equilibrium.

Figure 4 displays the coupled thermo-mechanical simulation and the considered interactions between both. External forces F and the spindle speed n combined with an initial preload F_{pre} and further parameters like the spindle geometry represent the input values. On the right side of figure 4, the external load F, a centrifugal force F_n, a thermal force F_{therm} and the current bearing stiffness $k_{bearing}$ lead to bearing contact forces, which are used to update the actual bearing stiffness. As a result, for equilibrium the process needs to be repeated iteratively. Once convergence is achieved, the resulting contact forces of each ball $F_{C,i}$ affecting the bearing's frictional behaviour are used to calculate the power losses. Here, a Palmgren-based model [10] that was expanded by Harris [6] is implemented. Friction torque of each ball element follows as a sum of a load-dependent part $M_{F,i}$ and a load-independent part $M_{n,i}$. While $F_{C,i}$ feeds into the first part, the spindle speed n mainly affects the second one. Furthermore, the friction torque leads to the total frictional power loss $\sum P_{F,i}$ warming up the structure, while convection (and radiation) dissipate heat into the environment ($\dot{Q}_{\alpha K}$). Other submodels describe the heat generation by dynamic air gaps and heat transfer coefficients of solid as well as air gap contacts. This leads to a transient field of temperatures T that in the end causes thermal forces F_{therm} closing the cycle.

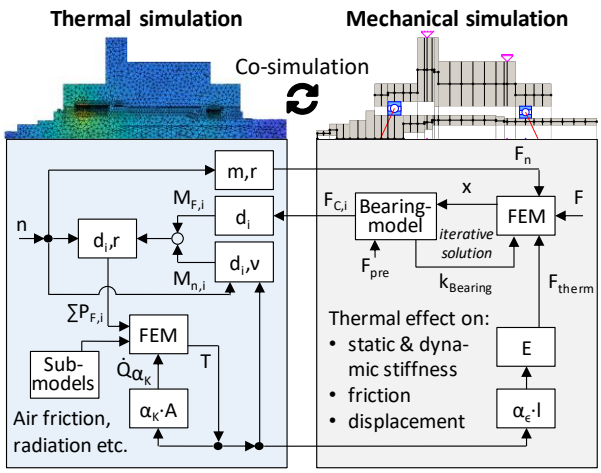

Figure 4. Co-simulation with considered interactions.

3.2. Thermal simulation

By combining an inverse Euler time discretisation with an explicit integration of heat flux densities $\{u_{i-1}\}$ a semi-explicit system follows for the transient thermal analysis problem.

$$([C] + \Delta t \cdot [K]) \cdot \{T_i\} = [C] \cdot \{T_{i-1}\} + [B] \cdot \{u_{i-1}\}$$

To achieve short calculation times, thermal system matrices (heat capacity matrix [C], conductivity matrix [K] and boundary condition matrix [B]) are reduced with a block Arnoldi algorithm. Dimension of system of equations (50 000 nodes) is reduced to 1 000 degrees of freedom (DoF).

Submodels deliver respective heat flux densities and heat transfer coefficients. Bearing heat input caused by friction is approximated with a Palmgren-Harris model to derive an individual heat input for each roller element. As a result, the effect of changed contact forces due to thermal deformation on bearing friction is taken into account. The heat flux density $u_{bearing}$ can be expressed as function of friction moment M, angular velocity ω and friction area A.

$$u_{bearing} = \frac{M \cdot \omega}{A} = \frac{\omega}{A} \cdot \sum_{i=1}^{n} (M_{n,i} + M_{F,i}) \,/\, \frac{W}{m^2}$$

Besides the coefficients f_0 and f_1, lubricant viscosity v, angular velocity of each ball ω_i, ball diameter d_i and the contact forces Q_i and Q_{max} are required for the following expressions for $M_{n,i}$ and $M_{F,i}$ (see figure 4).

$$M_{n,i} = 0.675 \cdot f_0 \cdot (v \cdot \omega_i)^{\frac{2}{3}} \cdot d_i^{\,2} \,/\, Nm$$

$$M_{F,i} = f_1 \cdot \left(\frac{F_{C,i}}{F_{C,max}}\right)^{\frac{1}{3}} \cdot F_{C,i} \cdot d_i \,/\, Nm$$

Empirical models for radiation, natural as well as forced convection, heat generation in air gaps and heat transfer through solid contacts lead to the respective coefficients [11, 12 and 13].

3.2. Mechanical simulation

In order to take thermal effect into account, temperatures coming from the linear tetraeder mesh of the thermal simulation are mapped onto the beam element mesh of the mechanical simulation. The interpolation of the mapping process can be expressed as matrix multiplication. For a fast and stable convergence into equilibrium of the iteratively solved mechanical model, the iteration is proceeded with either Newton-Raphson method or conjugate gradients method. Based on the convergence progress the solver automatically switches between the two mentioned methods.

4. Validation

For validation, measured temperature and stiffness are compared with simulated data. Results for T2 are shown in figure 5. The previously described effect of a rising temperature on the static radial stiffness can be reproduced with the co-simulation. In addition, the excessive temperature of the outer ring of the first bearing also matches the simulation. Due to the structure of the thermo-mechanical simulation environment, a process parallel application in thermal real time could been achieved.

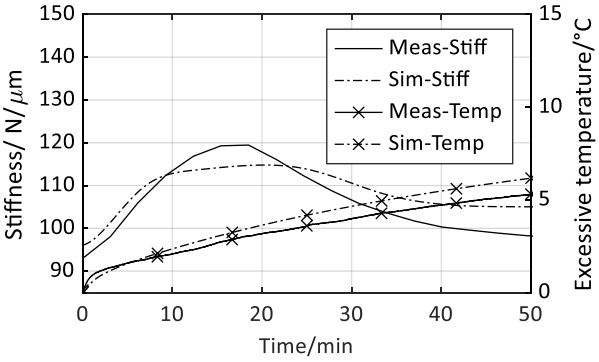

Figure 5. Comparison of measured (Meas) and simulated (Sim) static stiffness (Stiff) and average outer ring temperature (Temp) for T2.

5. Conclusion

This paper describes a co-simulation based approach to calculate the thermo-mechanical behavior of spindles efficiently. The model is validated and can be used process parallel. In future research, the co-simulation will be coupled to an empirical compensation model to predict overall TCP stiffness and deflection of an exemplary machine tool. Due to this procedure, interactions between thermal and mechanical domain occurring in the spindle can be considered and embedded in a TCP error compensation.

Acknowledgements

The Authors would like to thank the German Research Foundation (DFG) for financial support. The presented findings result from the transfer project T01 within the CRC/Transregio 96 “Thermo-Energetic Design of Machine Tools”.

References

[1] Gartung H 1985 *Beitrag zum thermischen, statischen und dynamischen Verhalten wälzgelagerter Spindeln* (TU Braunschweig)
[2] Bossmanns B 1997 *Thermo-Mechanical Modeling of Motorized Spindle Systems for High-Speed Milling* (Purdue University)
[3] Gebert K 1997 *Ein Beitrag zur thermischen Modellbildung von schnelldrehenden Motorspindeln* (TU Darmstadt)
[4] Jedrzejewski J, Kowal Z, Kwasny W and Modrzycki W 2004 Hybrid model of high speed machining centre headstock *CIRP Annals* **53** 285-288
[5] Uhlmann E and Hu J 2012 Thermal modelling of a high speed motor spindle *Proc. CIRP* **1** 313-218
[6] Harris T A 1991 *Rolling bearing analysis* **3** (Wiley)
[7] Altintas Y and Cao Y 2005 Virtual design and optimization of machine tool spindles *CIRP Annals* **54** 379–382
[8] Li H and Shin Y C 2004 Integrated dynamic thermo-mechanical modeling of high speed spindles, Part 1 *J of Man. Sc. And Eng.* **126** 148-158
[9] Holkup T, Cao H, Kolar P, Altintas Y, Zeleny J 2010 Thermo-mechanical model of spindles *CIRP Annals* **59** 365–368

[10] Palmgren A 1957 Neue Untersuchungen über Energieverluste in Wälzlagern *Wälzlagertechnische Mitteilungen* (SKF)
[11] Gesellschaft Verfahrenstechnik und Chemieingenieurwesen 2013 *VDI-Waermeatlas* **11** (Springer Vieweg)
[12] Bilgen E and Boulos R 1973 Functional Dependence of Torque Coefficient of Coaxial Cylinders on Gap Width and Reynolds Numbers *J of Fluids Eng.* **95** 122-126
[13] Bernhard F 2014 *Handbuch der Technischen Temperaturmessung* (Springer)

Special Interest Group Meeting on Thermal Issues
Laboratory for Machine Tools and Production Engineering (WZL) of
RWTH Aachen, Germany, February 2020
www.euspen.eu

Ambient temperature effect on the volumetric error of a large milling machine

Beñat Iñigo[1], Natalia Colinas-Armijo[1], Luis Norberto López de Lacalle[2], Gorka Aguirre[1]

[1]*Design and Precision Engineering Group, IDEKO, 20870 Elgoibar, Basque Country, Spain*
[2]*Department of Mechanical Engineering, EHU-UPV, 48013 Bilbao, Basque Country, Spain*

binigo@ideko.es

Abstract

Thermal errors represent one of the main error sources regarding to the volumetric accuracy of a machine tool. These errors can be induced by internal localized heat sources or by variations in the room temperature which affect to the whole volumetric performance. In this work a large milling machine model is presented and the effect of the ambient temperature in volumetric error is analysed. Model Order Reduction software allows to perform multiple evaluation at different machine position and temperature states, allowing full volumetric evaluation of the machine performance.

Machine tool, thermal error, ambient temperature, volumetric error, model reduction

1. Introduction

Thermal errors are amongst the main error sources regarding to the volumetric accuracy of a machine tool, along with the kinematic and dynamic errors [1]. These variations, which cause relative displacement between the Tool Center Point (TCP) and the workpiece, can be induced by internal heat sources, e.g. rotating spindle, linear axis drives or cooling system, or by variations in the room temperature.

Thermal errors caused by internal heat sources can be abrupt and less predictable, compared to those caused by the environment, but they are usually localized. Therefore, monitoring critical temperature variations and measuring its effects can be an easier task. Environmental effects usually lead to smooth temperature changes on the machine tool, but they affect the whole volumetric performance.

As in smaller machines environmental errors can be easier to characterize [2] measuring these effects in big machines represents a major challenge. Firstly, room temperature variations may be significant along the workshop volume, requiring a complete mapping of the machine temperature, with multiple probes in appropriate locations. Secondly, several points should be measured in the machine volume to properly characterize thermal error behaviour dependency with axes position, which involves difficulties in the implementation and accuracy of such measurements in large volumes. And last, implementing a compensation model that predicts thermal error is not straightforward, as several temperature inputs should be considered. These temperatures will usually show high correlation between them and lower signal-to-noise ratio to the displacements measured, compared to internal heat source effects.

Taking these aspects into account, characterization tests would require from several days to a week, involving specific measuring instrumentation [3], making this task time and cost ineffective. Hence, modelling and simulation play a major role on characterizing machines and efficient developing of compensation models.

Simulations using Finite Element models represent the most common approach, using them in different steps of the characterization and compensation process [4]. However, calculations usually require a considerable amount of time, especially in large machine models where the number of elements can be significant. Moreover, obtaining results in different axes position of the machine can be a difficult task in regular FEM programs, where the moving contacts between the axes are not prepared for such simulations.

Lately, Model Order Reduction (MOR) techniques has been used to reduce simulation time and analyse thermal error effects. Furthermore, FEM based reduction and simulation programs has been developed, that allow mechanical and thermal MOR and simulations in different machine positions using special interfaces between moving parts [5].

In this work environmental thermal effects will be analysed on a large moving-column milling machine model. MORe, a model order reduction software, will be used to simulate ambient temperature effects in the thermal error at different points of the machine volume. In section 2 the machine and several modelling aspects are presented. In section 3 some simulation results will be showed and analysed. Section 4 contains the main conclusions out of this work.

2. Modelling and methodology

In this section the machine model and the simulation procedure are presented.

2.1. Machine model

The machine modelled is a moving-column type milling machine with three linear axes. The moving parts of the machine, i.e. the column (X), the console (Z) and the ram (Y), along with the machine head, are supported by a bedplate (b2) that is fixed to the ground. The workpiece lays over another bedplate (b1), which is also fixed to the ground. Both bedplates have no other contact or bound between them. A schematic view of the machine is represented in figure 1 and table 1 summarizes main machine characteristics.

Table 1 machine specifications. Kinematic chain represented according to ISO 841 and ISO 10791-6 (t: tool; b: bed; w: workpiece).

Machine tool	X (mm)	Y (mm)	Z (mm)
Working volume	0-4000	0-1200	0-1500
Kinematic chain	t – Y – Z – X – b2 – b1 - w		

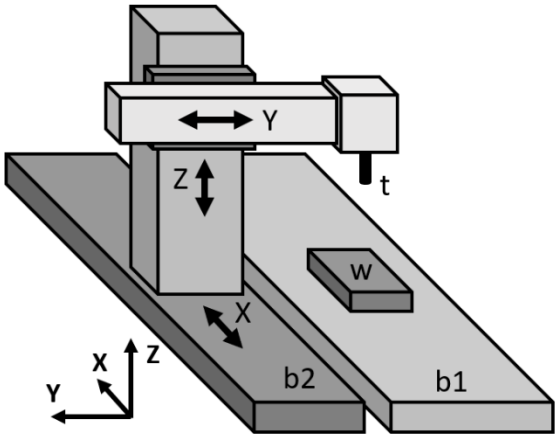

Figure 1. Schematic view of the machine structure.

All linear axes are position-controlled by the machine control using linear glass scales.

2.2. Modelling

A Finite Element model has been developed, including all the structural elements explained in section 2.1. A workpiece has not been included as these simulations aimed a more generalized analysis of the whole machine volume, nor has the tool, as its length may vary from case to case. The toolholder origin has been used as the reference point for the TCP instead. The metrics of the model are listed in table 2.

Most parts of the machine are made of structural steel, whose structural properties are available in most material libraries. The joints between moving parts, i.e. guidelines, carriages, ball screws and bearings has been modelled according to the mechanical and thermal properties provided by the manufacturers. Linear glass scale expansion effect has been included to consider its influence in the position control loop.

To simulate transient thermal effects in different axis positions thermal transient simulation is performed in the first place, varying ambient temperature. This way, complete temperature map of the machine is obtained for several time steps (T_1, T_2... T_n). Then, measuring points are defined in different axis positions ($\mathbf{X_1}$, $\mathbf{X_2}$ ... $\mathbf{X_m}$) and the thermomechanical model is used to evaluate all of them with the temperature field in each time step. Figure xx shows a diagram of the simulation process.

Table 2 FE Model metrics

FE Model DOF	Mechanic	Thermal
Full	~ 1 700 000	~ 560 000
Reduced	1720	490

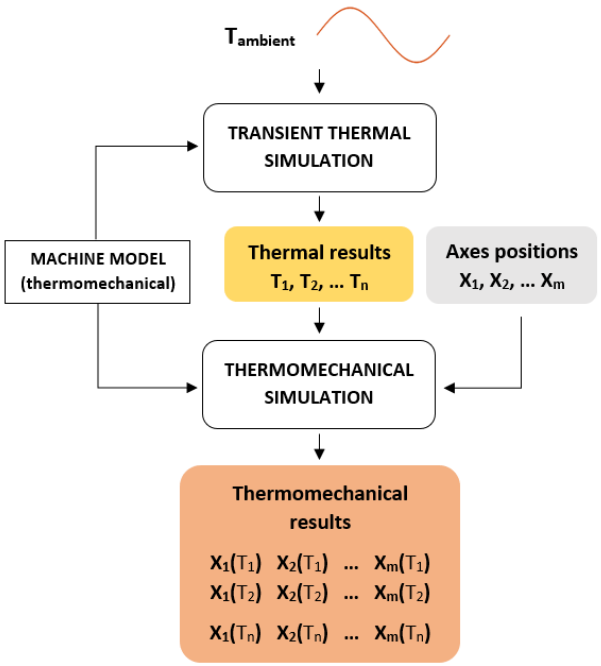

Figure 2. Diagram of the simulation process

3. Simulation and results

A 24h ambient temperature variations has been simulated, measuring the relative displacement between the TCP and the working bed (b1) at different axis positions. For that purpose, all external surfaces of the machine parts have been exposed to convection heat exchange with the air. The air temperature varies in a sinusoidal way, with ±5ºC variation, in a similar way workshop temperature may change due to day/night 24h cycle. Initial state has been set to 20ºC for all machine parts and transient thermal simulation has been perform.

Measured positions were generated by a 9x4x4 regular grid in all the machine volume, resulting in 144 points for each time step. These points have been evaluated every 30 minutes to obtain the thermal error of the machine through 24h. Table 3 summarizes simulation specifications.

Table 3 Ambient thermal simulation specifications

Ambient thermal simulation	
Ambient temperature	$T_{amb} = A \cdot \sin(2\pi f \cdot t)$; A = 5ºC ; f = 1/24h
Axes position grid	9x4x4 (**XxYxZ**) ; 144 total positions
Sampling period	30 min ; 49 total instants

Figure 3 shows the thermal error evolution for 24 hours in two different TCP positions. Deviations in X direction are plotted along with the ambient temperature. As it can be seen, X position affects to the thermal error in the machine volume. Both points show different behaviour in magnitude and phase through 24 h. As the first point (located at the middle of X, 2000mm) shows typical delayed behaviour with respect to the ambient temperature, the second one shows several effect, mainly related with the edge effect of both beds.

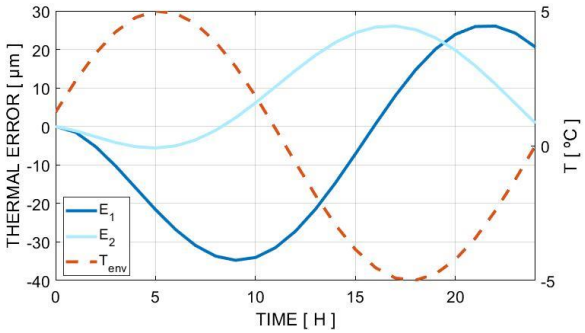

Figure 3. Thermal error through 24h for 2 measured points. E1 (dark blue) at X = 2000mm and E2 (light blue) at X = 3500mm, at same Y and Z positions. Thermal input is plotted in red.

Figures 4 shows the position-dependence behaviour of the thermal error, where the X direction error is shown for the XY plane at Z = 50mm position. 2 different time steps are shown to appreciate the evolution in time.

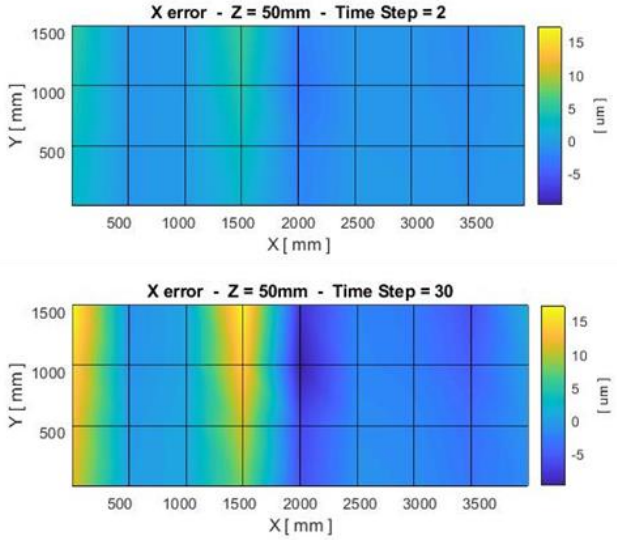

Figure 4. Thermal error through 24h for 2 measured points. E1 (dark blue) at X = 2000mm and E2 (light blue) at X = 3500mm, at same Y and Z positions. Thermal input is plotted in red.

4. Conclusions

- Complete thermal behaviour of a large machine tool has been simulated, allowing to evaluate the thermal error at any point of the machine volume. Such a volumetric evaluation has only been possible due to Model Reduction techniques applied with the mentioned software.

- Position dependency has been observed in the evolution of the thermal error. Along with the evolution over time, the study of such effects has allowed to understand different behaviour of the machine parts.

- In opposition to typical compensation strategies, this methodology approaches thermal errors as time and position dependent and will allow to develop compensation models that consider both aspects.

References

[1] J. Mayr, J. Jedrzejewski, E. Uhlmann, M. Donmez, W. Knapp, F. Härtig, K. Wendt, T. Moriwaki, P. Shore, R. Schmitt, C. Brecher, T. Würz, K. Wegener, Thermal issues in machine tools, CIRP Ann. - Manuf. Technol. 61 (2012) 771–791. https://doi.org/10.1016/j.cirp.2012.05.008.

[2] J. Yang, J. Yuan, J. Ni, Thermal error mode analysis and robust modeling for error compensation on a CNC turning center, Int. J. Mach. Tools Manuf. 39 (1999) 1367–1381. https://doi.org/10.1016/S0890-6955(99)00008-5.

[3] Z. Chengxin, G. Feng, L. Yan, Thermal error characteristic analysis and modeling for machine tools due to time-varying environmental temperature - ScienceDirect, Precis. Eng. 47 (2017) 231–238.

[4] P. Benner, R. Herzog, N. Lang, I. Riedel, J. Saak, Comparison of model order reduction methods for optimal sensor placement for thermo-elastic models, Eng. Optim. (2018) 1–19. https://doi.org/10.1080/0305215X.2018.1469133.

[5] P. Hernandez-Becerro, J. Mayr, P. Blaser, Model order reduction of thermal models of machine tools with varying boundary conditions - Research Collection, in: Conf. Therm. Issues Mach. Tools Proc., 2018: pp. 169–178.

Special Interest Group Meeting on Thermal Issues
Laboratory for Machine Tools and Production Engineering (WZL) of
RWTH Aachen, Germany, February 2020
www.euspen.eu

Extended discrete R-Test as on-machine measurement cycle to separate the thermal errors in Z-direction

Nico Zimmermann[1], Josef Mayr[1], Konrad Wegener[2]

[1] *inspire AG, Technoparkstrasse 1, 8005 Zürich, Switzerland*
[2] *Institute of Machine Tools and Manufacturing (IWF), ETH Zürich, 8092 Zürich, Switzerland*

zimmermann@inspire.ethz.ch

Abstract
This paper presents an on-machine measurement cycle based on the discrete R-Test, which separates the thermal errors of the different machine components in Z-direction. The error separation in Z-direction is particularly required for five-axis machining processes. The extended discrete R-Test separates the thermal position and orientation errors of a vertical rotation axis, the thermal errors of the machine table and the thermal position errors of the spindle and a horizontal rotation axis. The new measurement approach provides the foundation for more precise compensation results without requiring a more complex measurement setup.

Thermal error, on-machine measurement, error separation

1. Introduction

Five-axis machine tools are characterized by a high productivity for complex workpieces because of the reduced reclamping effort compared to 3-axis machine tools. However, this results in a more complex kinematic chain of the machine tool and a larger number of geometrical and thermal errors due to the two additional rotation axes. Among the different error sources, thermal errors have the most significant impact on the accuracy of machine tools [1].

Many different measurement strategies have been developed to evaluate the thermal behaviour of spindles and rotary axes. Commonly, the measurement setup described in ISO-230-3 [2] is applied to identify the thermal errors of spindles. Brecher et al. [3] propose an extension of this measurement setup to determine the thermal errors of a rotary axis and a spindle. The resulting measurement setup consists of five mandrels mounted on the machine table and a sensor setup with five displacement sensors fixed in the spindle. Furthermore, the R-Test developed by Weikert [4] is applicable to measure the thermal position and orientation errors of rotary axes. Ibaraki and Hong [5] propose a method based on the R-Test to evaluate the thermal influences on the error motions of a rotary axis. Gebhardt et al. [6] introduce a discrete R-Test to measure the thermal position and orientation errors of a vertical rotary axis and the thermal error of the machine table in axial and radial direction. Brecher et al. [7] developed a measurement method based on a dynamic R-Test to identify the volumetric thermal errors of five-axis machine tools. Ibaraki et al. [8] use a non-contact laser measurement system which is fixed on the rotary table to obtain the location errors of a rotary axis. This setup allows to measure the deviations at the same spindle speed as in the actual machining application.

Most of the measurement strategies for the thermal analysis of rotary axes need a specific measurement setup or expensive measurement devices. Therefore, Blaser et al. [9] present an on-machine measurement strategy for the discrete R-Test by using a touch trigger probe fixed in the spindle and a precision sphere mounted on the machine table. This on-machine measurement cycle identifies the thermal errors of a horizontal rotation axis which can be used for the Thermal Adaptive Learning Control (TALC) methodology [9,10].

The version of the on-machine measurement strategy described in [9] does not provide a detailed error separation in Z-direction between the different machine tool components. Consequently, the change of the effective direction of certain thermal errors is not considered for rotations of the swivelling axis. For robust thermal compensation results, it is required that the thermal errors are properly assigned to the different components so that they are also precisely compensated when the swivelling axis is rotated.

This paper presents an extended discrete R-Test for vertical rotation axes which enables a detailed error separation in Z-direction between errors with permanent and changing effective direction. Section 2 describes the methodology of the on-machine measurement approach and Section 3 presents the experimental results. To close the paper a conclusion and outlook is given in Section 4.

2. Methodology

The discrete R-Test for vertical rotation axes identifies the thermal position and orientation errors of a C-axis and the axial and radial thermal expansion of the machine table. Consequently, the axial thermal expansion of the machine table also includes the thermal error of the spindle and the position error of the horizontal rotational axis. In the case of the extended discrete R-Test the axial thermal growth of the machine table is clearly separated from the thermal error of the spindle and the thermal position error of the swivelling axis. Therefore, the extended discrete R-Test for vertical rotation axes enables to determine in total ten thermal errors, which are summarized in Table 1.

Table 1 Thermal errors identified by the extended discrete R-Test according to ISO 230-7 [11] with the addition of the machine table related errors according to [12]

Error	Description
E_{X0C}	Error of the position of C in X-axis direction
E_{Y0C}	Error of the position of C in Y-axis direction
E_{Z0T}	Position error of the table surface in Z-axis direction
E_{R0T}	Radial error of the functional surface table
E_{A0C}	Error of the orientation of C in A-axis direction: Squareness of C to X
E_{B0C}	Error of the orientation of C in B-axis direction: Squareness of C to Y
E_{C0C}	Zero position error of C-axis
E_{Z0S}	Error of the position of the spindle in Z-axis direction
E_{Y0A}	Error of the position of the A in Y-axis direction
E_{Z0A}	Error of the position of the A in Z-axis direction

2.1. Measurement cycle

The proposed measurement cycle combines laser measurement system and touch trigger probe measurements for a detailed separation of the thermal errors in Z-direction. Figure 1 illustrates the measurement procedure for the extended discrete R-Test. In the first step, the axial thermal error of the spindle is measured by a laser measurement system. However, the error separation between the spindle and the A-axis can only be realised if the laser measurement system is not mounted on the machine table. In the following, the measurements are performed using a touch trigger and a precision sphere placed on the machine table. The sphere is positioned at the circumference of the machine table to ensure a maximum distance from the rotational centre. The X-, Y-, and Z-positions of the sphere are measured at four positions reached by rotating the C-axis and two positions reached by additionally turning the A-axis. For the two A-axis measurements, the A-axis is turned to 90° and -90°. Thus, the proposed measurement cycle extends the standard discrete R-Test by a spindle measurement and two additional A-axis positions. The measurement time of the extended R-Test including all tool changes is around 2.5 minutes.

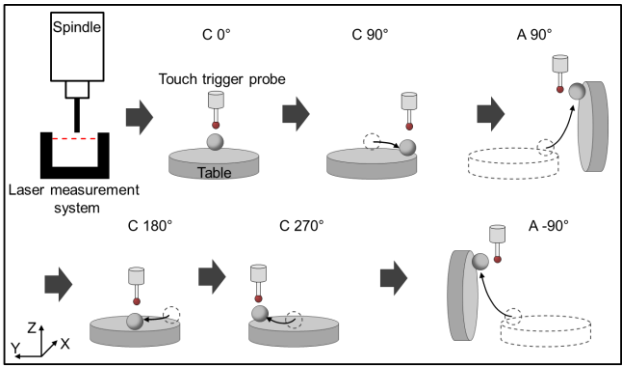

Figure 1. Measurement procedure of the extended discrete R-Test to identify the thermal position and orientation errors of the C-axis, the thermal errors of the machine table and the thermal position errors of the spindle and the A-axis.

2.2. Mathematical model

The calculation of the thermal position and orientation errors of the C-axis and the axial and radial thermal error of the machine table are described in [12]. The calculation of the axial thermal error of the machine table in Z-direction for the standard discrete R-Test is shown in Eq. (1).

$$E_{Z0T_i} = \frac{1}{4}\sum_{k=1}^{4} Z_{t_i,C_k} - \frac{1}{4}\sum_{k=1}^{4} Z_{t_1,C_k} \tag{1}$$

Compared to Eq. (1) the three additional measurement steps of the extended discrete R-Test allow a more accurate estimation of the thermal errors in Z-direction. The measurement of the laser measurement system is directly used to calculate the error E_{Z0S} as described in Eq. (2).

$$E_{Z0S,i} = -(Z_{t_i,laser} - Z_{t_1,laser}) \tag{2}$$

The thermal error of the spindle is defined at the tool side such that an elongation of the spindle results in an error in negative Z-direction. The thermal error of the spindle includes the thermal elongation of the spindle and the displacement of the laser measurement system due to thermal influences. The two additional measurement positions of the A-axis at 90° and -90° result in a reversal measurement in Y-direction, which enables an error separation between E_{Z0T} and E_{Y0A}. The thermal error E_{Z0T} changes its effective direction depending on the rotational angle of the A-axis. In contrast, the thermal error E_{Y0A} appears in the same direction at both rotation angles. Therefore, E_{Y0A} and E_{Z0T} can be separated by considering the Y-coordinate of the two additional positions. Eq. (3) defines the calculation of the thermal error E_{Z0T}.

$$E_{Z0T_i} = \frac{1}{2}\left(Y_{t_i,A_{-90}} - Y_{t_i,A_{90}}\right) - \frac{1}{2}\left(Y_{t_1,A_{-90}} - Y_{t_1,A_{90}}\right) \tag{3}$$

Eq. (4) is used to calculate the thermal error E_{Y0A}.

$$E_{Y0A_i} = \frac{1}{2}\left(Y_{t_i,A-90} + Y_{t_i,A90}\right) - \frac{1}{2}\left(Y_{t_1,A-90} + Y_{t_1,A90}\right) \tag{4}$$

The measurement data in Z-direction is required to determine the thermal error E_{Z0A}. However, the measurement results also depend on the thermal errors E_{R0T} and E_{Z0S}. These influences must be eliminated by subtracting them as shown in Eq. (5).

$$E_{Z0A_i} = \frac{1}{2}\left(Z_{t_i,A_{-90}} + Z_{t_i,A_{90}}\right) - \frac{1}{2}\left(Z_{t_1,A_{-90}} + Z_{t_1,A_{90}}\right) + E_{Z0S_i} - E_{R0T_i} \tag{5}$$

The thermal error E_{Z0A} describes the error between the laser measurement system and the position of the A-axis. However, a possible thermal zero position error of the A-axis has no influence on the identified E_{Z0A} because it is eliminated by the reversal measurement.

If no laser measurement system is available, it is not possible to separate the thermal errors of the spindle and A-axis in Z-direction. This separation is not required for the compensation but neglecting it results in a more complex compensation model for this thermal error due to a larger number of relevant inputs. For that case the calculation of the thermal error E_{Z0A} + E_{Z0S} is given in Eq. (6).

$$E_{Z0S_i} + E_{Z0A_i} = \frac{1}{2}\left(Z_{t_i,A_{-90}} + Z_{t_i,A_{90}}\right) - \frac{1}{2}\left(Z_{t_1,A_{-90}} + Z_{t_1,A_{90}}\right) - E_{R0T_i} \tag{6}$$

3. Experimental Results

The kinematic chain of the investigated machine tool can be described according to ISO 10791-2 [13] as following:

V [w – C' – A' – X' – b – Y – Z – S – t].

The laser measurement system of the considered machine tool is placed in the tool magazine. During the experiment, the spindle and the C-axis are rotated over 72 h with two randomly generated speed profiles. Figure 2 shows the speed variation for

the spindle and the C-axis and the measured temperatures. The speed of the spindle varies between 159 and 10’884 rpm and the speed of the C-axis is between 9 and 117 rpm. During the experiment a five minutes thermal load case interval and the measurement interval alternate.

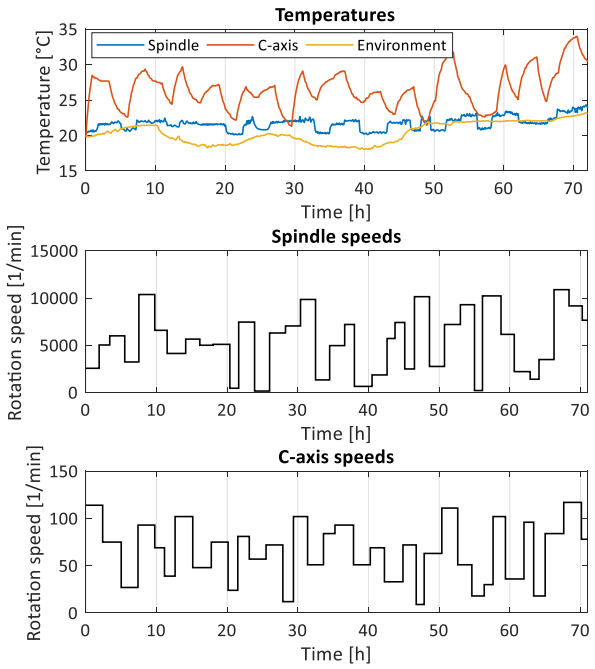

Figure 2. Speed profiles of the spindle and the C-axis and the measured temperatures.

Figure 3 presents the thermal error in Z-direction measured with the standard discrete R-Test for vertical rotation axis. Commonly, this error is described as thermal error of the machine table in axial direction. However, this represents the superposition of the thermal errors at the tool and the workpiece side. It is also apparent in Figure 2, that the underlaying source of the thermal error in Z-direction is a superposition of the two speed profiles and the changing environmental influences.

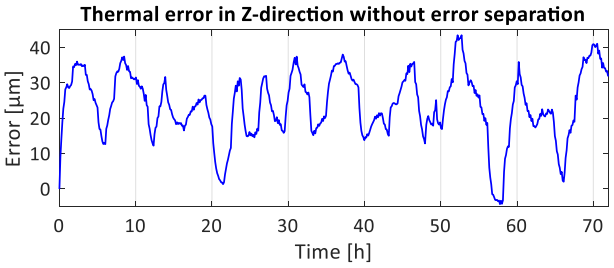

Figure 3. Error in Z-direction without separating the different influences.

Figure 4 illustrates the separated thermal errors in Z-direction obtained from the extended discrete R-Test. The thermal error E_{Z0S} relates to the speed variations of the spindle and the thermal error E_{Z0T} is mainly influenced by speed variations of the C-axis. The thermal error E_{Z0A} depends significantly on the environmental temperature. Consequently, the error separation enables a more detailed analysis of the thermal errors of the different machine components. Approximately one-half of the thermal error in Z-direction measured with the standard discrete R-Test corresponds to the spindle and the other half to the machine table. If the accumulated error in Z-direction was applied for thermal compensation, this would result in inaccurate compensation results when the swivelling axis is turned. This compensation error would be up to 26 µm in the conducted experiments.

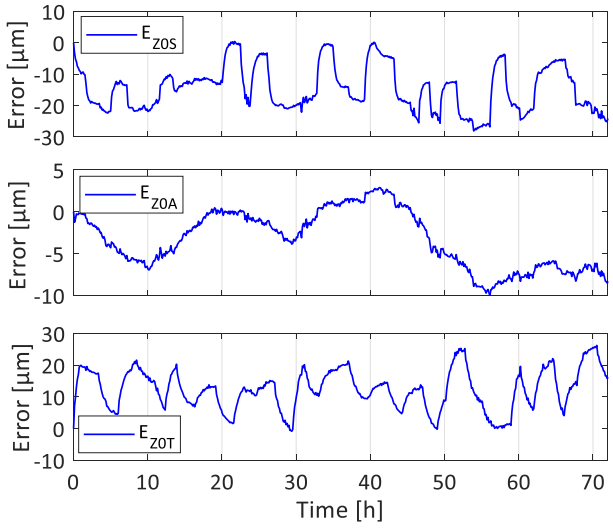

Figure 4. Separated errors in Z-direction of the spindle, A-axis and the table.

As described in Section 2.2 the extended discrete R-Test is also applicable if no laser measurement system is available on the considered machine tool. Figure 5 shows the error separation for this modified approach. The thermal error, which permanently appears in Z-direction, is the superposition of the thermal errors E_{Z0S} and E_{Z0A}. This thermal error must be compensated at the tool side and the thermal error E_{Z0T} should be compensated at the workpiece side.

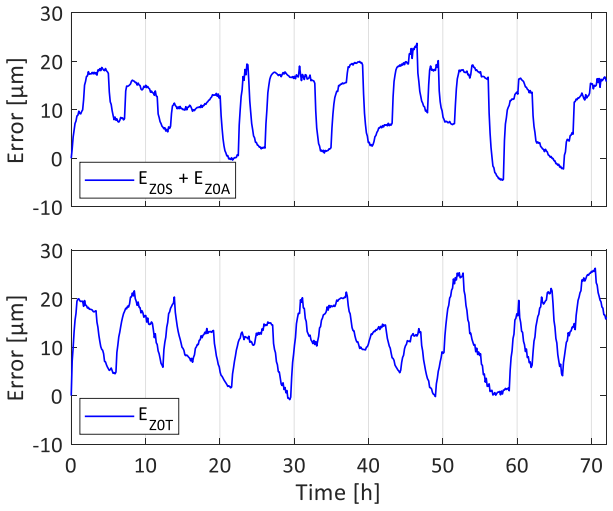

Figure 5. Separation of the errors in Z-direction without using the laser measurement.

4. Conclusion and Outlook

The extension to the discrete R-Test provides a detailed separation of the thermal errors in Z-direction so that the thermal errors are assigned to the correct machine components. This is especially important for five-axis machine tools when the swivelling axis is used in the machining process and a reorientation of the machine table takes place. The conducted experiments show exemplarily that in the case of the investigated machine tool a compensation without the error

separation results in compensation values which are around 50 % off. In the future, the on-machine measurement approach will also be extended to the orientation errors of the A-axis.

References

[1] Mayr, J., Jedrzejewski, J., Uhlmann, E., Alkan Donmez, M., Knapp, W., Härtig, F., Wendt, K., Moriwaki, T., Shore, P., Schmitt, R., Brecher, C., Würz, T., Wegener, K., 2012, Thermal issues in machine tools, CIRP Annals - Manufacturing Technology, 61/2:771–791.

[2] ISO 230-3:2007, Test Code for Machine Tools — Part 3: Determination of Thermal Effects, International Organization for Standardization ISO, Geneva, Switzerland.

[3] Brecher, C., Spierling, R., Du Bois-Reymond, F., Fey, M., 2017, Thermo-elastic deformation of rotary axes, Laser Metrology and Machine Performance XII - 12th International Conference and Exhibition on Laser Metrology, Machine Tool, CMM and Robotic Performance, LAMDAMAP 2017, pp. 111–121.

[4] Weikert, S., Knapp, W., 2004, R-test, a new device for accuracy measurements on five axis machine tools, CIRP Annals - Manufacturing Technology, 53/1:429–432.

[5] Ibaraki, S., Hong, C., 2012, Thermal test for error maps of rotary axes by R-test, Key Engineering Materials, 523–524:809–814.

[6] Gebhardt, M., von Cube, P., Knapp, W., Wegener, K., 2012, Measurement set-ups and -cycles for thermal characterization of axes of rotation of 5-axis machine tools, in *12th euspen International Conference*.

[7] Brecher, C., Behrens, J., Klatte, M., Lee, T. H., Tzanetos, F., 2018, Measurement and analysis of thermo-elastic deviation of five-axis machine tool using dynamic R-test, Procedia CIRP, 77/HPC:521–524.

[8] Ibaraki, S., Inui, H., Hong, C., Nishikawa, S., Shimoike, M., 2019, On-machine identification of rotary axis location errors under thermal influence by spindle rotation, Precision Engineering, 55:42–47.

[9] Blaser, P., Pavliček, F., Mori, K., Mayr, J., Weikert, S., Wegener, K., 2017, Adaptive learning control for thermal error compensation of 5-axis machine tools, Journal of Manufacturing Systems, 44:302–309.

[10] Mayr, J., Blaser, P., Ryser, A., Hernandez-Becerro, P., 2018, An adaptive self-learning compensation approach for thermal errors on 5-axis machine tools handling an arbitrary set of sample rates, CIRP Annals, 67/1:551–554.

[11] ISO 230-7:2015, Test Code for Machine Tools — Part 7: Geometric accuracy of axes of rotation, International Organization for Standardization ISO, Geneva, Switzerland.

[12] Gebhardt, M., 2014, Thermal behaviour and compensation of rotary axes in 5-axis machine tools.

[13] ISO 10791-2:2001, Test Conditions for Machining Centres − Part 2: GeometricTests for Machines with Vertical Spindle or Universal Heads with VerticalPrimary Rotary Axis., International Organization for Standardization ISO,Geneva, Switzerland.

Special Interest Group Meeting on Thermal Issues
Laboratory for Machine Tools and Production Engineering (WZL) of
RWTH Aachen, Germany, February 2020
www.euspen.eu

Thermal Qualification of Precision Systems

Maurice Limpens[1], Björn Bukkems[2], Theo Ruijl[3]

[1] *Maurice Limpens is Senior Thermal Architect at MI-Partners in Eindhoven, the Netherlands, having broad experience in troubleshooting and design improvement of industrial precision systems, based upon dedicated analysis and modelling.*

[2]*Björn Bukkems is Senior Mechatronic System Designer at MI-Partners in Eindhoven, The Netherlands, having a background in dynamics and control technology and thermal modelling, with focus on industrial precision systems.*

[3]*Theo Ruijl is CTO at MI-Partners and Senior Mechatronic System Architect. He initiated the TEMS (Thermal Effects in Mechatronic Systems) competence within Philips Applied Technologies about 15 years ago, and has more than 25 years of experience in designing high-end mechatronic systems.*

Maurice.Limpens@MI-Partners.nl

Abstract
Thermal qualification of a temperature conditioned heat shield for a precision motion system has been done using modelling and measurement tools at MI-Partners. Thermal qualification enables determination of thermal system performance without stringent demands on environmental conditions. It combines frequency domain modelling techniques with measurements on a real system in order to quantify thermal performance. It has shown to be an effective tool, enabling simple but accurate approval of thermal systems.

Thermal Qualification, Frequency domain, system approval

Special Interest Group Meeting on Thermal Issues
Laboratory for Machine Tools and Production Engineering (WZL) of
RWTH Aachen, Germany, February 2020
www.euspen.eu

Evaluation of optimal positioning methods of integral deformation sensors for the correction of thermal errors in machine tools

Christian Brecher[1], Roland Herzog[2], Robert Spierling[1], Filippos Tzanetos[3], Andreas Naumann[2]

[1]*Laboratory for Machine Tools and Production Engineering (WZL), Aachen, Germany*
[2]*TU Chemnitz, Faculty of Mathematics, Research Group Numerical Mathematics (Partial Differential Equations), Chemnitz, Germany*
[3]*Fraunhofer Institute of Production Technology (IPT), Aachen, Germany*

r.spierling@wzl.rwth-aachen.de

Abstract
Up to 75% of the overall workpiece error can be caused by the thermo-elastic behavior of the machine tool. Therefore, correction methods based on machine-integrated sensors were intensively researched in the last years, in order to determine the dislocation of the Tool Center Point (TCP) parallel to the process. One of these sensors is the integral deformation sensor (IDS), which detects the integral deformation along the length of a structural component of the machine. The integral deformation is the result of the directional temperature gradient along the length of the component. These measurements are fed into a mechanical model of each machine tool component to predict the deformation along the length of some significant outer surfaces, such as the guide ways on the component. Based on this information, the kinematic model of the machine tool can calculate the overall thermo-elastic TCP dislocation.
Before the installation of the IDS on the machine tool components, the optimization of the sensor arrangement is recommended, since it has a significant influence on the achievable TCP prediction accuracy. Several approaches to perform this step are known. This paper presents and compares an experienced-based approach and a mathematical optimization strategy. The arrangement of the IDS comprises the lengths and positions of the IDS within each machine tool component. The mechanical and the kinematic model using the IDS information are the basis for both the experienced-based and the mathematical approach. The first strategy is based on domain knowledge on the thermo-elastic behavior of the machine tool and on the interpretation of the IDS measurements. The mathematical strategy, on the other hand, changes the arrangement of the IDS on each machine tool component until the covariance with the overall TCP dislocation reaches its minimum.
Deformation, Measuring instrument, Optimization, Thermal error

1 Introduction

The integral deformation sensors (IDS) can provide a significant contribution to the determination of the thermo-elastic behavior of machine tools and subsequently the precision of the manufactured parts. A physical model, based on mechanical modeling and the kinematics of the machine tool, calculates the Tool Center Point (TCP) dislocation in real-time parallel to the machining process [1]. The determination of the optimal sensor placement can reduce the amount of sensors needed to reach the same prediction accuracy. It can also reduce the uncertainty propagation from the measurement uncertainty of the IDS data to the prediction of the TCP dislocation.

The application of optimal sensor placement techniques in practice is however bound to some challenges. Ideally, the optimal sensor placement is taken into consideration during the design and construction process of the machine tool. However, in case of a retrofit of the sensors on an existing machine tool, there are limitations with respect to the available installation space. The mathematical description of the allowable installation space has a direct impact on the computational effort that the optimization procedure will require. In practical terms, the installation space has to be discretized with a specific refinement, leading to a mesh with nodes indicating allowable positions of the sensors.

The arrangement of the IDS in this paper comprises the lengths and positions of the IDS within each machine tool component. This paper presents and compares two optimal sensor positioning methods in a simulation environment. On the one hand, an experience-based approach makes use of domain knowledge on the thermo-elastic behavior of the machine tool and on the interpretation of the IDS measurements. On the other hand, the mathematical optimization relies upon a general optimal experimental design criterion [3]. Every measurement contains measurement errors, which are often assumed to be independent and identically distributed. Under the assumption of a linear model, the true TCP lies inside the confidence ellipsoid around the computed (or expected) TCP. This method changes all sensor positions at the same time, until the longest axis of confidence ellipsoid of the predicted TCP dislocation reaches its minimum value.

The use case of this work is a 4-axis horizontal milling machine, as shown in Figure 1. The IDS will be placed at the column, the bed section underneath the column and the bed section underneath the table. There are practical limitations for the sensor placement due to piping, housings, measuring systems, drive elements and auxiliary systems. The figure below depicts the machine structure in grey, the ball screws in red, the guiding slides in blue, the guiding shoes in green and the measuring systems in orange.

2 Optimal Sensor Placement

The following sub-sections describe the working principles of the prediction and the optimal sensor positioning strategies. The

main goal of the optimal sensor placement is to maximize prediction accuracy, while using the least number of IDS. Both the propagation of measurement uncertainty though the model and the model simplifications and assumptions of the model hinder the overall prediction accuracy.

From the standpoint of the prediction model using the IDS data to derive the TCP dislocation of the machine tool, the sensor placement is a set of parameters of the model. The accuracy of the prediction model depends also on its parameters. Hence, changing the sensor positioning and the corresponding parameters to the model should lead to changes on the overall prediction. The extent to which these parameters can change the outcome depends on the physical principles of the model used to interpret the behavior of the machine tool and the meaning of the IDS measurements.

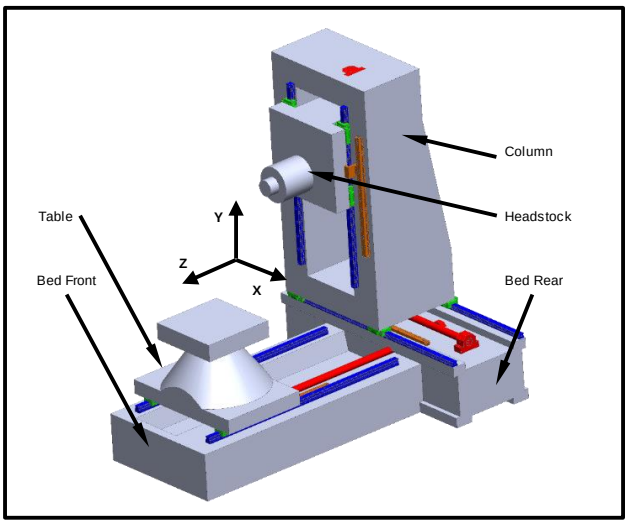

Figure 1. Demonstrator machine tool and areas of possible IDS placement

2.1 Prediction model and experience-based optimal positioning of IDS

The measuring principle of the IDS was explained in detail in [1], a brief summary is given in the following lines. An IDS measures the relative deformation of its two end points in one direction. When it is used for the detection of thermos-elastic behavior of machine tools, this measurement can be interpreted as the integral of the temperature distribution along its measuring length, multiplied by the specific heat expansion coefficient of the machine tool component. This leads to the resulting deformation distribution due to all thermal effects and heat transport phenomena that inflicted the machine tool component. The physical model that uses the IDS information contains two separate steps:

- the mechanical modelling of each machine tool component to calculate the overall deformation field of the component,
- the kinematic modelling of the entire machine tool to calculate the overall dislocation between tool and workpiece.

Both modeling steps influence the prediction accuracy. The overall chain of data and calculations from the collection of IDS data to the prediction of TCP dislocation is depicted in Figure 2. The model parameters for each modeling step are specific for the machine tool and do not depend on the thermal load.

The mechanical model follows the Euler-Bernoulli beam assumptions, which consider each machine tool component as a three-dimensional deformation and inclination field that can be described with one variable: the current position along the neutral fiber of the beam. The IDS are always parallel to the neutral fiber, so they measure only the longitudinal deformation of the machine tool component at their position. The distance of the IDS to the neutral fiber is a vital component to the interpretation of the IDS data: the farther away an IDS is from the neutral fiber, the larger the deformation this IDS is expected to detect.

The position of the IDS along the length of the beam is however a more complex parameter, because it includes the combinatorial consideration of all IDS on the machine tool component. The reason for this is that each IDS delivers a one-dimensional information, leading at first to a conclusion about the thermal expansion of the machine tool component. However, in order to detect bending modes with respect to one or two directions in space, another one or two IDS are necessary. Each bending mode would lead to one IDS getting elongated on the one side of the neutral fiber, while the other gets contracted. The presence of two bending modes on top of the thermal expansion would require three IDS in overall, for which the combination of expansion and / or contraction detected at each IDS can come from three different deformation modes: (1) thermal expansion; (2) bending around one transverse direction of the beam; (3) bending around another transverse direction of the beam.

On the other hand, the specific solution leading to the overall deformation field of a machine tool component depends also on the mechanical boundary conditions. A typical comparison to showcase this effect is the apparent difference of the resulting deformation between a fixed-free-end beam and a simply-supported beam. This information is also fed to the mechanical model, which in turn combines this information with the interpretation of the IDS data and tries to fit a polynomial equation of 2nd or 3rd degree to these known values of deformation at different points along the length of the neutral fiber. A 2nd degree polynomial, for example, is solvable with three known values and leads to a quadratic deformation distribution.

It is thus evident how complicated it is to decide where to position the sensors on each machine tool component, in order to maximize the prediction accuracy of the TCP-dislocation. The higher the number of deformation modes, the more complex this deduction process becomes. This paper applies the optimal positioning methods based on the model calculations for up to three deformation modes, as described above.

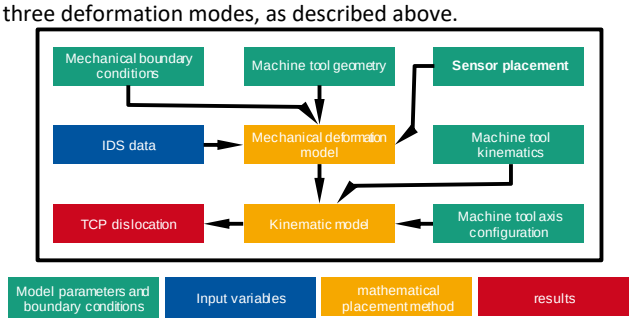

Figure 2. Overview of prediction model with model parameters, as well as input and output variables

It should be noted that additional deformation modes, that can be present in practice, such as torsion and shear strain, are not included. However, these deformation models are negligible in machine tool configurations such as the demonstrator machine tool used in this paper (Figure 1). Shear strain is negligible when one dimension is significantly longer than the other two, which is the case for all machine tool components considered for sensor placement. Torsion is not expected in such machine tool configurations, because it arises mostly on cross-beams, portals or horizontal headstocks.

The experience-based optimal positioning approach makes use of the information described above and combines them with analyses and experience gained about the thermo-elastic behavior of machine tools and their components.

2.2 Mathematical approach for the optimal positioning of IDS

The two approaches require different types of initial knowledge and different processes to find a set of optimal sensor positions, as can be seen in Figure 3. The mathematical model starts from the geometric and kinematic structure of the machine. The two main building blocks for the optimization are the optimization loop *sensor position -> svd -> sensor positions* and the *Bernoulli beam model*. These blocks lead to the optimal sensor positions. In contrast the experience based approach requires only the domain knowledge.

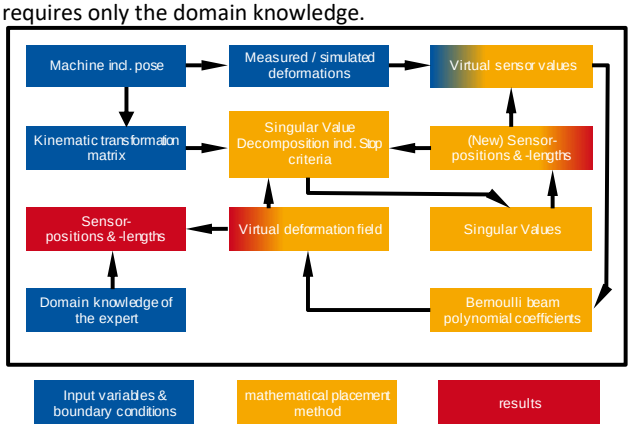

Figure 3. The model-based optimization approach

The mathematical model of the sensor measurement to machine displacement map can be written as

$$u(f) = A(x_c) \cdot B_c(x_s, l_s) \cdot (f + \theta) \qquad (1)$$

where the coefficient matrices B_c and A represent a constant and a nonlinear local sensor model respectively and the coefficient matrix $A(x_c)$ maps the local displacements to the global space. Hence, the last coefficient depends only on the local orientation of the machine components, whereas the first two depend only on the sensor locations and configuration.

Furthermore the sensor measurements are not exact, but contain independent normally distributed measurement errors $\theta \sim$ N (0, σ^2 2I) with zero mean and standard deviation σ. Let us first neglect the nonlinear part B_n. Then the Jacobian J of the machine displacement u is then given by

$$J(x_c, l_s) = A(x_c) \cdot B_c(x_s, l_s) \qquad (2)$$

Our aim are highly confidential computations of the machine distortion from the measured displacement. In other words, we wish to find sensor positions x_s and lengths l_s , such that the confidence ellipsoids are small. Due to the geometric nature, there are several choices [3]:

(i) One can minimize the length of longest axis. This corresponds to the largest singular value of the Jacobian matrix J.

(ii) One can minimize the volume of the ellipsoid. This corresponds to the product of the singular values of J.

We use the criterion (i) and look for the optimal sensor position and sensor lengths, such that the largest singular value becomes minimal. Furthermore, we constrain the sensor positions to their initial faces and orientation.

All optimization variables are continuous, but bounded by geometric constraints. As suitable numerical algorithm for these problem is the interior point method [5].

First, we start from an initial sensor placement, see for example Figure (4a). These initial sensor positions are symmetric in the centers of the surfaces and every surface contains exactly one sensor. This initial placement has the largest singular value around 2.7. After optimization, we obtain the placement in Figure (4b) with largest singular value around 1.3. In other words, the optimization halved the length of the longest confidence axis.

The basis for this optimization approach is a mathematical model of the sensors. Therefore the optimal sensor positions are only as good as the model describes the sensors and the machine kinematics and cannot correct any modelling error. In particular the optimization does not add any additional information, but increases the information from every sensor.

3 Results and comparison

In order to compare the experience-based with the mathematical approach, a probability distribution of random values will be used as a reference input value. The standard deviation of this distribution will be the measurement uncertainty of the IDS, which is known to be ±1 µm per meter IDS length from past experimental investigations [1]. The average value of the distribution will be zero, in order to evaluate the propagation of distributions with the so-called Monte-Carlo method [5]. The deformation model that predicts the TCP-dislocation will run twice for this input value: once with the sensor placement derived from the experience-based method and once with the sensor placement derived from the mathematical optimal positioning approach. The output values of each prediction run will be statistically evaluated.

A good sensor placement should not allow for an amplification of the scattering interval, nor a shift of the average value. The 95% confidence interval will quantify the scattering interval in this paper. The bigger such effects are present, the less trustworthy is the sensor placement and consequently the methods that derived it would be less effective. A shift of the average value indicates a non-linearity in the model calculation, which exists only in the kinematic model. In order to investigate the influence on the scattering interval, the model was linearized around the local deformation in the work-space of the test machine tool.

The mathematical optimization strategy leads to a significant reduction of the scattering interval on the prediction of the TCP dislocation as shown in Figure 4. Since the test machine tool is symmetrical with respect to the YZ-plane, the scattering along this direction is very low in both sensor placements and changes inconsiderably. The scattering in Y-direction is reduced to more than 50% and in Z-direction to almost 60%. This indicates a higher repeatability for the model prediction, which means that the overall prediction uncertainty is improved. Based on the fact that the optimization run lasted only a few minutes, the application of this method in practice can be beneficial. The Monte-Carlo simulation that allows the evaluation of the results also lasts only a few minutes.

4 Summary and Outlook

A comparison of the strategies in this paper leads to the conclusion that the mathematical optimization can provide useful results with reasonable numerical effort. The optimization for one kinematic pose lasts only a few seconds. The reason for this is that the physical model that the

mathematical optimization is built upon is a non-linear algebraic equation system. Since the model consists solely of algebraic equations, the Jacobian (2) is given explicitly. Therefore the singular values are available from standard numerical software. The results in Fig. 4 clearly indicate a significant optimization of the prediction of the TCP dislocation. As described in Ch. 3, the results of the optimization can be interpreted with the domain knowledge of the experts. More specifically, the results lead to conclusions about the mechanical behavior due to the mechanical boundary conditions and/or the relevance of deformation modes of each machine tool component due to the machine tool kinematics. These conclusions can only be drawn by such mathematical approaches.

Nevertheless, it must be noted that the mathematical strategy requires an initial sensor placement, which can only be deduced based on domain knowledge. Hence, this approach cannot replace the domain knowledge of the experts competely. A sensitivity analysis of the initial sensor placement has to be studied in the future. Another drawback of the mathematical method in this paper is that it does not optimize the sensor placement for all kinematic poses of the machine tool axes simultaneously. Instead, the authors ran an optimization of the sensor placement for the combination of three positions for each machine tool axis (the combination of 3 positions for each of the three axes leads to 10^3 = 1.000 combinations) separately.

Also, experimental data with the optimal sensor placement must be gathered and compared with the experience-based sensor placement, in order to validate the effectiveness of the mathematical optimization strategy in an industrially relevant environment.

The methods proposed in this paper were focused on parallel configurations of the IDS, which means that all IDS on a machine tool component are parallel to each other and to the axis of the longest dimension of the machine tool component (beam neutral fiber). There is no validated interpretation model yet of IDS being arranged with an inclination to each other or to the neutral fiber of the machine tool component. The mathematical optimization method presented in this paper calculates analytically the covariance of the predicted TCP dislocation based on the model equations, which classified this method as a so-called "white-box" strategy.

A "black-box" strategy, on the other hand, which is based on measurements of the IDS and the real TCP dislocation instead, will be also evaluated in the future. However, such a strategy is bound to higher installation and optimization effort, since a higher amount of pre-defined, possible optimal IDS positions have to be installed on the machine tool of interest. Then, experiments will have to be designed, in order to measure the real TCP dislocation while applying test thermal loads on the machine tool. Such strategies are limited by the fact that the test thermal loads are not the same as the real loads on the machine tool under operating conditions and by the pre-defined IDS positions.

Acknowledgement

Funded by the German Research Foundation – Project-ID 174223256 – TRR 96 – Subprojects B06, B08 and C03.

References

[1] Brecher C, Klatte M, Lee T H, Tzanetos F. Metrological analysis of a mechatronic system based on novel deformation sensors for thermal issues in machine tools, Proc CIRP Vol 77 Special Issue for the 8th CIRP Conference on High Performance Cutting (HPC 2018), 2018, pp. 517-520, https://doi.org/10.1016/j.procir.2018.08.245

[2] Herzog R, Riedel I, Uciński D. Optimal Sensor Placement for Joint Parameter and State Estimation Problems in Large-Scale Dynamical Systems with Applications to Thermo-Mechanics, D. Optim Eng Vol 19 Issue 3, 2018, pp. 591-627, https://doi.org/10.1007/s11081-018-9391-8

[3] Atkinson, A. C.; A. N. Donev; R. D. Tobias (2007). Optimum experimental designs, with SAS. Vol. 34. Oxford Statistical Science Series. Oxford: Oxford University Press.

[4] JCGM 101:2008 Evaluation of measurement data – Supplement 1 to the "GUM" – Propagation of distributions using a Monte Carlo method

[5] Wächter, A. (2002). "An interior point algorithm for large-scale nonlinear optimization with applications in process engineering". PhD thesis. PhD thesis, Carnegie Mellon University, Pittsburgh, PA, U

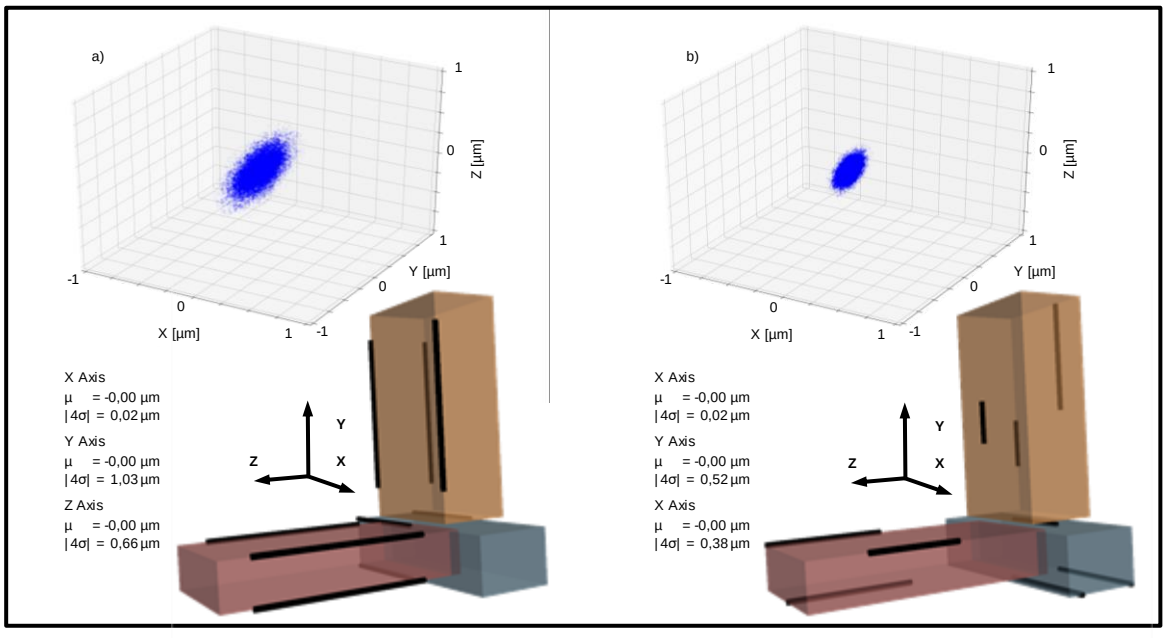

Figure 4. Sensor placement a) based on the experience-based method and b) based on the mathematical method. Prediction of the TCP-dislocation for a measurement uncertainty of **±1µm** per meter IDS length c) based on the experience-based method and d) based on the mathematical method

Modelling and Model Reduction Techniques

Special Interest Group Meeting on Thermal Issues
Laboratory for Machine Tools and Production Engineering (WZL) of
RWTH Aachen, Germany, February 2020
www.euspen.eu

Efficient thermo-mechanical model of a precision 5-axis machine tool

Pablo Hernández-Becerro[1,2], Josef Mayr[1], Konrad Wegener[2]

[1]*inspire AG, Technoparkstrasse 1, 8005 Zürich, Switzerland*
[2]*Institute of Machine Tools and Manufacturing (IWF), ETH Zürich, Leonhardstrasse 21, 8092 Zurich, Switzerland*

hernandez@inspire.ethz.ch

Abstract
Thermally induced deviations of machine tools result in geometric errors of manufactured parts. Thermo-mechanical models are a great asset in order to predict the thermal response of machine tools and understand the thermal design. This paper presents a thermo-mechanical model of a 5-axis precision machine tool, focusing on the thermal response during the rotation of the C-axis. In order to reduce the computational effort, this work uses a surrogate model by means of projection-based Model Order Reduction (MOR). The model setup, reduction, and analysis are performed in MORe, an simulation package designed for the development of efficient model of machine tools. The response of the thermo-mechanical model is compared to the measured thermo-mechanical deviations during the rotation of the C-axis. The validated thermo-mechanical model enables analysis of the thermal design of the machine tool, in frequency and in time domain.

Thermo-mechanical model; model order reduction (MOR); machine tool

1. Introduction

The review paper of Mayr et al. [1] pointed out that the thermal error sources are one of the main contributors to geometric errors in manufactured parts. Recent advances in modelling techniques facilitate the understanding of the thermal behavior of machine tools. Physical models, based on the finite element (FE) discretization of the heat transfer and elasticity equations, serve as virtual prototypes to test different design alternatives. However, the thermo-mechanical FE-models are computationally expensive due to the geometrical complexity of the machine tools. This limits the applicability when a large number of model runs or real time capabilities are required. Therefore, developing efficient modeling approaches is necessary to ensure the usability of physical models. Surrogate models are computationally efficient models reproducing the response of a high-fidelity model. Projection-based surrogate model or Model Order Reduction (MOR) is based on the projection of the original model in a lower dimensional subspace. The main advantage of MOR is that it retains the system structure while it allows tracing the system dynamics, as explained by Benner et al. [2].

2. MORe: an efficient simulation framework

MORe [3] is a software package developed at inspire AG for the simulation of the static, dynamic, and thermo-mechanical behavior of machine tools. The simulation platform offers tools to analyze efficiently the behavior of machine tools and optimize their design.

The simulation platform provides an efficient workflow to develop physical models of machine tools. Figure 1 illustrates the tool chain for the creation of a model of a machine tool assembly. A commercial FE software, Ansys, performs the FE discretization of each of the components of the assembly. As shown in Figure 1, MORe imports the geometrical information and system matrices delivered by the FE commercial software. After importing the required information, the model setup, analyses and postprocessing of the simulation results is performed in the software MORe.

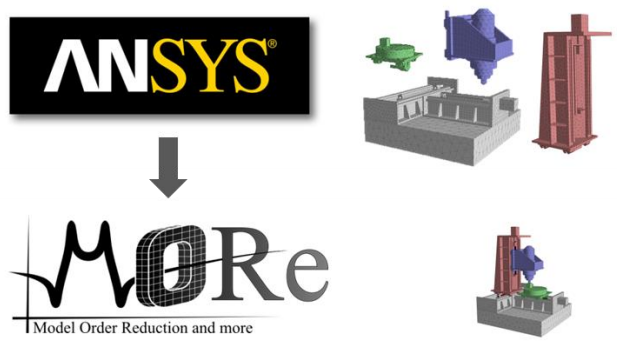

Figure 1. Tool chain of MORe: an efficient simulation framework

The model setup requires the definition of the different boundary conditions, e.g. moving or stationary thermo-mechanical contacts between the different components or convective boundary conditions. These boundary conditions are interfaces of the system, i.e. independents inputs considered for the reduction. After the complete definition of the model interfaces, the system equations are reduced by means of projection-based MOR. The Krylov Modal Subspace (KMS) approach is used for the creation of the projection basis. The work of Spescha [4] and Hernández-Becerro [5] provides a more detailed description of the reduction methods. The reduced models enables the efficient evaluation of the thermo-mechanical behavior of machine tools.

MORe offers dedicated analysis tools designed to investigate the design of machine tools. The thermo-mechanical transfer function in frequency domain evaluates the thermal response of the machine tool at characteristic frequencies, such as the 24

hours periodicity of the environmental temperature associated to the day-night cycle. The thermal transient response provides the thermo-mechanical response of the system under internal and external thermal influences. A full-featured postprocessor with cutting-edge visualization tools supports the evaluation of the simulation results.

3. Thermo-mechanical model of a 5-axis machine

This paper investigates of the thermo-mechanical behavior of the machine tool of Figure 2. The investigated machine tool is a 5-axis milling machine with a rotary table, a swiveling axis, and a vertical spindle. The kinematic configuration according to ISO 10791-1:2015 adapted for vertical spindles is:

$$V\ [w\ C2'\ B'\ b\ [Y1\ Y2]\ X\ [Z1\ Z2]\ (C1)\ t]$$

The dimensions of the working space is 730x510x510 mm for the investigated machine tool. The rotary table has a diameter of 500 mm. The C-axis of this machine tool provides the possibility to perform turning operations, enabling a maximal rotational speed of 1200 rpm. The rotation of the C-axis results in thermally induced deviations that directly affect the accuracy of the machine tool. This section presents an efficient thermo-mechanical model of the rotation of the C-axis. The thermal error model is performed in software environment MORe, introduced in Section 2.

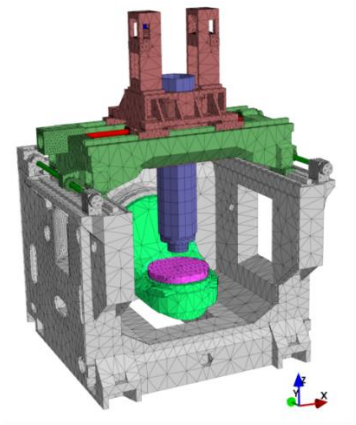

Figure 2. Model of the Mori Seiki NMV 5000 DCG in MORe

3.1. Setup of the thermo-mechanical model

In order to create the thermo-mechanical model, a commercial FE software performs the FE-discretization of the geometry of each of the components of the machine tool assembly. According to the workflow presented in Figure 1, the data is then imported into MORe where the thermal contacts, mechanical contacts, and other boundary conditions are defined. Among the thermal contacts at the different machine elements, the thermal contact conductivity (TCC) of the bearing of the C-axis plays a relevant role to describe the response of the machine tool to the investigated load case. For the estimation of the TCC of the bearing, the empirical correlations proposed by Wiedermann [6] are used. These formulas are based on the geometry of the bearing (e.g. diameter of the rolling elements) and rotational speed. The description of the thermal behavior requires the estimation of the convective boundary conditions. Pavliček et al. [7] presented a meta-model for the evaluation of the HTC inside the enclosure of the machine tool of Figure 2. The meta-models, validated with full CFD models, provide an estimation of the convective heat transfer inside the working space during the rotation of the C-axis.

The thermal response to the rotation of the C-axis originates heat losses at the machine elements. In order to quantify these heat losses, thermo-energetic models are a useful tool. Thermo-energetic models predict the different energy flows between the different components, providing an accurate estimation of the thermal boundary conditions. Züst [8] developed a simulation platform, EMod, to quantify the different energy flows in machine tools. Mohammadi et al. [9] used this simulation platform to create a thermo-energetic model of the investigated machine tool.

Figure 3 shows the different energy flows occurring during the rotation of the C-axis. The electrical power (P_{axis}) of the axis unit is supplied to the amplifiers. The amplifiers receive AC signal and rectify it in order to deliver a pulse width modulated (PWM) signal to the torque motor (P_{motor}). A power measurement system provides the power supplied to the axis unit during the rotation of the C-axis. A part of the power supplied to the amplifier is transformed into thermal energy ($Q_{amplifier}$). The amplifiers are structurally disconnected from the structural parts and the heat is removed from the EC by the ventilation system. Thus, the thermo-mechanical model of the C-axis does not consider the heat dissipated by the amplifiers. At a constant rotationally speed, i.e. after the acceleration of the axis, the energy supplied to the motor (P_{motor}) is converted into heat losses at the stator (Q_{stator}) and bearings ($Q_{bearing}$). Provided the characteristics of the torque motor and bearings the thermal losses at these elements can be quantified, as suggested by Züst [8].

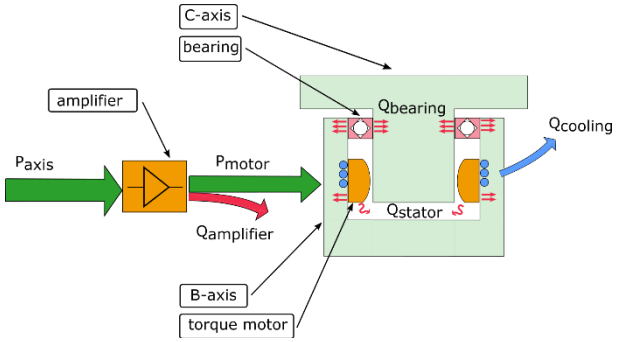

Figure 3. Energy flow in the rotary table unit of the NMV 5000 DCG

The cooling system is responsible for evacuating part of the heat dissipated in the machine elements, as depicted in Figure 3. External pumps supply pressurized fluid to the cooling channels arranged around the torque motor. An external unit controls the inlet cooling temperature to a reference temperature provided by a sensor located in the machine tool bed. Measuring the difference of the inlet and outlet temperature as well as the volumetric flow provide an estimation of the heat removed by the cooling system.

After the definition of the inputs of each of the parts of the machine tool assembly, a surrogate model by means of MOR is created. MORe provides a set of reduction methods based on the Krylov Modal Subspace (KMS) [4] method for the efficient simulation of machine tools. The projection basis captures the steady state part of the response including a basis of the Krylov subspace with an expansion point at a low frequency, i.e. 10^{-8} rad/s. Furthermore, the projection basis includes the eigenmodes of the system in order to reproduce the transient response. The a priori error estimator of the KMS ensures that the relative error between the reduced and original system remains below 0.05 for a frequency up to 0.01 rad/s. The MOR transforms the original thermal system of 508,462 dofs to a

reduced system of 392 dofs. In order to evaluate the mechanical response, a reduced thermo-coupled system needs to be also created. For the thermo-mechanical coupled system, an expansion point at 30 rad/s is chosen in order to capture the static mechanical response. The original mechanical model of 1,525,386 is reduced to 1,164. The reduced models enable the efficient simulation of the thermo-mechanical behavior of the investigated machine tool, facilitating the validation process.

3.2. Validation of the thermo-mechanical model

After completing the model setup and quantifying the boundary conditions, the comparison of the simulated and measured thermally induced deviations provides a validation of the thermo-mechanical model.

Weikert [10] developed the an indirect volumetric measurement technique, the R-Test, for geometric calibration of 5-axis machine tools. The R-Test evaluates the linear deviations between a sensor nest located on the spindle and the precision sphere located on the table. Measuring the relative deviation at four different indentations of the rotary table provides the thermally induced position and orientation of the C-axis. Blaser et al. [11] adapted R-Test measurement by including an on-machine measurement system. Instead of a sensor nest with displacement sensors, the measurement setup uses a 2.5D touch trigger probe. The main advantage of this measurement setup is that it facilitates its integration for online compensation strategies. This work uses this measurement system for the validation of the thermo-mechanical model.

In order to characterize the thermal behavior of the rotary table, the C-axis rotates at 1200 rpm over 3 hours. During the rotation of the C-axis, the inlet and outlet temperature is measured, as depicted in Figure 4. The difference between the inlet and the outlet temperature remains 0.8°C over the measurement time. This difference of temperature provides the the heat removed by the cooling system, which is an input of the thermo-energetic model. The chiller of the cooling fluid causes the fluctuations of the absolute values of the cooling temperature, as illustrated in Figure 4.

In order to define the boundary conditions, the fluctuations of the temperature of the air needs to be considered. For the validation of the thermo-mechanical model, the C-axis is rotated over 3 hours, which is a short time in order to observe significant fluctuations of the environmental temperature in the workshop outside the machine tool enclosure. Therefore, the temperature of the air outside the machine tool housing is assumed constant during the rotation of the C-axis. However, this is not valid for the air inside the machine tool enclosure, rising over 3.3 °C during the measurement time. The temperature increase stabilizes after 150 min of the rotation of the C-axis. Figure 4 shows the temperature rise inside the machine room (MR), which is an input for the thermo-mechanical model.

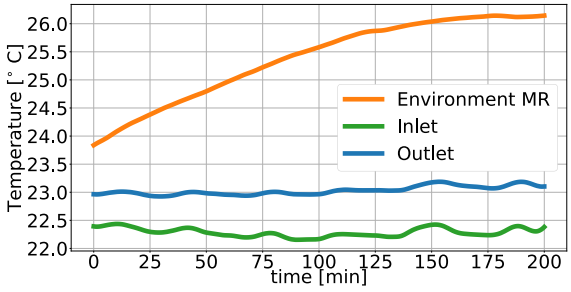

Figure 4. Measured temperatures during the rotation of the C-axis at 1200 rpm over 3 h. MR: machine room

In order to validate the model, the simulated thermal response is compared with the measured deviations. The investigated thermal load is the rotation of the C-axis at 1200 rpm over 3 h. The measurement system evaluates the thermally induced linear deviations every 6 min during the rotation of the C-axis. Figure 5 shows the comparison between the simulated and measured thermal behavior of the investigated machine tool. Due to the symmetry of the design of the machine tool, the machine tool does not show any deviations in X-direction. The dominant thermally induced deviations are in Y- and Z-direction. The model succeeds in representing the absolute values as well as the transient trends of the thermal deviations. Figure 5 shows that the thermo-mechanical model reproduces the thermal response of the investigated machine tool during the rotation of the C-axis. The main discrepancies between model and simulation are in Z-direction during the first hour. These discrepancies can be attributed to the lack of detail in modeling the thermal behavior of the measurement system.

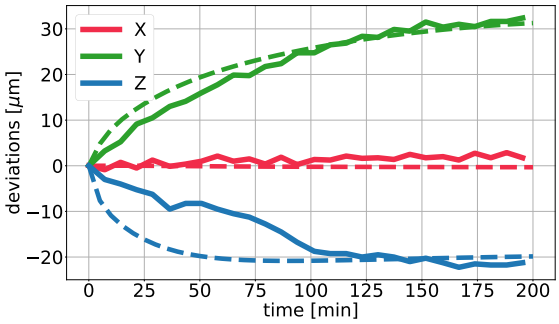

Figure 5. Comparison between measured and simulated thermal deviations due to the rotation of the C-axis at 1200 rpm over 3 h

3.3. Investigation of thermal design of the machine tool

After validating the thermo-mechanical model of the machine tool, the thermal design of the machine tool to internal heat sources can be further investigated. Mayr et al. [12] proposed the analysis of the thermal response of machine tools in frequency domain. The transfer function describes the effect of the variation of the thermal inputs on the outputs of the system for a given frequency range. For the thermal load under consideration, the input of the transfer function is the energy provided to the motor, P_{motor}, which transforms into heat dissipated at the bearings and stator. The outputs of the transfer function are the deviations between the TCP and the workpiece in X-, Y-, and Z-direction. The transfer function, shown in Figure 6, describes the thermal behavior in a frequency range between 10^{-6} and 0.01 rad/s. The thermal transfer illustrates that internal heat losses affect predominately the deviations in Y-direction, as observed also in the transient response of Figure 5. Furthermore, the transient function of Figure 6 provides the time constants of the response of the system. The model predicts that the time constant associated to the deviations in Y-direction is larger than the time constant of the response in Z-direction. The information about the different time constants of the response of the machine tool in different directions is of great interest when designing thermal error compensation strategies.

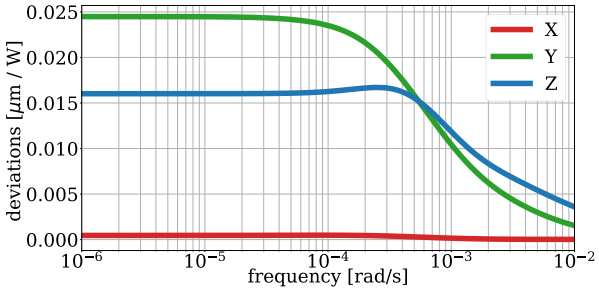

Figure 6. FRF response of the machine tool of Figure 2. Input: heat losses at the machine elements. Output: TCP deviations relative to the workpiece for the X-, Y- and, Z-direction.

A combination of the internal heat losses and the increase of the temperature inside the MR determines the thermal response of the machine tool during the rotation of the C-axis. The thermo-mechanical model enables the separation of these two the influences. Figure 7 shows the deformation of the machine tool, displaying the structural parts of the Z-, B-, and C-axis. The left part of Figure 7 illustrates the effect of the internal heat losses, i.e. losses at the stator and bearings, while the right side shows the deformation due to the increase of the air temperature inside the enclosure. On one hand, the internal heat sources affect predominantly the workpiece-sided axes, leading to deformations in Y- and Z-direction. On the other hand, the variation of the MR air temperature affects the workpiece-sided axes as well as the part of the Z-axis inside the working space. Therefore, the tool-sided axes are accountable for part of the thermally induced deviations. If the TCP deviations are measured relative to the inertial system, i.e. not considering the workpiece as a reference, the thermal deviations in Z-direction are -2.4 µm. This corresponds to 12% of the relative deviation between TCP and workpiece. For other direction, the contribution to the total thermal deviations of the tool-sided axes is negligible. The fact that part of the thermal deviations are originated in the tool-sided axes have a great significance during the design of the thermal error compensation strategies. The workpiece-sided deviations in Z-direction measured at B = 0° result in deviations both in Z- and X-directions for other positions of the B-axis different from 0°. However, the tool-sided deviations in Z-direction are unaffected by the position of the B-axis. Therefore, the possibility to quantify and separate between the tool- and workpiece-sided deviations benefits directly the quality of the thermal error compensation.

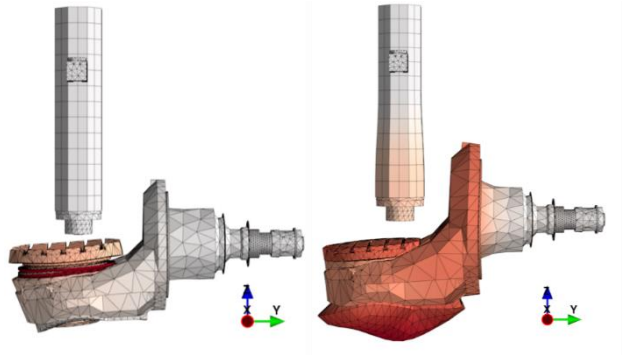

Figure 7. Structural deformation of the machine tool. Only the Z-, B-, and C-axis are shown. Right: thermal response to the internal heat sources. Left: thermal response to the increase in the temperature of the MR

4. Conclusions and outlook

This paper investigates the thermal response of a precision 5-axis machine tool during the rotation of the C-axis. The heat losses determine the thermal response of the machine tool. Therefore, the model requires considering the different energy flows during the rotation of the C-axis. In order to ensure an efficient simulation, this work creates a surrogate model by means of MOR. The simulation platform MORe enables an efficient workflow for the setup of the thermo-mechanical model. The software package MORe integrates reduction approaches to approximate the thermo-mechanical behavior of the original system. This paper compares the predicted and the measured thermally induced deviations, concluding that the developed thermo-mechanical model can represent the thermal response of the machine tool during the rotation of the C-axis. The validated model serves as a virtual prototype to investigate the thermal design of the machine tool and assess the validity of the thermal error compensation strategies. Future work will concentrate on the investigation of the thermal response of the machine tool to other load cases as well as improving current thermal error compensation models.

5. Acknowledgments

The authors would like to thank the Swiss Innovation Agency (Innosuisse) and the Machine Tool Technologies Research Foundation (MTTRF) for their financial support.

References

[1] Mayr, J., Jedrzejewski, J., Uhlmann, E., Alkan Donmez, M., Knapp, W., Härtig, F., Wendt, K., Moriwaki, T., Shore, P., Schmitt, R., Brecher, C., Würz, T., Wegener, K., 2012, Thermal issues in machine tools, CIRP Annals - Manufacturing Technology, 61/2:771–791.

[2] Benner, P., Gugercin, S., Willcox, K., 2015, A survey of model reduction methods for parametric systems, MPI Magdeburg Preprints, MPIMD/13–14:1–36.

[3] inspire AG, 2019, MORe. [Online]. Available: https://www.more-simulations.ch/. [Accessed: 12-Dec-2019].

[4] Spescha, D., 2018, Framework for efficient and accurate simulation of the dynamics of machine tools.

[5] Hernández-Becerro, P., Mayr, J., Blaser, P., Pavliček, F., Wegener, K., 2018, Model Order Reduction of Thermal Models of Machine Tools with Varying Boundary Conditions, in *Euspen Conference in Thermal Issues in Machine Tools - CIRP sponsored*.

[6] Weidermann, F., 2001, Praxisnahe thermische Simulation von Lagern und Führungen in Werkzeugmaschinen, in *19th CAD-FEM User's Meeting*.

[7] Pavliček, F., Pamies, D. P., Mayr, J., Züst, S., Blaser, P., Hernández Becerro, P., Wegener, K., 2018, Using meta models for enclosures in machine tools, in *Conference on Thermal Issues in Machine Tools: Proceedings*, pp. 159–168.

[8] Züst, S. D., 2017, Model Based Optimization of Internal Heat Sources in Machine Tools, ETH Zurich, Zurich.

[9] Mohammadi, A., Züst, S., Mayr, J., Blaser, P., Sonne, M. R., Hattel, J. H., Wegener, K., 2017, A methodology for online visualization of the energy flow in a machine tool, CIRP Journal of Manufacturing Science and Technology, 19:138–146.

[10] Weikert, S., 2004, R-Test, a New Device for Accuracy Measurements on Five Axis Machine Tools, CIRP Annals - Manufacturing Technology, 53/1:429–432.

[11] Blaser, P., Pavliček, F., Mori, K., Mayr, J., Weikert, S., Wegener, K., 2017, Adaptive Learning Control for Thermal Error Compensation of 5-Axis Machine Tools, Journal of Manufacturing Systems, 44.

[12] Mayr, J., Ess, M., Pavliček, F., Weikert, S., Spescha, D., Knapp, W., 2015, Simulation and measurement of environmental influences on machines in frequency domain, CIRP Annals - Manufacturing Technology, 64/1:479–482.

Special Interest Group Meeting on Thermal Issues
Laboratory for Machine Tools and Production Engineering (WZL) of
RWTH Aachen, Germany, February 2020
www.euspen.eu

Simulation-based approach for optimized tempering of concrete machine frames by thermo-elastic FEM and model coupling

Janine Glänzel[1)], Alexander Geist[1)], Arvid Hellmich[1)], Steffen Ihlenfeldt [1,2)]

[1]*Fraunhofer Institute for Machine Tools and Forming Technology IWU, Reichenhainer Str. 88, 09126 Chemnitz*
[2]*Technische Universität Dresden, Helmholzstraße 7a, 01069 Dresden, Germany*

janine.glaenzel@iwu.fraunhofer.de

Abstract
The thermal stabilization of machine components by demand-actuated temperature control opens up far-reaching potential for minimizing thermo-elastic deformations of machine tools while reducing energy requirements. High-performance concrete materials offer opportunities for the integration of cooling circuits, which must be operated with adapted control strategies. For example, demand oriented cooling in the vicinity of existing heat sources can be realized. The main aspect of the research project deals with issues concerning the best possible positioning and design of the cooling circuits. For this purpose, CFD and FEM simulations are created, integrated into key parameters and optimized and converted by methods of model order reduction to a fast computable digital model of the component (in this case a machine frame).

cooling system, Finite Element Method, machine tools, machine frame, heat transfer coefficient

1. Introduction

Thermal measurements on machine tools show repeatedly that despite the thermo-symmetrical design it is not possible to achieve a uniform temperature distribution. Feasible causes are asymmetric drive arrangements even on symmetrical structures, one sided external heat sources such as solar radiation or thermal losses from the machine and/or the process in the working space [1, 2]. These local or area wide heat inputs can have a significant influence on the resulting deformation behavior of the machine tool structure, e. g. the machine frame [3, 4]. In order to compensate for this effect and the resulting TCP error, the heat must be dissipated as efficiently as possible.

In order to reduce thermally induced displacements, EPUCRET has carried out an appropriate temperature control of concrete frame structures. Initially, simple prismatic bodies were measured under defined thermal stress series in order to be able to independently adjust the cooling system from the central control unit. For example, the error in straightness of guide rails has been reduced from ±35 µm to ±2 µm. In subsequent tests, this approach was applied to complete machine tools, where several individual circuits are coupled or work separately. The most important TCP shifts were measured and reduced by at least 50 %. In this context, energy aspects have not been taken into account [7] and transferability to other systems is not known.

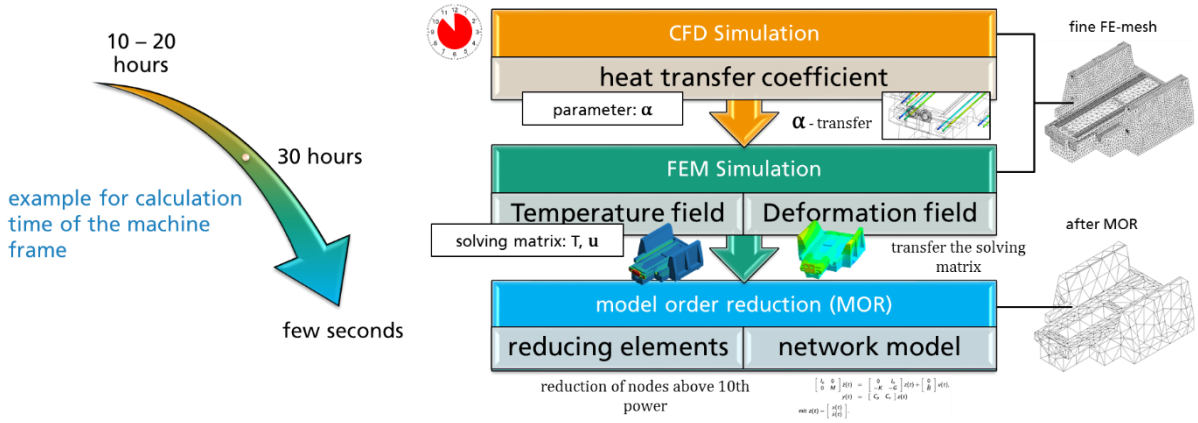

Figure 1. Decoupling approach

For this purpose, cooling circuits are usually integrated into active components and passive structures, which are subsequently adapted to the temperature of the structure [5]. The use of high performance concrete (HPC) in casting opens up completely new possibilities for the integration of cooling liquid circuit structures for an active temperature control [6].

As the example DMG MORI [8] shows, structurally integrated cooling circuits are already established. These stabilize precision-relevant components, such as the machine frame or the gantry, but also linear guides and drives. In this way, the heat

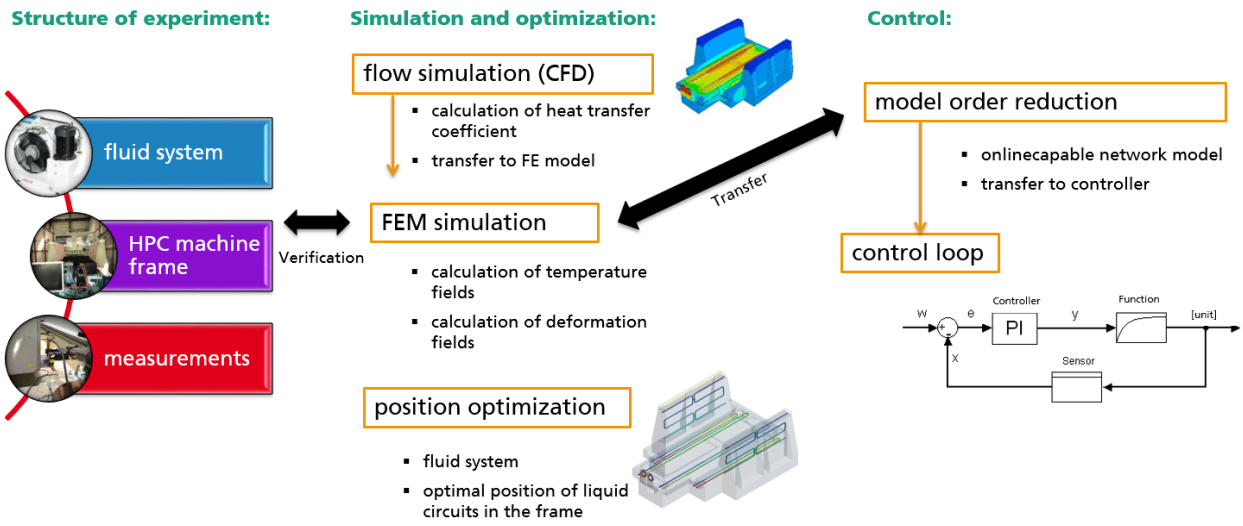

Figure 2. Methodology for calculation the optimal liquid circuit

input from internal heat sources can be dissipated, which leads to an improvement of the thermal behavior.

The aim is to present the methodological approach for the simulation-based analysis and optimization of cooling systems in machine frames made of HPC.

Figure 1 shows the decoupling approach for a faster calculation time without reducing of the model accuracy.

2. Methodology to use heat transfer coefficient in FE-models

Thermal stabilization of machine and machine components through adapted and demand-oriented temperature control opens up far-reaching potential for minimizing unwanted thermo-elastic displacements at the tool center point (TCP) while reducing energy consumption. High-performance concrete materials offer in this context a large variety of possibilities for the integration of adapted temperature control circuits in various forms, e.g. meander, spiral structures etc., which can be operated with adjusted control strategies as needed and thus energy-efficient. For example, an active temperature in the vicinity of existing heat sources can be realized, whereby the effect of unwanted heat sources can be minimized and used for more homogeneous temperature distribution of the machine frame.

As part of a transfer project in the Collaborative Research Center [9] research project, the goal is to consider the best possible positioning and design of the cooling circuits in the geometry of the machine frame as well as heat sources arising in the production process already in the development phase. For this purpose and as a basis for a demand oriented temperature control system, a suitable model is required. Therefore, the CFD and FEM simulation tools are used in a first step (fig. 2), whereby the tempering system is created taking into account all boundary conditions. These are for example environmental influences, flow velocity of the fluid in the tempering circuits or geometrical influences like circuit length and diameter. The heat transfer coefficients on the inner surface of the tempering system can be calculated in time-consuming calculations by using CFD simulation. In order to reduce the simulation effort, a procedure was developed, which transfers the significant heat transfer coefficients from the CFD simulation as input data to the FEM simulation. Moreover, it was calculated the resulting temperature fields and deformation fields. For the mapping of the heat transfer coefficients, the cooling circuits of the fluid

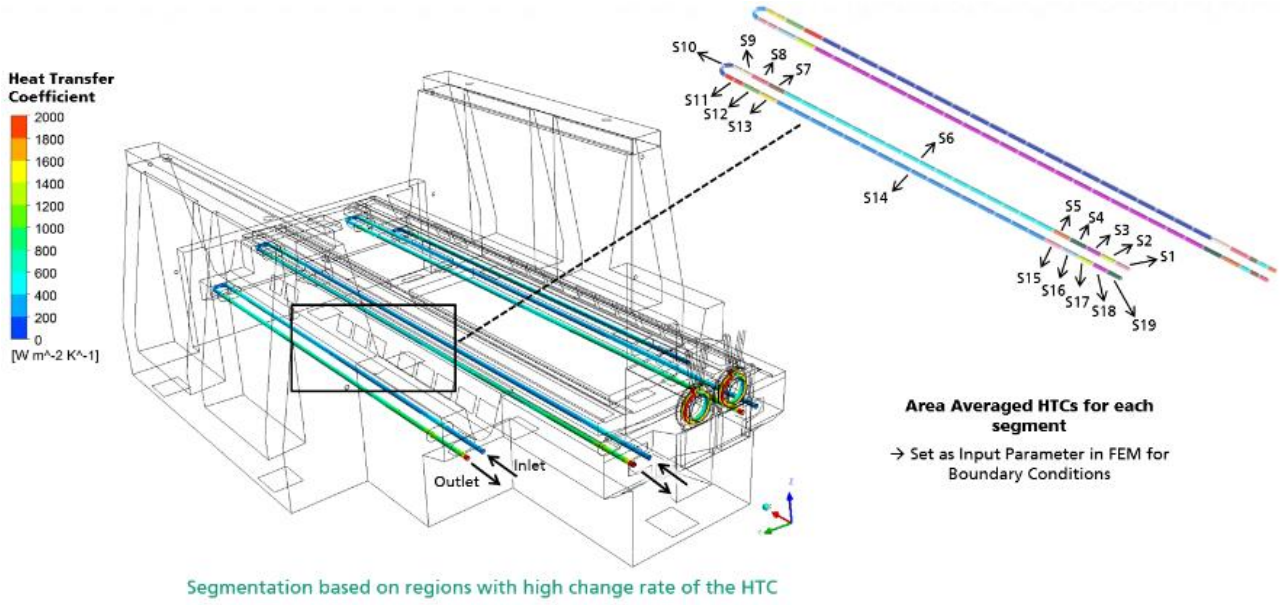

Figure 3. Segmentation of the circuits

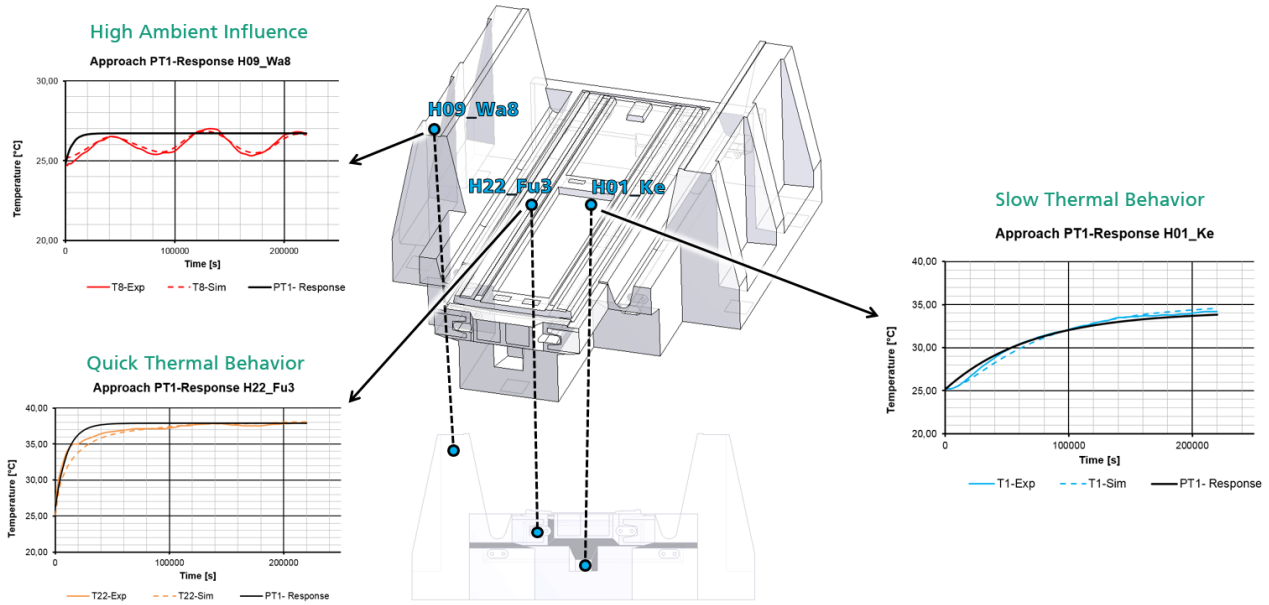

Figure 4. Transient thermal behaviour of the machine frame

system are subdivided into adaptive segments. Heat transfer coefficients are assigned to each segment as a boundary condition (convection). The level of detail of the segmentation depends on the rate of change of the HTC values. Areas of high rates of change such as inlet and outlet areas, deflections are segmented in detail whereas is roughly segmented. Further information to the procedure for segmentation is given in[5]. In the present example, the fluid circuits are divided into 19 segments. For each segment, the area-averaged HTC is calculated and then assigned as an input parameter to the FEM boundary conditions (see Fig. 3). For automatic FEM simulations, a parameterized model to calculate different thermal load cases and the resulting thermal effects of the machine frame are used. For further optimization of the calculation effort of the FEM simulation methods for model order reduction [10] are applied. The modification leads to a model with low calculation time, which provides the parameters for a decentralized controllable pump system. Therefore, the nonlinear and multi-input-multi-output temperature control system of a machine frame can be investigated and commissioned. The main goal of this new approach is to create a homogenized temperature field of machine frames.

3. Sample Application for a cooling system in an machine frame

The transfer of the developed method for the position optimization of the cooling circuits is carried out on a real machine frame, which consists of high performance concrete, steel reinforcement and a cooling system.

Figures 3 and 5 show the CAD-model of the machine frame together with an autarkic and mobile 5-spindle parallel processing unit. Inside the machine frame, six independent cooling circuits and 23 temperature sensors for a thermo-stabile structure behaviour is integrated. The research goal is to develop a decentralized controlled tempering concept for thermo-stabile machine frames and structures. The measurement of the machine frame amounts circa 5 x 3 m and has a weight of 18 t. Depending on the position (see Fig. 4), the machine frame shows a different time behavior. While areas around the vertical wall structures are almost exclusively affected by the environment (radiation), areas in the inner structure are thermally sluggish. Time constants from 20h to 29h were identified. Other areas closer to components or cooling circuits react faster, with time constants of 5000 s to 10000 s. The machine frame can be separated in three areas referenced to the surface: area for the guide rails, area for the chip transport and an area of the stringboard with the inclusion of the processing unit.

The machine table is positioned on the guide rails and can be driven in a linear direction. A chip conveyor is between the guide rails and the stringboard. The two main drives for the machine table are placed frontal on a water-cooled flange. The other four cooling circuits are placed nearly the chip canal and the guiding rails to lead heat fluxes away quickly. For the experiments and verifying of the FE-simulation of the machine frame the cooling circuits have a warming function, because the influence of the heat conduction effects could be better displayed.

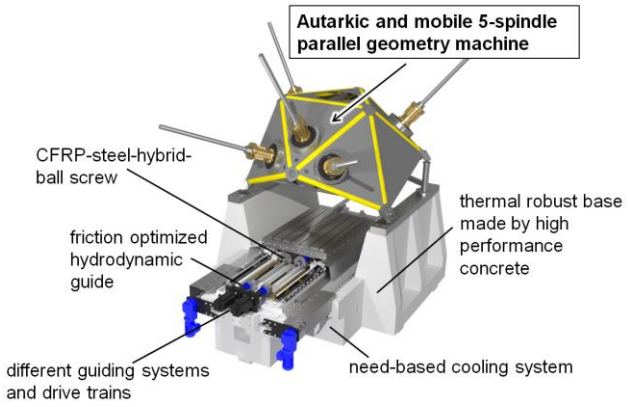

Figure 5. Machine frame with processing unit

The modelling work is concentrated only on the machine frame with the integrated cooling system since the machining unit is equipped with a separate tempering system. Based on the CAD-data a computation-intensive CFD-model in CADFEM Ansys CFX was created for calculating the heat transfer coefficient along the six cooling liquid circuits. The calculation time needs more than 20 hours per load case. Subsequently, the results of the flow field inside the liquid circuits are used for computing the heat transfer coefficients and transfer on the segmented circuits in the FE-mesh for the thermal-mechanical simulation. According to that, the computing time for transient temperature

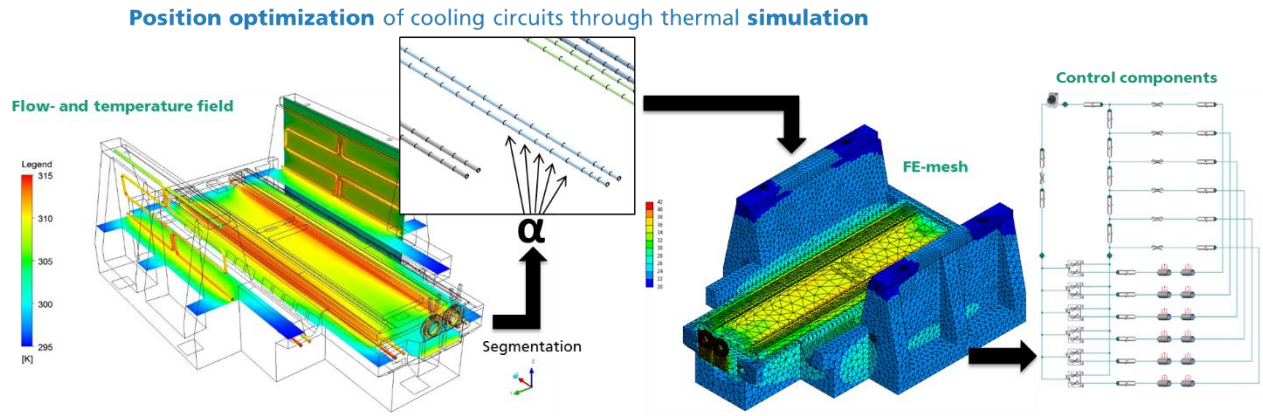

Figure 6. Computing example of cooling system in a machine frame of High performance concrete

field and resulting deformation field of the machine frame geometry could be reduced to 30 min.

Figure 6 presents one exemplary load case for ten liquid circuits inside the machine frame. The four additional cooling circuits have been added as part of a position optimization to create additional spheres of freedom for the control of the temperature fields. Because vertical wall structures with a large hight to thickness- ratio react directly to environmental influences such as changes in ambient temperature or solar radiation, additional cooling circuits are available. The subdivision into four independent cooling circuits can also compensate for asymmetrical heat radiation. The results shows the flow simulation on the left side of figure 6 and on the right side the computed temperature field of the thermo-mechanical simulation. The next steps are to use the MOR method for further time reducing and link the resulting temperature fields to the controlling system for the volumetric flow rate in cooling system.

4. Conclusion and Outlook

This paper presents a new methodology for optimization the inner tempering system of machine tool frames. Therefore, an approach to transfer the significant heat transfer coefficient from of the CFD simulation to the thermo-mechanical simulation for calculation the resulting temperature and deformation fields was developed. This FE-model is the basic for a network model, which, based on the MOR method and will be used for optimization calculations in the future. Also the position of the tempering liquid circuits can be optimized based on the model. The next steps are that the new methodology will be validated a real demonstrator machine frame with eight included cooling circuits which will be controlled through decentral controlling system.

Acknowledgement

Funded by the German Research Foundation – Project-ID 174223256 – TRR 96.

References

[1] BRYAN J., 1990, International status of thermal error research, CIRP Annals – Manufacturing Technology, 39/2, 645–656.

[2] GROSSMANN K., et. al., 2015, Thermo-energetic design of machine tools, Lecture Notes in Production Engineering, Springer.

[3] DROSSEL W.-G., WITTSTOCK V., REGEL J., RICHTER C., NOFFKE F., 2014. Auswirkungen lokaler Erwärmung von Mineralguss, wt Werkstatttechnik Online, 104/9, 602–607.

[4] NEUGEBAUER R., DROSSEL W.G., IHLENFELDT S., NESTMANN S., RICHTER C., 2012. Inherent thermal error compensation of machine tool structures with graded mineral casting, International Conference on Machine Tools, Automation, Technology and Robotics. Prag, Czech Republic.

[5] WEBER J., GLÄNZEL J., POPKEN J., SHABI L., WEBER J., 2018, Combined and Fast Computable Thermal Models for Situationally Optimal Tempering of Machine Components, Institute of Fluid Power, TU Dresden, Fraunhofer Institute for Machine Tools and Forming Technology IWU, Chemnitz.

[6] HELLMICH A., GLÄNZEL J., IHLENFELDT S., 2018, Methods for Analyzing and Optimizing the Fluidic Tempering of Machine Tool Beds of High Performance Concrete, CIRP Conference on Thermal Issues in Machine Tools, Dresden.

[7] SCHNEIDER M., 2013, Das „intelligente“ Mineralgussbett, VDI-Z Integrierte Produktion, 155/3.

[8] DMG MORI SEIKI Schweiz AG, 2013. Mehr Präzision für den Werkzeug- und Formenbau, Technische Rundschau, KW 9.

[9] CRC/TR96: http://141.76.19.93/SFBweb/

[10] Model order reduction for thermo elastic models Galant A.; Großmann K.; Mühl A.: Model Order Reduction (MOR) for Thermo-Elastic Models of Frame Structural Components on Machine Tools ANSYS Conference & 29, CADFEM Users’ Meeting 2011 19.-21.10.2011, Stuttgart

Special Interest Group Meeting on Thermal Issues
Laboratory for Machine Tools and Production Engineering (WZL) of
RWTH Aachen, Germany, February 2020
www.euspen.eu

Modelling & Identification for Thermal Control of Cooling Water with Varying Flow

Bas Scheepens[1,2], Björn Bukkems[2], Theo Ruijl[2], Enzo Evers[1], Tom Oomen[1]

[1]*Eindhoven University of Technology, Groene Loper 3, 5612 AE Eindhoven, the Netherlands*
[2]*MI-Partners, Habraken 1199, 5507 TB Veldhoven, the Netherlands*

s.j.m.c.scheepens@student.tue.nl

Abstract
Thermal effects can have a significant impact in precision engineering applications. To reduce this impact, thermal conditioning of the system via circulating water can be applied. The accuracy with which a system can be conditioned depends on the temperature variations of the water. A heater system with temperature sensors has been designed to enable active control of the water temperature. This system has shown to achieve millikelvin accuracy. With the aim of achieving this accuracy over multiple flow rates, modelling and identification techniques are explored and applied. This work forms a basis on which controllers can be designed that can attenuate temperature disturbances over a wide operating range.

Thermal Modelling, Identification, FRF, varying flow

1. Introduction

For high precision systems, thermal effects can have a large impact on performance. Changes in temperature can cause deformations of critical components within a system, reducing the system's accuracy. Thermal control is therefore desired to counteract these fluctuations and condition the temperature of the system components. Previous approaches achieved millikelvin temperature control [1], using a local fluid stream heater shown in figure 1. With a local fluid stream heater (LFSH), circulating cooling water can be thermally conditioned. Although important developments have been made to achieve the results in [1], at present the accuracy cannot be obtained for varying flows. The aim of this paper is to achieve the performance in [1] for a large range of varying flows. To achieve this next level of resilience, it is important to understand the effect flow variations have on the system. A combined approach of modelling and identification is used to determine the thermal behaviour of the LFSH. With an accurate and verified model, new controllers can be designed to ensure temperature stability for a wide range of flows, whilst attenuating temperature fluctuations disturbing the system. Different modelling approaches exist for thermal systems, so approaches are compared. The desired model properties for controller design are sketched. Since an accurate model of the existing setup is desired, the step towards identification is made. Using the insight and results from the modelling process, high accuracy identification is made possible. Using existing identification techniques, the system dynamics can be identified for varying flow rates, resulting in a set of models. These models can then be combined into a linear parameter varying (LPV) model that fully describes the LFSH dynamics. Results of this work are analysed and its applicability in future work of this research is shown.

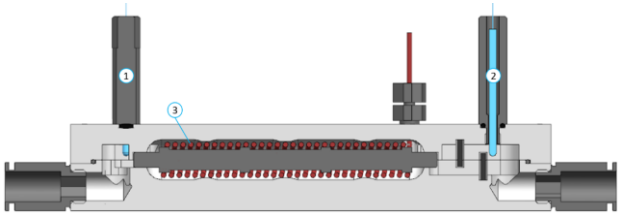

Figure 1. A cross-section of the Local Fluid Stream Heater used in this research, with incoming temperature sensor (1), outgoing temperature sensor (2) and heater coil (3).

2. Modelling

Thermal systems typically have slow transient behaviour and dynamics at low frequencies compared to the electrical and mechanical dynamics in precision mechatronics. Within the LFSH, an important and dominant factor is the mass flow of water.

2.1. Analytic Modelling

An initial approach is to model the behaviour from first principles of heat and mass transfer. The elegance of this approach is its physical origin, where the formulae arise from describing the heat transfer via conduction, convection and radiation [2].

Despite this being a good starting point when describing the thermal properties of a system, there are multiple drawbacks to this approach. The size and complexity quickly grows with nontrivial geometry, making it near impossible to fully model and simulate a system. Just describing the fluid dynamics and flow of water through the heater is worth a study of its own. A multitude of parameters is needed to describe all the materials and their interactions. These parameters are difficult to determine exactly. Therefore, measurements are needed to determine accurate parameters and validate the model. The question also arises to what accuracy the system needs to be described and if by simplifying and/or assuming simplified

properties similar results can be achieved, since parameters are calibrated to fit the model on data.

2.2. Lumped Mass Modelling

Lumped mass modelling, also called the lumped capacitance method, is an attractive way to model heat transfer. A material is divided into multiple smaller masses for which it neglects temperature gradients within the lumped masses, allowing linear modelling of the thermal dynamics [2]. The linearity of these models make them computationally viable and thus allows for fast simulation and analysis. Transient behaviour is captured in these models and mass flow can be added as an additional interaction.

The maximum mass size for which internal temperature gradients can be neglected, is determined by the ratio between the internal thermal resistance and the thermal resistance to its surroundings [2]. This ratio is called the Biot-number, and it depends on the material properties and the thermal interactions of the mass. A possible drawback can be that the amount of lumped masses becomes large for certain systems and consequently also the model size becomes impractically large. Furthermore, a solid is modelled as multiple lumped masses in series with heat transfer between them, giving first order dynamics between lumps. This first order behaviour comes with a 90° phase lag for between adjacent masses. A series connection results in a multiple of this lag dependent on the amount of masses. This means that the overall modelled phase relation is ambiguous, with increased phase lag for an increased amount of lumped masses. Experimental validation can be used to ensure accuracy of the model. Similar to the analytical approach, the multitude of parameters describing the system can then be calibrated to fit the model to the measured data.

2.3. Desired Model

The desired result of the modelling process is a model that can capture the thermal dynamics and heat transfer from the incoming water temperature and heater coil to the outgoing water temperature. The model should be sufficiently complex to capture the relevant dynamics between these points, but also have restricted complexity to facilitate computation. A low order model can also allow for more advanced controller designs, like H-infinity control, for which the order of the controller is minimally as large as the modelled plant. The model is also required to take varying flow into account.

For all modelling approaches, it is beneficial to validate and tune the model using measured data to ensure accuracy. Since the accuracy then depends on measurement, a data-driven approach can be beneficial.

3. System Identification

System responses can be obtained from measurements via system identification. Commonly, the frequency response function (FRF) is estimated. By designing the experiments with carefully selected frequency content, the response can be measured at the output. FRF identification is fast, inexpensive and accurate [3]. Little to no knowledge or modelling is needed to obtain an estimate of the response, although it can be used to improve the accuracy.

FRF identification assumes a system to be in steady state, which often is not the case. Thermal systems often have a large transient response, meaning a significant amount of time is needed to reach a steady state. Therefore, identification techniques that take the transient response into account are desired. The Local Polynomial Method (LPM) approximates the local transfer function by a polynomial such that the transient can be estimated and removed [4]. This method can be generalized into the Local Rational Method (LRM), which uses a rational function for the local approximation [5]. By using a rational function, linearity is lost in the parameters, but improved estimation quality is shown [6]. This approach can be further improved by incorporating system knowledge of the system poles (LRMP) [3]. Other interesting extensions include identification of linear parameter varying system (LPV-LRM) [7].

Temperature control for varying flows is desired, and thus identification of the plant for varying flows is needed in accordance. Combining the identification and modelling over a range of flows, an accurate model of the system can be obtained.

4. Results

A lumped mass model has been constructed describing the LFSH consisting of 220 states. The frequency response from the inserted coil power to the outgoing water temperature is evaluated for multiple flow rates in figure 2. The figure shows that both the magnitude and phase change for varying flow. For comparison, the magnitudes at low frequencies at 1 l/min and 10 l/min are 0.0135 K/W and 0.0014 K/W, respectively. This is near a factor ten difference. With ten times the amount of water flowing through the system, it is to be expected that ten times the power is needed for the same temperature change.

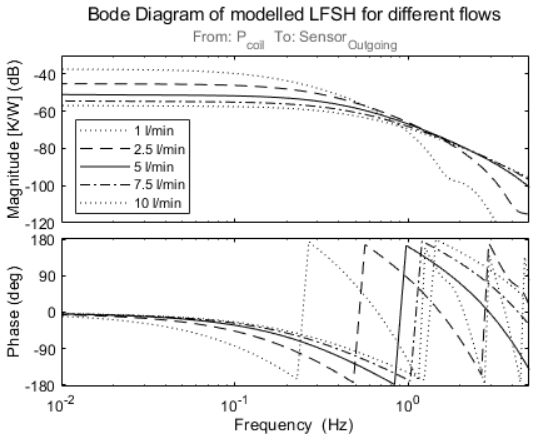

Figure 2. Frequency response from the coil power to the outgoing water temperature of the LFSH for multiple flow rates.

5. Conclusion and Outlook

Multiple modelling and identification techniques are researched and compared. By modelling the system using its physical parameters, the effect of parameter variations can be analysed. It is shown that the flow rate has a large impact on the dynamics. This insight can be used to define input signals and settings for the experiments used to identify the system.

It is concluded that the combined approach of modelling and identification provides accurate estimates of the responses, allowing controller design that can adapt to flow variations in ongoing work.

References

[1] Bukkems B, Ruijl T, Ronde M and Lamers R 2018 Milli-kelvin temperature control using a local fluid stream heater *DSPE Conf. on Precision Mechatronics (Sint Michielsgestel, the Netherlands, 4 - 5 September 2018)*

[2] Bergman T, Lavine A, Incropera F and Dewitt D 2011 *Fundamentals of heat and mass transfer 7th ed* Wiley (Hoboken, NJ)

[3] Evers E, de Jager B and Oomen T 2018 Improved local rational method by incorporating system knowledge: with application to mechanical and thermal dynamical systems. *18th IFAC Symp. on sys. id.* (Stockholm, Sweden)

[4] Pintelon R, Schoukens J, Vandersteen G and Barbé K 2010 Estimation of nonparametric noise and FRF models for multivariable systems *Mech. Systems and Sig. Proc.* **24-3** pp 573-95
[5] McKelvey T and Guérin G 2012 Non-parametric frequency response estimation using a local rational model *IFAC Proceedings Volumes* **45-16** pp 49-54
[6] Geerardyn E and Oomen T 2017 A local rational model approach for H ∞ norm estimation: with application to an active vibration isolation system. *Cont. Eng. Practice* **68** pp 63-70
[7] van der Maas R, van der Maas A and Oomen T 2015 Accurate frequency response function identification of LPV systems: a 2D local parametric modelling approach *54th IEEE Conference on Decision and Control (CDC)* (Osaka, Japan) pp 1465-1470

Modelling & Identification for Thermal Control of Cooling Water with Varying Flow

Author: Bas Scheepens[1,2], Björn Bukkems[1], Theo Ruijl[1], Enzo Evers[2], Tom Oomen[2]

Date: 26-02-2020

Version: 1.0

[1]MI-Partners B.V.

[2]Eindhoven University of Technology

Problem: milliKelvin Control

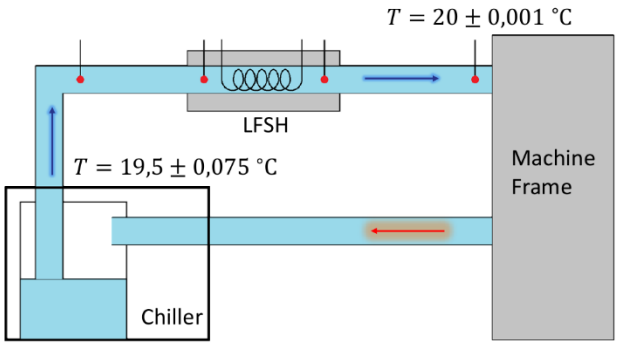

Specifications:
- $T_{req} = 20$ °C
- $\Delta T = 1$ mK
- $Flow = 2{,}5$ l/min

Bukkems B, Ruijl T, Ronde M and Lamers R 2018 Milli-Kelvin Temperature Control using a Local Fluid Stream Heater *DSPE Conf. On Precision Mechantronics*

Current Problem: Varying flow

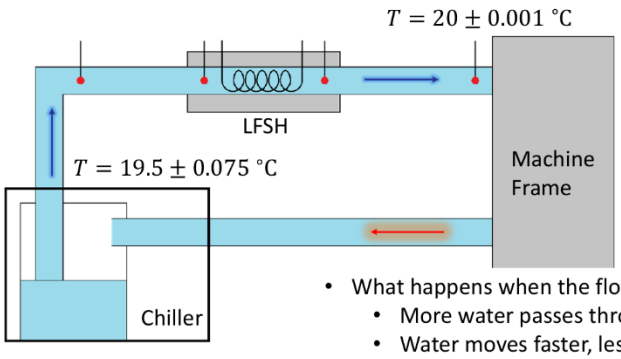

Specifications:
- $T_{req} = 20$ °C
- $\Delta T = 1$ mK
- $Flow \in (1, 4.5)$ l/min

- What happens when the flow rate increases?
  - More water passes through, more water to heat
  - Water moves faster, less transport delay

Approach

White box approach:
Lumped-Mass Modelling
- No setup needed
- All temperatures and heatfluxes available
- Built upon known physics

Black box approach:
Identification using LPM
- Fast
- Inexpensive
- Accurate
- Data-driven

Grey box approach:
Low order model fitting
- Simple physics
- Suitable for advanced controller design
- Accuracy by fitting

Analytic Lumped-Mass Model

- 223 states, >40 parameters
- Bode plots show Frequency Response
- Effect of Increased Flow:
  - Magnitude decrease at low frequencies
  - Magnitude increase at higher frequencies
  - Less phase-lag
- What does the actual setup do?

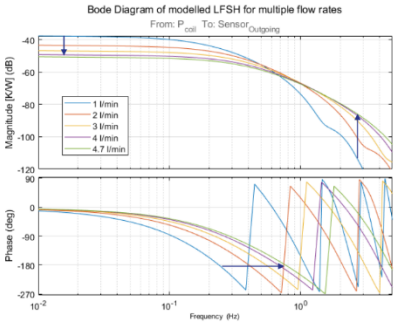

Identification

- Multi-sine excitation, 0,01 upto 10 Hz
- Local Polynomial Method (LPM) used
  - Determines Transfer
  - Takes noise and Transient into account

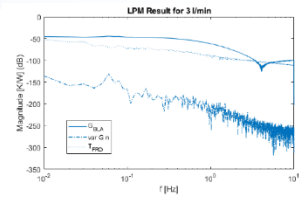

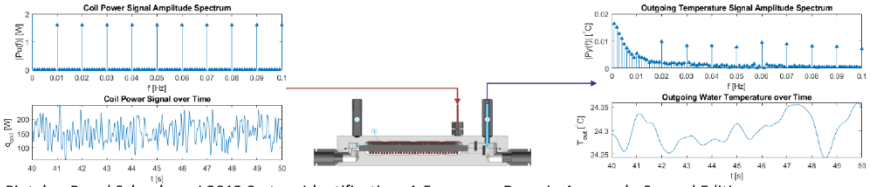

Pintelon R and Schoukens J 2012 System Identification: A Frequency Domain Approach, Second Edition

Model and Identification compared

Model:

- Lower magnitude at low and mid-range frequencies
- Higher magnitude at high frequencies for high flow
- More phase lag for low flow
- Less phase lag for high flow

- Can we do better?

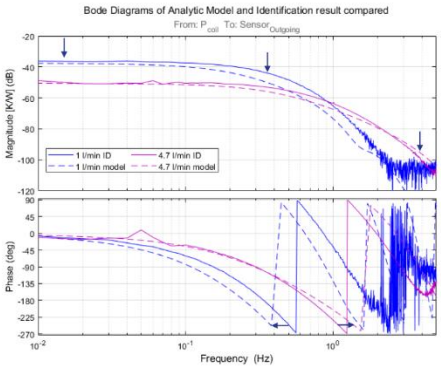

Grey box: Simple Lumped-Mass Model

- Only two lumped-masses
- Added 3rd order Low Pass to match roll-off
  - $LP_3 = \left(\frac{1}{\frac{1}{f_c \cdot 2\pi}s+1}\right)^3$
- Added delay to model transport delay

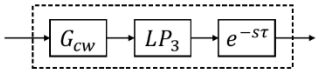

$G_{low\ order}$

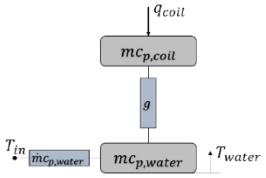

Transfer function:

$$G_{cw} = \frac{g}{a_2 s^2 + a_1 s + a_0}$$

$$a_2 = mc_{p,coil}\, mc_{p,water}$$
$$a_1 = \left(\dot{m}\, c_{p,water} + g\right) mc_{p,coil} + g\, mc_{p,water}$$
$$a_0 = g\, \dot{m} c_{p,water}$$

Model fitting

- Only 8 Parameters describe dynamics
- 4 Parameters tuned for each flow rate:
  - Mass flow $\dot{m}\ [\frac{kg}{s}]$
  - Heat transfer $g\ [\frac{W}{K}]$
  - Corner frequency $f_c\ [Hz]$
  - Transport delay $\tau\ [s]$

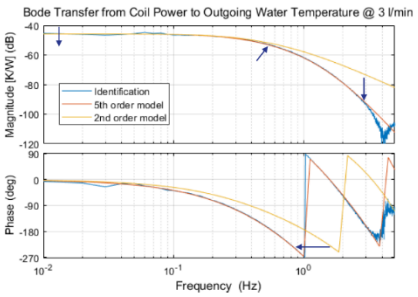

$$G_{cw}(s) = \frac{g}{\left(mc_{p,coil}\, mc_{p,water}\right)s^2 + \left(\left(\dot{m}\, c_{p,water} + g\right)mc_{p,coil} + g\, mc_{p,water}\right)s + g\, \dot{m} c_{p,water}} \cdot \left(\frac{1}{\frac{1}{f_c \cdot 2\pi}s + 1}\right)^3 \cdot e^{-s\tau}$$

Linear Parameter Varying model

- Varying Parameters:
  - $\dot{m} = [0{,}95 \;\; 1{,}85 \;\; 2{,}8 \;\; 3{,}6 \;\; 4{,}5 \;] \frac{998}{60*1000} \frac{\text{kg}}{\text{s}}$
  - $g = [135 \;\; 81{,}0 \;\; 43{,}9 \;\; 43{,}9 \;\; 43{,}9 \;] \frac{\text{W}}{\text{K}}$
  - $f_c = [0{,}9 \;\; 1{,}1 \;\; 1{,}65 \;\; 1{,}8 \;\; 1{,}8 \;] \text{ Hz}$
  - $\tau = [0{,}41 \;\; 0{,}21 \;\; 0{,}17 \;\; 0{,}14 \;\; 0{,}13] \text{ s}$

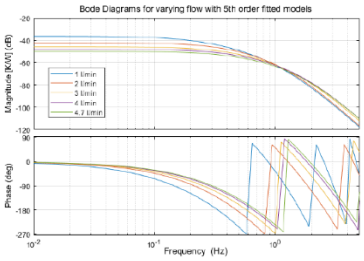

- Static Parameters:
  - $m_{coil} = 0{,}0319 \text{ kg}$
  - $cp_{coil} = 444 \frac{\text{J}}{\text{kg·K}}$
  - $m_{water} = 0{,}0092 \text{ kg}$
  - $cp_{water} = 4183 \frac{\text{J}}{\text{kg·K}}$

- Linear interpolation over flow range → LPV model

Conclusion

Grey Box Modelling approach combines physics and measurements

- Low Order Model
- High accuracy by fitting Identification results
- Meaningful parameters + unconsidered dynamics
- Allows for future advanced controller design

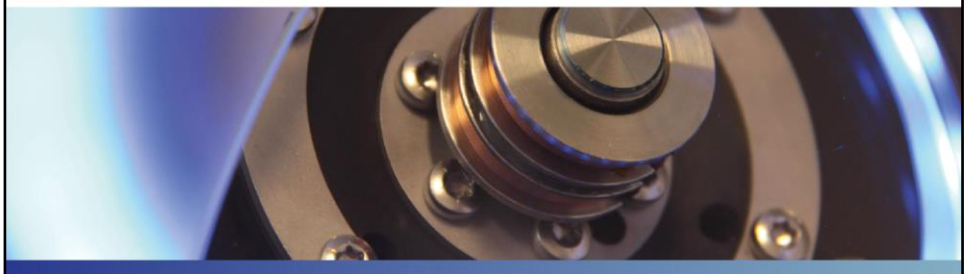

www.mi-partners.nl

Habraken 1199
5507 TB Veldhoven
The Netherlands

T +31(0)40-2914920
E info@mi-partners.nl

Analytic Lumped-Mass Model

- No hardware needed
- 223 lumped-masses
- >40 parameters
- Temperature and heatflux of each mass available
- Flow dependance
- Transport delays modelled by consecutive masses

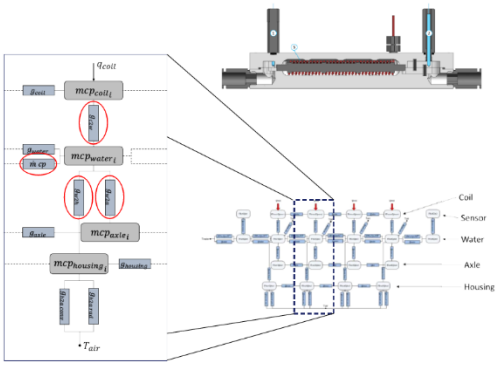

LPM: Local Polynomial Method

- $T(k) = G\ U_0(k) + V(k) + T(\Omega_k)$
- Goal: determine transfer G accurately
- Noise V: random function of frequency
  - Covariance on non-excited bins
- Transient T: smooth function of frequency
  - Locally fit with polynomial
- Plant G: smooth function of frequency
  - Determined after removing noise and transient
  - $G = U_0(k)^{-1}\big(T(k) - V(k) - T(\Omega_k)\big)$

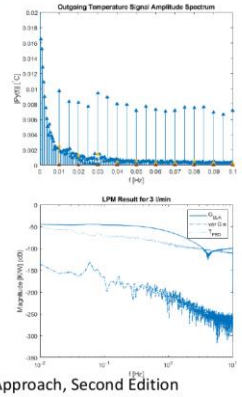

Pintelon R and Schoukens J 2012 System Identification: A Frequency Domain Approach, Second Edition

Special Interest Group Meeting on Thermal Issues
Laboratory for Machine Tools and Production Engineering (WZL) of
RWTH Aachen, Germany, February 2020
www.euspen.eu

A novel FEM-CFD interface for multi-physical simulations to model the effects of cutting fluid on the tool temperature during orthogonal cutting

Hui Liu[1], Thorsten Helmig[2], Thorsten Augspurger[1], Reinhold Kneer[2], Thomas Bergs[1]
[1]*Laboratory of Machine Tools (WZL) RWTH Aachen University*
[2]*Institute of Heat and Mass Transfer, RWTH Aachen University*

Corresponding Author: h.liu@wzl.rwth-aachen.de

Abstract

Numerical modelling is a widely used method for predicting machining process variables such as cutting forces, chip formation and temperature development. The coupled Eulerian-Lagrangian method (CEL) is one of the most important methods due to its robust handling of large deformations occurring during machining. So far, the CEL method has mainly been used for dry machining simulation. In order to simulate the influence of the cutting fluid on the tool temperature, a coupling between fluid simulation and CEL model needs to be implemented. To enable a simulation of the thermo-mechanical as well as fluid-structural interaction, the simulation results from the CEL model are transferred to the flow simulation. The proposed paper presents a Python script-based interface for coupling the CEL simulation with the fluid dynamics simulation and vice versa. First, the chip formation, the temperature fields in the cutting zone and the heat source were calculated in the CEL simulation and then the chip shape as well as the temperature distribution and the heat flow in the cutting zone were imported into the fluid simulation as initial conditions by the interface program. In the fluid simulation, the cooling effect of the cutting fluid was calculated. For the validation of the heat transfer model, fundamental investigations on orthogonal cutting of the nickel-base super alloy (Inconel 718) under cooling-lubrication were performed. The tool temperature was measured with a pyrometer and provided together with the measured cutting force a validation of the simulation.

Orthogonal cutting; Finite Element Simulation (FEM); FEM-CFD interface; INCONEL 718

1. Introduction

Cutting is a complex process associated with a variety of different mechanical and thermal physics. The mechanical energy applied to the chip formation is largely converted into heat in the shearing and friction zones. The resulting extraordinarily high mechanical and thermal stresses lead to thermally induced displacement of the tool tip and tool wear [1]. This limits the tool life and the applicable cutting speeds and thus the productivity of the machining process. In order to reduce tool wear and carry away the chips, cutting fluids are often used in machining operations. However, for different cooling strategies, the use of energy and resources and the impact on the environment are very different, which leads to enormous cost differences. Therefore, the knowledge of the suitable cooling strategy for different applications is an essential part of the efficient and economical design of the manufacturing process. However, due to the limited measuring conditions, the influence of the coolant on the temperature and heat distribution and the effect on chip formation cannot be observed directly during the machining process. This insufficient understanding of the process leads to the fact that the cutting fluid cannot be used to its full extent.

In addition to the empirical method, numerical simulation is increasingly used in the design of cooling systems. Compared to the experimental method, the simulation method reduces the cost of experiments and it is possible to analyze the mechanism of cooling effects in the cutting processes. So far, various numerical models and methods for the analysis of the cooling effect have been developed, such as [2], [3], [4]. Many of the methods simulate the cutting process and the cooling effect of the cutting fluid separately and do not consider the thermal and mechanical interactions between process and coolant. This leads to a large deviation in the simulation results, which cannot analyze the effect of the coolant quantitatively. Therefore, for a comprehensive modeling of the coolant effect on the tool temperature, mechanical and thermal effects and their interaction need to be considered, which consequently requires the coupling of finite element method (FEM) and computational fluid dynamics (CFD) models. The present work shows a method for coupling the CEL cutting simulation with the CFD fluid cooling simulation. First the chip formation, the heat source and the temperature distribution are calculated in the FEM simulation without considering the effect of the fluid. The results are then imported into the fluid simulation via the interface program as initial boundary and geometric boundary conditions. The influence of the coolant on the tool temperature is then calculated in the CFD simulation. By comparing the measured tool temperature with the calculated tool temperature, the accuracy of the simulation can be evaluated. In order to automate this procedure, a Python-based program has been developed which automatically performs the conversion and transfer of the simulation results.

2. FE-CFD Interface

The numerical method shown in this article is based on two simulation software. First, the heat development and chip formation during the machining process was modelled with the coupled Eulerian-Lagrangian (CEL) formulation. The model was solved with the commercial simulation program ABAQUS. Then the cooling effect of the cutting fluid is calculated by the CFD

software OpenFOAM. The task of the interface program is to realize the exchange of physical parameters and geometric conditions between the two programs in order to simulate the thermo-mechanical interaction between the cutting process and the cutting fluid. The workflow of the interface program is shown in Figure 1.

First, ABAQUS calculates the stationary state of the orthogonal cutting without considering the effect of cutting fluid. The interface program accesses the result file (ODB file) via the ABAQUS python library and reads the chip geometry as well as the temperature and heat flow distribution. Then the data is converted into the VTK format (Visualization Toolkit). The rules for writing VTK files refer to the literature [5]. The generated VTK file can be post-processed through the python library provided by the open source software PARAVIEW, so that it can be directly imported into the CFD simulation. The fluid properties of the coolant and the cooling effect are then calculated in the CFD simulation. The result of the simulation is the temperature of the tool in steady state under the influence of the cutting fluid.

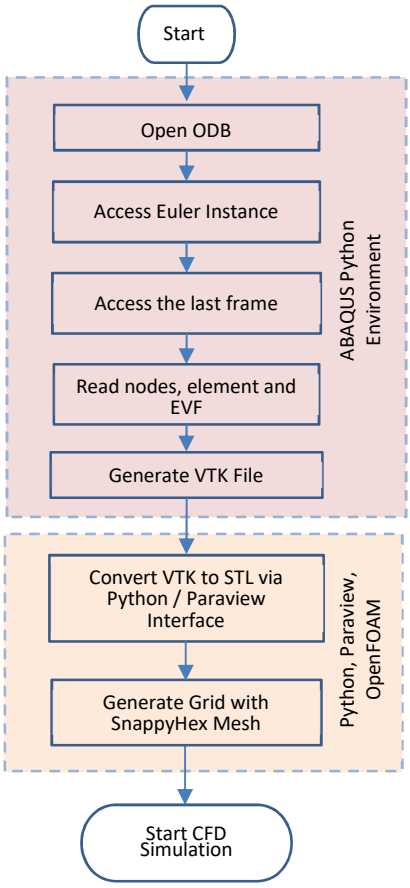

Figure 1. Major working procedures of the interface program

3. FEM modelling of orthogonal cutting

The chip formation simulation is performed using the CEL approach, in which the workpiece is modelled with Euler elements and the tool is modelled with Lagrange elements. Model structure, boundary conditions and mesh types are shown in Figure 2. The tool shown in grey is considered to be the ideal rigid body. The blue area in the Euler grid is the initial position of the material, and it moves at a constant velocity v_c through the Euler grids towards the tool. To describe the visco-plasticity of the Inconel 718, the Johnson Cook material model (Eq. 1) and the Johnson Cook damage model (Eq. 2) were used.

Both models are described in [6] and [7]. The parameters for the equation were obtained from the work of Erice [8] and are listed in Table 1 and Table 2.

$$\sigma_{yld} = (A + B \cdot \varepsilon^n) \cdot \left[1 + C \cdot \ln\left(\frac{\dot{\varepsilon}}{\dot{\varepsilon}_0}\right)\right] \cdot \left[1 - \left(\frac{T - T_0}{T_{melt} - T_0}\right)^m\right] \quad (1)$$

$$\varepsilon_f = (D_1 + D_2 \cdot e^{D_3 \cdot \eta}) \cdot \left[1 + D_4 \cdot \ln\left(\frac{\dot{\varepsilon}}{\dot{\varepsilon}_0}\right)\right] \cdot \left[1 + D_5 \cdot \left(\frac{T - T_0}{T_{melt} - T_0}\right)\right] \quad (2)$$

Table 1. Johnson-Cook constitutive model parameters of INCONEL 718 [7]

A [MPa]	B [MPa]	n	C	m	$\dot{\varepsilon}_0$ [s^{-1}]	T_0 [°C]	T_m [°C]
1200	1284	0.54	0.006	1.2	0.001	25	1800

Table 2. Johnson-Cook damage model parameters of INCONEL 718 [7]

D_1	D_2	D_3	D_4	D_5
0.04	0.75	-1.45	0.04	0.89

The friction between workpiece and tool during cutting is described by the temperature-dependent friction model published by Puls [8]. The parameters of the friction model for the Inconel 718 were obtained from the literature [9] as shown in Table 3.

$$\mu_{app} = \mu_0 \cdot \left[1 - \left(\frac{T - T_f}{T_{melt} - T_f}\right)^{m_f}\right] \quad (3)$$

Table 3. Friction model parameters of INCONEL 718 [9]

μ_0	T_f [°C]	m_f
0.46	200	2.4

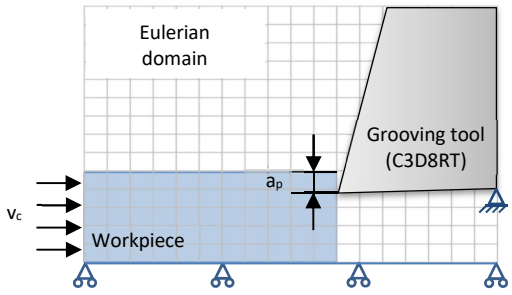

Figure 2. Concept of FE modelling of orthogonal cutting with coupled Eulerisch-Lagrangian (CEL) formulation

Figure 3 shows the chip shape from the simulation. The simulation results presented in this section are processed in the FE-CFD interface and used as boundary condition in the CFD simulation.

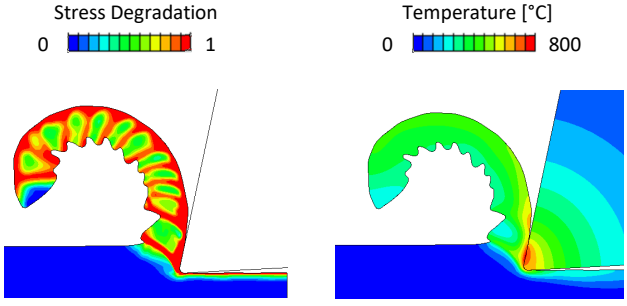

Figure 3. Chip formation and temperature distribution from the simulation (v_c = 50 m/min, a_p = 0.175 mm)

4. Computational Fluid Dynamics

The framework for the CFD simulation is provided by the OpenSource software OpenFoam using the exported 2-D chip geometry to generate the grid. This is done by converting the VTK output file from FEM into a STL (stereolithography) file format by using a python script with an embedded PARAVIEW library. Following this STL file used by the snappy hex mesh meshing tool of OpenFoam to generate the CFD geometry and boundaries conditions.

The used OpenFoam solver accounts for multiphase fluids meaning that gaseous ambient air as well as liquid cooling lubricant are modelled. Further, conjugate heat transfer between lubricant (fluid) and chip, workpiece (solid) is considered.

$$\rho c_p \frac{\partial T}{\partial t} + \rho c_p u_i \frac{\partial T}{\partial x_i} = \lambda \frac{\partial^2 T}{\partial^2 x_i} + \dot{q} \tag{4}$$

$$\rho \frac{\partial u_i}{\partial t} + \rho \frac{\partial u_i u_j}{\partial x_j} = \frac{\partial p}{\partial x_i} + \nu \frac{\partial^2 u_i}{\partial^2 x_j} \tag{5}$$

Exemplary results of the CFD simulation are presented in Figure 4 showing the volume fraction of cooling lubricant and the corresponding redirection of fluid due to the chip geometry.

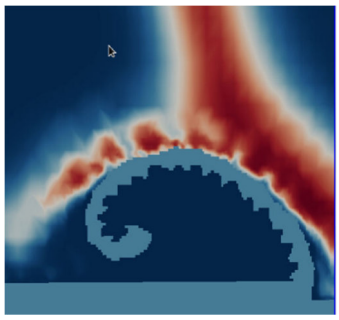

Figure 4. Exemplary CFD Simulation Results of the Cooling Lubricant approaching the Chip

5. Experimental Setup

To validate and evaluate the simulation models, orthogonal cutting tests are carried out on a broaching machine. The experimental setup is shown schematically in Figure 1. The test material INCONEL 718 was machined into 2.5 mm thick sheets and fastened to the slide of the broaching machine. A grooving insert made of uncoated cemented carbide was fixed to the Kistler Multi-Component Dynamometer Z21289 and mounted on the worktable of the broaching machine. The applied grooving insert has a rake angle of 12°, a clearance angle of 3° and a cutting radius of 5 µm. The temperature inside the tool is measured by a pyrometer. Thereby the infrared radiation is captured by a glass fibre integrated in the grooving tool and transmitted to the pyrometer. During the test, the workpiece moves with the broaching slide against the tool at constant speed v_c and cutting depth a_p. The chip formation process as well as temperature distribution and process forces were recorded and used as validation parameters for the simulation.

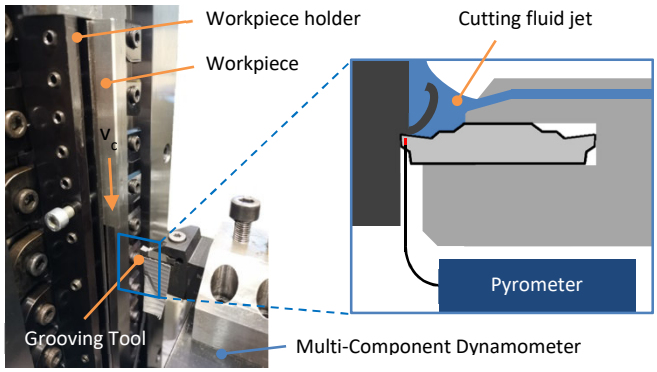

Figure 5. Experimental setup of orthogonal cutting

6. Acknowledgements

The authors would like to thank the German research foundation (DFG) by founding the project collaborative research project TRR 96 Project-ID 174223256.

Reference:

[1] Klocke, F., 2011, “Manufacturing Processes 1”, Springer-Verlag Berlin Heidelberg

[2] Shet, C.; Deng, X.; E. Bayoumi, A., 2003, “Finite element simulation of high-pressure water-jet assisted metal cutting” In: International Journal of Mechanical Sciences. Jg. 45, Nr. 6-7, S. 1201–1228

[3] Dix, M.; Wertheim, R.; Schmidt, G.; Hochmuth, C., 2014, “Modeling of drilling assisted by cryogenic cooling for higher efficiency” In: CIRP Annals - Manufacturing Technology. Jg. 63, Nr. 1, S. 73–76

[4] Aurich, J. C.; Zimmermann, M.; Schindler, S.; Steinmann, P., 2013, “Analysis of the machining accuracy when dry turning via experiments and finite element simulations” In: Production Engineering

[5] Liu Q.B., Li J., 2016, “ParaView visualization of Abaqus output on the mechanical deformation of complex microstructures”, Computers & Geosciences, Volume 99, 135–144

[6] Johnson, G.R., Cook, W.H., 1983, “A constitutive model and data for metals subjected to large strains, high strain rates and high temperatures”, In: 7th International Symposium on Ballistics, The Hague, pp. 541–547.

[7] Johnson, G.R.; Cook, W.H., 1985, “Fracture characteristics of three metals subjected to various strains, strain rates, temperatures and pressures”, Engng. Fracture Mechanics, 21, 31–48.

[8] Erice B, G´alvez F., 2014, “A coupled elastoplastic-damage constitutive model with lode angle dependent failure criterion”, Int J Solids Struct 51(1):93–110.

Development of a novel FEM-CFD interface for multiphysical simulations to model the cooling effect of cutting fluid

Hui Liu[1],
Thorsten Helmig[2], Thorsten Augspurger[1], Reinhold Kneer[2], Thomas Bergs[1]

[1] Laboratory for Machine Tools, RWTH Aachen University
[2] Institute of Heat and Mass Transfer, RWTH Aachen University

Introduction and Motivation

Motivation

Increasing demand in high precision manufacturing and components during the last decades

Inaccuracies caused by thermal expansion of the machine tool

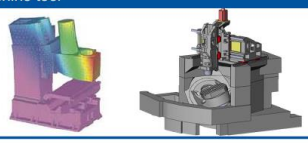

Quantification and Modelling of Heat Sources during Processing

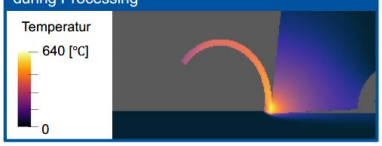

Thermo-mechanical modelling with consideration of cooling lubricant effects

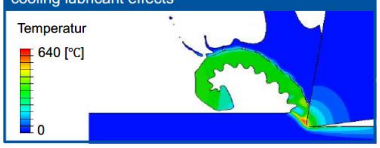

[KLINKEL05]

Introduction and Motivation

Potentials of numerical simulations

Empirical Models

Modelling based on empirical observations

Lack of knowledge and limited measurement capabilities restrict the optimization potential of the process.

Numerical Models

Process analysis with simulation models derived from measurement data.

FEM: Modelling of the chip formation process and heat generation during cutting process

CFD: Modelling of convective heat transfer

Cutting simulation extends the optimization potential of process design and offers the possibility to reduce development time and costs.

Development of the flow simulation for the analysis of cutting fluid

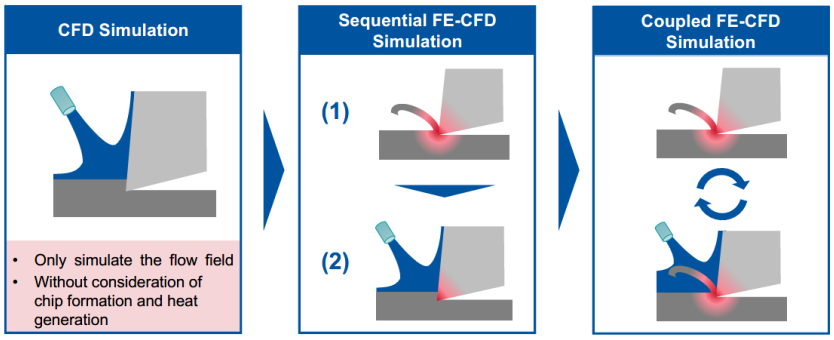

[OBIKAWA13], [PERVAIZ15], [HELMIG19]

Agenda

Requirements of the co-simulation

Model based analysis of the influence of cutting fluids on the cutting tool temperature

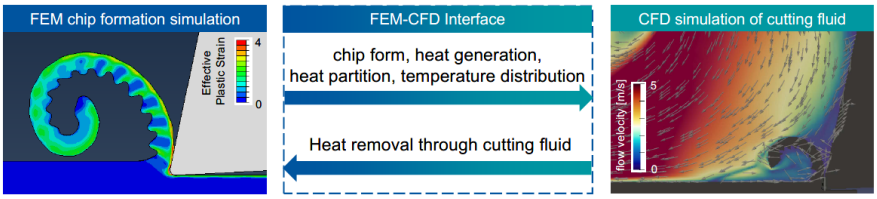

- The interface program exchanges physical and geometric data between FEM and CFD simulations.
- The simulation process is controlled by the interface program, so that data exchange is possible during the whole simulation.

Development of the FE-CFD Interface

Simulation approach of the cutting process

FE-Modelling of the chip formation process with Coupled-Eulerian-Lagrangian method (CEL)

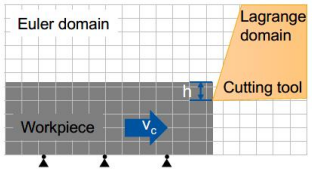

- Software: ABAQUS 6.14
- Solver: Explicit – Solver

- High stability
- Low computing performance required
- Controllable via python script

INCONEL 718

Cutting speed:
v_c = 50 m/min

Undeformed chip thickness:
h = 0.075 mm

Tool orthogonal clearance:
α_0 = 12°

Tool orthogonal rake angle:
γ_0 = 3°

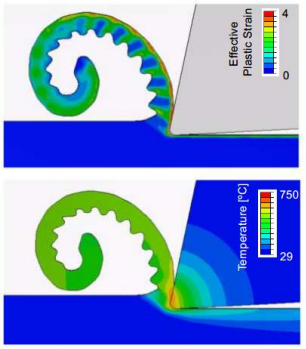

Development of the FE-CFD Interface

Simulation approach of the cooling process

Modeling of the cutting fluid by OpenFOAM CFD

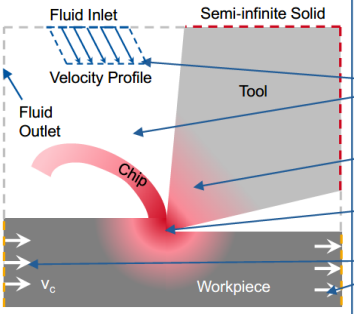

- Multiphase – liquid fluid and gaseous air
- Heat conduction inside the solid
- Heat source terms at chip and rake face
- Relative movement of chip, tool and workpiece is considered

Development of the FE-CFD Interface

Simulation approach of the cutting process

Modeling of the cutting fluid by OpenFOAM CFD

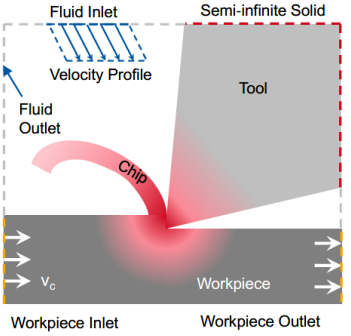

- Software: OpenFOAM v3.2
- Solver: Multiphase Volume-of-Fluid Approach
- Fluid Regime: Laminar

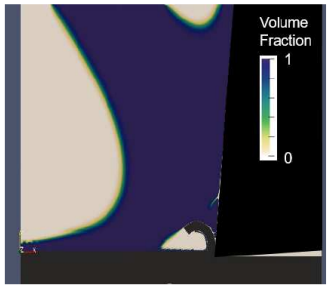

FE-CFD Interface

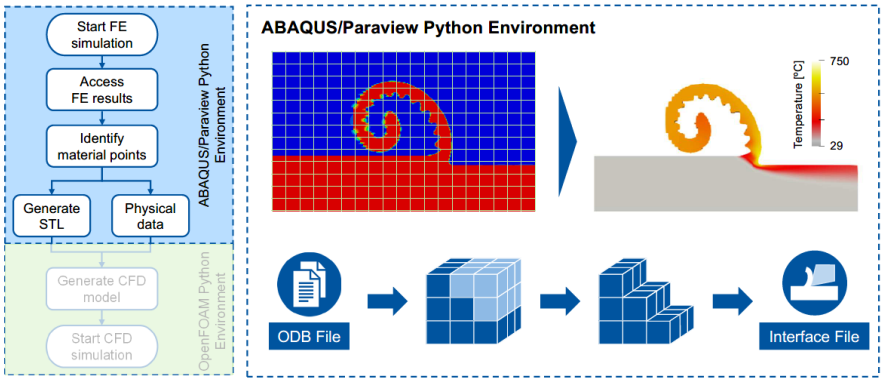

FE-CFD Interface

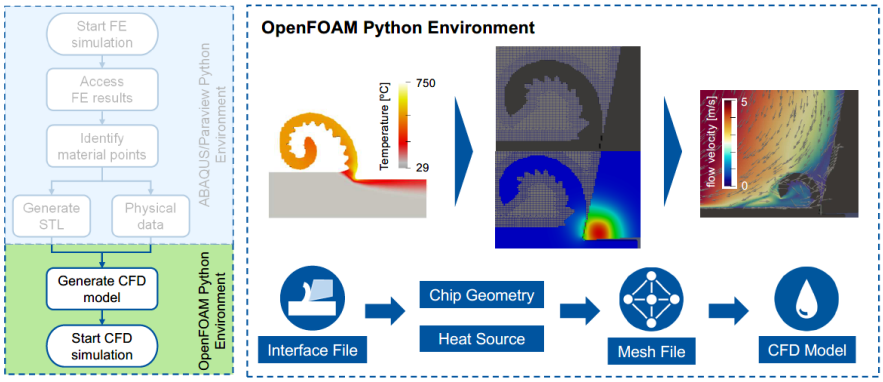

Agenda

Simulation Results and Validation Procedure

Simulation results

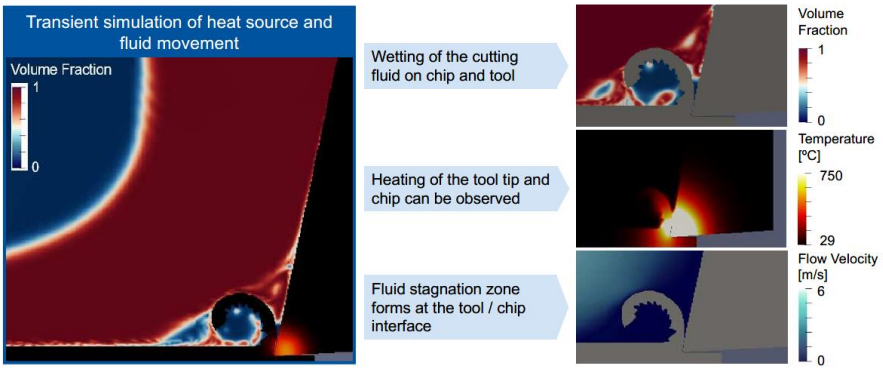

Simulation Results and Validation Procedure

Design of the test bench

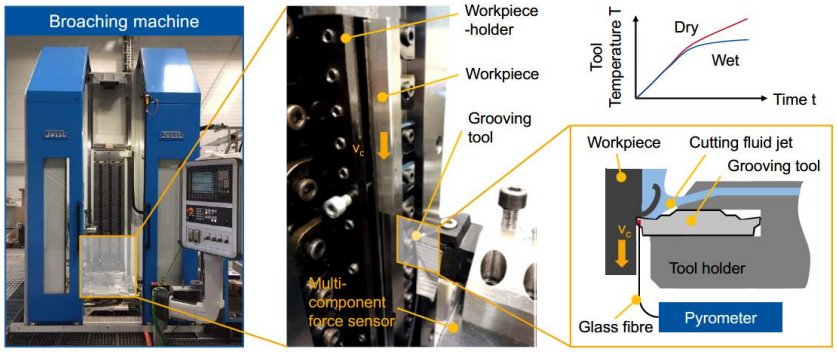

Simulation Results and Validation Procedure

Experimental investigation of the dry cutting process

INCONEL 718

Cutting speed:
v_c = 50 m/min

Undeformed chip thickness:
h = 0.075 mm , 0.175 mm

Tool orthogonal clearance:
α_0 = 12°

Tool orthogonal rake angle:
γ_0 = 3°

Measuring point of the tool temperature

d = 0.3 mm to the cutting edge

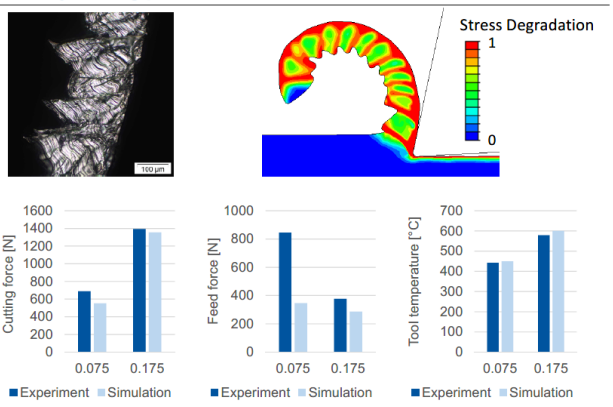

Agenda

1	Introduction and Motivation
2	Development of the FE-CFD Interface
3	Simulation Results and Validation Procedure
4	**Conclusion**

Conclusion

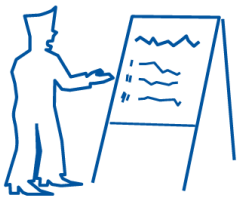

Summary

- The interface program enables a direct coupling of the chip formation simulation with the flow simulation.
- The cooling effect of the cutting fluid can be simulated under consideration of the chip formation process
- The entire simulation process can be performed automatically by the interface program.

Outlook

- The simulation models of contact heat transfer between cutting fluid and solid body are being further developed.
- The cooling effect of the coolant jet will be investigated simulatively and compared with empirical data.

Thank you for your attention

Hui Liu
H.Liu@wzl.rwth-aachen.de

Laboratory for Machine Tools
RWTH Aachen University

www.wzl.rwth-aachen.de

Thorsten Helmig
helmig@wsa.rwth-aachen.de

Institute of Heat and Mass Transfer
RWTH Aachen University

www.wsa.rwth-aachen.de

References

[KLINKEL05] Kinkel S.: Anforderungen an die Fertigungstechnik von morgen. Fraunhofer ISI, Karlsruhe, 2005

[OBIKAWA13] Obikawa T, Yamaguchi, M.: Computational Fluid Dynamic Analysis of Coolant Flow in Turning, 2013

[PERVAIZ15] Pervaiz, S.; Deiab, I.; A novel numerical modeling approach to determine the temperature distribution in the cutting tool using conjugate heat transfer analysis, 2015

[HELMIG19] Helmig T.; Peng B.; Augspurger, T: A coupling approach combining CFD and FEM methods to predict cutting fluid effects on the tool temperature in cutting processes, 2019

Special Interest Group Meeting on Thermal Issues
Laboratory for Machine Tools and Production Engineering (WZL) of
RWTH Aachen, Germany, February 2020
www.euspen.eu

Thermal Modal Analysis including Static correction: an efficient tool to model and design thermal compensation systems

Nicolas JOBERT[1] , Muriel THOMASSET[1], Gilles CAUCHON[1], David DENNETIERE[1]

[1]*Synchrotron SOLEIL, l'Orme des Merisiers, Gif-sur-Yvette, 91192 Saint-Aubin, France*

nicolas.jobert@synchrotron-soleil.fr

Abstract
Designing a thermal compensation system always involves dealing with conflicting requirements, such as minimizing the number of sensors and transducers, cable routing and control power while ensuring maximal disturbances rejection. To assist in the trade-off process, it is essential to have a means to quickly investigate the merits of various configurations. Starting from the dynamics of the thermal systems, the residual position error for any control loop can be quickly evaluated provided that such a model is given in an efficient and compact manner. State-space models provide a convenient way to capture the system dynamics, and allow for the exploration of dozens of control configurations with no appreciable computational burden. However, conventional finite element packages do not have built-in capacities to efficiently generate such compact models, and it is extremely inefficient to work with the original detailed models.

In this paper, it is shown that using thermal modal analysis, thermal mechanical state-space models can be efficiently built. In particular, it is shown that adding one extra state per actuator allows for capturing the full static response of the system. While the impact on the thermal response is generally limited, the mechanical response fidelity is very significantly improved, particularly in bending dominated problems. The method is validated against the full, detailed thermal mechanical response, and it shows that the reduced models are both efficient and conservative.

Model reduction, thermal modal analysis, state-space, thermal effects compensation

1. Scope and motivation

The idea of using modal analysis to reduce the complexity of thermal transient analyses is nothing new (see [1] or [2] for example). However, in contrast with structural dynamics where it is *de facto* the standard approach, for thermal effects modal superposition techniques have never seemed to have received a broad acceptance. One reason for this might be that convergence is comparatively slow, i.e. generally a large number of thermal modes are needed to obtain acceptable agreement with the original model.

Firstly, it must be acknowledged that this limitation is a fact, and arises particularly in situations where point-like heat loads are applied. However, as noted in [3], while the temperature distribution can be underestimated in the vicinity of the load, this does not mean that the quantity of interest (generally, positional or angular deviation) is severely affected.

Secondly, when higher accuracy is required, then the modal basis can be simply augmented using the so-called residual vector approach. A nice discussion of the method as applied in the field of structural dynamics, where it originated, can be found in [4]. To the best of the knowledge of the authors, the method has never been applied to thermal response estimation. In the following sections we outline the corresponding procedure and show its benefits when applied to ultra-precision components.

2.1. Thermal response using residual modal vector method

Mathematically, including a residual vector this simply amounts to evaluating the offset between the static response vector of the system obtained firstly using the original model, and secondly using a modal basis, as follows:

$$T_{exact} = K^{-1} P \text{ , and}$$

$$T_{reduced} = \sum_{i=1}^{n} {}^{t}\Phi_i P . \Phi_i / \lambda_i$$

Where K is the conductivity matrix, P is the nodal load vector (thermal power fed into the system on a node basis) and (λ_i, Φ_i) are the eigenvalues and eigenvectors of the thermal system, i.e solutions to the following matrix equation.

$$\lambda C + K = 0$$

Physically, for each mode the corresponding eigenvalue is equal to the inverse of the corresponding time constant, that is, the modes with the lowest eigenvalues correspond to solutions to the free thermal response of the system with the longest decay time. The residual vector R is obtained by :

$$R = T_{exact} - T_{reduced}$$

The process can be repeated with each load case, i.e. the response to the jth load vector will need to account for the jth residual vector to be exact in the static domain.

2.2. State-space thermal-mechanical model using residual modal vector

Thanks to linearity the mechanical response $\Phi_{i,s}$ to all of the n_m thermal modes $\Phi_{i,t}$ can be evaluated and superimposed to obtain the complete thermal mechanical

response. By the same procedure, the responses to the n_a residual vectors are estimated.

This is sufficient to conveniently build a state-space model for the thermal-mechanical response, i.e.:

$$x' = Ax + Bu \text{ , and}$$
$$y = Cx + Du$$

Where:

- x is the state vector, i.e containing the n_m modal amplitudes
- y is the output vector, containing responses at the n_s sensors
- u is the input vector, containing the thermal power delivered by each of the n_a actuators

By definition, A is a square diagonal matrix containing the eigenvalues, B is a $n_m x n_m$ matrix containing the load vectors. C is a $n_s x n_m$ matrix containing the modal amplitudes at each of the sensor locations.

Under normal circumstances, D would be zero. When adding residual vectors, each of their contributions will appear as a *feedthrough*, i.e. an additional response whose contribution linearly (and instantly) follows the excitation, hence in the D matrix. Mathematically, D will be a $n_s x n_a$, each column of which will correspond to the j-th residual vector. See for example [5] for a discussion of the residual vector as a feedthrough for structural dynamics.

3. Practical application

The methodology outlined previously is applied to a geometrically simple optical component for which flatness requirements are tight, while thermal effects are of crucial importance. This is the typical configuration for primary mirrors used in Synchrotron Light Source facility such as SOLEIL. In this example, the heat deposited can exceed 10^3 W/cm^2, while the local slope error should be kept within 1 µrad, down to 0.2 µrad in the near future. In order to control the temperature, the mirror is cooled via water or liquid nitrogen circulating into a copper heat exchanger, tightly on each of the mirrors side. The mirror itself is fitted with regularly spaced holes in order to allow bolting of each half of the heat exchanger to the mirror. Such a mirror is shown on Figure 1.

Figure 1. primary mirror for high-energy X-ray beamline (SOLEIL Synchrotron)

While both heat load and heat sinks are aimed at being stationary, there are inevitable residual fluctuations. The heat load deposited on the optical surface will change over time, in intensity, and in space because of the photon beam jitter, or whenever because of required changes in undulator gap. Conversely, the cooling water will neither keep its temperature constant to better than 1 °C nor will the flow rate remain stable within less than 10 to 20 %. This will induce some modification of the heat circulating in the mirror, then of the temperature distribution and ultimately the mechanical distortions of the optical surface.

In order to evaluate the optical surface distortions due to thermal transients, a thermal mechanical finite element model has been developed (using ANSYS rev 19.1), as shown on figure 2. It consists of both the mirror and the cooler, and is meshed using 20-nodes brick elements. In order to simplify the interpretation, we assume a uniform thermal conductance at the mirror/cooler interface of 50 000 W/m²/K, as would be obtained using a thermal contact enhancement foil (indium) as is typically employed in such a situation.

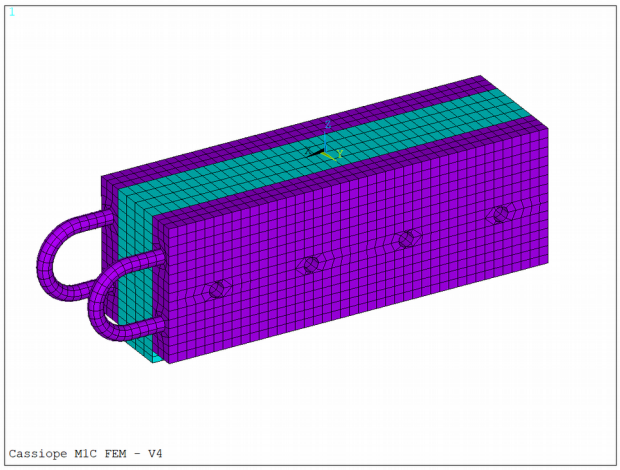

Figure 2. Finite Element model - mirror and cooler

The heat load is provided by the photon beam. It is assumed to be centered on the optical surface, with a maximum flux of 2500 W/cm^2. The beam profile is assumed to be gaussian, with a full-width-at-half-maximum equal to half the optical surface dimensions (160x25 mm^2), hence a total input power of about 400 W.

This system is cooled by circulating water, and again we simplify things by assuming that the flow rate is large enough to maintain a fluid bulk temperature at 21°C, and the fluid convection (film) coefficient is equal to 8000 W/m²/K .

Under those hypotheses, the temperature distribution is shown in figure 3, and the out-of-plane motion (with respect to the optical surface) in figure 4. Although the temperature elevation is about 23 K, and the resulting distortion is about 5 µm, this is already enough to cause some loss of performance for the overall system, since the corresponding slope is of the order of 100 µrad.

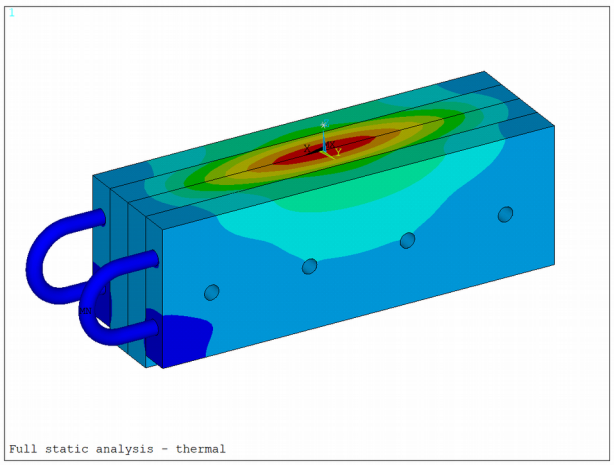

Figure 3. Temperature for nominal beam power (Tmax=42.8 °C)

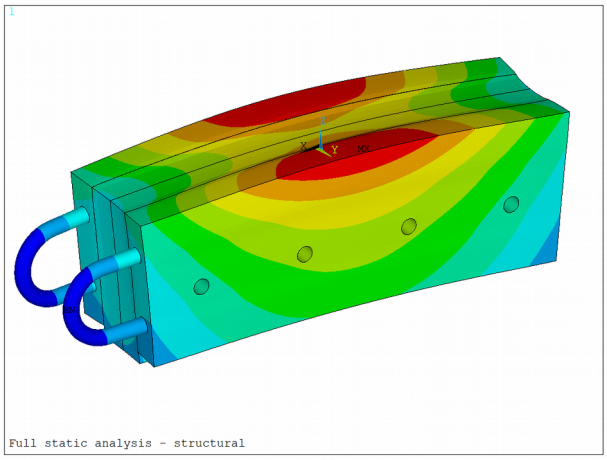

Figure 4. Distortion for nominal beam power dZmax=5.1 µm)

Equipped with those reference values, we can estimate the convergence rate of the modal superposition method.

First of all, we begin by estimating the modes, see [6] for generalities about the ANSYS matrix manipulation language (APDL Math), [7] for details specific to thermal modal analysis practical implementation and [8] for thermal harmonic analysis.

Table 1 - Thermal Modes

Mode		Description
#	τ [s]	
1	12.0	Heat dumped into water
2	8.1	Heat traveling longitudinally (order 1)
3	4.3	Heat traveling longitudinally (order 2)
4	3.0	Heat travelling vertically (order 1)

Obviously, modes 1 and 4 involve differential expansion of the upper and lower part of the system (bi metal effect), and should be a major contributor to both the temperature and structural response. Other modes might contribute to temperature distribution, but minimally to the distortions of the optical surface.

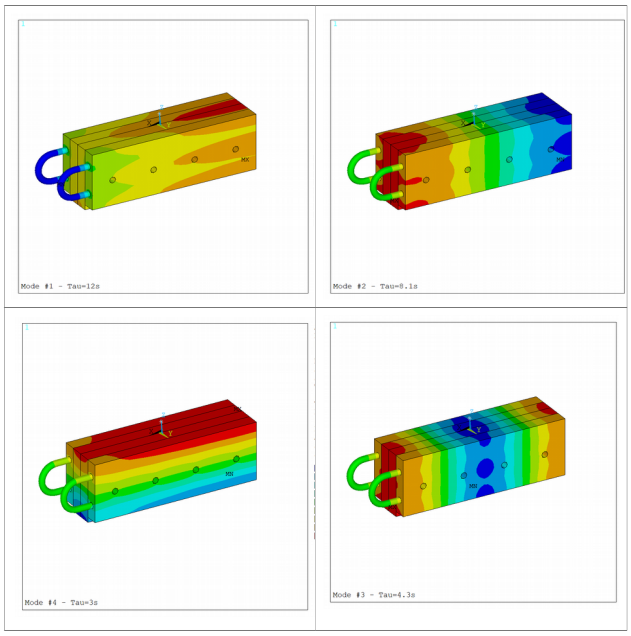

Figure 5. Temperature distribution for modes 1 to 4.

The thermal time constants distribution is given in figure 6. Since we are aiming at building a model that would have a useful bandwidth extending up to 1 Hz, we need to include modes with time constants shorter than approximately 0.5 to 1 s. From the thermal model (half model using the XZ plane of symmetry), we see that there are less than 10 modes with thermal time constants longer than 2 s, but more than 100 modes when setting the limit at 0.5 s. Obviously, the modal method is extremely efficient for slow dynamics, but there is a cliff-edge effect in the required number of modes as soon as one tries to extend the bandwidth further.

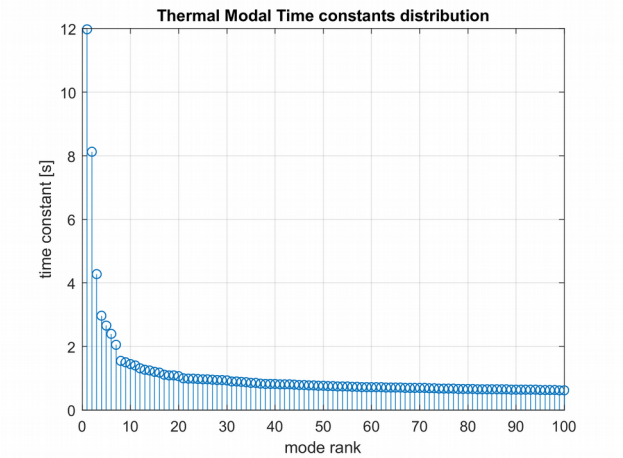

Figure 6. Thermal time constants distribution

In our case we might want to track the accuracy of temperature and structural responses obtained by including an increasing number of modes. Again, the static response is straightforward to obtain. The states (thermal modes) are obtained as $x = -A^{-1}Bu$ and hence the static response reads (including the residual vector):

$$T_{static} = Cx_{static} + Du = \left(-CA^{-1}B + D\right)u$$

Applying the procedure to the peak local temperature (on the optical surface), it appears that the convergence rate is terribly slow. The relative error exceeds 30% even for 100 modes included, and shows no sign of decrease (see Figure 7). On the contrary, the bump magnitude can be estimated within 1% by using as few as 20 modes.

In this context, it is clear that adding a single residual vector would definitely help to overcome convergence problems.

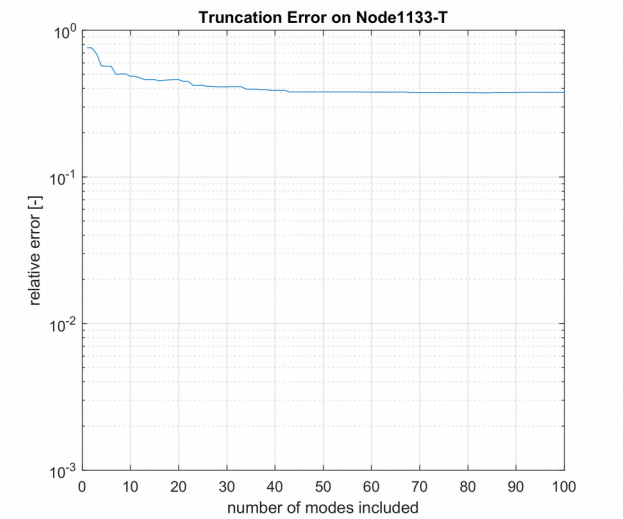

Figure 7. Relative error on local temperature

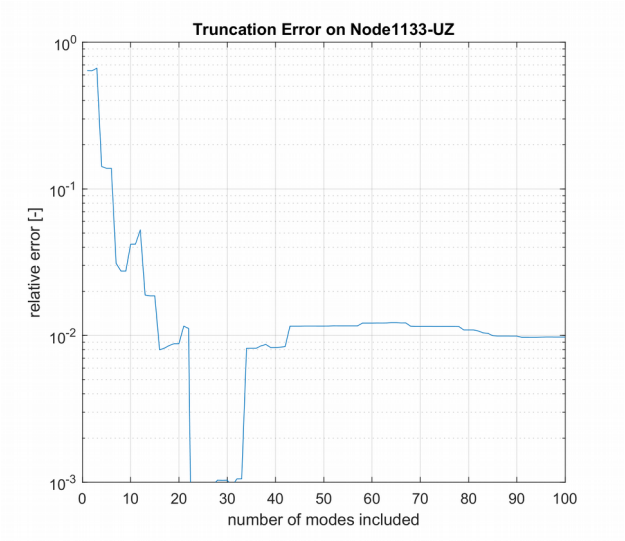

Figure 8. Relative error on bump amplitude

Residual vector effect on transfer functions

Since the quantity of interest is the optical surface distortion, from this point on we will focus on the thermal bump. The frequency response estimated *in the absence of residual vector* is given in figure 9 below. The input is expressed as a fraction of total thermal power, and the output is the thermal bump (in mm). We can check that for 10 and 100 modes, the static response is close to the reference value of 5.1µm.

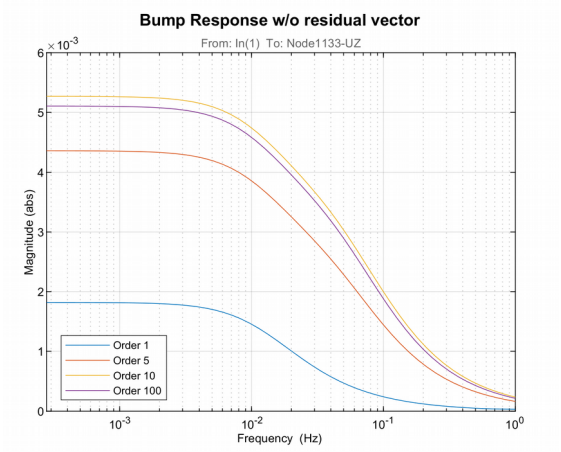

Figure 9. Transfer function without residual vector : magnitude

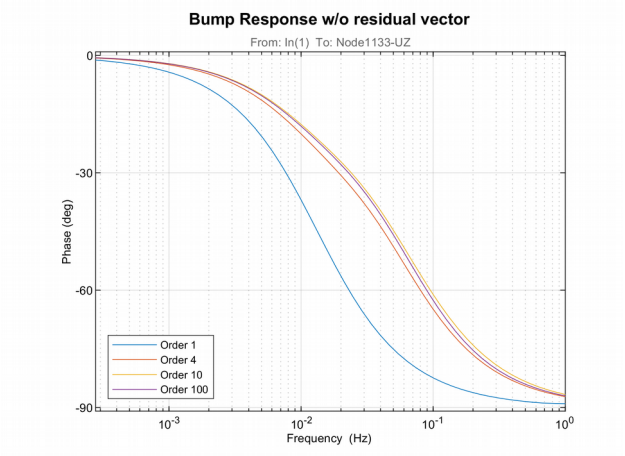

Figure 10. Transfer function without residual vector : phase

The benefit of including a residual vector is shown in figures 11 and 12, for magnitude and phase. Clearly, as far as magnitude is concerned, the model validity is greatly improved, and the usable bandwidth extends largely above 0.1Hz. In terms of phase, however, it is clear that it cannot be reliably estimated for frequencies above 0.5 Hz. Inconsistent results are obtained, clearly showing limitations of the model (and to begin with, space discretization is probably insufficient: for silicon, thermal diffusivity is about 90 mm^2/s, and a mesh with an element size 6 mm might not be fine enough).

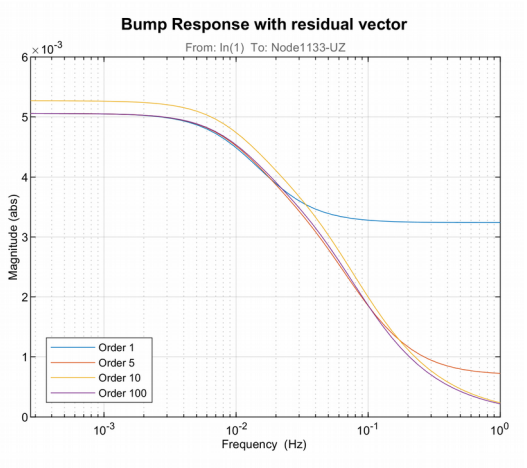

Figure 11. Transfer function with residual vector : magnitude

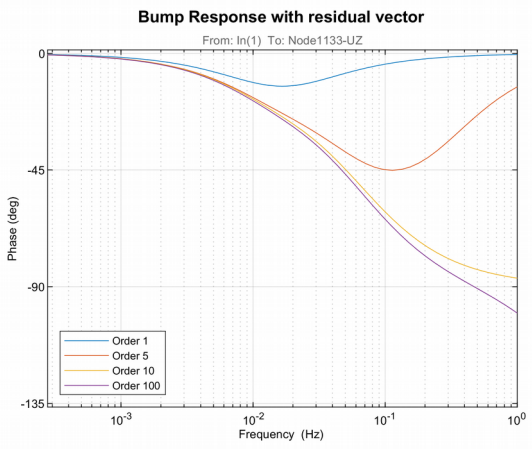

Figure 12. Transfer function with residual vector : phase

4. Conclusion

In this paper, we have shown that thermal mechanical state-space models can be efficiently built by using the modal method. In particular, it is shown that adding one extra state per actuator allows for capturing the full static response of the system. While the impact on the thermal response is generally limited, the mechanical response fidelity is very significantly improved, particularly in bending dominated problems, or if local results are to be obtained. In particular, it has been shown that convergence can be obtained at drastically different rates, depending on the quantity of interest: for the same number of modes included in the analysis, the relative error could vary by as much as two order of magnitudes.

Since it is not feasible to obtain accurate results with confidence by solely relying on engineering judgment, it is recommended to systematically add a residual vector, thus largely improving the robustness of the analysis. It has been shown, however, that while the system response in the low

frequency range is clearly improved, the asymptotic (high-frequency) response is biased, and in particular, starting from a limit frequency the phase is clearly corrupted (i.e. it begins to increase), a clear warning sign that the model should not be used above that particular frequency. To summarize, the residual vector method only dramatically enhances the fidelity of model in the low frequency range, but does not extend its validity in the higher frequency range.

This work could be improved by modifying the correction: the residual vector could be modified into a residual mode, with a specific time constant chosen so as to minimize the deviation from the exact response above the model cut-off frequency.

References

[1] Palmieri and Rathjen 1978 - CAVE3 - A General Transient Heat Transfer Computer Code Utilizing Eigenvectors and Eigenvectors – NASA Contractor Report 145290

[2] Ruijl, Compensation model based on thermal mode shape. In Euspen SIG Seminar2006, Eindhoven, The Netherlands

[3] Morishima, 2016, Novel thermal error reduction techniques in temperature domain

[4] Roy and Girard, 2005, Impact of Residual Modes in Structural Dynamics, European Conference on Spacecraft Structures, Materials and Mechanical Testing.

[5] Preumont, 2017, Vibration Control of Active Structures 3rd edition

[6] ANSYS Inc, Mechanical APDL, ANSYS Parametric Design Language Guide

[7] Jobert, 2017, Working Wonders with APDL Math: Thermal Modal Analysis, PADT Blog «The Focus»

[8] Jobert, 2019, Working with APDL Math Illustrated : Thermal Harmonic Analysis, ANSYS White Paper

Thermal Modal Analysis with Static Correction: an efficient tool to model and design thermal compensation systems

Nicolas JOBERT

Synchrotron SOLEIL
Accelerators and Engineering Division

EUSPEN - SIG Meeting on Thermal Effects
Feb 26, 2020 Aachen

Outline

Outline

Objective (1/2)

Models in the context of thermal compensation systems

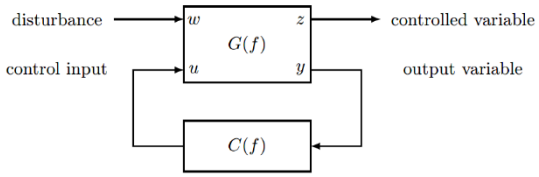

Objectives:

- minimize closed-loop response $T_{zw} = [G_{zw} + G_{zu}C(I - G_{yu}C)^{-1}G_{yw}]$
- guarantee stability

Need to know $G_{zw}, G_{yw}, G_{zu}, G_{yu}$

Objective (2/2)

What do we expect from a thermal model

Ideally, a model for thermal/thermal-elastic problems should be:

1. built on existing thermal and structural models (minimize manual workload)
2. computationally efficient (fast and accurate)
3. compact in size (lightweight)
4. physically meaningfull (supports engineering judgment)

Modal decomposition only partially fullfils those requirements.

Outline

Thermal Response - Direct approach

Starting from conductivity [**K**] and capacity [**C**] matrices:

In time domain:

$$[\mathbf{C}]\dot{T} + [\mathbf{K}]T = P \tag{1}$$

In frequency domain:

$$(j\omega[\mathbf{C}] + [\mathbf{K}])T = P \tag{2}$$

Hence

$$\mathbf{G}(\omega) = (\mathbf{j}\omega[\mathbf{C}] + [\mathbf{K}])^{-1} \tag{3}$$

Most accurate numerically, but computationally demanding. Completely extensive but not really informative. Not suited for control loop design.

Thermal Response - Modal approach

Thanks to symetry, we can solve for the modes:

$$([\mathbf{C}] + \tau_i[\mathbf{K}])\Phi_i = 0 \tag{4}$$

Then the system "thermal compliance" reads:

$$G_{kl}(\omega) = \sum_{i=1}^{n_{dof}} \frac{\Phi_{ki}\Phi_{il}}{1 + j\omega\tau_i} \tag{5}$$

As accurate as direct method but only if all modes are extracted. Not feasible nor necessary in practice.
No clear-cut criterion to accept/reject truncated model.

Modal truncation error: simplification

Retaining only the first n_m modes ($n_m < n_{dof}$).

$$G_{kl}(\omega) = \sum_{i=1}^{n_m} \frac{\Phi_{ki}\Phi_{il}}{1 + j\omega\tau_i} + \sum_{i=n_m+1}^{n_{dof}} \frac{\Phi_{ki}\Phi_{il}}{1 + j\omega\tau_i} \tag{6}$$

Let ω_b be the bandwidth of the controller to be designed. Including all modes with $\tau_i >> 1/\omega_b$, the truncation error can be approximated as a *frequency independent* term.

$$R_{kl}(\omega) = \sum_{i=n_m+1}^{n_{dof}} \frac{\Phi_{ki}\Phi_{il}}{1 + j\omega\tau_i} \simeq \sum_{i=n_m+1}^{n_{dof}} \Phi_{ki}\Phi_{il} \tag{7}$$

Modal truncation error: estimation

Rewriting compliance in the static domain ($\omega = 0$)

$$G_{kl}(0) = \sum_{i=1}^{n_m} \Phi_{ki}\Phi_{il} + \sum_{i=n_m+1}^{n_{dof}} \Phi_{ki}\Phi_{il} \tag{8}$$

So that

$$R_{kl} = G_{kl}(0) - \sum_{i=1}^{n_m} \Phi_{ki}\Phi_{il} \tag{9}$$

This term cand be added to "thermal compliance" so as to compensate for the "thermal flexibility" of discarded modes.

Outline

Beamline Primary Mirror

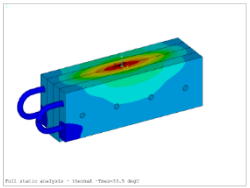

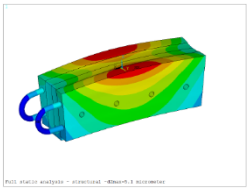

$160x25mm^2$ optical surface
SiC / Water cooled
heat load: 400W
drift rate: 1%/s
allowable slope error: 1μrad

Technical Procedure:

1. Build plant thermal-elastic state space model (ANSYS / APDL Math)
2. Shape controller using LTI models (Matlab)
3. Build prototype
4. Validate optical performance (HASO at SOLEIL Optical Metrology Lab)

Controller Architecture

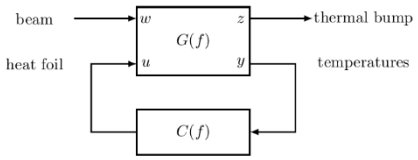

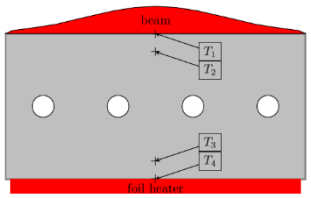

T_1	On upper surface
T_2	10mm below upper surface
T_3	10mm above lower surface
T_4	On lower surface

Ideal Case: $y = T_1 - T_4$
Real Case: $y = T_2 - T_3$
Performance: controlled by G_{yw}
Stability: controlled by G_{yu}

Plant Response - Reference Results Using Full Method

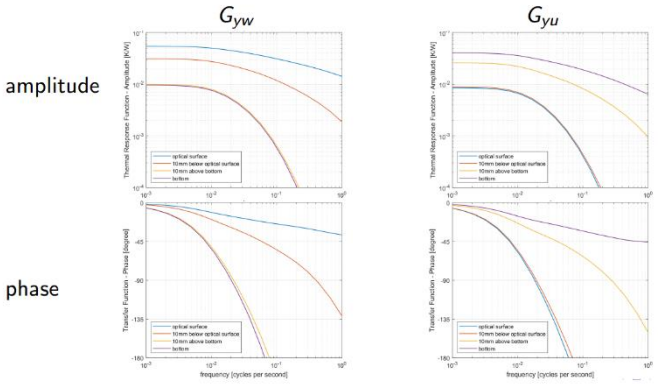

Results (1/5): Thermal Time Constants

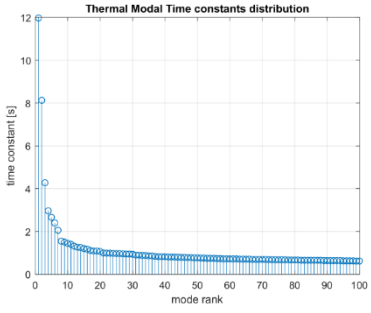

Desired controller bandwidth $[0 - 10^{-1}Hz]$

- retain modes with $\tau > 1.6s$, hence 20
- is that enough? too much?

Results (2/5) : First 6 Thermal Mode Shapes

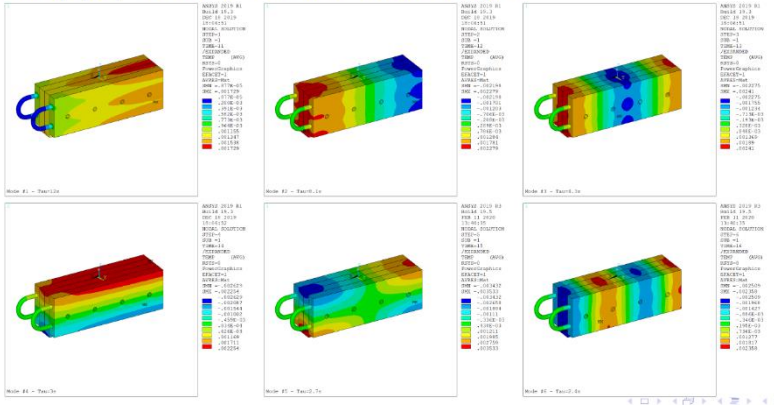

Results (3/5): Modal Method Convergence Rate

Static responses close to beam heat load

T_1

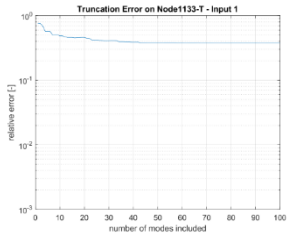

T_2

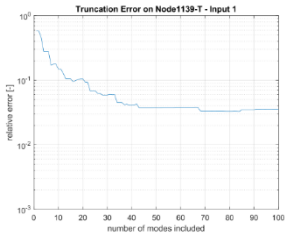

Close to heat load convergence is extremely slow: over 30% error with 100 modes included
Away from heat load convergence is faster

Brute force cannot be employed.

Results (4/5): Frequency Responses Compared

Direct vs Modal FRFs - Thermal probes at IDEAL positions

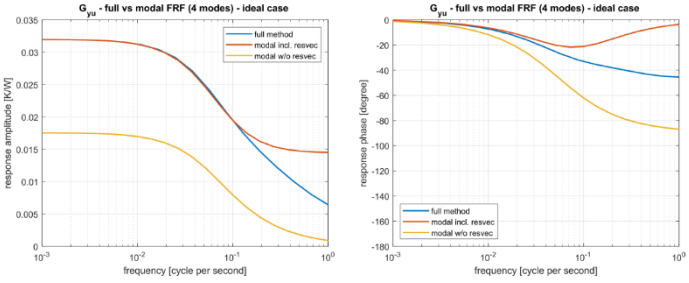

With residual vector, modal method yield exact results (±1dB).
Above cutoff frequency gain and phase are overestimated, though

Results (5/5): Frequency Responses Compared

Direct vs Modal FRFs - Thermal probes at REAL positions

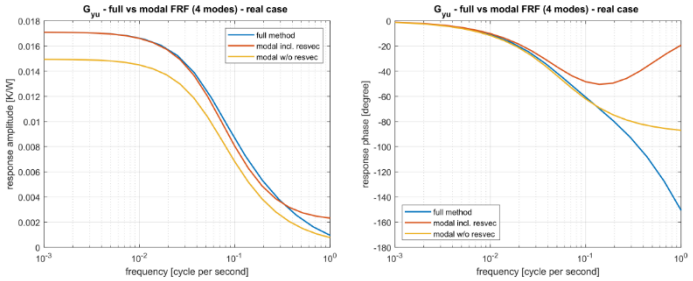

Again, modal method yield almost exact results
Above cutoff frequency phase becomes largely **overestimated**

Outline

Summary

Applicability and Benefits

For cases where *localized* thermal loads exist:

1. high spatial frequency thermal modes are excited
2. this requires including a very large number of modes to capture the local response
3. however, those modes have short time constants, hence respond quasi-statically
4. they can be lumped into a single, additionnal contribution, directly proportionnal to input, i.e. a residual vector
5. the modal basis can then be restricted to those modes that respond dynamically

In terms of state-space representation, this amounts to adding a feedthrough (D) term

Outlook

Possible evolutions

Functionnality:

- Performance: Gain can be accurately obtained, even with a small number of modes, so that controller performance estimates will be accurate
- Stability: phase is overpredicted at higher frequencies, hence stability *cannot* be guaranteed. This could be solved by replacing residual *vectors* by residual *modes*

Usability:

- Protoyping phase completed : APDL Math procedures perform Modal Analysis, Frequency Response, Residual Vector, State-Space Model creation
- Next step: Encapsulate as an add-on ("ACT App")

Questions ? Comments?

Outline

Thermal Modal Analysis

```
/SOLU
ANTYPE,MODAL,NEW ! Modal analysis
modopt,LANB,nbModes,-1e-6,1/(2*PI*SQRT(TauMin)),,OFF ! Normalize to
unit mass
*EIGEN,MatK,MatC,,EiV,MatPhiSolv
!  internal to Boundary conditions mapping
*MULT,Nod2Bcs,TRAN,MatPhiSolv,,MatPhi
!  Check mass normalization
*MULT,MatC,,MatPhiSolv,,APhi
*MULT,MatPhiSolv,TRANS,APhi,,PhiTMPhi
!  PRINT THIS MATRIX: IT SHOULD BE [I]
*PRINT,PhiTMPhi,PhiTMPhi.txt
```

Extracts nb modes with τ > TauMin

Estimate Generalized forces (Load vector)

```
!  Fi=matPhi x VecF
!  internal to Boundary conditions mapping
*MULT,MatPhiSolv,TRAN,vecF,,modalForcesVec
*IF,indLoad,EQ,1,THEN
*DMAT,modalForces,D,COPY,modalForcesVec
*ELSE
*MERGE,modalForces,modalForcesVec,indLoad,COL
*ENDIF
```

Fills the modalForces matrix with generalized forces (nbModesxnbLoad)

Residual Vectors (1/2)

```
*LSENGINE,BCS,MyBcsSolver,MatK
*LSFACTOR,MyBcsSolver
*do,indLoad,1,nbLoad *SMAT,vecF,D,IMPORT,MAT,RunThermalVecF%indLoad%
!  CONSTRUCT EXACT SOLUTION *LSBAC,MyBcsSolver,VecF,TBcsExact
*MULT,Nod2Bcs,TRAN,TBcsExact,,T_Exact
!  CONSTRUCT THE APPROXIMATE SOLUTION
*VEC,T_MODAL,D,ALLOC,T_EXACT_ROWDIM
*do,indMode,1,nbModes !  Extract one mode at a time
*VEC,currVec,D,LINK,MatPhi,indMode
*AXPY,TauArray(indMode)*modalForces(indMode,indLoad),0,currVec,1.,0,T_Modal
*enddo
```


Residual Vectors (2/2)

```
!  Estimate Error (=residual vector)
*VEC,T_RESVEC,D,ALLOC,T_EXACT_ROWDIM
*AXPY,1.,0.,T_EXACT,1.,0.,T_RESVEC *AXPY,-1.,0.,T_MODAL,1.,0.,T_RESVEC
*ENDDO
!  Store Residual Vector into matrix
*IF,indLoad,EQ,1,THEN *DMAT,T_RESVEC_MAT,D,COPY,T_RESVEC *ELSE
*MERGE,T_RESVEC_MAT,T_RESVEC,indLoad,COL
*ENDIF
```

Constructs Temperature Residual Vectors (nbNodesxnbLoad)

Special Interest Group Meeting on Thermal Issues
Laboratory for Machine Tools and Production Engineering (WZL) of
RWTH Aachen, Germany, February 2020
www.euspen.eu

Applied thermo-elastic model reduction

Walter Aarden[1], Björn Bukkems[1], Maurice Limpens[1] and Theo Ruijl[1]

[1]*MI-partners BV*

W.Aarden@mi-partners.nl

Abstract
Errors induced by thermal deformations, i.e. undesired deformations and/or relative displacement differences due to temperature fluctuations, are becoming one of the more significant contributions to the overall accuracy budget during the design of high precision equipment. In order to optimize the system design for performance, transient thermo-mechanical analyses are performed. However, these analyses can become computationally very expensive and thus time intensive. In order to accelerate this process, while retaining accurate models, model reduction techniques are used in practice. This paper presents a short overview of commonly used model reduction techniques for thermo-elastic systems and gives an insight on the advantages and the ease with which they can be applied in the actual development of high precision equipment. As an example an actual developed high precision stage is used, which has nanometre performance requirements.

Keywords: Thermal-elastic model, model order reduction, modal analysis, Krylov subspace method, design optimization.

1. Introduction

When accounting for thermal induced deformation errors, during the concept and/or design stage of the development of a high precision machine, transient simulations of thermal-mechanical models are needed. When thermal models become quite complex and when multiple variations of thermal loads need to be investigated, these simulations can become very computational expensive. To accelerate this process model reduction techniques are used.

The following section gives a very short overview of the mathematical framework together with commonly used reduced bases.

2. Model reduction framework and reduced bases

Given a full order model (FOM) Σ of a MIMO LTI system with N states, p inputs and m outputs:

$$\Sigma: \begin{cases} \boldsymbol{E\dot{x}(t) = Ax(t) + Bu(t)} \\ \boldsymbol{y(t) = Cx(t) + Du(t)} \end{cases} \quad (1)$$

Model reduction assumes that state trajectories, $\boldsymbol{x(t)}$ are contained in lower dimensional subspaces of size $\boldsymbol{k \ll N}$ and can be written as $\boldsymbol{x(t) = Vq(t)}$, with $\boldsymbol{V} \in \mathbb{R}^{N \times k}$, the reduced basis vector matrix and $\boldsymbol{q(t)} \in \mathbb{R}^{k}$, the reduced state vector. By applying the standard Galerkin projection [1, 2] the full order model $\boldsymbol{\Sigma}$ can be projected to a reduced order model (ROM) $\boldsymbol{\Sigma_k}$:

$$\Sigma_k: \begin{cases} \boldsymbol{\hat{E}\dot{q}(t) = \hat{A}q(t) + \hat{B}u(t)} \\ \boldsymbol{y(t) = \hat{C}q(t) + Du(t)} \end{cases} \quad (2)$$

With $\boldsymbol{\hat{E} = V^T EV, \hat{A} = V^T AV} \in \mathbb{R}^{k \times k}, \boldsymbol{\hat{B} = V^T B} \in \mathbb{R}^{k \times p}$ and $\boldsymbol{\hat{C} = CV} \in \mathbb{R}^{m \times k}$.

Most commonly used reduced basis vectors are the *eigenvectors* (modal method), *Krylov basis vectors* (moment matching method) of the system Σ or the basis vectors calculated from a proper orthogonal decomposition (POD) method. The POD method can be applied when the actual inputs of the system are well known and/or state-trajectory data is already available, see [1, 2].
Methods for solving the eigenvalue problem are standard available in e.g. Matlab, ANSYS and Comsol. However for the Krylov basis vectors or POD methods one has to implement the commonly available algorithms, see [2] for more details. In this paper only the application of eigenvectors and the Krylov basis are considered. The use of POD basis vectors will be a topic for another paper.

3. Thermo-mechanical case

As a case, an actual developed high precision positioning stage is considered. This stage, with a total mass of 6.2 kg, is part of a larger machine and its movement is limited to one direction only. The other degrees of freedom are constrained by means of 3 bearings and 2 guidance rails. The actuation, along the X direction, is performed by an ironless linear motor. See figures 1 and 3 for a more detailed overview.

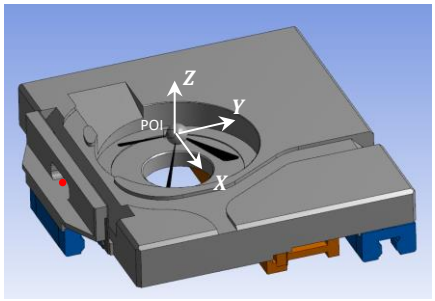

Figure 1: Top view model high precision positioning stage. Red dot indicates encoder location. Sphere at (0,0,0) of coordinate system is POI.

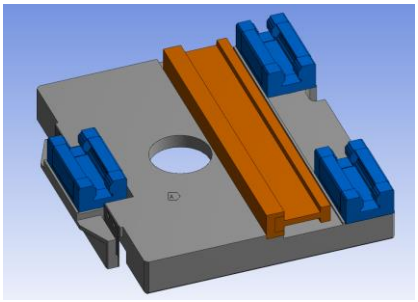

Figure 2: Bottom view model high precision positioning stage. Bearings are indicated in blue and the actuator is indicated in orange.

It is assumed that the stage is in ambient conditions at a nominal environment temperature of 22 $°C$. Faces in contact with air have appropriate convection boundary conditions, ranging from 2.5 – 5 W/m^2/K, depending on the face orientation. Additionally linearized radiation is taken into account, in the order of 0.6 – 1.5 W/m^2/K, as temperature offsets, due to heat loads are expected to be in the sub Kelvin range.

For this example two inputs are considered, i.e. the air temperature at the top surface (+Z side) of the stage and heat generation in the linear motor. However it is not uncommon to have a larger amount of inputs, i.e. $\mathcal{O}(10)$, can easily be incorporated in the framework. As for temperature outputs, the nodes on the outer faces of the large carrier part (grey coloured part in Figure 1 and 2) are used.

To assess the resulting thermal induced deformations, the displacement of a point-of-interest (POI) is considered in conjunction with constraints at the three bearings and in the encoder degree of freedom, i.e. along the X-axis. The POI can be seen in Figure 1, coinciding with the coordinate system and is rigidly connected to the stage. In this example it is assumed that the POI is thermally isolated from the stage.

4. Implementation and model reduction details

The finite element (FE) implementation, i.e. meshing, boundary conditions and contacts, is done using ANSYS and the model reduction steps are performed in an ANSYS/Matlab developed toolbox. The toolbox combines the efficient ANSYS solvers with the flexibility of Matlab.

The first input is heat generation in the linear motor and results from a $300\ mm$ scanning setpoint, i.e. the stage scans multiple times back and forth within a fixed time of $7.5\ s$. The maximum achieved velocity is $0.5\ m/s$ and has maximum acceleration levels of $22\ m/s^2$. This setpoint results in a maximum dissipating power of 225 W. In figure 3 the first two seconds of the heat generated in the linear actuator is shown.

As for the second input, the topside air temperature is stepped to 32$°C$ at the beginning of the simulation.

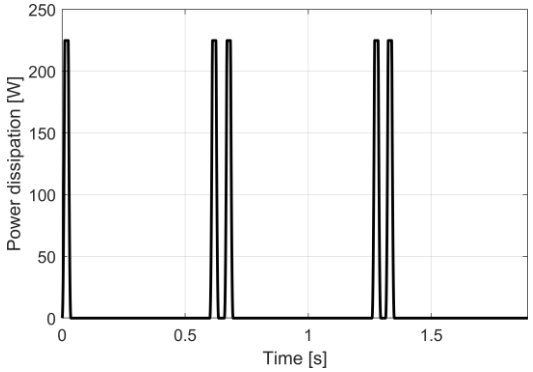

Figure 3: First two seconds of the actuator internal heat generation.

The defined inputs will be used for transient simulations of three systems, i.e. the FOM, the modal ROM and the Krylov ROM. Initially, a thermal simulation will be performed, which calculates temperature fields with a time-step of $1\ ms$. Next the thermally induced deformations, $\vec{d}(t)$, are calculated, by solving the following set of linear equations for each time step:

$$K_s\vec{d}(t) = K_{th}T_{FOM}(t) \tag{3}$$

with K_s the FE stiffness matrix, K_{th} the thermo-elastic coupling matrix and $T_{FOM}(t)$ the calculated FOM temperature field at time t. To be able to calculate the deformations for the ROMs, it is only necessary to calculate the so-called thermo-elastic basis vectors, V_d, which is found by solving a similar set of equations as (3), i.e.

$$K_sV_d = K_{th}V_{ROM} \tag{4}$$

with V_{ROM} the reduced, *modal* or *Krylov,* basis vectors. Note that by changing the output matric $\hat{C}$ of (2) to $\hat{C} = CV_d$, the reduced system Σ_k can calculate the deformations for any *other* given input and time. Giving a large flexibility in input variation/sensitivity analysis.

The size of the thermal ROMs is chosen by using a rule of thumb value of $k = 30$ per input for the Krylov method and $k = 120$ per input for the modal method. The reason the modal method requires a factor four more states, is slower error convergence for thermal systems than for the modal method than for Krylov based methods , see [1, p. 284]. Additionally, the modal method requires the use of residual vectors in order to compensate for relatively large DC errors. The effect of taking this correction into account will be shown in the next section.

Although the modal method requires a significantly larger order, the modal method is still a preferred method, due to the efficient calculation of the eigenvalue problem in FE packages. Furthermore, there is an intuitive physical interpretation of mode shapes and an extensive knowledge, toolboxes and experimental techniques are available originating from structural dynamic related problems.

5. Results and conclusions

First the impact on computational performance is considered and afterwards the accuracy of the ROMs are analysed.

Implementing the models with the inputs as described above, results in transient simulation timings given in Table 1. It can be seen that by applying model reduction, a computational performance increase for transient simulations of a factor $7\ (modal) - 117(Krylov)$ can be achieved. Also the timings for generating the ROMs are significant less when compared to performing one FOM simulation. Indicating that there is no significant impact on overall calculation timings when recalculating the ROM.

When considering the calculations of the deformations, the time for evaluating a data-set with 50 time-steps of the FOM or 50 basis vectors is approximately $28\ min$. Note that after generating the thermo-elastic basis vectors, V_d, every alternative input can be simulated efficiently. For the FOM, however, this would imply that the thermal transient and deformation calculations need to be redone completely, which will take approximately $50\ min$ per new loadcase.

Table 1. Overall timings for one transient thermal simulation, performed on an i7-7700HQ mobile workstation with 32 Gb RAM

Timings [s]	Full model N ≈ 240k	Modal k=240	Modal k=240 + residual vector correction	Krylov k=60
Basis vector calculation		148	148	21
Correction term		-	2.4	-
Projection + state space		0.2	0.5	0.7
Thermal Simulation	1290	181	187.4	11

To evaluate the accuracy of the ROMs the following spatial RMS error measure over time is used:

$$\varepsilon_{rms}(t) = \frac{\sqrt{\sum_{i=1}^{N_{nodes}}[T_{FOM}(i,t) - T_{ROM}(i,t)]^2}}{\sqrt{\sum_{i=1}^{N_{nodes}} T_{FOM}^2(i,t)}} \qquad (5)$$

with N_{nodes} the number of FE nodes, T_{FOM} and T_{ROM} the temperature of the FOM and respectively the ROM. Figure 4 shows $\varepsilon_{rms}(t)$ for the 3 different ROMS, i.e. modal, modal + residual vectors correction terms and the Krylov model. Figure 5 shows the relative spatial temperature error at the final simulation time ($t = 7.5\ s$).

It can be concluded that the Krylov method can very accurately estimate the temperature fields over space as well as time, i.e. $\varepsilon_{rms} < 0.04$ within 0.3 s. For this case it out performs the modal method. However the modal method is sufficiently accurate at the spots where there is a significant temperature offset from $22°C$. See e.g. the hot-spot at location $(x, y, z,) = (0, -0.15, 0.13)\ m$ in the top-left of figure 5. What is also interesting to note is that the addition of the residual correction vectors, significantly improves the accuracy of the modal method and that it should therefore be included when the actual inputs are known.

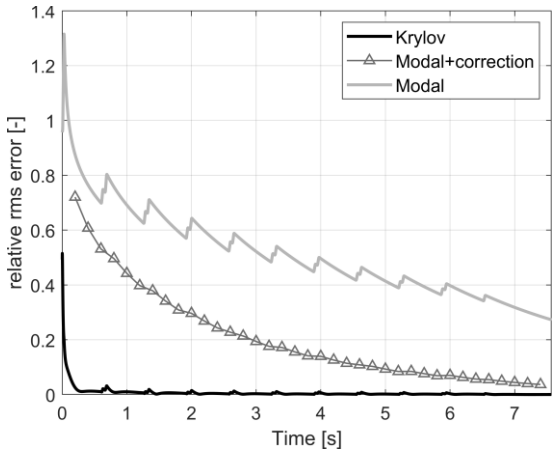

Figure 4. $\varepsilon_{rms}(t)$, relative RMS temperature error over time.

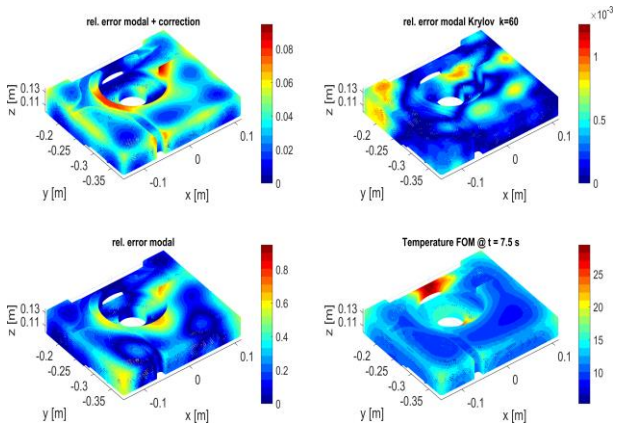

Figure 5. Relative temperature errors, compared to the FOM temperature field at t =7.5 s.

Finally the accuracy with regard to the POI deformations is shown in figure 6. In this figure the 2-norm of the calculated deformation vector over time is compared. These deformation calculations only take the first 50 basis vectors into account in order to limit the overall computation time. From figure 6 it can be seen that both reduction methods accurately (within 1 nm absolute difference) describe the POI thermally induced drift.

Note that for this case only a smaller subset of the reduced basis vectors is sufficient to accurately estimate the POI deformations and indicates that not all basis vectors contribute equally to the final deformation.

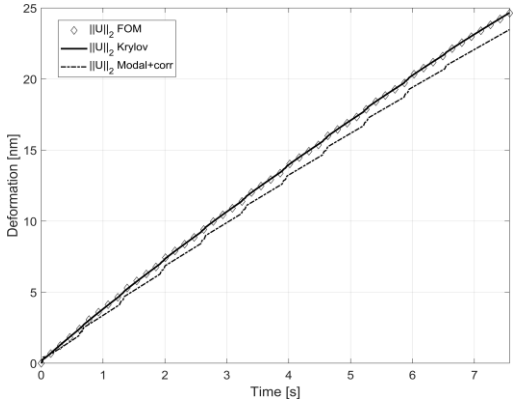

Figure 6. Norm of the POI deformations in [nm].

Current practical limitations of model reduction techniques are a lack of a-priori knowledge on what the accuracy will be, which basis vectors should be taken into account and which size of the reduced order should be chosen given a certain tolerance on allowed errors.

Taken these practical limitations into account, it can still be stated that using model reduction techniques in practice, the development high precision systems can be effectively and accurately be accelerated. Especially when used early on in the concept / design phase.

As a final note, one of the main benefits of using ROMs is the huge flexibility in applying input variations and different initial conditions. This flexibility is very helpful in determining critical sensitivities of the system and selecting the most demanding inputs for future analysis.

6. Future work

This paper only presented a short overview what can be achieved with model reduction techniques. Future work will focus more on the application of advanced model reduction related topics. These topics will go into more depth regarding automated reduced order selection, optimal selection of basis vectors for thermo-elastic deformations calculations and optimal sensor/actuator placement together with thermal error correction models, see e.g. [3].

References

[1] Antoulas A C 2005 Approximation of Large-Scale Dynamical System. *SIAM* Philadelphia PA

[2] Antoulas A C, Sorensen D C, Gugercin S 2000 A survey of model reduction methods for large-scale systems.

[3] Van der Sanden J, Philips P 2013 FEM model based POD reduction to obtain optimal sensor locations for thermo-elastic error compensation. *Proceedings of the 13th euspen International Conference*

Design Principles for Thermally Robust Production Equipment

Special Interest Group Meeting on Thermal Issues
Laboratory for Machine Tools and Production Engineering (WZL) of
RWTH Aachen, Germany, February 2020
www.euspen.eu

Methodology for thermal optimization of motor spindles

Berend Denkena[1], Benjamin Bergmann[1], Heinrich Klemme[1]

[1]*Institute of Production Engineering and Machine Tools (IFW), Leibniz Universität Hannover, 30823 Garbsen, Germany*

klemme@ifw.uni-hannover.de

Abstract

Heat losses in motor spindles lead to thermal loads and thus to undesired effects on the spindle performance. To minimize these effects, the development of spindles must ensure a thermally advantageous design. Nowadays, a variety of software tools exist to support the design process. In particular, simulation models based on the Finite Element Method (FEM) have become widely established. Some commercially available simulation software offer specific tools for time-efficient optimization of multi-physical tasks. This article describes a methodology for an iterative optimization of the thermal behavior of a newly developed motor spindle applying these tools. An initial spindle is modelled, parameterized and thermally advantageous modification potential is identified by means of a parameter correlation analysis. The spindle is thermally optimized by appropriate adjustments to the design. The validity of the simulation model is evaluated by comparing the simulation results with experimental data of prototype analysis. The experimental findings are used to improve the simulation model by applying a parameter optimization. Lastly, improvements that could be achieved in the scope of an exemplary design iteration applying this methodology are shown.

Keywords: Motor spindle, FE-simulation, Thermal optimization

1. Introduction

The achievable accuracy in machining is significantly affected by the thermal properties of main spindle drives [1]. Today, motor spindles with roller bearings are mainly used in industrial practice [2]. Due to the conversion of electrical energy into mechanical energy, electrical losses occur in the motor resulting in heat. Bearing and fluid friction causes additional thermal load, which has an effect on the spindle system [3].

The effects of thermal loads can already be counteracted during the development phase of a spindle by skilfully selecting the design parameters. The variety of possibilities for improving the thermal behavior and the design parameters to be varied is large. Due to the high complexity of modern motor spindles and a wide range of available design parameters and materials, the identification and derivation of suitable measures for improvements is not trivial. Although simple, linear correlations can be quantified by analytical approaches. Such approaches fail with increasing complexity of the system. An analytical description of the thermal behavior of modern high-performance spindles is therefore not possible [4]. Simulations based on the Finite Element Method (FEM) have become widely established as a supporting tool for designers. Modern FEM programs offer possibilities for time-efficient modelling of multi-physical correlations. The determination of realistic parameter values, as well as sufficient mesh quality and a suitable modelling approach, is a challenge when developing simulations. If, however, a thermal model of a spindle exists, it can be used to improve its design with regard to the desired target values.

The aim of this project is to increase the maximum rotational speed or the initial bearing preload. Therefore, the temperature differences between inner and outer rings of the front and rear fixed bearing ($d\vartheta$ (FB_f), $d\vartheta$ (FB_r)) must be reduced [4]. In many simulation programs, analysis and optimization tools are already integrated to treat these problems. By using these tools, complex correlations between parameters and their interactions can be identified. Genetic algorithms can also be used to solve multicriterial thermal optimization tasks [5, 6]. In [7], a self-developed FE algorithm is used to optimize the dynamic behavior of a motor spindle. In [6], a genetic algorithm for the identification of realistic heat transfer coefficients is used to improve the thermal simulation model of a motor spindle.

In this article, a novel approach for multicriteria thermal optimization of a motor spindle is presented. Optimization measures are derived using a correlation analysis. The optimization is carried out manually within the scope of this work. As stated in[6], an additional optimization of the FE-model is carried out to improve the model validity. This is done by using a genetic algorithm. An illustration of the optimized spindle can be seen in Fig. 1. This concept with integrated lamellar heat exchangers and heat pipes is also shown in [8].

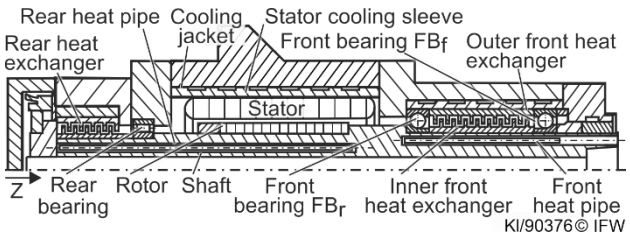

Figure 1. Considered spindle design according to Denkena et al. [8].

2. General approach

In the herein described design process, an initial spindle design is optimized in multiple design loops. The design loop is illustrated in Fig. 2. First, a primary CAD model of the spindle is geometrically simplified, so that a time-efficient meshing is possible for the next step. The model is then parameterized. During parameterization, thermal and mechanical boundary conditions are defined and modelled. In addition, material properties are associated to the bodies. Values of parameter inputs are determined analytically, experimentally and by considering tabular

data. The established simulation model is used to carry out a parameter correlation. This is done to quantify effects of model parameter value variations on the target parameter values ($d\vartheta(FB_f)$, $d\vartheta(FB_r)$). The results of this parameter correlation are used for the direct manual optimization of the spindle design. This allows an initial improvement to be carried out at an early stage. For the purpose of this article, one spindle design was also prototypically realized. This prototype is described and metrologically evaluated in [8]. In addition, results of the experimental analyses are used to verify the simulation model and to improve the validity of the model parameters. Model parameters with improved validity were determined by applying an optimization algorithm. The aim of this optimization was to achieve a better agreement between simulation results and experimentally determined values (model fitting). Based on the verified and fitted simulation model, subsequent design iteration could be simulated with increased validity. The process of spindle design optimization ends when certain target values of the target parameters ($d\vartheta(FB_f)$, $d\vartheta(FB_r)$) are reached or no significant optimization progress can be stated. In the following chapters, the individual steps of an exemplary design loop with prototype verification are explained in more detail.

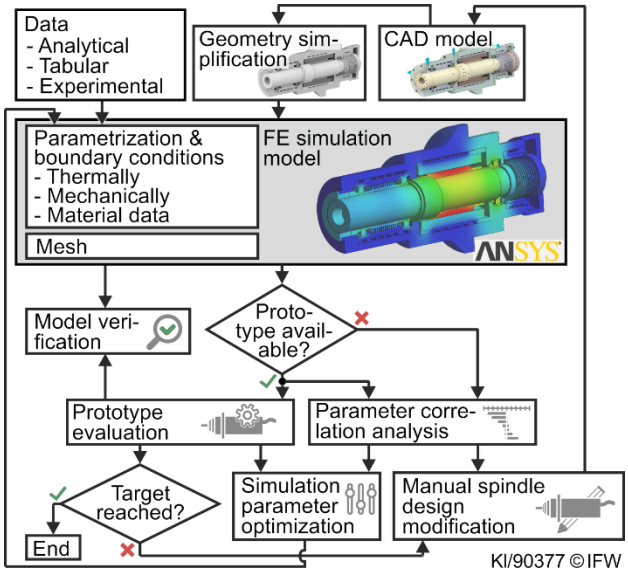

Figure 2. Process of spindle design optimization.

3. Simulation model

Simulations were carried out time-independently since only steady-state values were relevant. First, an initial CAD drawing of the spindle was geometrically simplified. This facilitated subsequent meshing and reduced the model size. During simplification, chamfers, undercuts, screw as well as through and blind holes were removed. Bearing rolling elements were modelled according to [9] as circumferential bodies. The sufficient meshing of bodies was ensured by a mesh study following the modelling and parameterization. The spindle was modelled according to [10]. Parameter values were determined according to Tab. 1. Analogy parameters were defined to simplify the parameterization. For example, material thermal conductivities were varied, instead of varying a body's wall thickness. A decrease of material conductivity led to a proportional decrease of thermal resistance. By reducing the length of heat transport by the same percentage, the same quantitative effect was achieved due to the linear correlation between thermal resistance and length of heat transport. Consequently, the influences of the spindle components' wall thicknesses could be evaluated by varying their materials' thermal conductivities instead of varying the geometry itself.

Table 1. Sources for the determination of parameter values.

Model parameter	Source
Convection at rotating cylinders, cooling channels, ambient	[11]
Convection in air gap of two cylinders	[12]
Convection at rotating discs	[13]
Convection on rolling bearing elements	[14, 15]
Heat transfer between bearing elements	[16]
Heat transfer coefficient, heat exchanger & conductivity heat pipes	experimental
Heat losses of bearings & motor	manufacturer
Heat transfer between solid bodies	[17, 18]

In consultation with the spindle manufacturer, variable design parameters and their value ranges were agreed according to this procedure. Tab. 2 summarizes some of these parameters and their values determined for one load case (20 000 rpm, idle run) according to Tab. 1. The heat transfer parameters were parameterized using an APDL script so that they could be used and varied for the following parameter correlation analysis and parameter optimization.

Table 2. Considered control parameters and initial values (20 000 rpm)

Nb.	Control parameter	Initial value
P1	Heat transfer coefficient inner lamellas – outer lamellas of heat exchanger front	185 W/m²/K
P2	Heat transfer coefficient outer front heat exchanger – outer bearing ring FB_r	5 200 W/m²/K
P3	Thermal conductivity heat pipes front	10 000 W/m/K
...	...	...
P41	Thermal conductivity material outer heat exchanger lamellas at front	120 W/m/K
P42	Thermal conductivity stator cooling sleeve material	43 W/m/K

4. Parameter correlation

The parameter correlation is based on the determination of the thermal transfer functions between individual control and target parameters. For this purpose, the value of each control parameter is varied around an initial value. The values of other parameters remain constant. The effect of this parameter value change on the target value change is then determined. The target parameters are given by $d\vartheta(FB_f)$ and $d\vartheta(FB_r)$. The control parameters and their initial values are defined according to Tab. 2. Within the scope of this work, the parameter correlation according to Pearson [19] is used. The Pearson correlation determines the magnitude of a linear correlation between two parameters. The determined significance S adopts values between -1 and +1. It is approximately 0 if there is no correlation at all. A negative value indicates a shift of the target parameter value to lower values due to an increasing control parameter value. An increase of the target parameter value due to an increasing value of the control parameter results in positive values of S.

Before the correlations are calculated, a lower and upper value limit (P_- and P_+) of the variation range must be defined for

each parameter. The range size $|P_+ - P_-|$ has significant influence on the results of the parameter correlation. It is particularly important to determine the initial parameter values as realistically as possible. If these are determined insufficiently, non-linear correlations between control and target parameters may result in considerably lower or higher significance of a control parameter than actually present. If the parameter values do not have to be defined stepwise due to technical reasons (e.g. number of heat pipes (see [8]), it is advisable to define relatively equal limits for each parameter [20]. For the purpose of this investigation, the initial values of each parameter were varied by ± 15% as this is the average expected inaccuracy of the parameter value determination. The prioritized target parameter in this work is $d\vartheta$ (FB_r) since the temperature rise of the inner ring of the fixed bearing close to the motor is particularly critical due to its proximity to the motor's secondary part. The number of applied samples for the correlation analysis is 100.

The results of the parameter correlation are shown as bar charts in Fig. 3. A significant decrease of both target values is achieved by increasing the value of design parameter P1 from P_- to P_+. This is indicated by the relative significances S which are -0.66 for FB_r and -0.36 for FB_f. Thus, an optimization of the heat transfer behavior of the fin-shaped heat exchangers leads to a significant decrease of the temperature differences as more heat is transferred from both inner bearing rings. Increasing P2 results in a comparatively high increase of 0.15 for $d\vartheta$ (FB_r). The effect of P2 on $d\vartheta$ (FB_f) is less significant. However, increasing P2 leads to lower values of $d\vartheta$ (FB_f). This is due to increased heat transport between the outer bearing ring of FB_r, which reduces the outer ring temperature of FB_r. However, this leads to an increased heating of the outer front heat exchanger. Hence, temperature difference between the outer front heat exchanger and the outer bearing ring of bearing FB_f is reduced. This in turn leads to a decrease of $d\vartheta$ (FB_f). Increasing the value of P3 leads to a significance of -0.13 for $d\vartheta$ (FB_r). The effect on $d\vartheta$ (FB_f) is negligible with a value of 0.02. Better heat conduction of the heat pipes results in increased heat transfer from FB_r in direction of FB_f. As a result, $d\vartheta$ (FB_r) is reduced and the front area of the spindle heats up. This leads to an increase of $d\vartheta$ (FB_f). Increasing the values of P41 and P42 leads to an increase of S and thus an increase of target parameter values. These effects, however, are minor.

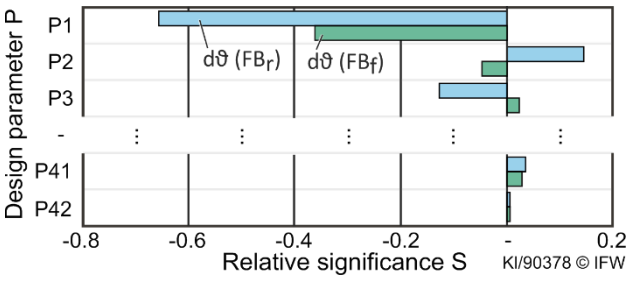

Figure 3. Parameter correlations with determined significances.

The results of this correlation analysis are used to derive measures for optimizing the spindle design. The adequate order of the optimization steps is based on the level of the determined significances. The optimization of a parameter with high significance is prioritized. However, the spindle designer must consider the degree to which a parameter value can be changed. Otherwise, inadequate changes of geometrical or material parameters may worsen the mechanical behavior. In addition, the manufacturability and assembling ability as well as other cost-related effects of design changes must be evaluated and taken into account by the designer.

5. Model fitting

The aim of the model fitting is to adjust the simulation parameters in such a manner that the simulated temperature values correspond as closely as possible to the measured temperatures. For this purpose, ANSYS provides a toolbox for handling multi-criteria optimization tasks. A particular challenge of parameterization is the dependency of parameters on mechanical and thermal load variations as well as variations of other boundary conditions [2]. The model fitting was therefore only carried out for the thermally most critical load case at 20 000 rpm.

Prior to optimization, the simulation parameters were parameterized so that they could be varied in the optimization algorithm. The procedure is similar to that of the correlation analysis in chapter 4. Instead of design parameters, however, thermal loads of the bearings and the motor as well as the convection coefficients values and heat transfer coefficients were varied. The thermal conductivities of the materials were also parameterized. For the optimization of the parameters, the genetic MOGA algorithm (multi-objective genetic algorithm) was applied. This algorithm was implemented in ANSYS. MOGA is a variant of the NSGA-II algorithm (non-dominated sorted genetic algorithm-II), based on the controlled elitism concepts [21]. By searching for global optima, several optimization goals can be defined.

In the simulation, temperature values were obtained as target values. These points correspond to the sensor locations in the experimental investigation of the spindle prototype. In the experimental analysis of the prototype, the temperatures of the bearing inner and outer rings were determined. The experimentally determined temperatures served as constraints for the optimization. The algorithm attempted to achieve the specified constraints by varying the parameter values within these limits. The principle of this optimization is shown in Fig.4.

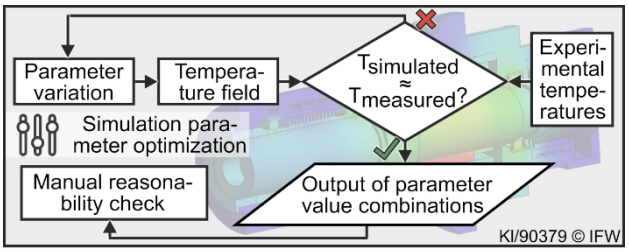

Figure 4. Simulation model optimization principle.

A range for each parameter, in which its values are to be varied, must be defined prior to optimization. The upper and lower limits of a parameter value result from uncertainties to be expected when determining the initial value. The limits of the parameter value ranges were defined by values of ± 30% of the initial value in this paper. By considering this comparatively wide range, possible global optima located further away from the previously determined parameter values were also taken into account. Otherwise, it is possible that the optimal approximation of actual parameter values could not be determined by the optimization algorithm. This may occur especially in cases where a precise determination of parameter values is difficult. Especially the convection boundary conditions of high-speed bearings and contact heat transfer parameter are difficult to determine [2]. As a result of the optimization, several parameter value combinations were obtained, achieving similar simulation results. If parameter values of different parameter value combinations are nearly similar, it can be assumed that these values are more likely to be physically valid. If individual or several values differ significantly, the relevance of the affected parameters must be

weighted and evaluated using a correlation analysis. Such a correlation analysis of the simulation parameters was carried out automatically in ANSYS during the optimization, analogous to chapter 4. If the parameter significance is high, the value determined by the optimization algorithm must be adjusted with higher priority to the respective optimized value. Consequently, deviations from values of a parameter with high significance lead to particularly high deviations between simulation and experiment. Parameters with low significances < ± 0.1 are not considered to optimize the model. Values of parameters with low significances vary when comparing different parameter sets and can often already be identified in this way. These parameters were kept to their previously determined values. Due to the widely selected value range of some parameters, individual parameters may dominate disproportionately. This makes it difficult to interpret the optimization results. Nevertheless, this procedure is particularly suitable for identifying parameters with very low significances.

6. Evaluation of the methodology

An initial spindle design was optimized in several steps according to the procedure described above. Fig. 5 illustrates the result of an exemplary optimization of a design i to a design i+1. A design i was initially used for the simulative evaluation of optimization measures. By simulating the load case at 20 000 rpm, the temperature differences (ϑ_i - ϑ_o, see Fig. 5 top) were determined with dϑ (FB_f) = 14.8 K and dϑ (FB_r) = 16.0 K. Based on the knowledge obtained from the simulations, the spindle design was then optimized by the spindle manufacturer. The optimized design i+1 was again simulatively evaluated and also prototypically realized. The metrological evaluation of the design i+1 can be found in [8]. The temperature differences of the design i+1 dϑ (FB_f) and dϑ (FB_r) were determined to be 7.5 K and 8.2 K, respectively. The results of the metrological analyses were used to validate the i+1 simulation model. The deviations between simulated and experimentally determined values were 1.7 K (dϑ (FB_f)) and 2.7 K (dϑ (FB_r)). So far, no model fitting has taken place. For this reason, the agreement between simulation and experiment is very good. The experimental results were used in the further course of the project to carry out a fitting according to chapter 5. The fitted model was then used for more precise simulation of further optimization potential. The methodology of further optimization steps is similar to those described in this article.

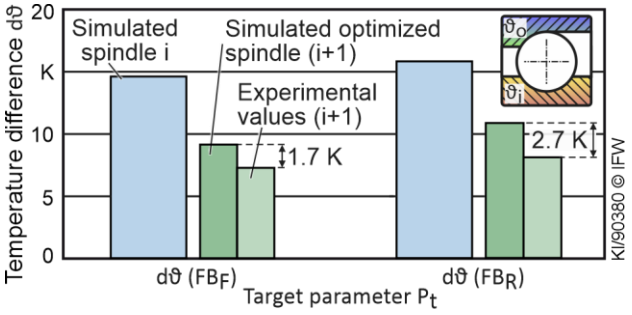

Figure 5. Evaluation of the simulation and optimization measures.

7. Conclusion and outlook

In this article, a methodical approach for the iterative thermal and thermo-elastic optimization of a motor spindle design was presented. With the help of an FE model and a parameter correlation analysis, parameters, which had significant effects on the defined target values, were first identified. These findings were used to optimize the design. In addition, the results of the parameter correlation were used to optimize the FE model. The optimization was carried out with the help of a multi-criteria optimization algorithm. Experimentally determined values of a prototype were used to define target functions for the algorithm. This fitting improved the validity of the model parameters and thus the interpretability of the simulated significances. This methodology was used to optimize the spindle shown in [8] so that the highest possible efficiency of the therein applied heat transfer elements was achieved. By applying this method, simulatively determined temperature differences between the bearing inner and outer rings of the front fixed bearing were reduced by 38% and those of the rear fixed bearing were reduced by 31%.

References

[1] Brecher C, Shneor Y, Neus S, Bakarinow K, Fey M 2015 Thermal Behavior of Externally Driven Spindle: Experimental Study and Modelling *Engineering* **7**(2) 73–92

[2] Abele E, Altintas Y, Brecher C 2010 Machine tool spindle units *CIRP Annals - Manufacturing Technology* **59**(2) 781–802

[3] Gebert K 1997 Ein Beitrag zur thermischen Modellbildung von schnelldrehenden Motorspindeln *Darmstädter Forschungsberichte für Konstruktion und Fertigung* Dr.-Ing. Diss. Technische Hochschule Darmstadt (Shaker)

[4] Tüllmann U 1999 Das Verhalten axial verspannter schnelldrehender Schrägkugellager *Berichte aus der Produktionstechnik* Dr.-Ing. Diss. RWTH Aachen (Shaker)

[5] Gosselin L, Tye-Gingras M, Mathieu-Potvin F 2009 Review of utilization of genetic algorithms in heat transfer problems *International J. of Heat and Mass Transfer* **52**(9-10) 2169–2188

[6] Tan F, Yin Q, Dong G, Xie L, Yin G 2017 An optimal convective heat transfer coefficient calculation method in thermal analysis of spindle system *Int J Adv Manuf Technol* **91**(5-8) 2549–2560

[7] Maeda O, Cao Y, Altintas Y 2005 Expert spindle design system *International J. of Machine Tools and Manufacture* **45**(4-5) 537–548

[8] Denkena, B, Bergmann, B, Klemme, H, Dahlmann, D 2018 Cooling Potential of Heat Pipes and Heat Exchangers Within a Machine Tool Spindle in Ihlenfeldt S, Brecher C, Putz M, Billington D (Eds.) *Conference on Thermal Issues in Machine Tools: Proceedings CIRP* Dresden 2018 1st ed. Auerbach/Vogtland (Wiss. Scripten) 295–305

[9] Hu J, Uhlmann E (Eds.) 2014 Modellierung und Simulation des thermischen Verhaltens einer Werkzeugmaschine mit der Finite-Elemente-Methode *Berichte aus dem Produktionstechnischen Zentrum Berlin* Dr.-Ing. Diss. Fraunhofer IPK Berlin (Fraunhofer)

[10] Uhlmann E, Hu J 2012 Thermal Modelling of a High Speed Motor Spindle *Procedia CIRP* **1** 313–318

[11] VDI-Gesellschaft Verfahrenstechnik und Chemieingenieurwesen 2013 *VDI-Wärmeatlas: 11th ed*. Berlin (Springer Vieweg)

[12] Tachibana F, Fukui S, Mitsumura H 1960 Heat transfer in an annulus with inner rotating cylinder *Bulletin of JSME* **3**(9) 119–123

[13] Kreith F 1969 Convection Heat Transfer in Rotating Systems Advances in *Heat Transfer* **5** 129–251

[14] Harris T A 2001 *Rolling bearing analysis*. 4th ed. New York (John Wiley & Sons)

[15] Zahedi A, Movahhedy M R 2012 Thermo-mechanical modeling of high speed spindles. *Scientia Iranica* **19**(2) 282–293

[16] Muzychka Y S, Yovanovich MM 2001 Thermal Resistance Models for Non-Circular Moving Heat Sources on a Half Space *J. Heat Transfer* **123**(4) 624–632

[17] Yovanovich M M 1981 New Contact and Gap Conductance Correlations for Conforming Rough Surfaces *AIAA 16th Thermophysics Coference* Palo Alto CA, June 23-25

[18] Zhao H L, Huang Y M, Xu, J L, Jiang, L Y, Zhang, W H, Sheng, B H 1999 Experiment Research on Thermal Contact Resistance of Normal Used Joints *J. of Xi'an University of Tech.* **15**(3) 26–29

[19] Akoglu H 2018 User's guide to correlation coefficients *Turkish J. of emergency medicine* **18**(3) 91–93

[20] Siebertz K, van Bebber D, Hochkirchen T 2010 *Statistische Versuchsplanung: Design of Experiments (DoE)* Heidelberg (Springer)

[21] Deb K, Pratap A, Agarwal S, Meyarivan T 2002 A fast and elitist multiobjective genetic algorithm: NSGA-II. *IEEE Trans. Evol. Computat* **6**(2):182–197

Special Interest Group Meeting on Thermal Issues
Laboratory for Machine Tools and Production Engineering (WZL) of
RWTH Aachen, Germany, February 2020
www.euspen.eu

Thermal stabilization of ultraprecision turning machines

Jan Behrens[1], Christian Wenzel[1]

[1]*Innolite GmbH*

jan.behrens@innolite.de

Abstract

For the production of optics with form errors below 100 nm, single point diamond turning machines require extremely stable temperatures within their key components. These key components include all parts that are relevant for positioning of the tool or the workpiece, namely the machine bed, the linear axes, and the main spindle. The design goal of the Innolite IL300 turning machine is to achieve a temperature stability of under ±0.1°C in all key parts. Reasonable operating conditions, which take into account a warm-up process and preconditioning of the outside temperatures (room, cooling water) to ±1°C, are presupposed. The envisaged ten-fold thermal stabilization requires a dedicated system which protects the temperature sensitive machine parts by providing continuous flows of temperature-controlled air, oil and water. For this purpose, the IL300 follows a thermally robust mechanical design. The granite machine bed, the hydrostatic linear axes, and the aerostatic main spindle are all protected by at least one cover structure from environmental changes. The two-level cascade temperature control system also focuses on robustness. First of all, external circuits with low precision mixing valves reduce the temperature variation of externally provided cooling water down to ±0.1°C. Internal circuits then use this pre-conditioned water to continuously provide air, water and oil flows with a much higher precision of ±0.01°C. This paper describes the general design as well as a detailed performance analysis of all subsystems

Accuracy, Machine, Temperature

Temperature Measurement & Control

Special Interest Group Meeting on Thermal Issues
Laboratory for Machine Tools and Production Engineering (WZL) of
RWTH Aachen, Germany, February 2020
www.euspen.eu

Input-Output Linearized Control of a Thermoelectric Actuator using an Extended Kalman Filter Observer

Koen Bos[1], Dennis Heck[2], Robert van der Kall[2], and Marcel Heertjes[3]

[1]*ASML, Development & Engineering, Thermal Architecture EUV Scanner*
[2]*ASML, Development & Engineering, Thermal Architecture DUV Scanner*
[3]*Eindhoven University of Technology, Mechanical Engineering, Dynamics & Control*

Corresponding author: koen.bos@asml.com

Abstract
In ASML's wafer scanners, thermal management is becoming increasingly important as a result of Moore's law driving the performance and throughput requirements. To this end, thermoelectric modules (TEMs) or Peltier elements are increasingly considered in active control of the temperature of several wafer scanner modules. TEMs are thermal actuators that have the appealing property that they are able to both cool and heat. As a disadvantage, the thermal dynamics of a TEM are nonlinear, which complicates the control design for thermoelectric systems. Due to the inherent nonlinearity, the input-output response varies significantly for different setpoints and operating conditions. This complicates the controller tuning for desired performance and compromises closed-loop stability properties for, e.g., unreachable setpoints or (unknown) disturbances, possibly causing machine downtime and damage. To deal with these problems, an input-output linearizing controller in conjunction with a linear (e.g. PID) controller is used. More specifically, to eliminate the need for temperature sensors, that might limit the thermal efficiency and performance of the actuator, we propose to use an observer to estimate the temperatures required for the IO linearization.

Thermal Control, Thermoelectric modules, Nonlinear control, Feedback Linearization, Observer

1. Introduction

In advanced lithography systems that are used to manufacture integrated circuits (ICs) (see Figure 1), thermal management in terms of accurate temperature control becomes increasingly important. For next-generation thermal conditioning, active methods using thermoelectric modules (TEMs) are receiving increased attention. TEMs are solid-state thermal actuators that use the Peltier effect to transfer heat. These actuators are broadly applied in temperature control applications, e.g. lab-on-a-chip applications, laser diodes, and scanning electron microscopes [1, 2]. Unfortunately, the thermal dynamics of TEMs are highly nonlinear [2], which complicates control design for these actuators.

To address this problem, several approaches have been studied in literature. In [1], an input-output (IO) linearizing controller is proposed, which is able to deliver fast and accurate closed-loop control of a thermoelectric system. However, stability of this controller is not guaranteed *a priori*. In another approach, a nonlinear Lyapunov-based controller is used to control a thermoelectric system with guaranteed stability [3]. However, closed-loop performance in terms of settling time, rise time, and overshoot may be difficult to guarantee, because of the nonlinear nature of the controller.

To deal with these problems, Bos *et al.* propose to use an input-output (IO) linearizing controller in conjunction with a Lyapunov-based saturation function in a generic control application of a TEM [4]. This control architecture enables linear closed-loop behaviour with a well-defined performance for nominal operating conditions, and guarantees input-to-state stability (ISS) outside these nominal operating conditions. This approach requires state knowledge pertaining to the temperatures of both sides of the TEM. Temperature sensors are placed directly on the TEM, but this introduces an additional thermal resistance between the TEM and the conditioned object on one side and the cooling water on the other side. This additional thermal resistance limits the achievable energy efficiency, and hence, the achievable performance of the TEM.

To overcome this problem, we propose to use an extended Kalman filter (EKF) to estimate the required states for the IO linearization. This eliminates the need for sensors placed directly on the TEM. As such, the first key contribution is the design of the EKF for a nonlinear thermoelectric system. The second contribution is the implementation and verification of the results on an experimental setup.

The remainder of this abstract is organized as follows. Section 2 introduces the system at hand and summarizes the control architecture proposed in [4], as it forms the basis for this work. Section 3 presents the observer design for the thermoelectric system. Section 4 shows experimental results obtained from an experimental setup. Finally, Section 5 presents concluding remarks and recommendations for further research.

Figure 1. ASML's EUV System

2. System Description

In accordance with [4], an experimental setup is considered that resembles a simplified thermal control application in a wafer scanner, as illustrated in Figure 2 and Figure 3.

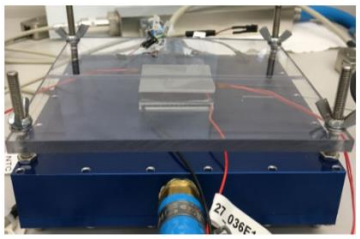

Figure 2. Experimental thermoelectric setup [4].

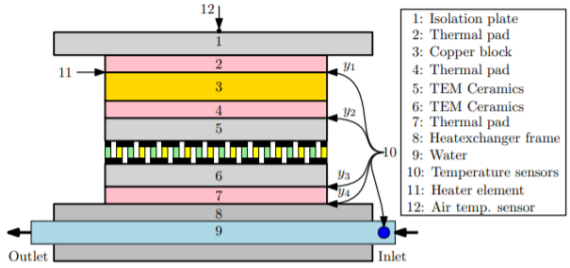

Figure 3. Schematic of the experimental thermoelectric setup [4].

2.1. Experimental Setup

The setup consists of a copper block (element 3 in Figure 3) attached to a thin film heater (element 11) that resembles a heat dissipating module, a thermoelectric module (type UWE UEPT-140-127-036E120) (element 5,6) used as a thermal actuator to condition the copper block, a heat exchanger (element 8) connected to a cooling water circuit (element 9) to remove waste-heat from the system. These components are assembled using thermal pads (element 2,4,7). The top plate (element 1) is used for assembly purposes. In the setup, four negative temperature coefficient (NTC) sensors are located between components of the setup (y_1 to y_4 in Figure 3), and two NTC sensors are used to measure the inlet water temperature of the heat exchanger and the surrounding air temperature, respectively.

2.2. Thermal Dynamics & IO linearization

The setup is modelled using a lumped mass approach, resulting in the following set of ordinary differential equations (ODEs):

$$\begin{aligned}
E_1\dot{x}_1 &= \frac{1}{R_{12}}(x_2 - x_1) + \frac{1}{R_\infty}(w_2 - x_1)\\
E_2\dot{x}_2 &= \frac{1}{R_{12}}(x_1 - x_2) + \frac{1}{R_{23}}(x_3 - x_2)\\
E_3\dot{x}_3 &= \frac{1}{R_{23}}(x_2 - x_3) + \frac{1}{R_{34}}(x_4 - x_3) + w_3\\
E_4\dot{x}_4 &= \frac{1}{R_{34}}(x_3 - x_4) + \frac{1}{R_{45}}(x_5 - x_4)\\
E_5\dot{x}_5 &= \frac{1}{R_{45}}(x_4 - x_5) + \frac{1}{R_{56}}(x_6 - x_5) + u^2R_e/2 - Sx_5u\\
E_6\dot{x}_6 &= \frac{1}{R_{56}}(x_5 - x_6) + \frac{1}{R_{67}}(x_7 - x_6) + u^2R_e/2 + Sx_6u\\
E_7\dot{x}_7 &= \frac{1}{R_{67}}(x_6 - x_7) + \frac{1}{R_{78}}(x_8 - x_7)\\
E_8\dot{x}_8 &= \frac{1}{R_{78}}(x_7 - x_8) + \frac{1}{R_{89}}(x_9 - x_8)\\
E_9\dot{x}_9 &= \dot{m}c_w(w_1 - x_9) + \frac{1}{R_{89}}(x_8 - x_9),
\end{aligned} \tag{1}$$

with $x_i, i \in \{1,2,\dots,9\}$ representing the temperatures of the lumped elements in Figure 3, E_i the thermal capacitance of the elements, $R_{i,i+1}$ the thermal resistances between elements, R_∞ the thermal resistance between the surrounding air and the top plate. These parameters are calibrated using a dedicated experiment, see [4] for the details. Furthermore, w_1 is the temperature of the water at the inlet of the heat exchanger, w_2 the surrounding air temperature, w_3 the thermal power of the thin film heater (representing thermal disturbance loads), $\dot{m}$ the mass flow of the water, and c_w the specific heat capacity of the water. Finally, S represents the Seebeck coefficient, u the applied electric current, and R_e the electrical resistance of the TEM. The control output y is the temperature of the copper block measured by the sensor y_1 (see Figure 3), and is defined as

$$y = y_1 = \alpha_1 x_2 + (1 - \alpha_1)x_3, \tag{2}$$

with α_1 a scaling factor to account for the fact that the sensor is located in between element 2 and 3.

In (1) the (input) nonlinearity is clearly visible in the terms containing u^2 and x_5u and x_6u, that relate to the Joule heating effect and Peltier and Seebeck effect of the TEM [2, 4]. To overcome the nonlinearity between the input u and the output y, the IO linearization as proposed in [4] is considered with a newly defined input:

$$v = \frac{1}{R_{56}}(x_6 - x_5) - Sx_5u + u^2R_e/2. \tag{3}$$

After substitution of the new input v of (3) in (1), the IO dynamics of the system can be written as

$$\begin{aligned}
E_1\dot{x}_1 &= \frac{1}{R_{12}}(x_2 - x_1) + \frac{1}{R_\infty}(w_2 - x_1)\\
E_2\dot{x}_2 &= \frac{1}{R_{12}}(x_1 - x_2) + \frac{1}{R_{23}}(x_3 - x_2)\\
E_3\dot{x}_3 &= \frac{1}{R_{23}}(x_2 - x_3) + \frac{1}{R_{34}}(x_4 - x_3) + w_3\\
E_4\dot{x}_4 &= \frac{1}{R_{34}}(x_3 - x_4) + \frac{1}{R_{45}}(x_5 - x_4)\\
E_5\dot{x}_5 &= \frac{1}{R_{45}}(x_4 - x_5) + v.
\end{aligned} \tag{4}$$

The remaining nonlinear zero-dynamics are then constituted by

$$\begin{aligned}
E_6\dot{x}_6 &= \frac{1}{R_{56}}(x_5 - x_6) + \frac{1}{R_{67}}(x_7 - x_6) + u^2R_e/2 + Sx_6u\\
E_7\dot{x}_7 &= \frac{1}{R_{67}}(x_6 - x_7) + \frac{1}{R_{78}}(x_8 - x_7)\\
E_8\dot{x}_8 &= \frac{1}{R_{78}}(x_7 - x_8) + \frac{1}{R_{89}}(x_9 - x_8)\\
E_9\dot{x}_9 &= \dot{m}c_w(w_1 - x_9) + \frac{1}{R_{89}}(x_8 - x_9),
\end{aligned} \tag{5}$$

with u the linearizing control law (following from (3)) as

$$u = \frac{Sx_5 - \sqrt{S^2x_5^2 - 2R_e(\frac{1}{R_{56}}(x_6 - x_5) - v}}{R_e}. \tag{6}$$

This control poses a lower-limit on the allowed input v, as to guarantee that the input u remains real-valued, or

$$v \geq \frac{1}{R_{56}}(x_6 - x_5) - \frac{S^2x_5^2}{2R_e}. \tag{7}$$

Physically, this lower bound is the maximum possible cooling power the TEM, that depends on the temperatures of the cold and hot-side of the TEM (x_5 and x_6, respectively). For this reason, it is important to ensure input-to-state stability of the nonlinear differential equations in (5), as to prevent the state x_6 from becoming too large and consequently limiting the cooling power of the TEM through (7).

2.3. Control Architecture

In [4], the linearizing control law (6), is implemented in a control loop in combination with a saturation function Φ and linear feedback controller C_{fb}, as shown schematically in Figure 4. The saturation function ensures that the computed control

input by the feedback controller $\bar{v}$ stays within predetermined Lyapunov-based bounds, or

$$\Phi: \quad v = min\{max\{\bar{v}, \beta_2\}, \beta_3\}, \tag{8}$$

with β_2 and β_3 bounds derived from a Lyapunov stability analysis. This effectively guarantees input-to-state stability of the closed-loop system, while allowing for linear closed-loop IO behaviour in normal operating conditions.

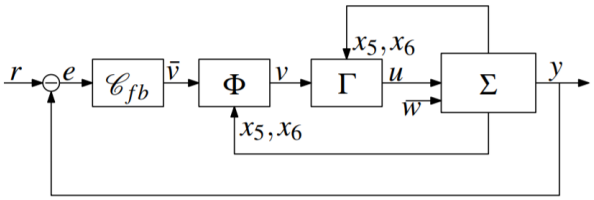

Figure 4. Schematics of the IO linearizing controller architecture [4].

3. Observer

As shown in Figure 4, the IO linearizing controller Γ and the saturation function Φ require state knowledge of x_5 and x_6 (the TEM temperatures). In [4], sensors are used to measure these states, but this sensor placement negatively affects the contact resistance and thus the thermal performance.

As a solution to this problem, an observer will be used to estimate the required states, using only sensors y_1 and y_4 that are not attached to the TEM, but are usually already available for diagnostics and feedback control. Furthermore, we consider the known inputs of the system to be the electric current u, inlet water temperature w_1 and air temperature w_2. The heat load of the heater is considered as an unknown disturbance w_3.

With this, system (1) is written in state-space formulation according to

$$\Sigma: \begin{cases} \dot{x} = F(x, u, w) \\ y = Cx + \eta \end{cases} \tag{9}$$

with $y = [y_1 \quad y_4]^T$ the measurements of the connected sensors, $w = [w_1 \quad w_2 \quad w_3]^T$ the disturbances acting on the system and η representing measurement noise. Note that $F(x, u, w)$ represents the equations in (1).

3.1. Extended Kalman Filter

The extended Kalman filter (EKF), which is commonly used in nonlinear state estimation, is known to deliver accurate results for temperature estimation [5]. The continuous-time EKF for the system (9) reads

$$\hat{\Sigma}: \begin{cases} \dot{\hat{x}} = F(\hat{x}, u, \hat{w}) - K(t)(C(x - \hat{x}) + \eta) \\ K(t) = P(t)C^T R^{-1} \\ \dot{P} = A(t)P + PA^T(t) - PC^T R^{-1} CP + Q, \end{cases} \tag{10}$$

with $\hat{x}$ the state estimate, $\hat{w} = [w_1 \; w_2 \; 0]^T$ the measured (known) disturbances, $K(t)$ the time-varying Kalman gain, $P(t)$ the estimated error covariance, Q and R tuning matrices, and $A(t)$ a linearization of the process $F(\hat{x}, u, \hat{w})$, which is defined as

$$A(t) = A(u(t)) = \frac{\partial F(x, u, w)}{\partial x} = \frac{\partial F(\hat{x}, u, w)}{\partial \hat{x}}. \tag{11}$$

Note that the resulting matrix $A(t)$ only depends on $u(t)$ and does not depend on x nor $\hat{x}$. Therefore, the linearization of F around $\hat{x}$ is equal to the linearization of F around x, as stated in (10). Exploiting the latter, stability of the EKF itself can be shown by means of Lyapunov theory. To this end, consider the Lyapunov function candidate

$$V = \epsilon^T P(t)^{-1} \epsilon, \tag{12}$$

with $\epsilon = x - \hat{x}$ the estimation error and $P(t)^{-1}$ the inverse of the error covariance matrix. The time-derivative of this Lyapunov function can be expressed as

$$\begin{aligned} \dot{V} \leq & -\epsilon^T (P^{-1} Q P^{-1} + C^T R^{-1} C)\epsilon + 2\epsilon^T P^{-1} B_d (w - \hat{w}) \\ & + 2\epsilon^T P^{-1} P C^T R^{-1} \eta \end{aligned} \tag{13}$$

with $B_d = \partial F / \partial w$. By using the fact that $\dot{P}^{-1} = -P^{-1}\dot{P}P^{-1}$ and $C^T R^{-1} C \geq 0$, and substituting (12) into (13):

$$\begin{aligned} \dot{V} &\leq -\frac{\underline{q}}{\bar{p}^2}\|\epsilon\|^2 + \frac{2}{E_3 \underline{p}}\|\epsilon\|\|w_3\| + \frac{2\bar{c}}{\underline{r}}\|\epsilon\|\|\eta\| \\ &\leq -\frac{\underline{q}\underline{p}}{\bar{p}^2} V + \frac{2}{E_3 \underline{p}}\sqrt{\bar{p}V}\|w_3\| + \frac{2\bar{c}}{\underline{r}}\sqrt{\bar{p}V}\|\eta\|, \end{aligned} \tag{14}$$

with $\underline{q}, \underline{p}, \underline{r}$ (norm-based) lower bounds on the matrices Q, P and R, and $\bar{p}, \bar{c}$ (norm-based) upper bounds on the matrices P and C, respectively. Using a new function $W = \sqrt{V}$, analogous to [6], the following bound on the estimation error can be derived from (14):

$$\begin{aligned} \|\epsilon(t)\| \leq & \sqrt{\frac{\bar{p}}{\underline{p}}}\|\epsilon(0)\| e^{-\theta t} + \frac{\bar{p}}{\theta E_3 \underline{p}}\left(1 - e^{-\theta t}\right) \sup_{t \geq t_0} w_3(t) \\ & + \frac{\bar{c}\bar{p}}{\theta \underline{r}\underline{p}}\left(1 - e^{-\theta t}\right) \sup_{t \geq t_0} \eta(t), \end{aligned} \tag{15}$$

with $\theta = \underline{q}\underline{p}/2\bar{p}^2$. With this bound, the EKF is concluded to be input-to-state stable in the presence of the unknown disturbance $w_3(t)$ and measurement noise $\eta(t)$.

3.2. Implementation

The EKF in (10) is used in closed-loop with the control architecture from [4], as illustrated in Figure 5. The estimated states $\hat{x}$ that are computed by the EKF, are used as inputs to the IO linearizing controller Γ and the saturation function Φ. In linear systems, the separation principle guarantees stability for a closed-loop system with a separately designed stable observer and controller. However, for nonlinear systems, the separation principle often does not hold [7], meaning that stability cannot be automatically concluded when using a stable EKF for closed-loop control. In [8], a separation principle for a class of nonlinear systems is presented. However, the method used in [8] requires that the control law is continuously differentiable, which is in this case not applicable because of the saturation function Φ. In [9], an analysis is conducted on closed-loop stability of a system under EKF-based feedback, however, the analysis used is limited to systems that can be written in a special normal form, which is found not possible in this case. In the remainder of this work, closed-loop stability is assumed and verified experimentally in the next section.

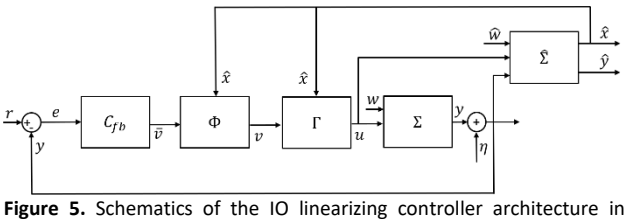

Figure 5. Schematics of the IO linearizing controller architecture in conjunction with the extend Kalman filter.

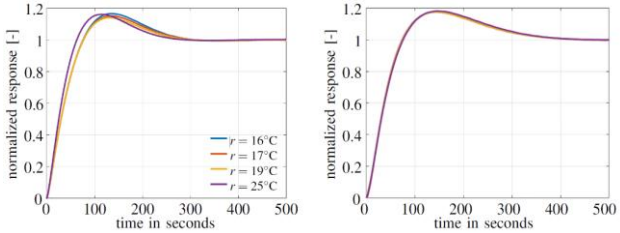

Figure 6. Measured (normalized) closed-loop step responses with a PID controller (left) [4], and the responses with IO linearization and EKF (right).

4. Measurement Results

To verify the obtained results in this work, an experiment is conducted by varying the setpoint temperature and using the estimated state by the EKF in the IO linearization. Analogous to [4], Figure 6 depicts the *normalized* step response without (left) and with (right) IO linearization. From this figure, it is observed that the estimation error of the EKF has little impact on the linearization of the IO dynamics, because all responses in the right plot are identical.

To verify the closed-loop stability of the system as a whole, a second experiment is conducted by applying a heat-load of $w_3(t)$ =12W with the heater, and commanding an unreachable setpoint of $r = -20$ °C, similar to the experiment conducted in [4]. This experiment does not come with any stability guarantees, but the closed-loop system is still found to be stable, as shown in Figure 7. In the left part of Figure 7, the outputs y_1 and y_4 are shown. The output y_1 is controlled toward the setpoint $r = -20$ °C, but this temperature cannot be reached, because of the applied heat-load and the limitations of the TEM. As also shown in [4], this situation would lead to instability if only a PID controller would be used. However, the stability bound β_2 limits the input $\bar{v}$ (as computed by the linear controller C_{fb}) and applies a limited input v to ensure stability, as shown in the right part of Figure 7.

By comparing this result to the results depicted in Figure 8 as obtained from [4], it can be concluded that the performance with the EKF exceeds the performance (in terms of reachable temperature y_1) of using sensors to estimate the required state variables x_5 and x_6. It is worth noting that, although not used, the sensors y_2 and y_3 are still physically present in the setup, in order to make a fair comparison to the results obtained in [4].

It is assumed that the difference in performance is due to the location of the sensors (in between elements) and that they therefore do not exactly measure the states they are assumed to represent. This, in turn, would lead to a larger error than the error of the state estimation by the EKF. This larger error caused by the sensor placement leads to a more conservative bound β_2, such that less cooling power is available when compared to using the EKF. This can partly be explained by the performed calibration of model parameters in [4], where an accurate match is obtained between measurements and model simulations. The model-based EKF naturally benefits from this calibration of parameters.

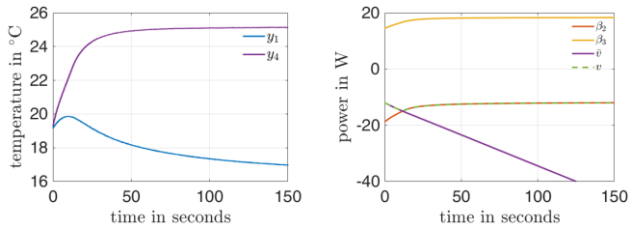

Figure 7. Measured output (left) and input bounds (right) of the experiment with the EKF and the nonlinear controller obeying the bounds $\beta_2(\hat{x}_5, \hat{x}_6), \beta_3(\hat{x}_5, \hat{x}_6)$.

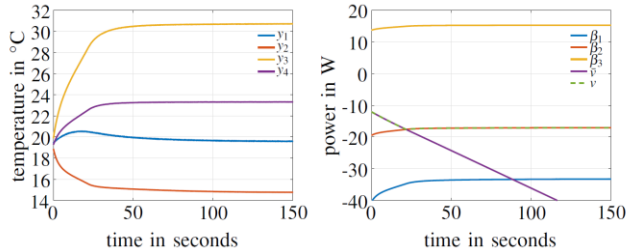

Figure 8. Measured output (left) and input bounds (right) of the experiment without EKF [4] .

5. Conclusions and Recommendations

For a thermoelectric system, this paper demonstrates the successful design and implementation of an extended Kalman filter with the IO linearizing control architecture proposed in [4]. The observer eliminates the need for sensors to be attached to the TEM, which otherwise limits performance. The estimated states can directly be used in the IO linearizing controller and saturation function. In the conducted experiment, the achieved performance supersedes the performance obtained in [4], in which sensors are used instead of an observer. This performance increase is attributed to the accuracy of the state-estimation by the EKF, because the unused sensors (that are attached to the TEM) are still physically present in the setup, meaning the thermal contact resistances are equal in both experiments. It is concluded that the accurate state-estimation allows for a less conservative stability bound with respect to the situation where sensors are used to estimate the required temperatures. Furthermore, no stability issues pertaining to using an observer in closed-loop were observed.

For future work, our research focusses on applying the control architectures with and without EKF to a system with multiple thermoelectric actuators. Furthermore, we will focus on obtaining stability guarantees for using the observer in the loop. Finally, we will investigate the sensitivity of the EKF to uncertainty in the model parameters.

References

[1] R. van Gils, "Practical thermal control by thermo-electric actuators," *2017 23rd Int. Workshop on Thermal Investigations of ICs and Systems (THERMINIC*), Amsterdam, 2017, pp. 1-6.

[2] J. Jiang, G. Kaigala, H. Marquez, and C. Blackhouse, Nonlinear Controller Designs for Thermal Management in PCR Amplification, *IEEE Tr. on Control Systems Technology*, 20(1), pp. 11-30, 2012.

[3] A. Mironova, P. Mercorelli, A. Zedler, Robust Control using Sliding Mode Approach for Ice-Clamping Device activated by Thermoelectric Coolers, *In IFAC-PapersOnLine, 49(25),* pp. 470-475, 2016.

[4] K. Bos, D. Heck, M. Heertjes and R. van der Kall, "IO Linearization, Stability, and Control of an Input Non-Affine Thermoelectric System," *2018 Annual American Control Conference (ACC),* Milwaukee, WI, 2018, pp. 526-531.

[5] A. Yanou, N. Hosoya, K. Wada, M. Minami, and T. Matsuno, “Estimation of thermal conductivity for model with radiative heat transfer by extended Kalman filter,” in 2016 IEEE 21st Int. Conf. on Emerging Technologies and Factory Automation (ETFA), pp. 1–4, Sept 2016.

[6] H. Khalil, *Nonlinear Systems, ch. 5*, pp. 223–225. Edinburgh Gate, Harlow: Pearson, second ed., 1996.

[7] A. Fossard and D. Normand-Cyrot, *Nonlinear Systems: Modeling and Estimation, ch. 5*, pp. 173–213. Nonlinear Systems, Springer US, 1995.

[8] A. E. Golubev, A. P. Krishchenko, and S. B. Tkachev, “Separation principle for a class of nonlinear systems,” *IFAC Proc. Volumes, vol. 35*, no. 1, pp. 447 – 452, 2002. 15th IFAC World Congress.

[9] J. H. Ahrens and H. K. Khalil, “Closed-loop behaviour of a class of nonlinear systems under EKF-based control,” *IEEE Tr. on Automatic Control, vol. 52*, pp. 536–540, March 2007.

ASML

IO Linearized Control of a Thermoelectric Actuator using an Extended Kalman Filter

Koen Bos[1], Dennis Heck[1], Marcel Heertjes[1,2] & Robert van der Kall[1]

(1) ASML – Development & Engineering
(2) Eindhoven University of Technology

euspen

February 27th 2020 - Special Interest Group Meeting: Thermal Issues
Laboratory for Machine Tools and Production Engineering (WZL) of RWTH Aachen

ASML & Thermal Challenges

ASML

- ASML scanners are used in the lithography process to create computer chips
- Principle: DUV or EUV light via reticle to expose 2D image on wafer
- Overlay error future machines < 1nm
- To meet future demands, we require:
  - mK-level temperature conditioning
  - Sub-nm thermal deformations

Thermal Conditioning of Lithography Systems

ASML

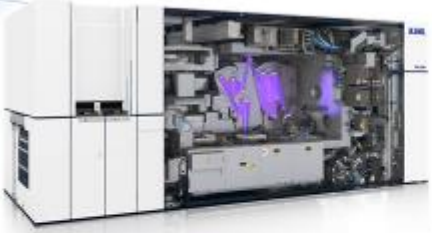

Passive temperature control
(open-loop)

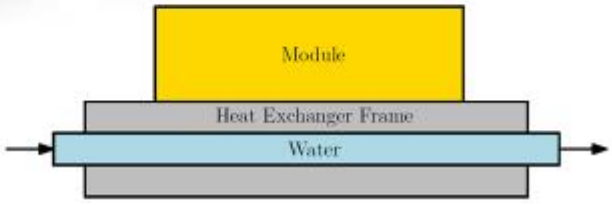

Thermal Conditioning of Lithography Systems

ASML

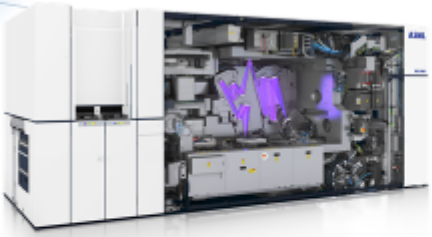

Increasing Requirements→ Active control

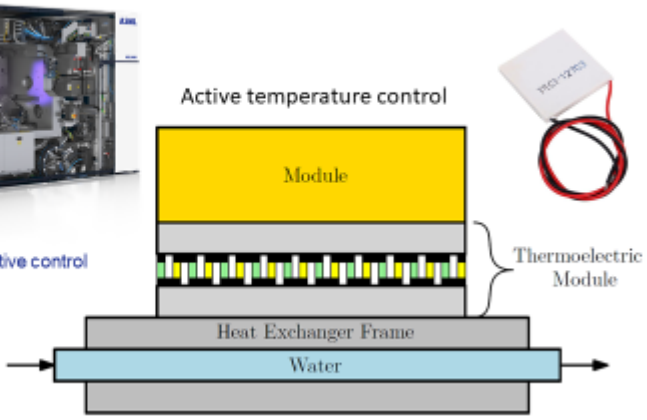

Peltier Element / Thermoelectric Module

ASML

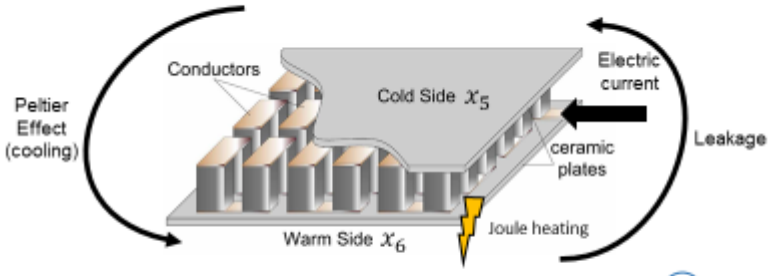

Nonlinear dynamics:

$$E_5\dot{x}_5 = \frac{1}{R_{45}}(x_4 - x_5) + \frac{1}{R_{56}}(x_6 - x_5) + u^2R_e/2 - Sx_5u$$

Peltier effect

Joule effect

Conduction leak

[1] E. Bos, D. Heck, M. Heertjes and R. van de Kaa, "IQ Linearization, Stability, and Control of an Input Non-Affine Thermoelectric System," 2018 Annual American Control Conference (ACC), Milwaukee, WI, 2018, pp. 528-533.

Problem Statement

ASML

- Varying input-output response (non-linearity)
- Unstable for some operating conditions

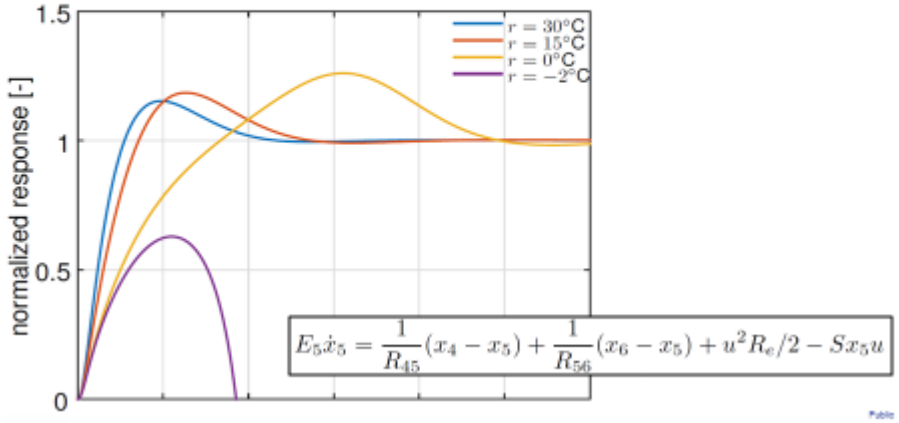

Problem Statement & Agenda

ASML

- Problem formulation:
  - Varying input-output response → Performance not constant
  - Stability not guaranteed
- Contents:
  - Experimental Setup & Modelling
  - IO Linearization, Feedback Control, and Observer Design
  - Experimental Results
  - Conclusions & Recommendations

Modelling of Experimental Setup

ASML

Experimental Setup

ASML

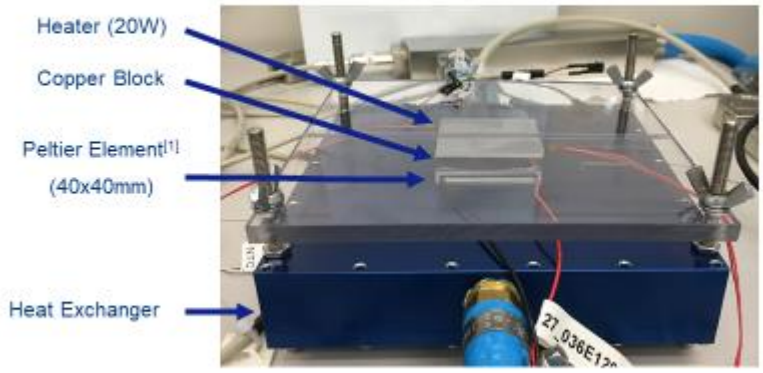

[1] Peltier element type: UWE UEPT-140-127-096E120

Setup Overview

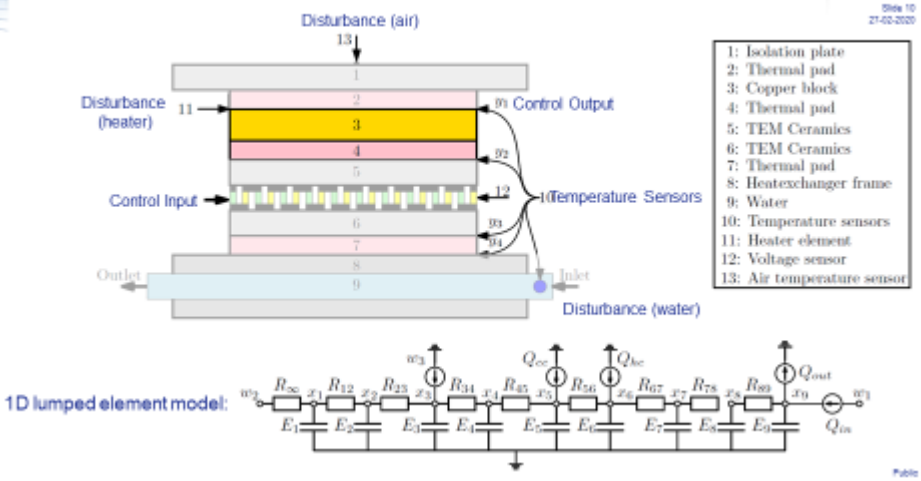

1D lumped element model:

IO Linearization & Feedback Control

Input-Output (IO) Linearization

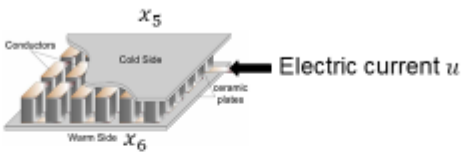

Thermal dynamics (cold-side):

$$E_5\dot{x}_5 = \frac{1}{R_{45}}(x_4 - x_5) + \underbrace{\frac{1}{R_{56}}(x_6 - x_5) + u^2 R_e/2 - S x_5 u}_{\text{Peltier-related dynamics}}$$

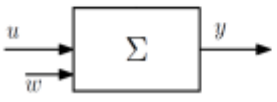

Contains thermal dynamics of complete setup

Input-Output (IO) Linearization

ASML

Net transferred heat v

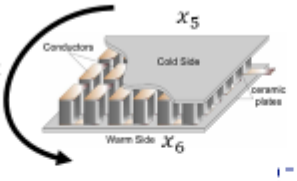

$$E_5\dot{x}_5 = \frac{1}{R_{45}}(x_4 - x_5) + v$$

$$v = \frac{1}{R_{56}}(x_6 - x_5) - Sx_5u + \frac{R_e}{2}u^2$$

Peltier-related dynamics

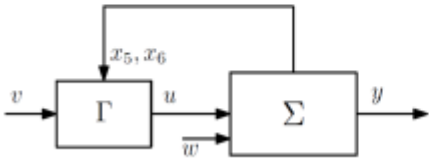

$$\Gamma: \quad u = \frac{Sx_5 - \sqrt{S^2x_5^2 - 2R_e(\frac{1}{R_{56}}(x_6 - x_5) - v)}}{R_e}$$

New input is limited by maximum possible cooling power: $v \geq v_{min}(x_5, x_6)$

Public

Control Architecture

ASML

- Linear (PID) controller to control output to setpoint
- Lyapunov-based saturation function (state-dependent) → Input-to-State stability

- Two possibilities:
  1. Saturation not active $v = \bar{v}$: Linear behavior in **nominal operating range**
  2. Saturation active $v \neq \bar{v}$: Stability **outside nominal operating range**

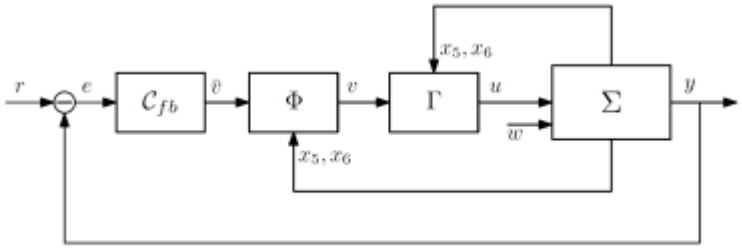

[1] E. Bos, D. Heck, M. Heertjes and R. van der Kall, "IO Linearization, Stability, and Control of an Input Non-Affine Thermoelectric System," 2018 Annual American Control Conference (ACC), Milwaukee, WI, 2018, pp. 528-533.

Public

Available Sensors

ASML

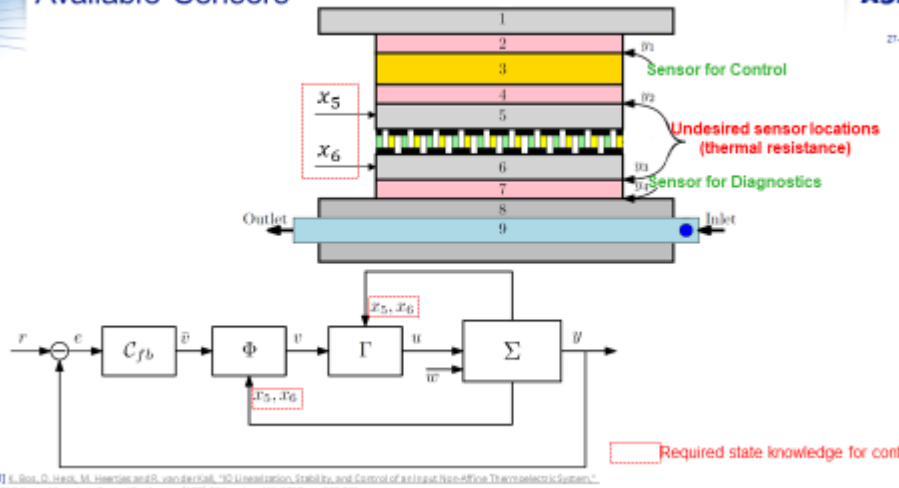

[1] E. Bos, D. Heck, M. Heertjes and R. van der Kall, "IO Linearization, Stability, and Control of an Input Non-Affine Thermoelectric System," 2018 Annual American Control Conference (ACC), Milwaukee, WI, 2018, pp. 528-533.

Public

Control Architecture

ASML

- C_{fb}: Linear (PID) controller to control output to setpoint
- Φ: Lyapunov-based saturation function (state-dependent) → Input-to-State stability
- Extended Kalman Filter (EKF): observer to estimate states → No sensors @ Peltier

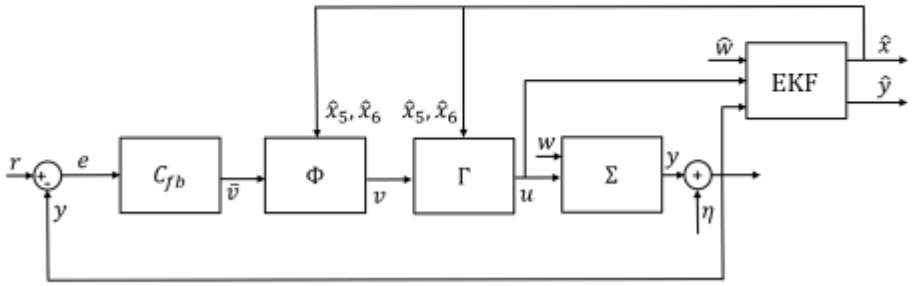

Measurement Results

ASML

Possibility 1: Nominal operating range

- Linear closed-loop behavior

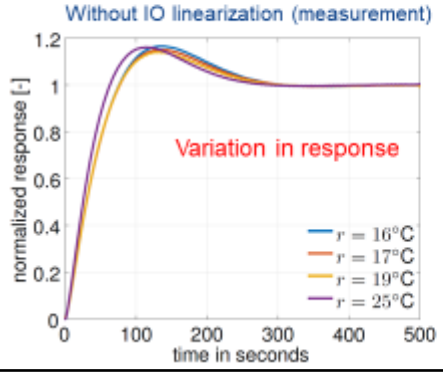

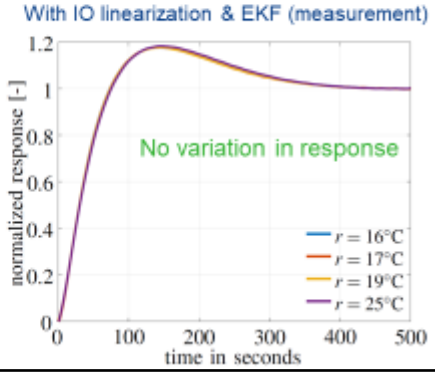

Measurement Results

ASML

Possibility 2: Outside nominal conditions (e.g. large disturbances)

- Applied large heat load with heater (12W), applied infeasible setpoint (-15°C)
- Input-to-state stable response (assumed)

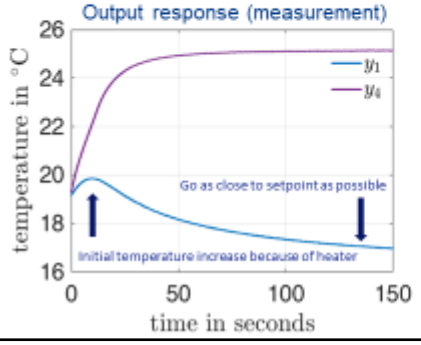

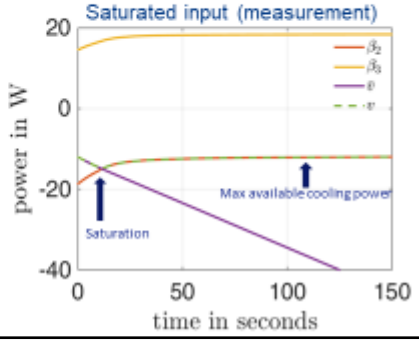

Summary

ASML

Recap: Linear Control Simulation

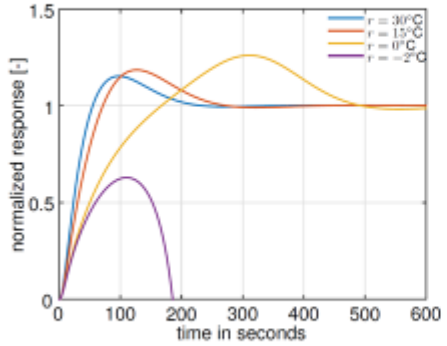

- Variation in response
- Unstable for some conditions

IO linearization & EKF Simulation

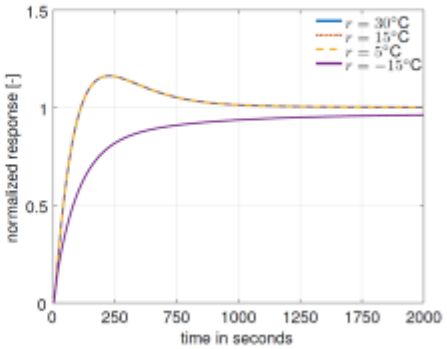

- No variation in response for nominal conditions
- Stable outside nominal conditions

Conclusions & Recommendations

ASML

Conclusions:

- Successfully combined EKF with IO Linearization
  - Linear closed-loop IO behavior
  - Stable in the face of large disturbances (experimentally verified)

Recommendations:

- Extend to multi-Peltier systems
- Theoretical stability guarantees for EKF in closed-loop
- Sensitivity analysis to model uncertainty
- Include temperature dependency Peltier parameters

ASML

ASML

Slide 22
27-02-2020

Back-up Slides

Public

ASML

Slide 23
27-02-2020

Model Validation

Copper block

Peltier top

Peltier bottom

Heat exchanger

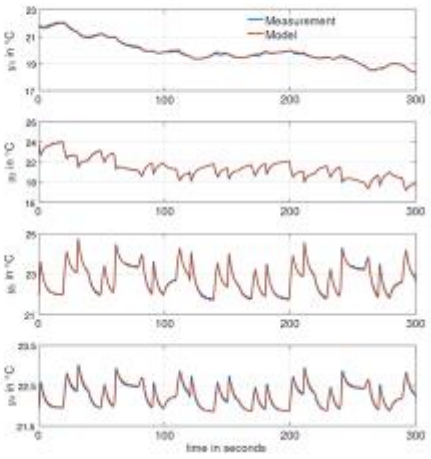

Public

ASML

Slide 24
27-02-2020

Disclaimer

- This publication is subject to change without notice and contains confidential and proprietary information of ASML Holding N.V. or its affiliates ("ASML").
- This documentation is for the intended purpose only and for the use the intended recipient only. Please retain control of this documentation. It is not to be forwarded or distributed. Any unauthorized review, copying, use, disclosure or distribution is strictly prohibited.
- The material herein is provided "AS-IS" and ASML makes no warranty of any kind with regard to this material. ASML shall not be liable for errors and omissions contained herein.
- If this document is in a language other than English, please read the following text carefully.
- While we strive to ensure that the information is translated correctly, no warranty or guarantee, express or implied, is given as to its accuracy or that it is as current as the English version. We accept no liability for any errors or omissions. If there is any conflict or difference between the translated version of this document and its English version, the English version is leading. If any part of the translated version is unclear, reference should be made to the English version.
- We shall not be liable for any damages (including, without limitation, damages for loss of business or loss of profits) arising in contract, tort or otherwise from the use of or inability to use this document, or any material contained in it, or from any action or decision taken as a result of using such material.

Public

Special Interest Group Meeting on Thermal Issues
Laboratory for Machine Tools and Production Engineering (WZL) of
RWTH Aachen, Germany, February 2020
www.euspen.eu

Precision Core Temperature Measurement of Metals for Use in Manufacturing Applications

Olaide F. Olabode[1*], Simon Fletcher[1], Andrew P. Longstaff[1], Naeem S. Mian[1]

[1]*Centre for Precision Technologies, University of Huddersfield, Huddersfield, UK.*

**olaide.olabode@hud.ac.uk*

Abstract
Core temperature variation in metals during manufacturing processes affects both the dimensional accuracy and the surface integrity of manufactured workpieces. Different types of temperature measurement techniques have been applied for obtaining workpiece temperature. However, their main limitations have been an inability to give the core temperature of the workpiece and the reduction in accuracy due to the harsh environment of some manufacturing processes. The velocity of sound in any medium of propagation is dependent on the temperature of that medium. This relationship can be used to obtain a medium's temperature, provided that the velocity of sound through the medium can be measured. This paper investigates the use of ultrasonic waves sent in the continuous mode to measure the temperature variation in a 100 mm steel sample (type EN24T) using the ultrasonic phase-shift method. Simulations and bench tests were performed to obtain a resolution and accuracy better than 0.5 °C and ±1 °C respectively. The results show that the method gives reliable results well within the target specification. Based on these results, ultrasonic thermometry experiments will be carried out during subtractive machining processes to determine the effects of the harsh environment on the accuracy of the proposed method.

Keywords: core temperature measurement; phase-shift method; manufacturing; ultrasonic thermometry

1. Introduction

The quality of manufactured products is determined by the conformance of the product to key specifications such as the dimensional accuracy and the surface integrity of the finished product. These two specifications are influenced by the temperature variation during manufacturing and inspection. Therefore, there is a need for temperature control or compensation of the thermal effects during manufacturing and measurement to produce high quality components.

No exact value is given for temperature variation during manufacturing. This is because there are many different types of manufacturing processes as well as different degrees of temperature variation for different materials. However, subtractive machining is a method in which high temperature variation can be reached. Typical temperature variation in this type of manufacturing process can reach 10 °C. In precision manufacturing, workpieces often need to be produced with dimensional error of less than 5 µm. The required temperature measurement accuracy to achieve this varies for different materials. Aluminium has a relatively high coefficient of thermal expansion compared with other common materials used in manufacturing. In order to achieve less than 5 µm dimensional error in aluminium, assuming a thermal expansion coefficient of 24 µm/m/°C, there is a need to measure temperature with accuracy of ±1 °C and a resolution of 0.5 °C. These are the accuracy and resolution this paper seeks to achieve in order to satisfy the requirement for precision manufacturing.

There have been many methods applied for measuring temperature during manufacturing processes, most of the methods described in literature deal with either the temperature of the machine [1] or of the tool [2]. Some temperature measurement methods such as the tool/workpiece thermocouple [3]–[5] and infrared thermometry [6] have been used to measure workpiece temperature. The major limitations of these and other methods previously used are the low accuracy in harsh manufacturing environments and the inability of the methods to measure the core temperature of the workpiece, which is the parameter that affects the dimensional expansion of the workpiece.

The velocity of sound in any material is dependent on the density, which is a function of temperature. This relationship can be used to obtain the temperature of any material provided that the velocity of sound through the material can be reliably obtained. Ultrasound thermometry requires sound signals at frequencies above 20 kHz. The pulse-echo method is traditionally used for ultrasonic thermometry [7]. However, the cost of pulser/receiver needed for high resolution temperature measurement is relatively high [8]. The resolution may also reduce in larger workpieces due to attenuation of the echo signal [9]. The main alternative to the pulse-echo method is the phase-shift method. In the phase-shift method, a continuous wave rather than pulses is used, the time-of-flight of ultrasonic wave is computed by measuring the difference between the phases of the transmitted and the received ultrasonic signals [10].

In this paper, the phase-shift method is used for the precise measurement of the temperature of a steel workpiece (type EN24T). Initial simulations were performed in MATLAB using the k-Wave toolbox – an open toolbox for time-domain acoustic and ultrasound simulations [11]. Based on the simulations, ultrasonic phase-shift experiments were carried out in a metrology laboratory. The results showed that this temperature variation in steel can be measured with this method with

resolution of up to 0.1 °C. As part of future work, this method will be used in different manufacturing and inspection processes.

2. Materials and method

The pulse-echo method of ultrasonic measurement is widely used because of its simplicity. The method works based on the principle of time-of-flight (*tof*). The ultrasonic velocity is calculated using the time difference between sending the signal and receiving its echo [12]. The relationship between the *tof*, distance of travel and the ultrasonic velocity is given as:

$$c = \frac{d}{tof} \qquad (1)$$

where *c* is the ultrasonic velocity, *d* is the distance between the transmitter and receiver and *tof* is the time-of-flight [12].

The Phase-shift method is another technique for ultrasonic measurement. To obtain the ultrasonic velocity, the phase-shift method uses the difference between the phases of the sent and received signal of a continuous ultrasonic wave. The relationship between the phase-shift and the velocity of a steady state frequency ultrasonic wave is governed by the following equation:

$$c = \frac{Lf}{\left(n + \frac{\phi}{2\pi}\right)} \qquad (2)$$

where *L* is the path length between the ultrasonic transmitter and receiver, *n* is the integer number of wave periods, ϕ is the phase-shift, *f* is the ultrasonic frequency and c is the ultrasonic velocity.

2.1. Simulations

The pulse-echo and the phase-shift methods were both simulated to choose the most appropriate method for core temperature measurement of metals. The simulation was done in MATLAB R2017b using the k-Wave toolbox. Steel was chosen as the medium of propagation. For the pulse-echo simulation, the *tof* technique was used to resolve 0.1 °C. The k-Wave grid (Nx) was set as 6.561e+3 grids, the spacing (dx) was set as 1.2e-4. The ultrasonic velocity used for the simulation is based on the temperature-velocity relationship given by Ihara et al [13] which is given as:

$$c(T) = -0.636T + 5917.6 \qquad (3)$$

Where c(T) is the temperature dependent ultrasonic velocity and T is the temperature.

To achieve a 0.1 °C resolution, a 1.2 MHz tone burst and 10 GHz sampling frequency were used. Figure 1 and Table 1 show the tone burst and the *tof* for the whole simulation respectively.

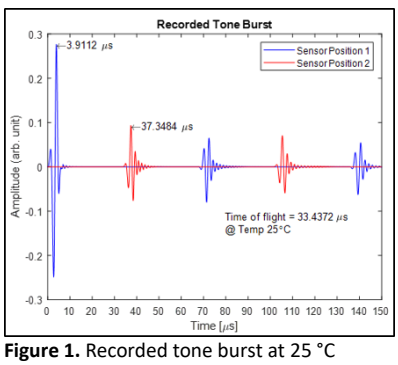

Figure 1. Recorded tone burst at 25 °C

Table 1. Time of flight at different material temperature.

Temperature (°C)	Velocity (m/s)	Tof (μs)
25.0	5901.70	33.4372
25.1	5901.63	33.4376
25.2	5901.57	33.4380
25.3	5901.51	33.4384
25.4	5901.45	33.4388
25.5	5901.38	33.4392

The phase-shift method was also simulated, using a frequency of 5 MHz, 0.1 °C change was successfully resolved and this is shown in table 2.

Table 2. Phase-shift simulation result.

Temperature (°C)	Phase-shift (5 MHz) (°)	Used ultrasonic velocity (m/s)
20	167.64	5894.0
20.1	168.83	5893.9
20.2	170.02	5893.8
20.3	171.21	5893.7
20.4	172.40	5893.5
20.5	173.59	5893.4

Both pulse-echo and phase-shift methods resolved 0.1 °C change in temperature. However, the resolution of the pulse-echo method may reduce due to attenuation [9]. However, with the phase-shift method, resolution of 0.1 °C can be achieved even with attenuated echo signal. Also, to use the pulse-echo method, a pulser/receiver of sampling frequency of approximately 10 GHz needs to be used, the cost of such device can be as high as €20,000. However, using the phase-shift method requires the use of a phase detector just under €400. Because of these, the phase-shift method was chosen over the pulse-echo method. The experiments described in the next section are based on the phase-shift method.

3. Experiments

The ultrasonic phase-shift thermometry experiment was set up as shown in figure 2.

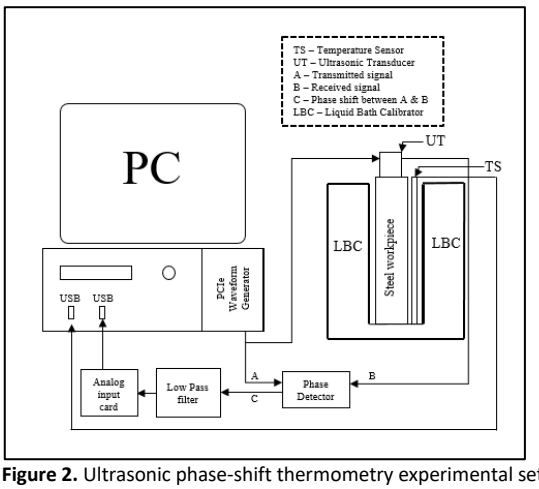

Figure 2. Ultrasonic phase-shift thermometry experimental setup.

For the phase-shift thermometry experiment, a sinusoidal waveform was generated using a Spectrum M2i.6022-exp arbitrary waveform generator (Spectrum Instrumentation, Ahrensfelder, Grosshansdorf, Germany). The signal was then sent to the transmitter probe of a transducer (5 MHz centre frequency and bandwidth of ±1 MHz) and the input A port of an Analog Devices AD8302 (Analog Devices, Norwood, MA, USA) phase detection board using a 100 mm steel sample (EN24T) - as the medium of propagation. Using a single transceiver on a 100 mm sample has the equivalent path length to the simulation, where a transmitter and receiver were at opposite ends of a 200 mm sample. The received signal was sent through the receiver probe of the transducer to the input B port of the phase detector board. The phase difference between the transmitted and received signals is computed by the phase detector and the equivalent voltage value is sent out through the phase-out port. Signal noise from the phase-out value was reduced with a low pass filter. A filter with cut-off frequency of 3.4 Hz was used. Using an NI-9239 analogue input card (National Instruments, Austin, TX, USA), the filtered phase-out values were saved to a PC through NI LabVIEW. Using a TCS140 liquid bath calibrator (E Instruments, Langhorne, PA, USA), the temperature of the steel workpiece was varied in steps of 1 °C and 0.1 °C and the corresponding phase-shift was recorded. The result of this experiment will be discussed in the next section.

4. Discussion

The AD8302 outputs voltage values represent the phase-shift between the transmitted and received signals. The relationship between the phase-shift and phase-out voltage values is given in figures 3 and 4. Figure 3 is the datasheet plot while figure 4 was obtained experimentally using the same parameters as those used for the phase-shift experiments – 2V input, 40 mV received signal with 5.5 MHz signal frequency. 5.5 MHz frequency was used in order to utilize the linear region of the phase output curve; this frequency was chosen experimentally.

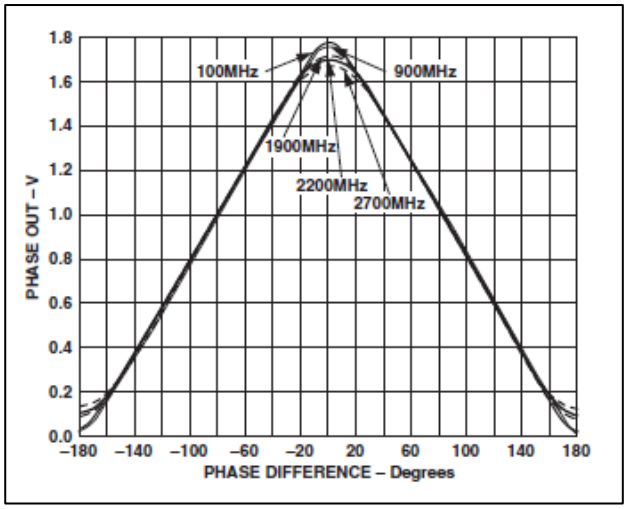

Figure 3. Phase Output vs. Phase Difference [14].

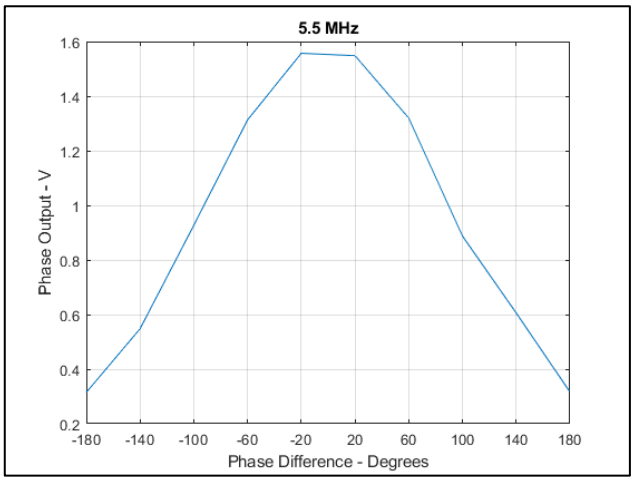

Figure 4. Phase Output vs. Phase Difference for 5 MHz signal.

The first experiment was for a temperature range of 20 to 30 °C in steps of 1 °C. The phase out values which represent the phase-shift between the transmitted and received signals for the temperature range and the micron equivalent values of the residuals of the phase out values are given in the figures 5 and 6 respectively.

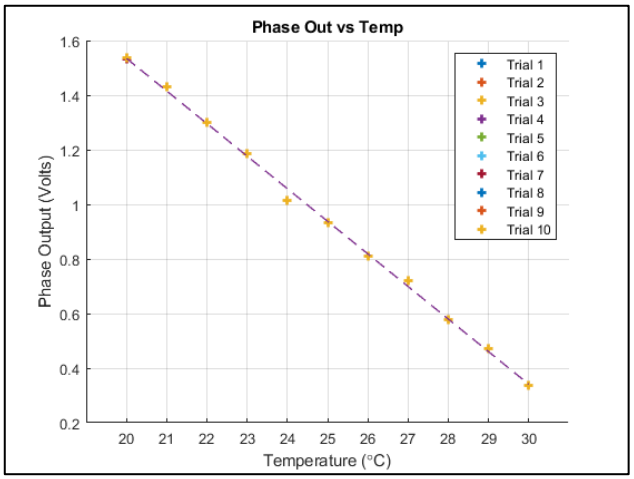

Figure 5. Results of 20 to 30 °C range in steps of 1 °C.

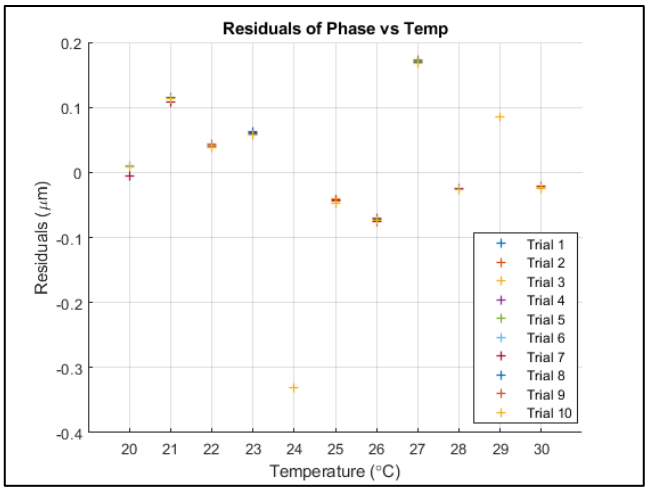

Figure 6. Residual plot of 20 to 30 °C

The second experiment was designed to focus on achieving the required resolution. A range of 20 to 21 °C in steps of 0.1 °C was used. The recorded phase out and the residual plots are given in figures 7 and 8 respectively.

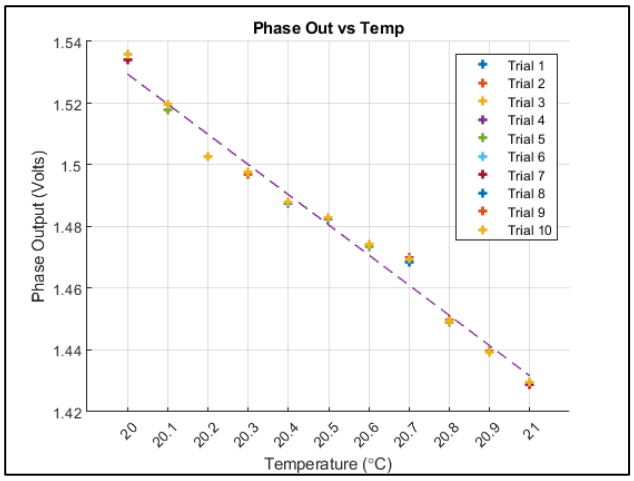

Figure 7. Results of 20 to 21 °C range in steps of 0.1 °C.

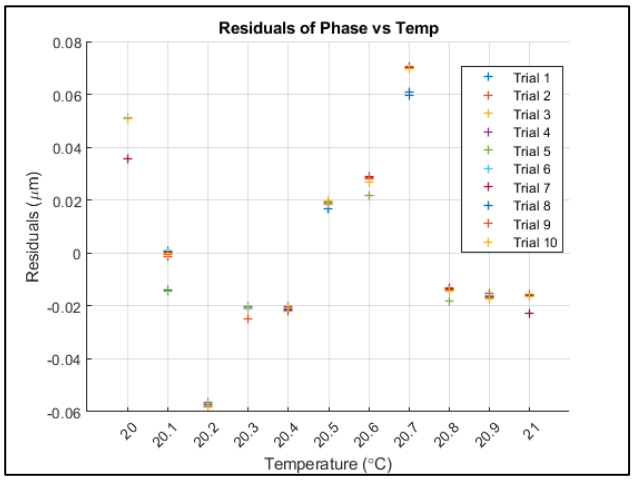

Figure 8. Residual plot of 20 to 21 °C

The results of the simulations as well as the experiments confirm that temperature variation in metals can be measured using the phase-shift technique of ultrasonic thermometry.

5. Conclusions

This study showed that with phase-shift ultrasonic thermometry, core temperature of metals can be measured with a resolution and accuracy of better than 0.5 °C and ±1 °C respectively, even with an attenuated echo signal of 40 mV. For these experiments, a 100 mm steel sample (EN24T) was used. The range of temperature measurement can be increased by combining multiple ultrasonic signals of different frequencies. Two main limitations of the AD8302 board are the nonlinearities at the extremes and at the centre (-180°, 180° and 0°) as seen in figures 3 and 4, and the lack of clarity on the sign of the phase difference from the phase-out value. Choosing a suitable frequency for which phase out values are within the linear region will reduce the possibilities of values falling in the non-linear region as shown in the results of the experiments. The sign of the phase difference is needed for absolute temperature measurement. However, relative temperature variation can be measured without the knowledge of the sign of the phase difference. A possible application of this study would be for temperature monitoring during co-ordinate metrology. As part of future work, more experiments will be carried out in order to deploy this setup in subtractive manufacturing processes. Also, the suitability of the method to different materials as well as the possibility of measuring material temperature at a specific region or point using ultrasound will be studied

6. Acknowledgement

The authors gratefully acknowledge the UK's Engineering and Physical Sciences Research Council (EPSRC) funding of the Future Metrology Hub (Grant Ref: EP/P006930/1).

References

[1] L. Olson, R. Throne, and E. Rost, "Improved Inverse Solutions for On-Line Machine Tool Monitoring," *J. Manuf. Sci. Eng.*, vol. 126, no. 2, p. 311, 2004.

[2] M. Bacci da Silva and J. Wallbank, "Cutting temperature: prediction and measurement methods—a review," *J. Mater. Process. Technol.*, vol. 88, no. 1–3, pp. 195–202, 1999.

[3] E. G. Herbert, "The measurement of cutting temperatures," *Proc. Inst. Mech. Engnrs*, vol. 110, no. September 1925, pp. 289–329, 1926.

[4] N. Dhar, S. Islam, M. Kamruzzaman, and T. Ahmed, "The Calibration of Tool-Work Thermocouple in Turning Steels," in *Proceedings of National Conference on Industrial Problems on Machines and Mechanisms (IPROMM-2005)*, 2005.

[5] M. C. Santos, J. S. Araújo Filho, M. A. S. Barrozo, M. J. Jackson, and A. R. Machado, "Development and application of a temperature measurement device using the tool-workpiece thermocouple method in turning at high cutting speeds," *Int. J. Adv. Manuf. Technol.*, vol. 89, no. 5–8, pp. 2287–2298, 2017.

[6] M. B. Da Silva and J. Wallbank, "Temperature measurements in machining using infrared sensor, COBEM97, Cong," *Bras. Eng. Mecânica, Bauru SP, Brazil*, 1997.

[7] M. Takahashi and I. Ihara, "Ultrasonic monitoring of internal temperature distribution in a heated material," *Jpn. J. Appl. Phys.*, vol. 47, no. 5 PART 2, pp. 3894–3898, 2008.

[8] O. F. Olabode, S. Fletcher, A. P. Longstaff, and N. S. Mian, "Precision Core Temperature Measurement of Metals Using an Ultrasonic Phase-Shift Method," *J. Manuf. Mater. Process.*, vol. 3, no. 3, p. 80, 2019.

[9] D. Marioli, C. Narduzzi, C. Offelli, D. Petri, E. Sardini, and A. Taroni, "Digital Time-of-Flight Measurement for Ultrasonic Sensors," *IEEE Trans. Instrum. Meas.*, vol. 41, no. 1, pp. 93–97, 1992.

[10] F. E. Gueuning, M. Varlan, C. E. Eugène, and P. Dupuis, "Accurate distance measurement by an autonomous ultrasonic system combining time-of-flight and phase-shift methods," *IEEE Trans. Instrum. Meas.*, vol. 46, no. 6, pp. 1236–1240, 1997.

[11] B. Treeby, B. Cox, and J. Jaros, "k-Wave: A MATLAB toolbox for the time domain simulation of acoustic wave fields - User Manual," vol. 1. 2016.

[12] R. Queirós, R. C. Martins, P. S. Girão, and a C. Serra, "A New Method for High Resolution Ultrasonic Ranging in Air," *Xviii Imeko World Congr.*, pp. 1–4, 2006.

[13] I. Ihara and M. Takahashi, "A novel ultrasonic thermometry for monitoring temperature profiles in materials," *19th IMEKO World Congr. 2009*, vol. 3, pp. 1635–1639, 2009.

[14] Analog Devices, "LF–2.7 GHz RF/IF Gain and Phase Detector AD8302." [Online]. Available: https://www.analog.com/media/cn/technical-documentation/evaluation-documentation/AD8302.pdf. [Accessed: 18-Sep-2019].

Special Interest Group Meeting on Thermal Issues
Laboratory for Machine Tools and Production Engineering (WZL) of
RWTH Aachen, Germany, February 2020
www.euspen.eu

Deformation-based control of a thermo-mechanical system

Dennis Heck[1], Nic Dirkx[1], Wijnand Hoitinga[2], Johan Kunnen[1], Marc van de Wal[1]
[1]ASML, 5504 DR Veldhoven, The Netherlands
[2]Evalf, Burgwal 45, 2611 GG Delft, The Netherlands

dennis.heck@asml.com

Abstract
In this work, we introduce the concept of a Deformation-Based Controller (DBC) to improve the performance, in terms of thermal deformations, of a temperature controlled thermo-mechanical system subject to unpredictable thermal disturbances. In a traditional temperature controlled system, thermal actuators are used to control the temperature *at sensor locations* towards a desired setpoint. Since the temperature is not controlled in-between the sensor locations, there can arise thermal gradients in the system, which result in undesired thermal deformations in the whole system. DBC aims to reduce these thermal deformations while using only the existing thermal actuators and sensors, such that hardware changes are not required. Experiments with a system subject to unpredictable evaporation loads demonstrate that a significant reduction in thermal deformations is achieved, compared to a traditional temperature controller.

Control, Temperature, Deformation, Observer

1. Introduction

In many industrial high precision applications, such as electron microscopes and lithography machines, thermal specifications are continuously tightened to improve the performance in terms of accuracy and availability [1]. As a result, reducing temperature fluctuations and the resulting thermal deformations of components, often resulting from unpredictable and uncontrollable thermal disturbances, becomes highly important.

A reasonable thermal performance can often be achieved with a good thermal design and insulating or shielding of thermal loads. When thermal disturbances cannot be insulated completely, (multiple) thermal actuators (e.g. heaters) and (temperature) sensors can be added and combined with a temperature feedback controller (e.g. a PID-controller) to suppress the effect of the thermal disturbances by controlling the temperature to a desired setpoint. In this way, a satisfying thermal performance can be achieved, but *only at the sensor locations*. Thermal gradients might still exist between the sensor locations and these result in undesired thermal deformations, limiting the precision of optical elements [2, 3].

To reduce the thermal deformations, we propose to control these thermal deformations instead of the temperatures. In practice it is not always possible (volume restrictions) or desired (extra costs and complexity) to add extra sensors to measure deformations. Therefore, we focus on a 'software-only' solution, where only the existing thermal actuators and sensors are used. This means that the resulting Deformation-Based Controller (DBC) is based on a high accuracy thermo-mechanical model of the system to estimate the thermal deformations from measured temperatures and these deformations are controlled using the thermal actuators.

There are many challenges in designing such a DBC. These challenges include the design of a high order thermo-mechanical model (>10 000 states), the identification of physical model parameters (e.g. contact resistances and heat transfer coefficients) to improve the model accuracy, model order reduction to make control design feasible, disturbance modelling, Multiple Input-Multiple Output (MIMO) controller design and closed-loop controller order reduction to compute the model-based controller in real-time. The main contribution of this work is to provide a framework for DBC, illustrating the steps taken, and how the previously mentioned challenges can be overcome.

This abstract proceeds as follows. In Section 2, the physics of the considered thermo-mechanical system are explained. The DBC design steps and solutions to the previously mentioned challenges are explained in Section 3. Subsequently, Section 4 shows experimental results to illustrate the reduction in thermal deformations that can be obtained with DBC over a commonly used temperature controller. Finally, the conclusions and future work are described in Section 5.

2. System description

The system considered in this work consists of a 300 mm disk of 10 mm in height, with water cooling channels, as illustrated in Figure. 1. The top surface of this disk should remain as flat as possible. Due to the operation process of the machine, the top edge of the disk is irregularly wetted with water. To keep the top surface dry, the water is first extracted via small holes into an Edge Channel (EC), inside the edge of the disk, and then from the EC via several extraction holes at the bottom of the disk. A part of this water evaporates in the EC, thereby extracting up to 15 W of heat from the disk. As a result, the edge of the disk cools down (in the order of 100 mK) and this results in several nanometres of thermal deformations of the edge, affecting the flatness of the top of the disk. To compensate for the evaporative load, 12 segmented heaters are attached to the edge (covering the whole edge) and 12 sensors are attached (8 cm apart) to the bottom of the disk, below the EC, as illustrated in Figure 1. These heaters and sensors are available for control.

2.1. Thermo-mechanical model

A spatially discretized and parametrized thermo-mechanical finite element model of the system is created using Nutils [4].

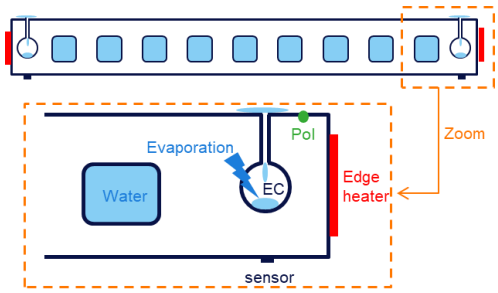

Figure 1. Impression of the cross section of the disk with cooling water, EC with evaporation load, edge heaters, temperature sensors and the Point of Interest (PoI) for DBC.

The resulting dynamics are described in descriptor state-space form as

$$\begin{aligned} E(p)\dot{T} &= A(p)T + B_1 u + B_2 w \\ y &= C_y T \\ d &= C_d T \end{aligned} \tag{1}$$

with $T \in \mathbb{R}^n$ the states (temperatures) of the full system, consisting of $n = 50\,000$ states, $u \in \mathbb{R}^{12}$ the heater power inputs, $w \in \mathbb{R}^{100}$ the evaporation loads in the EC, modelled over 100 segments, $y \in \mathbb{R}^{12}$ the temperatures measured by the sensors and $d \in \mathbb{R}^{100}$ the stacked deformations in x- and y-direction of 50 uniformly distributed points at the top edge of the disk (see Figure 2), also referred to as the Points of Interest (PoI). The matrices B_1 and B_2 are the input matrices of u and w, respectively, and C_y and C_d are the output matrices related to y and d, respectively. The capacity matrix $E(p)$ and conductivity matrix $A(p)$ depend linearly on the physical model parameters $p \in \mathbb{R}^{50}$, i.e.

$$E(p) = \sum_{i=1}^{50} p_i E_i\,, \qquad A(p) = \sum_{i=1}^{50} p_i A_i. \tag{2}$$

with E_i and A_i representing the structural contribution of parameter p_i, $i = 1,2,\ldots,50$, to E and A, respectively. The parameters p consist of the physical parameters of the disk (e.g. thermal masses, heat transfer coefficients, conductivities, water flow, etc.) and the dynamics of the heaters and sensors (modelled with a time constant). The uncertainty on the parameters is on average ~10 % due to production tolerances and variations in flows between different systems.

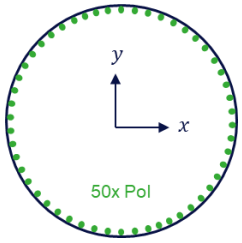

Figure 2. Top view of the disk with the 50 deformation nodes (PoI).

2.2. Characteristics of disturbance w

The evaporation disturbance $w_i \in \mathbb{R}_{\leq 0}$ of an element in w can be characterized by the illustration in Figure 3. The thermal evaporation load is present at ① when there is water in the EC segment and the local humidity is below 100 %. The load drops to zero when the humidity is 100 % or when all the water is extracted via the bottom holes or evaporated in the EC. The humidity reaching 100% could be a local effect ②, when the supply of dry air via the holes is blocked (due to the production process), or it could be a global effect ③ when the extraction flow is switched off (also due to the production process). The local effect, which causes the largest temperature gradients and disk deformations, occurs for each of the 100 segments at different time instances during production and is not known in advance.

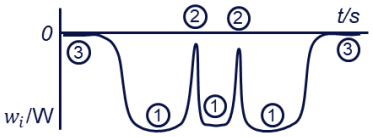

Figure 3. Impression of the repetitive disturbance characteristic w_i. At ① evaporation takes place, at ② the evaporation stops due to a blocked hole and at ③ the extraction flow (sucking dry air in the EC) is switched off.

3. Deformation-based control design

The goal of the DBC is to minimize the deformations d when the system is subject to the unmeasurable disturbance w, characterized in Section 2.2. The deformations cannot be measured directly. Instead, only the temperature measurements y are available. To estimate the deformations, an observer is used, as illustrated in Figure 4. The challenges involved in designing an accurate observer are discussed in Section 3.1. Thereafter, Section 3.2 discusses the design of the MIMO controller to minimize d, and Section 3.3 discusses how the observer and the MIMO controller can be combined and efficiently implemented on a control board.

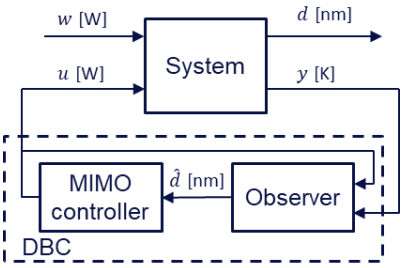

Figure 4. Block diagram of the DBC controller, consisting of an observer and a MIMO controller. The observer estimates d from the measurements y and the applied input u and the MIMO controller computes u to drive $\hat{d}$ to zero.

3.1. Observer design

The main challenge when designing an observer is to obtain an accurate thermo-mechanical model. For our system, the model structure in (1) is used as a basis. Due to the uncertainty on the model parameters p, an identification experiment is conducted using only u and y to accurately identify these parameters. When calibrating these parameters it is important that the input signal u results in a sufficiently high sensitivity of each parameter in the measured response and that the contribution to each parameter can be separately identified (limited correlation). We experienced for our system that the best results can be obtained when calibrating the parameters based on a measured Frequency Response Function (FRF) of the system (both magnitude and phase), rather than performing the calibration on a time-domain signal. The main reason is that time-domain signals for thermal systems are usually dominated by low frequency dynamics far below the desired bandwidth of the controller. To accurately measure the FRF, a standard system identification, e.g. using white noise- or multi-sine injection [5], is sufficient. Note that the same measured FRF is often already measured to tune a traditional temperature controller.

Using the measured FRF of the MIMO system, the parameters are calibrated following the optimization procedure illustrated in Figure 5. In this iterative optimization procedure, the gradient

of the FRF with respect to each parameter is used to determine the parameter update direction. This gradient is determined using the perturbation method [6], where, per iteration, for all 50 parameters the FRF of the model with one perturbed parameter is compared with the FRF of the unperturbed model. Per iteration this yields 50+1 computed model FRFs to be computed, which is computationally very expensive when using the full order model of (1) with 50 000 states. To speed up the process, we propose to use the parametric model-order reduction technique of [7], which is an extension of the commonly used Arnoldi reduction technique [8], to obtain a parametrized reduced order model (of 500 states) that needs to be computed only once, outside the iterative loop. The calibration of the 50 parameters of the 12x12 MIMO system takes only ten minutes using Matlab on a Lenovo P52 with Intel Xeon E-2176M processor.

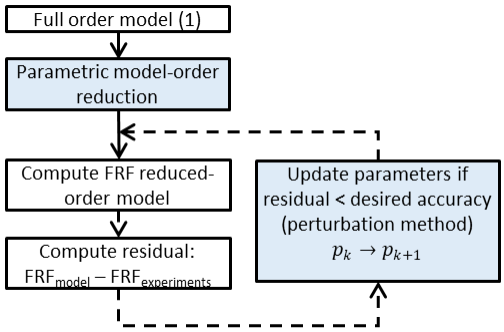

Figure 5. Outline parameter calibration procedure. The dashed arrows represent an iterative loop that stops when the desired accuracy is achieved.

The observer to estimate d is a Kalman filter [9] based on a reduced order version (500 states) of the model (1), obtained using the reduction method of [7]. Since the disturbance w cannot be modelled by white noise (one of the requirements for using a Kalman filter), the system dynamics are augmented with a dynamical model of the disturbance to map a white noise input $w_{white} \in \mathbb{R}^{100}$ to w used in (1), i.e.

$$\begin{aligned} \dot{x}_w &= A_w\, x_w + B_w\, w_{white}, \\ w &= C_w x_w, \end{aligned} \tag{3}$$

with $x_w \in \mathbb{R}^{100}$. An integrator model is considered sufficient for the problem at hand, so $A_w = O$ and $B_w = C_w = I$. The augmented Kalman filter is then expressed by

$$\begin{aligned} \begin{bmatrix} \dot{\hat{T}} \\ \dot{x}_w \end{bmatrix} &= \begin{bmatrix} \hat{A} & \hat{B}_2 C_w \\ O & A_w \end{bmatrix} \begin{bmatrix} \hat{T} \\ x_w \end{bmatrix} + \begin{bmatrix} \hat{B}_1 \\ 0 \end{bmatrix} u + L\,(y - \hat{y}), \\ \hat{y} &= \begin{bmatrix} \hat{C}_y & O \end{bmatrix} \begin{bmatrix} \hat{T} \\ x_w \end{bmatrix}, \\ \hat{d} &= \begin{bmatrix} \hat{C}_d & O \end{bmatrix} \begin{bmatrix} \hat{T} \\ x_w \end{bmatrix}, \end{aligned} \tag{4}$$

with $\hat{(\ )}$ an estimate of the actual matrices (obtained after parameter calibration) and signals. The Kalman gain L is obtained by solving a Riccati equation with a disturbance covariance matrix Q_w and measurement noise covariance matrix $R = \gamma_r I$, $\gamma_r = (10^{-4})^2$ K². Due to the nature of the disturbance (in particular effect ① in Figure 2), w is strongly correlated. The correlation of w is included in Q_w as illustrated by the matrix structure in Figure 6.

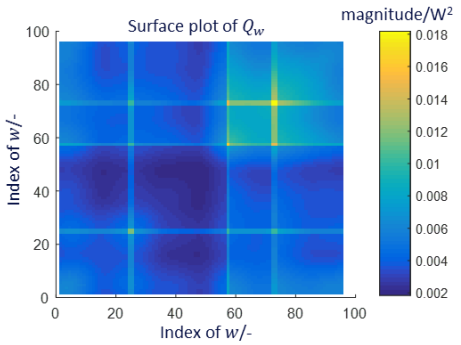

Figure 6. Structure of the covariance matrix Q_w, illustrating the correlation of elements in w (an uncorrelated signal is represented by a diagonal structure). The lines standing out are related to locations where water is extracted from the EC at the bottom of the disk. Here, the evaporative load is larger compared to the other EC elements.

3.2. Feedback control design

Due to the large number of input signals (12 heater powers) and performance variables (100 deformations), manually designing and tuning a feedback controller is too cumbersome. Instead, a Linear-Quadratic Regulator (LQR) [9] is used as MIMO controller. LQR is a state-feedback controller that computes the input u based on the estimated states $\hat{T}$ via

$$u = -K\hat{d} = -KC_y\hat{T}, \tag{5}$$

with $K \in \mathbb{R}^{12\times 500}$, and $\hat{T}$ the estimate state from the observer (4). The matrix K follows from solving a Riccati equation to minimize the following cost function

$$J = \int_{t=0}^{\infty} \left(\hat{d}^T Q_d \hat{d} + u^T\, u\ \right) dt, \tag{6}$$

which is modified to drive $\hat{d}$ to zero, instead of $\hat{T}$. Here, $Q_d = \gamma_d I$, γ_d being a positive scalar to tune the aggressiveness of the controller.

3.3. DBC implementation

The total DBC consists of the observer (4) and the controller (5), indicted by the dashed box in Figure 3, and has 500 states. This controller is too expensive to compute in real-time. Therefore, the DBC controller with 12 *controller* inputs y and 12 *controller* outputs u is reduced to only 100 states using a closed-loop model order reduction technique (see [10, 11, 12]).

4. Experimental results

The DBC of Section 3 is implemented on the experimental system described in Section 2 and the estimated deformations are compared to the estimated deformations obtained when using a standard PID temperature controller $u = \left(K_p + K_d s + \frac{K_I}{s}\right)(y_{set} - y)$, where s is the Laplace variable, y_{set} is the temperature setpoint and K_p, K_d and K_I are the proportional, derivative and integral gains, respectively. Both controllers were tuned for maximal performance, with similar robustness margins.

During both experiments, the controller was implemented with a 200 Hz sampling frequency. The Kalman filter was implemented in parallel to estimate the deformations in real-time during both experiments. The x-component of these estimated deformations is shown in Figure 7 (the y-component shows similar results).

The left plot shows the deformations when using the temperature controller. The temperature error $y_{set} - y < 5$ mK throughout the whole experiment, but because the temperature gradient in-between the sensor locations is not controlled, this

results in a too large thermal deformation for the specific process in the lithography machine.

The right plot of Figure 7 shows that with DBC the deformations are suppressed to 40 % compared to the temperature controller, which is considered a huge performance gain for a software solution. Finally, note that with DBC not all deformations can be controlled to zero, because the system is underactuated (nr. of actuators << nr. deformations to control), but the average can be steered to zero.

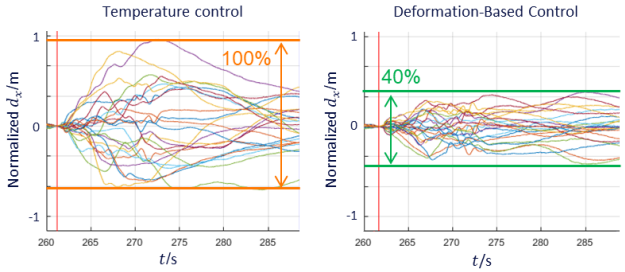

Figure 7. Real-time estimated deformations (x-component, normalized) of the 50 points at the top edge of the disk under closed-loop temperature control (left) and DBC (right). With DBC, the deformations are reduced to 40 %.

5. Conclusion and recommendations

In this work, we have shown for a temperature controlled thermo-mechanical system subject to unpredictable thermal disturbances that the performance, in terms of thermal deformations, can be improved significantly with a deformation-based controller. The advantage of the DBC controller is that it uses the same thermal actuators and sensors as the temperature controller, so no hardware changes are required. We have given a framework for the DBC and illustrated how to use parameter calibration, based on the measured FRF of the system, to obtain a high accuracy thermo-mechanical model, how to include disturbance information in the observer and how to design a MIMO controller to minimize the thermal deformations. Finally, we have demonstrated on an experimental system with unpredictable evaporation disturbances a performance improvement of 60 %, in terms of thermal deformations, over a standard temperature controller.

Future work focusses on developments towards an efficiently automated calibration and tuning of the DBC to be robust for variations in dynamics and disturbance loads between different systems.

References

[1] DSPE Mikroniek 2019 Vol 59 Issue 2 Eindhoven, the Netherlands

[2] Bikcora C, Weiland S and Coene W M J 2014 Thermal deformation prediction in reticles for extreme ultraviolet lithography based on a measurement-dependent low-order model *IEEE Tr. on Semiconductor Manufacturing* 27(1) p 104–117

[3] Habets M, Merks R, Weiland S and Coene W 2015 A multiphysics modelling approach for thermal aberration prediction and control in extreme ultraviolet lithography *Imaging and Applied Optics* p AOM4B.2, Washington D.C., USA

[4] nutils.org/en/latest

[5] Pintelon R and Schoukens J 2012 System identification: A frequency domain approach *Wiley-IEEE Press* 2nd edition

[6] Spall J C 1992 Multivariate stochastic approximation using simultaneous perturbation gradient approximation *Tr. on Automatic Control* p 332-341, 37(3)

[7] Lou D and Weiland S 2018 Parametric model order reduction for large-scale and complex thermal systems *IEEE 2018 European Control Conference* p 2593-2598 June 12-15 2018, Limassol, Cyprus

[8] Arnoldi W E 1951 The principle of minimized iterations in the solution of the matrix eigenvalue problem *Quart. Appl. Math.* P 17–29, Vol 9

[9] Skogestad S and Postlewaite I 2005 Multivariable feedback control – Analysis and design, Chapter 9 *John Wiley & Sons, Inc.*, Chichester, West Sussex, England

[10] Wortelboer P 1994 Frequency-weighted balanced reduction of closed-loop mechanical servo systems: Theory and tools. *Ph.d. dissertation,* Delft University of Technology

[11] Wortelboer P, Steinbuch M and Bosgra O H 1999 Iterative Model and Controller reduction using closed-loop balancing, with application to a compact disc mechanism *Int. J. of Robust and Nonlinear Control*, p 123-142, 9(3)

[12] Merks R 2019 Towards control relevant system design and constrained order controller synthesis: with a thermal control application in immersion lithography *Ph.d. dissertation,* Eindhoven University of Technology

ASML

Deformation-based control of a thermo-mechanical system

Dennis Heck, Nic Dirkx, Wijnand Hoitinga, Johan Kunnen & Marc van de Wal

euspen

February 27th 2020 - Special Interest Group Meeting: Thermal Issues
Laboratory for Machine Tools and Production Engineering (WZL) of RWTH Aachen

Introduction

ASML

Typical steps to improve thermal design

- Remove heat loads
- Reduce heat loads
- Insulate/shield heat loads
- Passive thermal conditioning
- Active thermal conditioning
  - actuators, sensors, control loop
- Active thermo-mechanical conditioning
  - deformation-based control

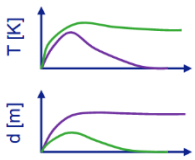

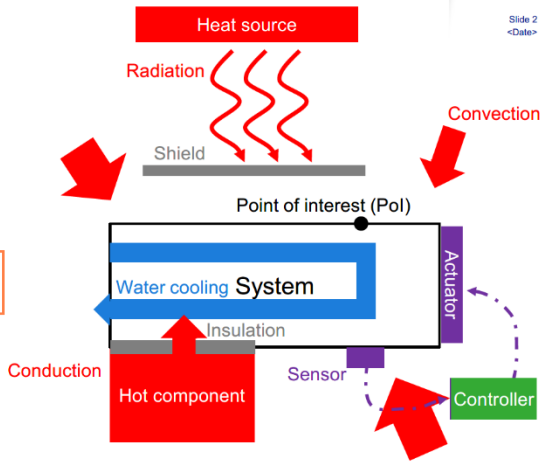

Introduction

ASML

Problem under consideration

- Lithography machines project images on wafers to create chips
- Liquid lens element loses water
- Water evaporates → unpredictable cold load
- Thermal deformation → image distortions on wafer

Expose light containing image

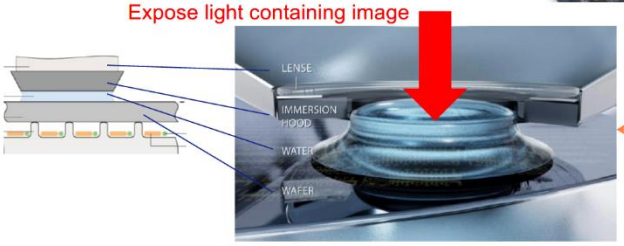

Introduction

ASML

Slide 4
<Date>

- Water collected and removed in Edge Channel (EC)
- Unpredictable evaporative load in EC

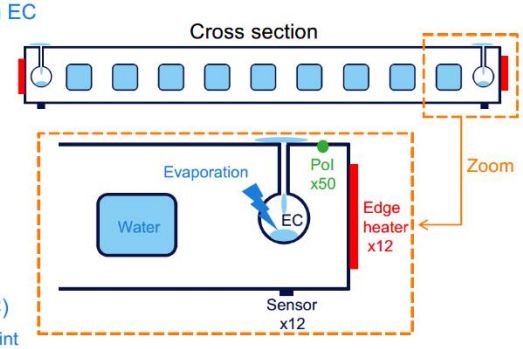

- Active thermal control
  - Sensor temperature → setpoint
  - Deformation PoI too large
- Deformation-Based Control (DBC)
  - Control PoI deformation → setpoint

Public

Introduction

ASML

Slide 5
<Date>

Steady-state temperature profile after step on heater

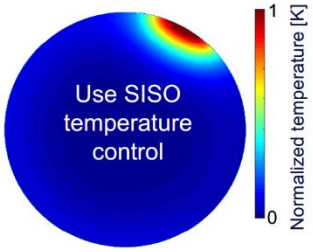

Resulting deformation profile

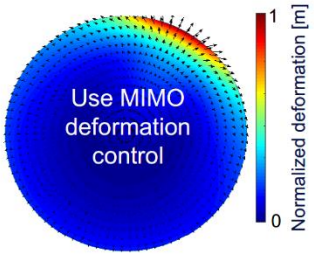

Public

Deformation-Based Control

ASML

Slide 6
<Date>

Idea of DBC

- Control the deformation d of the PoI subject to disturbances w
- Use only existing thermal actuators u & sensors y

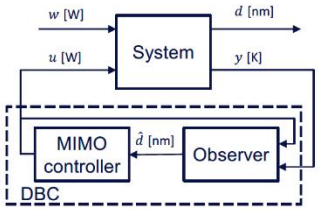

Challenges

- Deformation d cannot be measured ➡ Observer (Kalman filter)
- Disturbance w is unpredictable ➡ Use y to estimate w

Approach

Model → Parameter calibration → Observer design → MIMO controller → Experimental validation

Public

Model | Parameter calibration | Observer design | MIMO controller | Experimental validation

ASML

Slide 7
<Date>

Thermo-mechanical model created in Nutils:

$$E(p)\dot{T} = A(p)T + B_1 u + B_2 w$$
$$y = C_y T$$
$$d = C_d T$$

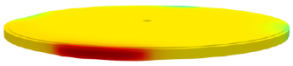

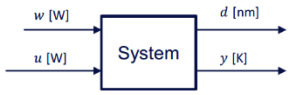

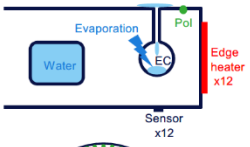

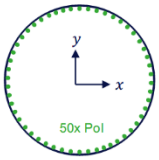

Property: system matrices depend linearly on parameters p
(thermal masses, conductivity, heat transfer coefficients, etc.)

$$E(p) = E_0 + p_1 E_1 + p_2 E_2 + \ \ldots$$
$$A(p) = A_0 + p_1 A_1 + p_2 A_2 + \ \ldots$$

Dimensions model: $T(t) \in \mathbb{R}^{50\,000}$, $u(t) \in \mathbb{R}^{12}$, $y(t) \in \mathbb{R}^{12}$, $w(t) \in \mathbb{R}^{100}$, $d(t) \in \mathbb{R}^{100}$

Public

Model | Parameter calibration | Observer design | MIMO controller | Experimental validation

ASML

Slide 8
<Date>

Variation between systems due to production process

- Using 1 model for all systems is inaccurate
- Calibrate parameters per system

Proposed parameter calibration for large scale systems

- Parametric model-order reduction [1]
  - From 50 000 → 500 states (only once)
  - Parametrization kept after reduction
- Use FRF residual to update parameters

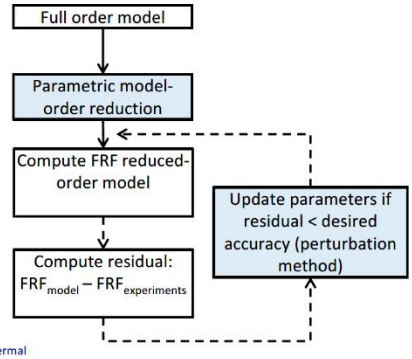

[1] Lou D and Weiland S 2018 Parametric model order reduction for large-scale and complex thermal systems *IEEE 2018 European Control Conference* p 2593-2598 June 12-15 2018, Limassol, Cyprus

Public

Model | Parameter calibration | Observer design | MIMO controller | Experimental validation

ASML

Slide 9
<Date>

Thermo-mechanical model

$$E(p)\dot{T} = A(p)T + B_1 u + B_2 w$$
$$y = C_y T$$
$$d = C_d T$$

Disturbance (integrator) model to map white noise to colored noise

$$\dot{x}_w = A_w x_w + B_w w_{white},$$
$$w = C_w x_w,$$

Augmented observer (Kalman filter)

$$\begin{bmatrix} \hat{E}(\hat{p}) & 0 \\ 0 & I \end{bmatrix} \begin{bmatrix} \dot{\hat{T}} \\ \dot{x}_w \end{bmatrix} = \begin{bmatrix} \hat{A}(\hat{p}) & \hat{B}_2 C_w \\ 0 & A_w \end{bmatrix} \begin{bmatrix} \hat{T} \\ x_w \end{bmatrix} + \begin{bmatrix} \hat{B}_1 \\ 0 \end{bmatrix} u + L\,(y - \hat{y}),$$

Correction for mismatch model and measurements due to evaporative load

$$\hat{y} = \begin{bmatrix} \hat{C}_y & 0 \end{bmatrix} \begin{bmatrix} \hat{T} \\ x_w \end{bmatrix},$$
$$\hat{d} = \begin{bmatrix} \hat{C}_d & 0 \end{bmatrix} \begin{bmatrix} \hat{T} \\ x_w \end{bmatrix},$$

The Kalman gain L follows from solving a Riccati equation

Public

Model | Parameter calibration | Observer design | MIMO controller | Experimental validation

ASML

Slide 10
<Date>

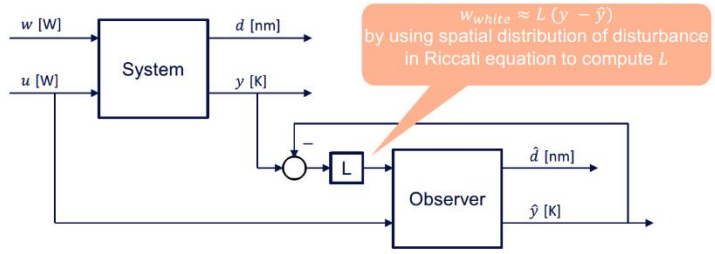

Public

Model | Parameter calibration | Observer design | MIMO controller | Experimental validation

ASML

Slide 11
<Date>

- Recall DBC concept
  - Observer estimates deformation $\hat{d} \in \mathbb{R}^{100}$
  - MIMO controller steers estimate $\hat{d} \rightarrow 0$
- MIMO controller based on Linear Quadratic Regulator (LQR) to minimize $J = \int_{t=0}^{\infty} \left(\hat{d}^T Q_d \hat{d} + u^T u \right) dt$

  $u = -K\hat{d} = -KC_d\hat{T}$
- Observer + MIMO controller = DBC

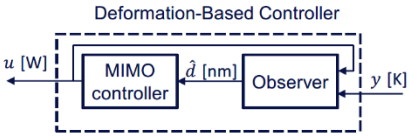

- Closed-loop controller order reduction: from 500 to 100 controller states
  - Makes online implementation feasible

Public

Model | Parameter calibration | Observer design | MIMO controller | Experimental validation

ASML

Slide 12
<Date>

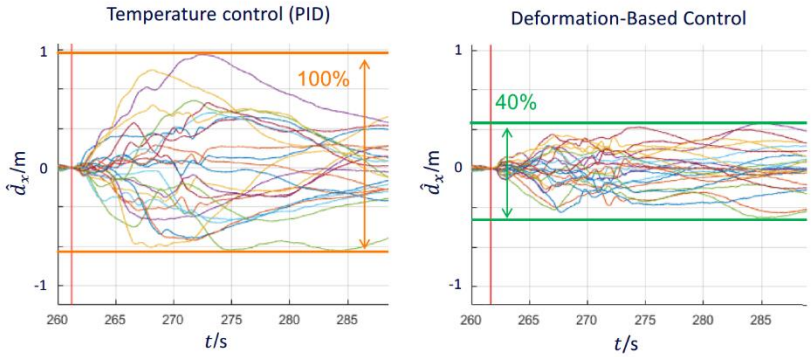

- With DBC, max estimated deformations are reduced to 40% compared to PID control
- Similar results in y-direction

Public

Summary & Future work

ASML

Summary

- Deformation-Based Control …
  - … is a software solution to control thermal deformations
  - … uses existing thermal actuators and sensors
  - … is observer-based and requires a good thermo-mechanical model
    - → parameter calibration
- 60% reduction over temperature controller obtained in experiments

Future work

- Further improve model of system and disturbance
- Automate parameter calibration and tuning

ASML

Disclaimer

ASML

- This publication is subject to change without notice and contains confidential and proprietary information of ASML Holding N.V. or its affiliates ("ASML").
- This documentation is for the intended purpose only and for the use the intended recipient only. Please retain control of this documentation. It is not to be forwarded or distributed. Any unauthorized review, copying, use, disclosure or distribution is strictly prohibited.
- The material herein is provided "AS-IS. and ASML makes no warranty of any kind with regard to this material. ASML shall not be liable for errors and omissions contained herein.
- If this document is in a language other than English, please read the following text carefully.
- While we strive to ensure that the information is translated correctly, no warranty or guarantee, express or implied, is given as to its accuracy or that it is as current as the English version. We accept no liability for any errors or omissions. If there is any conflict or difference between the translated version of this document and its English version, the English version is leading. If any part of the translated version is unclear, reference should be made to the English version.
- We shall not be liable for any damages (including, without limitation, damages for loss of business or loss of profits) arising in contract, tort or otherwise from the use of or inability to use this document, or any material contained in it, or from any action or decision taken as a result of using such material.

Special Interest Group Meeting on Thermal Issues
Laboratory for Machine Tools and Production Engineering (WZL) of
RWTH Aachen, Germany, February 2020
www.euspen.eu

Molecular heat transfer in rarefied gas: experimental determination of thermal accommodation coefficients

Joris P. Oosterhuis[1], Mohammadreza Gaeini[1], Petra van den Heuvel-Bijl[1]

[1] *Philips Innovation Services, Mechatronics department, Eindhoven, The Netherlands*

joris.oosterhuis@philips.com

Abstract
Molecular heat transport in rarefied gas can be a significant factor in the thermal system performance of vacuum applications. An experimental setup is realized to measure the relation between gas pressure and heat transfer coefficient, which is determined by the thermal accommodation coefficient. The influence of surface contamination on the thermal accommodation coefficient is investigated and found to be of significant impact on the heat transfer performance.

Thermal accommodation coefficient, vacuum, Sherman-Lees, rarefied gas, surface adsorption, monolayers, heat transfer coefficient

1. Introduction

Thermal management under vacuum conditions can be crucial in the performance of high-precision equipment. Two heat transfer mechanisms play a role in heat transport through a vacuum: thermal radiation and molecular heat transport. Especially at ambient temperatures (or lower) and when there is a considerable amount of gas (few Pascal and higher), the molecular heat transport will dominate the overall heat transfer rate.

Unlike in continuum conditions, the heat transfer coefficient in the free molecular regime is dependent on the gas pressure as well as on various gas and surface properties. This heat transfer process is illustrated in Figure 1: an incident gas molecule with temperature T_i interacts with a solid surface with (constant) temperature T_s, thereby exchanging energy such that the temperature of the reflecting molecule has changed to T_r.

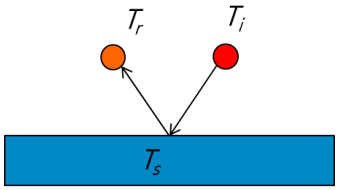

Figure 1. Illustration of molecular heat transfer process.

The efficiency of this molecular heat transport is expressed by means of the thermal accommodation coefficient α:

$$\alpha = \frac{T_r - T_i}{T_s - T_i}$$

The thermal accommodation coefficient is an important model parameter to predict the heat transfer rate. For two parallel solid plates with an intermediate gas medium, a commonly used model that describes the relation between heat transfer coefficient and gas pressure is the so-called Sherman-Lees relation [1], [2]:

$$\frac{1}{h_g} = \frac{d_g}{\lambda_g} + \frac{2-\alpha}{\alpha} \cdot \frac{\sqrt{\frac{\pi M_g T}{2R}}}{\left(1+\frac{\zeta}{4}\right)p} \qquad [\text{Eq. } 1]$$

with h_g the heat transfer coefficient between the two parallel plates, d_g the distance between the plates, λ_g the continuum gas conductivity, M_g the gas molecular mass, R the universal gas constant, ζ the atomic degrees of freedom of the gas, T the gas temperature and p the gas pressure. Figure 2 shows an example result of the Sherman-Lees relation for nitrogen and a 300 µm gap size with pressure on the horizontal axis and gap heat transfer coefficient on the vertical axis. Note that the heat transfer coefficient approaches a constant value for pressures inside the continuum regime whereas in the free molecular regime a clear pressure dependency can be observed.

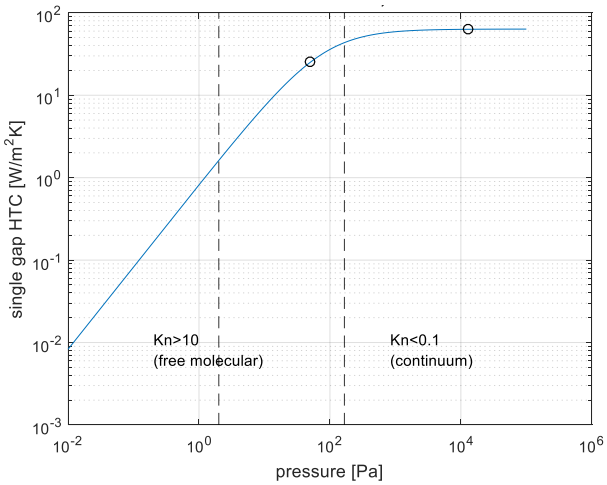

Figure 2. Result of Sherman-Lees relation for nitrogen at a 300 µm gap size.

It is apparent that knowledge on the thermal accommodation coefficient α is essential to predict the relation between heat transfer coefficient and gas pressure. However, α is dependent on both gas and surface characteristics such as surface material, surface roughness, gas composition, cleanliness of the surface (i.e., adsorped monolayers) and much more. In literature, some generic values α can be found for limited cases. For instance, comparable work has been performed at Sandia National Laboratories [3]. For practical applications where accurate

thermal modelling is required, the thermal accommodation coefficients needs to be determined for each specific situation.

The current work describes the development of an experimental setup at Philips Innovation Services to determine the thermal accommodation coefficient for different solid surfaces under a controlled gas composition and gas pressure. The focus is to achieve high accuracy on reproducibility (typically 1 %3σ) to be able to perform comparative measurements. In Section 2 the measurement principle and realized experimental setup is described. Section 3 is devoted to a brief discussion on measurement results. Finally, some conclusions are drawn in Section 4.

2. Experimental setup

An experimental setup is designed to realize and measure a steady-state heat flow in a slit between two parallel surfaces while controlling the gas conditions in the slit. The measurement principle is shown in Figure 3. The heat flow between the surfaces is induced by the temperature difference of the plenums that are water-conditioned at 35˚C and 15˚C. On the centre axis of each plenum, two temperature sensors (Amphenol SC30 NTC's) are embedded (T_1, T_2 and T_3, T_4).

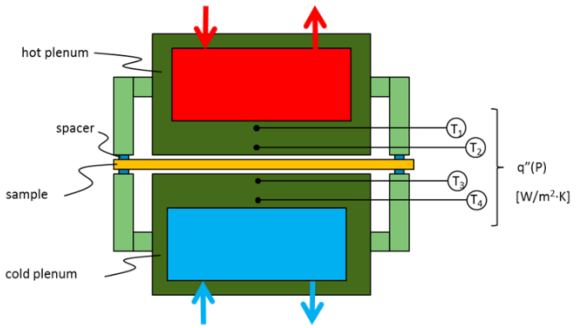

Figure 3. Schematic of measurement principle.

From the measured temperature difference, the mutual distance of the temperature sensors, and the thermal conductivity of the plenum material, the heat flux $\dot{q}$ through a plenum is calculated. Under the assumption of a purely one-dimensional heat flux (see Section 2.3), the heat transfer coefficient through the gap h_g can be calculated from:

$$h_g = \frac{\dot{q}}{T_{s,top} - T_{s,bot}} \qquad [\text{Eq. } 2]$$

with $T_{s,top}$ and $T_{s,bot}$ the surface temperatures of the top and bottom plenum, respectively. These temperatures are obtained through extrapolation from the measured temperatures. This measurement is carried out at two different pressure set points, typically at 50 Pa and 13000 Pa (see Section 2.2). As such, the thermal accommodation coefficient can be derived independent of the actual gap height (see Eq. 1).

2.1. Sample measurement

So far, this explains the measurement principle for a single gap (plenum-to-plenum). In order to examine various surface materials, a sample can be placed in between the two plenums (as depicted in Figure 3) and is typically spaced at 400 µm with respect to the plenum surfaces using ceramic studs (light green in Figure 3) and stainless steel spacers with a variable thickness. The gap height is a trade-off between temperature signal and mechanical tolerances. Consequently, two slits exist on either side of the sample and the Sherman-Lees relation can be extended accordingly to:

$$\frac{1}{h_g} = 2 \cdot \left(\frac{d_g}{\lambda_g} + \frac{\alpha_p + \alpha_s - \alpha_p \alpha_s}{\alpha_p \alpha_s} \cdot \frac{\sqrt{\frac{\pi M_g T}{2R}}}{\left(1 + \frac{\zeta}{4}\right) p} \right) + \frac{d_s}{\lambda_s} \qquad [\text{Eq. } 3]$$

with d_s and λ_s the thickness and thermal conductivity of the sample, respectively. The plenum-to-plenum thermal accommodation coefficient α_p is used as an input to finally derive the thermal accommodation coefficient for the sample, α_s.

2.2. Gas control

The setup as shown in Figure 3 is placed inside a vacuum vessel (CF DN160 6-way cross) that is equipped with a pump set (Pfeiffer HiPace80 turbo-molecular pump and Adixen ACP15 pre-pump). Two pressure sensors are mounted on the vessel, each covering a different measurement range (MKS Baratron 0 – 133 Pa and 0 – 13300 Pa). The 13000 Pa pressure set point is realized by filling the vacuum vessel with a carrier gas and then carrying out the temperature measurement. For the 50 Pa set point, a continuous flow of carrier gas is provided to the vacuum vessel and pumped away through the pumping system at approximately 190 mL_n/min. The flow rate is controlled using a mass flow controller (Bronkhorst F-201CV-200) and regulated using a control feedback loop with the pressure sensors to maintain a constant pressure throughout the measurement.

Next to the carrier gas flow, also traces of different components can be added to the gas stream in order to investigate the effect of surface monolayer adsorption on the thermal accommodation coefficient. Liquid substances (such as water) are evaporated using a Bronkhorst CEM system prior to mixing-in. A simplified flow diagram of the gas supply system is shown in Figure 4. To realize a dynamic range of partial pressure from $1 \cdot 10^{-4}$ – 1 Pa at a total pressure of 50 Pa, an optional dilution step is added (MFC2 in Figure 4) while the remainder of the mixed gas flow is vented.

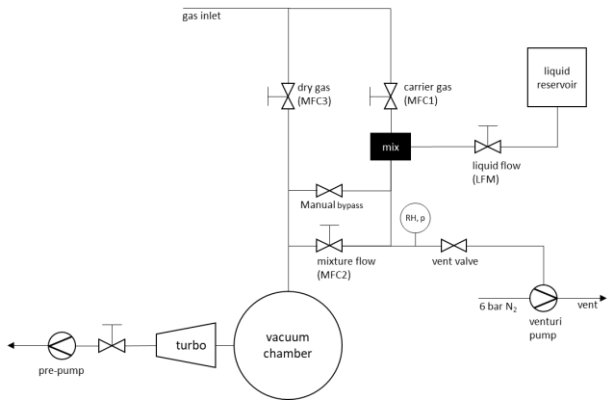

Figure 4. Simplified flow diagram of gas supply system.

2.3 Parasitic heat fluxes

The measurement principle is based on the assumption of one-dimensional heat flux through the plenums and no cross talk with other parts of the experimental setup. In reality, there will be a certain amount of heat transfer between the plenums and the vacuum vessel walls. This does result in an offset in the temperature difference measurement from both plenums. To minimize the impact of environmental temperature variations on the measurement reproducibility, the vacuum vessel walls are water-conditioned at 25 °C. As the residual parasitic heat flux to both plenums is comparable, the influence on the heat transfer measurement is largely mitigated by averaging the heat flux measurements from the top and bottom plenums.

3. Results and discussion

As a first step in order to quantify the setup measurement reproducibility, five consecutive measurements on the same sample are performed over a time span of two weeks (including sample mounting and removal) using nitrogen as a carrier gas. The relative difference in α_s with respect to the average value is depicted in Table 1. This results in a determined measurement reproducibility of 1.1 %3σ.

Table 1 Variation in $\boldsymbol{\alpha_s}$ for five consecutive measurements using nitrogen.

Number	$\Delta\alpha_s$ [%]
1	0.07 %
2	0.13 %
3	-0.51 %
4	-0.27 %
5	0.58 %

One of the key questions in this research is the impact of surface cleanliness on the thermal accommodation coefficient. As such, the difference between various metal engineering samples "as received" and after an additional cleaning procedure is measured, both using nitrogen as carrier gas. The cleaning procedure constitutes of a wipe with iso-propanol followed by a vacuum bake-out procedure of 24hr at 120 °C. Afterwards, the sample is transported from the collocated bake-out facility to the measurement setup. An in-situ bake-out would be more effective in removing water monolayers from the sample, but is not possible due to temperature limitations on the sensors in the setup.

Table 2 shows the change in thermal accommodation coefficient before and after this cleaning procedure. In general, there is a clear decay in α_s visible. This can potentially be attributed to the removal of hydrocarbons from the sample surface, originating from coolants used in machining steps. The impact of cleaning is very variable for the different samples, probably due to differences in the manufacturing processes.

Table 2 Change in $\boldsymbol{\alpha_s}$ after performing cleaning procedure on metal samples.

Sample	$\Delta\alpha_s$ [%]
A	-8.1 %
B	-12.4 %
C	0.5 %
D	-1.5 %
E	-4.1 %
F	-2.3 %

The previous investigation shows the vulnerability of the thermal accommodation coefficients to adsorped monolayers on the surface and is in line with prior research [3], [4]. In order to investigate this in a more controlled manner, a pre-defined concentration of traces is added to the vacuum. This allows in-situ monitoring of a change in heat transfer coefficient due to monolayer formation. One example of such an experiment is depicted in Figure 5. Here subsequently 0.6 Pa, 2.4 Pa, 4.2 Pa, and 5.5 Pa of water is added to a 50 Pa total pressure of nitrogen. Measured impact of adding water on the heat transfer coefficient is up to 4.0 % compared to the case where no additional water is added.

Note that this not necessarily resembles a change in the thermal accommodation coefficient as adding water to the carrier gas also changes the overall gas properties. Moreover, it is very likely that this result is influenced by initial monolayers of water being adsorbed on the sample surface while transporting from the vacuum bake-out facility towards the measurement setup. In order to examine this further, different trace gases and / or an in-situ water desorption facility needs to be realized.

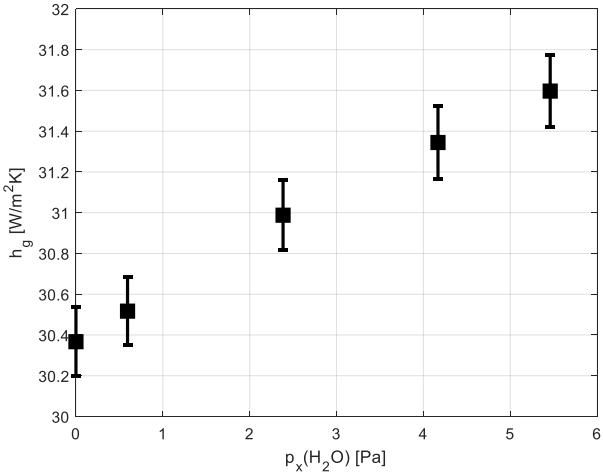

Figure 5. Impact of adding water on heat transfer coefficient in gap using nitrogen as carrier gas. Error bars indicate ±1σ on measurement data.

4. Conclusions

An experimental setup is realized to measure the thermal accommodation coefficient in rarefied gas conditions. From this coefficient, the pressure dependent heat transfer between two solid surfaces can be calculated using the Sherman-Lees relation. The measurement reproducibility of the setup is shown to be in the order of 1 %3σ. From the impact analysis on the cleaning procedure, it can be derived that it is crucial to apply a vacuum bake-out in applications where a predictable thermal accommodation coefficient is required. Future research will focus on gaining better physical understanding of the effect of surface cleanliness on the thermal accommodation coefficient.

References

[1] F. S. Sherman, "A survey of experimental results and methods for the transition regime of rarefied gas dynamics," *Rarefied Gas Dyn.*, vol. **2**, pp. 228–260, 1963.

[2] L. Lees and C.-Y. Liu, "Kinetic theory description of plane compressible Couette flow," *Rarefied Gas Dyn.*, pp. 391–428, 1961.

[3] W. M. Trott, J. N. Castaneda, J. R. Torczynski, M. A. Gallis, and D. J. Rader, "An experimental assembly for precise measurement of thermal accommodation coefficients," *Rev. Sci. Instrum.*, vol. 82, no. **3**, pp. 1–12, 2011.

[4] S. Song and M. M. Yovanovich, "Correlation of thermal accommodation coefficient for 'engineering' surfaces," in *American Society of Mechanical Engineers, Heat Transfer Division, (Publication) HTD*, 1987, vol. **69**, pp. 107–116.

Compensation and Correction of Thermal Effects

Special Interest Group Meeting on Thermal Issues
Laboratory for Machine Tools and Production Engineering (WZL) of
RWTH Aachen, Germany, February 2020
www.euspen.eu

Controlling Temperature Effects on Dimensional Measurements – Overview and new Approaches

Dietrich Imkamp, Aline Baumeister [1)]

[1] *Carl Zeiss Industrielle Messtechnik GmbH, D-73446 Oberkochen*

dietrich.imkamp@zeiss.com

Abstract
Temperature might be the most sensitive influence for dimensional measurements in industrial production because of thermal expansion of most materials used. Therefore, the temperature environment conditions and the workpiece temperature need to be observed carefully. The observation results are used to correct the thermal expansion of the workpiece considering certain constrains and to assure that the environment temperature does not exceed these constrains. Active climatization of workpieces helps to accelerate the measurement of work pieces heated by manufacturing.

Dimensional Metrology, Temperature Metrology, Climatization

1. Introduction

Temperature might be the most sensitive influence for dimensional measurements in industrial production because of thermal expansion of most materials used. The standards for Geometrical Product Specification define in ISO 1 the standard reference temperate to 20°C [1]. Most production facilities do not provide an environment with a constant temperature of 20°C. Furthermore, manufacturing processes heat up the product to be measured. Therefore, dimensional measurements are perfumed at temperatures that are different to 20°C and results must be corrected depending on temperature and thermal expansion.

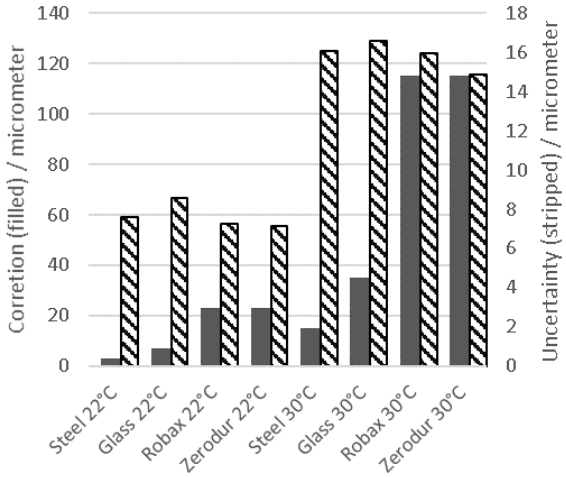

Figure 1. Correction and its uncertainty for measuring 1m length on a steel workpiece with different scale materials at 22 and 30°C

Most corrections are made based on a linear expansion model. The details of the correction calculation considering also the expansion of the used scale are describe in ISO/TR 16015 [2]. Moreover, this standard includes the determination of the corresponding uncertainty for the correction. Figure 1 shows example values of correction and uncertainty for measuring 1 m length on a steel workpiece (Coefficient of Thermal Expansion CTE=11.5*10-6 /K) with different scale materials considering information from [2-5].

The corrections for steel scales are the lowest one because thermal expansion of scale and workpiece compensate each other. Nevertheless, the lowest uncertainty is achieved using temperature insensitive material made of glass ceramic like Robax or Zerodur from Schott AG, Germany.

A closer look on the distributors to the uncertainty of the correction shows the dominating impact of workpieces's thermal expansion. The contribution of the scale in case of insensitive material is close to zero except for Robax scale due to its uncertain CTE (Figure 2) [6].

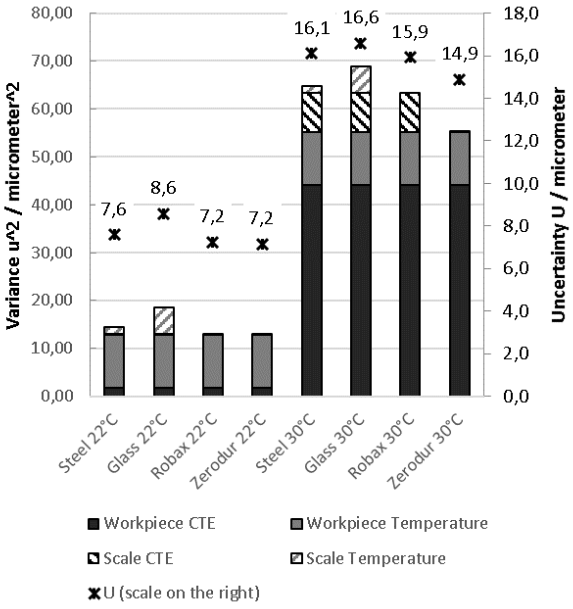

Figure 2. Uncertainty of correction for measuring 1m length on a steel workpiece with different scale materials at 22 and 30°C (The uncertainty is calculated from the square root of the linear combination of the different component's variances [2, 7]. Therefore, the variances are used here for the presentation of component's contribution in the bars.) [6]

2. Supervision of Temperature Conditions

Nevertheless, the performance of complex measuring systems for dimensional measuring tasks like Coordinate Measuring Machines (CMMs) cannot be described by the scale expansion only. Therefore, the manufacturers specify operating conditions for their system. In case of CMMs a temperature range and limits for spatial and temporal thermal gradients are defined. The supervision of these operating conditions requires a temperature measuring system with several sensors that combines the results from the different sensors to determine the gradients. The installation setup of the sensors depends on the individual CMM location and its environment conditions. Recommendations for the setup are available in German guideline VDI/VDE 2627 [8, 9], which also classifies the environment in relation to the temperature stability. The data from the sensors are recorded and a dashboard presents the results and indicates warnings in case of limit violations (Figure 3).

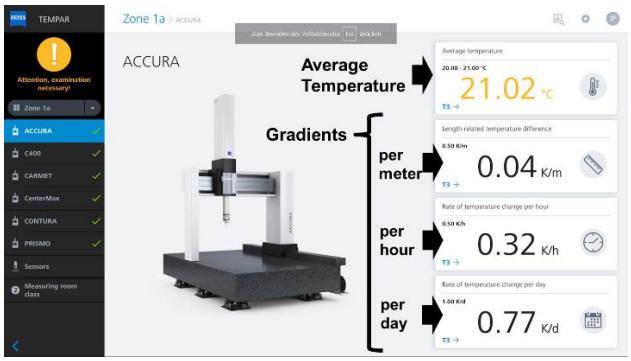

Figure 3. Dashboard of the temperature supervision system TEMPAR from ZEISS with visualisation of temperature and temperature gradients

3. Workpiece Temperature Recording and CTE Calibration

A prerequisite for correction of length temperature is the precise determination of workpiece's temperature. Different types of contact sensors are used for that purpose. Pallet integrated sensors with spring force contact are used for automatic loading. Also, the CMM itself can carry an automatic changeable temperature sensor instead of the dimensional sensor (Figure 4).

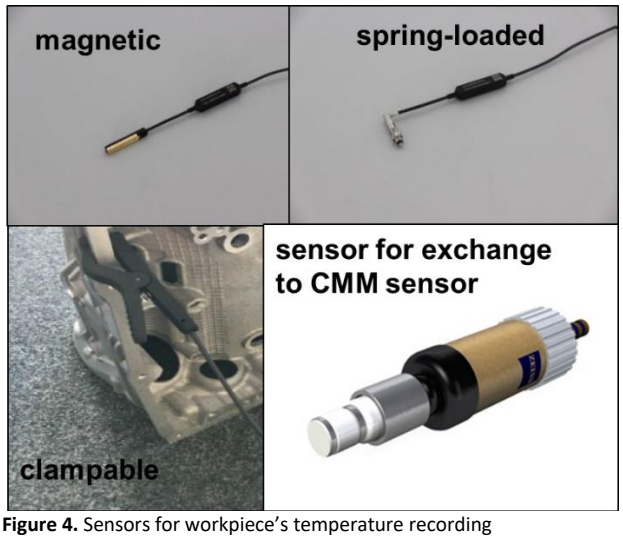

Figure 4. Sensors for workpiece's temperature recording

The recorded temperature data are used for correction as described above. This correction is a static correction and does not consider any gradients. This is an issue for measuring systems like CMMs that measure characteristics consecutively. The implementation of a dynamic correction does not seem possible due to the complex relationship between the consecutively measured characteristics and corresponding dates.

Beside the precision of workpiece's temperature measurement, the CTE (Coefficient of Thermal Expansion) influences the uncertainty of thermal expansion correction significantly. The variation of CTE among several heat treatments of the same steel reaches up to 10% [2]. Therefore, the calibration of CTE (Figure 5) may reduce the uncertainty of the thermal correction.

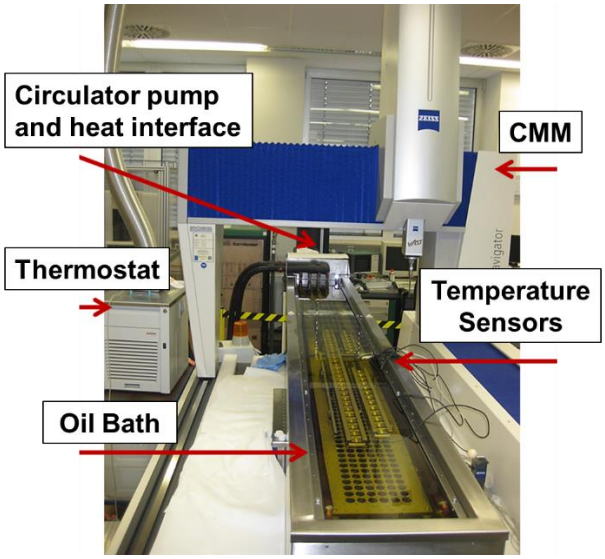

Figure 5. Calibration for coefficients of thermal expansion (CTE) at ZEISS's calibration lab

4. Active Climatization for Workpieces

Workpieces that come directly from machining are often heated up by the process. Afterwards they cool down and adapt to the ambient temperature. The cooling process can take several hours (Figure 6).

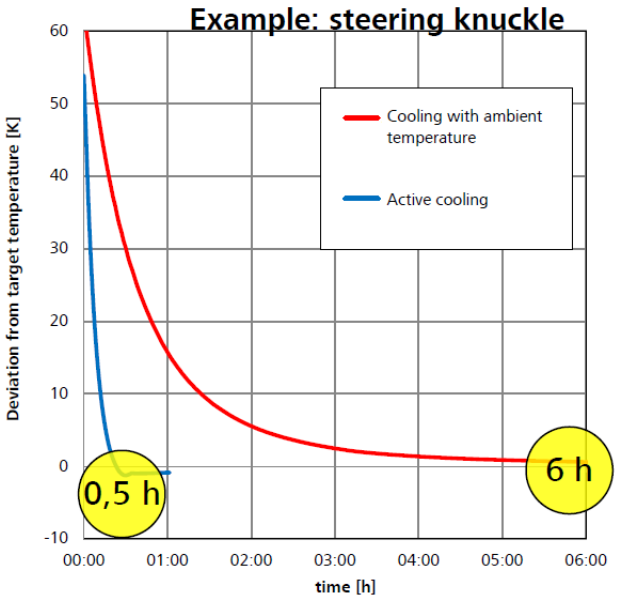

Figure 6. Cooling curves with and without active air conditioning

If a largely constant temperature is not reached measuring is not possible, because the dimensions of the workpiece are constantly changing, which cannot be compensated with static corrections. This delays rapid feedback to manufacturing. Using an active climate chamber (Figure 7) this time can be reduced dramatically. The coloured lighting shows workpiece's temperature gradient. Green indicates that the workpiece is ready to measure.

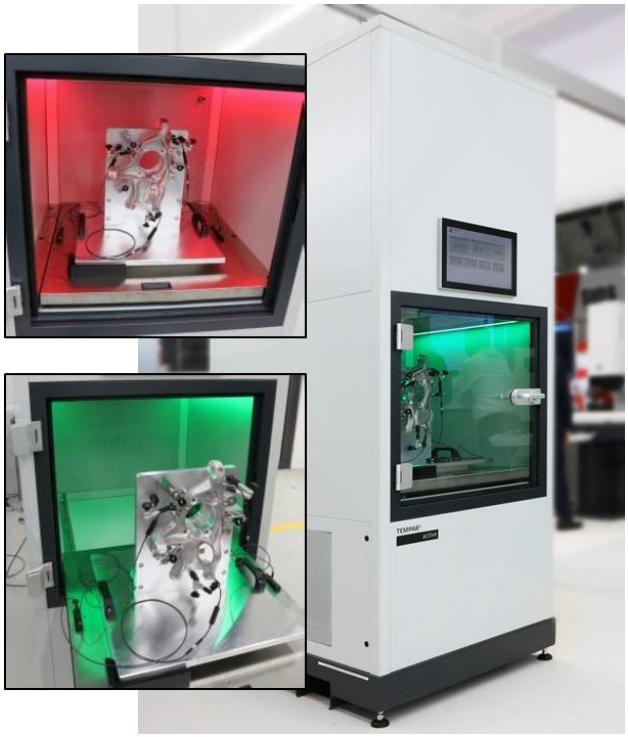

Figure 7. Active climatization for workpieces ("Zeiss TEMPAR active")

5. Summary and Outlook

The magnitude of workpieces' thermal expansion in industrial production reaches typical tolerances. Therefore, precise thermal expansion correction plays an important role in measuring dimensional characteristics. Beside accurate measurement of workpiece's temperature, calibration of workpiece's CTE and supervision of environment temperature to assure of specified operating conditions for measuring system, active workpiece climatization can accelerate the dimensional measurement process.

New ideas for more accurate thermal expansion correction may improve the accuracy of the correction [10]. But the effort increases dramatically.

References

[1] ISO 1: 2016 Geometrical Product Specifications (GPS) - Standard reference temperature for the specification of geometrical and dimensional properties, 2016-12.

[2] ISO/TR 16015: 2003 Geometrical product specifications (GPS) – Standard reference temperature for geometrical product specification and verification – Systematic errors and contributions to measurement uncertainty of length measurement due to thermal influences, 2004-02.

[3] ASM International (American Society for Metals): ASM Ready Reference: Thermal Properties of Metals, ASM International, Materials Park, Ohio, USA 2002.

[4] Neumann, H. J.: Messen mit geringem Temperatureinfluss, Lassen temperaturstabile KMG die Temperatur vergessen?, QZ, Qualität und Zuverlässigkeit, Carl Hanser Verlag, München Jg. 53 (2008), Nr. 1, S. 30-33.

[5] Dr. J. Heidenhain GmbH: Exposed Linear Encoders, Brochure, Germany 05/2019; (Internet, 10.11.2019 https://www.heidenhain.de/fileadmin/pdb/media/img/208960-2F_Exposed_Linear_Encoders_en.pdf)

[6] Imkamp, D.: Metrology on the shop floor, where else? – Potentials and Limitations, Presentation on Forum of Etalon AG, Volkswagenhalle, Braunschweig, Germany 03.-04.11.2016

[7] JCGM 100:2008 Evaluation of measurement data – Guide to the expression of uncertainty in measurement, JCGM (Joint Committee for Guides in Metrology) 2008 (Internet 05.11.2019: http://www.bipm.org/en/publications/guides/gum.html).

[8] VDI/VDE-Richtlinie 2627 part 1 Measuring rooms - Classification and characteristics, December 2015.

[9] VDI/VDE-Richtlinie 2627 part 2 Measuring rooms - Guide for planning, construction and operation, October 2005.

[10] Ohlenforst, M.: Model-Based Thermoelastic State Evaluation of Large Workpieces for Geometric Inspection; PhD thesis, University Aachen, Germany 2019

Special Interest Group Meeting on Thermal Issues
Laboratory for Machine Tools and Production Engineering (WZL) of
RWTH Aachen, Germany, February 2020
www.euspen.eu

Development of a method for the evaluative comparison of procedures for the correction and compensation of thermally induced errors on machine tools

Carola Gißke[1], Tom Albrecht[2], Hajo Wiemer[2], Werner Esswein[1], Steffen Ihlenfeldt[2]

[1]*Chair of Business Economics, esp. Systems Development, Technische Universität Dresden, Dresden, Germany*
[2]*Chair of Machine Tools Development and Adaptive Controls, Technische Universität Dresden, Dresden, Germany*

tom_morris.albrecht@tu-dresden.de

Abstract
The demands for increased productivity and manufacturing accuracy mean that the relevance of thermally induced displacements of the TCP on machine tools is constantly increasing.
In order to avoid errors in the resulting workpiece geometry, the SFB/TR 96 "Thermo-energetic design of machine tools" develops various solutions for correction and compensation.
This work presents a comprehensive assessment method of these solutions. In addition to the purely technical aspects, economic factors are also taken into account in order to be able to assess the solutions holistically. The aim is to classify the entire implementation effort and the benefits of the solutions.
With the help of this method it is possible to offer potential users an optimal selection taking into account their operational requirements and their requirements for the correction or compensation procedure.

Evaluation, Knowledge management, Methodology, Thermal error

1. Introduction

In order to increase the productivity of machine tools, it is often necessary to increase the drive power. The associated power losses lead to increased thermally induced deformation.
With the simultaneous demand for increased manufacturing accuracy, the resulting displacement of the TCP can lead to relevant errors in the workpiece geometry.
The aim of the project SFB/TR 96 “Thermo-energetic design of machine tools” is to research and develop compensation and correction procedures in order to solve the conflicting goals of energy input, precision and productivity within the chipping production. Within this project, a holistic evaluation of the developed procedures will be conducted, which considers both technical and economical aspects. A suitable valuation metric should take into account the thermo-energetic efficacy of each procedure, its applicability for defined use scenarios, as well as the impact on the amount of resources needed. To address the complexity of such a valuation method, an approach is being conducted that, on the one hand, evaluates the applicability of each procedure for predefined operational scenarios through measurements and, on the other hand, captures the procedure’s impact on all phases of the product life cycle by conceptual semi-formal modelling.
In the following section, the method of assessing the overall effort and costs for each solution procedure will be displayed. In section 3, the approach for the assessment of the efficiency will be explained. Furthermore, a concept of a rule-based recommender-tool will be presented in section 4, which will make the designed valuation method available. In the end, an outlook will be given on future work that needs to be conducted.

2. Assessment of the overall effort

In order to carry out a detailed and transparent assessment of the costs and effort, each developed solution procedure is being modelled with the Business Process Model and Notation (BPMN). BPMN is a modelling language for the representation of business processes and allows the illustration of actions, responsibilities, decision processes and artefacts such as documents or resources. The BPMN was chosen since it is broadly accepted in research and industry [1] and, moreover, allows a light-weighted definition of language extensions, which facilitates the representation of artefacts that are specific for the project context. For the inquiry of the process steps, an interview is being conducted with one expert each of the according solution procedure. For each process step, the material and immaterial resources needed are being displayed, as well as eventual related risks. Figure 1 illustrates an extract of a modelled procedure.
Furthermore, each expert is being asked to estimate the life cycle costs of the method examined. Therefore, the costs given in the VDMA guideline 34160:2006 are being used, which are subdivided into the phases installation and implementing, operations and recycling and dismantling [2]. Thus, the modelling of processes has two objectives. On the one hand, the procedures are made comprehensible and on the other hand, the estimated effort and costs become transparent and reasonable. Next to the assessment of effort, the interviews should enable a statement to be made about the flexibility and long-term behavior of the procedures. The estimations conducted in one-on-one interviews will be evaluated with an expert panel according to the Delphi method, if necessary in several runs [3].
Since the procedures that are to be examined are part of a

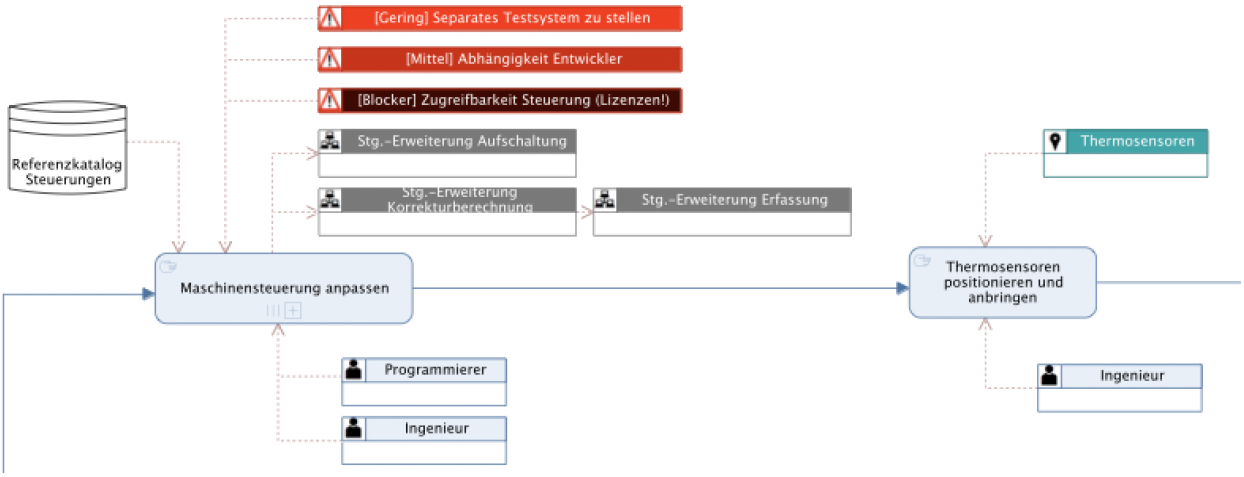

Figure 1. Extract of a modelled solution procedures

project which is still running, they are still in the research process and not fully developed, yet. Therefore, the estimated effort may change as the research goes on. In order to address this within the valuation metric, the concept of the technology readiness level (TRL) [4] will be utilized and included in the evaluation by considering the potential for improvement a higher level of technological readiness can entail.

3. Assessment of the efficiency

In addition to the experts' assessments from the interviews, an exemplary comparative measurement is necessary to prove the effectiveness and the evaluation of the working accuracy.
As described in [5], the relevant drives are loaded by cyclically executed traversing regimes without cutting process.
The regimes are designed in such a way that they represent the already defined technological applications as well as possible.
The thermally induced displacement of the TCP is determined with the developed test piece. With this method, the time course of the thermally induced displacement of the TCP in x, y and z direction relative to the initial state can be measured [6].
The test is carried out and the measurement results evaluated in accordance with the specifications of ISO 230-3 [7].
By comparing the results for the machine with and without the implemented solution method, the improvement of the accuracy in x, y and z direction can be evaluated.
The process stability is determined by multiple repetitions of these measurements.

4. Conception of a recommender tool

The results of the effort analysis and the measurements for the suitability assessment will now be used to carry out a comparative evaluation of the solution procedures. This will be done by using a multiple-criteria decision analysis method (MCDA). The rules of decision logic on which the method is based are to be implemented in a software-based tool. The evaluation is implemented on a case by case basis. That means that the available solution procedures are compared with an initial scenario defined by the user and examined for their solution potential. As a result, a selection of the procedures is issued that are suitable to address the initial problem, stating the expected effort and benefit. This may also include a combination of procedures. So, in the end the user can choose between a set of procedures, that are all suitable to solve the defined problem and build the decision according to personal preferences upon the expected efforts displayed.

5. Conclusion and outlook

This paper describes a method to evaluate and characterize different correction and compensation procedures for thermally induced defects on machine tools.
In addition to solely technical aspects, such as positioning accuracy and process stability, economic aspects are also considered in order to estimate the implementation and maintenance effort. Expert interviews and comparative measurements build the basis for this.
Based on these findings, a recommender tool will be developed. Potential users will be able to select a correction or compensation procedure that optimally suits their capabilities and needs. The characterization provides a better overview of the effort and benefits of a solution and thus, helps to reduce the inhibition threshold for its implementation.
The methods and procedures presented are still in the development stage and therefore, no definite results can be presented at this point.
In the future, it will be necessary to extend the recommender tool by further correction and compensation methods and to make them available to potential users. In this way, weak points and missing aspects will be revealed in the evaluation, which will have to be corrected and added.

References

[1] Kirchner K, Malessa, C, Scheuerlein, H and Settmacher, U 2014 Experience from collaborative modelling of clinical pathways. *In (Hess, M and Schlieter, H (eds.)): Modellierung im Gesundheitswesen: Tagungsband des Workshops im Rahmen der Modellierung ICB Research Report* 13-24
[2] Bünting, F 2018 VDMA Excel-Berechnung zur Prognose von Lebenszykluskosten https://www.vdma.org/v2viewer/-/v2article/render/15237352
[3] Ammon, U 2009 *Handbuch Methoden der Organisationsforschung*
[4] Mankins, J C 2009 Technology readiness assessments: a retrospective *Acta Astronautica* **65** 1216-23
[5] Wiemer H, Neidhardt L, Esswein W and Braun R 2014 Technical and Economic Benchmarking Guideline for the Compensation and Correction of Thermally Induced Machine Tool Errors *Thermo-energetic Design of Machine Tools* 233-246
[6] Neidhardt L, Höfer H and Wiemer H 2014 Prüfwerkstück zum Nachweis von thermisch bedingten Verlagerungen an Fräsmaschinen *ZWF Zeitschrift für wirtschaftlichen Fabrikbetrieb* 814-818
[7] ISO 230-3: Test code for machine tools - Part 3: Determination of thermal effects - [2007-8]

Special Interest Group Meeting on Thermal Issues
Laboratory for Machine Tools and Production Engineering (WZL) of
RWTH Aachen, Germany, February 2020
www.euspen.eu

Simulation based comparison of thermal error modelling methods for machine tools

Philip Blaser[1], Josef Mayr[2] and Konrad Wegener[1]

[1]Institute of Machine Tools and Manufacturing (IWF), ETH Zürich, Leonhardstrasse 21, 8092 Zurich, Switzerland
[2]inspire AG, Technoparkstrasse 1, 8005 Zurich, Switzerland

blaser@iwf.mavt.ethz.ch

Abstract
The temperature field of machine tool structures change constantly in response to external and internal heat changes, as do the thermal deviations of the TCP. This leads to inaccuracy of machined work pieces. Therefore it is necessary to minimize the occurring thermal errors of machine tools. This paper shows, that for accurate thermal error models based on input-output behaviour, a dynamic modelling approach is necessary to capture the time dependent thermal errors. It is shown, based on a simple thermo-mechanical FEM model, that the ARX model structure outperforms static as well as other dynamic models.

Thermal errors, modelling, dynamic, FEM

1. Introduction

In this work, a time series modelling approach of thermal errors based on the system identification theory is presented. System identification is the subject of constructing or selecting models of dynamical systems to serve certain purposes. This modelling approach is capable of describing the non-instantaneous relationship of input and output based on the dynamic nature of thermo-mechanical systems. The aim of the model is to predict thermally induced errors of machine tools in dependency of varying thermal loads.

2. Models of Time-Invariant Systems

The relationship between temperature data and the thermal position and orientation errors at the TCP can be described by a linear time-invariant dynamic system. As explained by Tangirala [1] the output of such systems can be expressed as weighted sum of a finite number of past inputs u and outputs y as well as a disturbance term e. The additive disturbance term e is introduced to describe modelling uncertainties, such as, modelling approximation, unrecognized and not modelled inputs, and noise-corrupted measurements. According to Ljung [2] a linear time-invariant system can be written in a general form as follows:

$$A(q)y[k] = \frac{B(q)}{F(q)}u[k] + \frac{C(q)}{D(q)}e[k] \quad (1)$$

$A(q)$, $B(q)$, $C(q)$, $D(q)$ and $F(q)$ denote five different polynomials influencing the input $u[k]$, the output $y[k]$ as well as the disturbance term $e[k]$. With the use of different combinations of these five polynomials, 32 unique model sets can be created. The structure of Equation (1) is too general for most practical purposes. One or several of the five polynomials can be fixed to unity in most applications. Additionally the time-shift operator q is used as follows:

$$q \cdot u[k] = u[k+1] \quad and \quad q^{-1}u[k] = u[k-1] \quad (2)$$

2.1. Autoregressive Model with Exogenous Inputs

The linear difference Equation (1) maps the past input and output data into the current output and provides a parsimonious system description. According to Mayr et al. [3] the input output description of thermo-mechanical systems can be written as:

$$A(q)E[k] = B(q)u[k] + e[k] \quad (3)$$

where $E[k]$ are the thermal position and orientation errors at the TCP. Such a model is called ARX, where AR refers to the autoregressive part $A(q)E[k]$ and X to the extra input $B(q)u[k]$, also called the exogenous input. A unique feature of this approach is the possibility to analytically estimate the model parameters with the least-squares estimator.

3. Simulation

The temperature field of the machine tool structure changes constantly in response to external and internal heat changes, as do the thermal deviations at the TCP. As pointed out by Yang and Li [4] the unmodelled dynamic characteristics of temperature variables and thermal errors are the major causes of inaccurate and non-robust thermal error modelling using a static modelling approach.

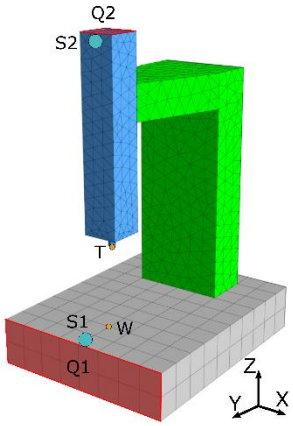

Figure 1. 3D FEM model of simplified machine tool structure. Indication of heat sources, Q1 and Q2, temperature recording spots, S1 and S2, as well as thermal deviation measurement points, T and W.

In this section, a comparison of different static and dynamic modelling methods are used to verify this theory. With the use

of a simulation framework the performance of the different models are compared. A three dimensional FEM model of a simplified machine tool structure is built as shown in Figure 1. The modelled machine consists of three bodies, base, column and spindle. All bodies are modelled with the same material. The FEM model is used to simulate both the transient temperature field as well as the thermo-mechanical deviations using the commercial FEM software MORe [5].

The machine model has two independent heat sources. Heat source Q1 is located at the front end of the base, the heat source Q2 is located at the top of the spindle body. In order to monitor the heat flux inputs of the two independent heat sources, two virtual temperature sensors S1 and S2 are located close to the heat sources. The relative drift between the points T and W is considered as the three dimensional thermal deformation, X, Y and Z direction, of this machine structure.

The model parameters and material properties are shown in Table 1. All material property coefficients are considered temperature independent, since the range of temperature is small.

Table 1. Material properties and model parameters of FEM model.

Thermal conductivity	k	60.5 W/mK
Specific heat capacity	c	434 J/kgK
Thermal expansion coefficient	α	12 µm/mK
Convection coefficient	h	5 W/m²K
Environmental temperature	T_{Env}	20 °C
Density	ρ	7850 kg/m³
Length	D_L	1 m
Width	D_W	0.8 m
Height	D_H	1.4 m

To excite a broad spectrum of dynamics of the system, the heat flux data is generated in a random pattern for a total of 48 hours. Two sets of input data for the two heat sources are generated, as shown in Figure 2. One is used for model training, while the other is used for model validation. To simplify the problem, the heat loads are switched and scaled for the validation data set, as can be seen in Figure 2.

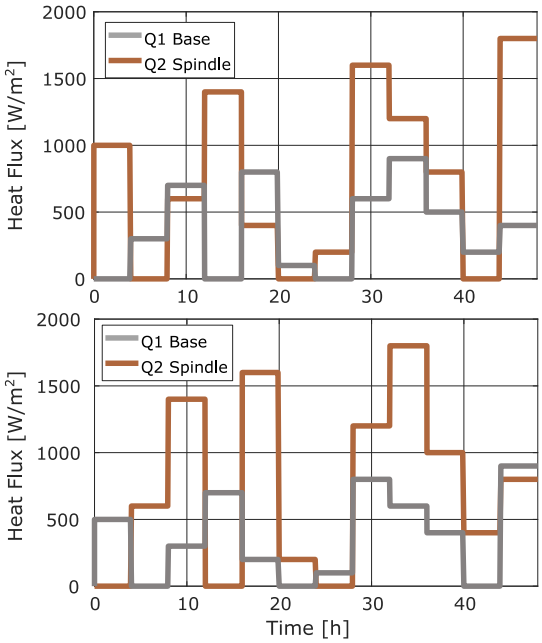

Figure 2. Heat flux input data for model training (top) and model validation (bottom).

The corresponding temperature values of the two virtual measurement points S1 and S2 are shown in Figure 3. These temperatures will be used in the following sections to model the thermal deviations. In Figure 1 the points T and W depict the location of the surfaces used to evaluate the relative deviation between tool and workpiece. The deviations in X-, Y- and Z-direction are depicted in Figure 4. The thermally induced deviations in X-direction are neglectable small, due to the symmetry of the modelled machine in the YZ-plane. A negative deviation in Z-direction occurs, when the distance between T and W is reduced, as it happens, when for example the spindle body is heated up.

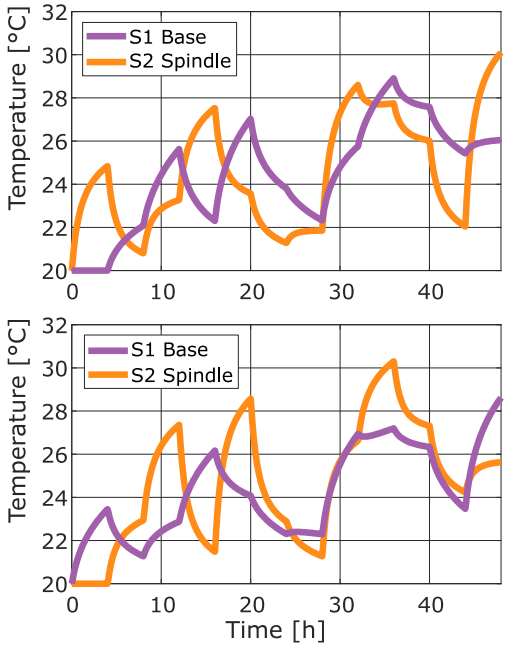

Figure 3. Temperature data for model training (top) and model validation (bottom).

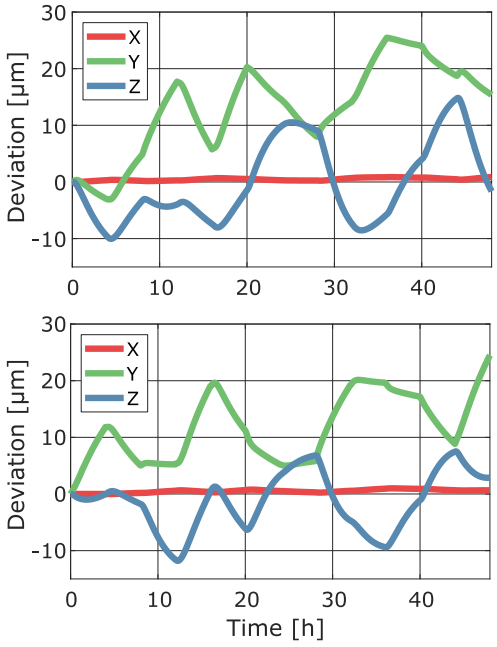

Figure 4. Relative deviations between T and W for model training (top) and model validation (bottom).

3.1. Static Modelling

The static modelling approach is widely used in industry to compensate thermal deviations of machine tools. The approach is based on the assumption of direct correlation between the

structural temperatures and the occurring deviations at the TCP. As shown by Yang and Li [4], the phenomena of pseudo-hysteresis can have a negative effect on the robustness and the compensation quality of such static models. To further proof these difficulties a static model based on FEM simulations of the simplified machine tool shown in Figure 1 is computed.

As seen in Figure 4 the deviations in X-directions are neglectable small and will not be considered for the modelling process. Therefore, only the deviations in Y- and Z-direction are modelled. As inputs for the regression model the virtually measured temperatures close to the two heat sources are used. This 2-input 2-output MIMO system can be partitioned into two 2-inputs 1-output MISO systems. The parameter estimation is performed on the training data set with the linear least squares criterion and results in the following equation:

$$\begin{aligned} E_Y &= 0.1976 + 3.3654 \cdot T_{S1} - 0.4747 \cdot T_{S2} \\ E_Z &= 1.1052 + 1.1560 \cdot T_{S1} - 1.4357 \cdot T_{S2} \end{aligned} \quad (4)$$

The estimation model of each direction consist of two temperature inputs, T_{S1} and T_{S2}, as well as the corresponding weighting parameters and the intercept term. Figure 5 shows the simulated and the modeled deviations of the FEM model in Y-direction. One can see, that the fit for the training as well as for the validation data set is satisfactory. The limitations of the static modelling method are obvious, when comparing the modelled and simulated deviations in Z-direction. Figure 6 shows that the model is not capable of capturing the thermal behaviour in Z-direction, neither in the training nor in the validation data set. This can be explained by looking at the underlying physical phenomena that leads to this deviation in Z-direction. The heat conduction into the column of the machine has a significant influence on the deviation but is due to the time delay of the conduction not covered by the static modelling approach. Therefore, the model can capture the fast and direct thermal responses of the system, as can be seen in Y-direction, but lacks of robustness when it comes to time delayed effects.

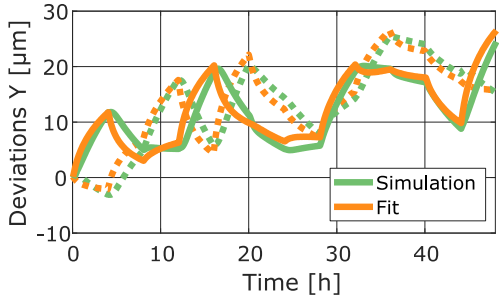

Figure 5. Simulated deviations and estimation for Y-direction using a static multivariable regression method for (dashed lines) model training and (solid lines) model validation.

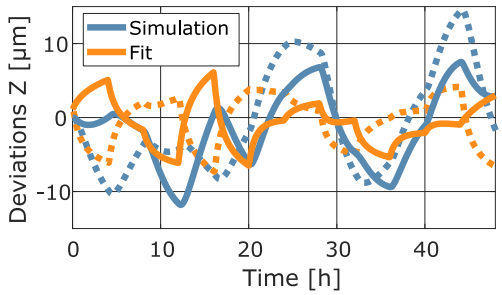

Figure 6. Simulated deviations and estimation for Z-direction using a static multivariable regression method for (dashed lines) model training and (solid lines) model validation.

3.2. FIR Modelling

Since thermo-mechanical deviations show a time dependent behaviour with certain time delay effects a dynamic modelling approach is investigated in more detail.

The only difference between the Finite Impulse Response (FIR) model and the static multiple regression model is, that also past inputs are considered to compute the occurring thermal deviation. In the following the time-shift operator q is used, where for example q^{-2} denotes that the input is shifted by two sample time instances. For the post-processing of the FEM model a sampling time of 5 minutes is chosen. Since the amount of considered past inputs is strongly influencing the prediction accuracy and the robustness, an optimum has to be found. This can be done with the Minimum Description Length (MDL) criterion introduced by Rissanen [6]. The MDL criterion evaluates the prediction quality and penalizes high model orders. Therefore an overfitting of the training data can be avoided and the model order is kept as small as possible.

The optimal input order for the deviations in Y-directions for the training load case was found to be $n_{b,S1} = 2$ and $n_{b,S2} = 4$. Therefore, the resulting model equation is as follows:

$$E_Y = 0.2249 + (-20.5312 + 23.8548q^{-1}) \cdot T_{S1} + (2.8056 - 4.2741q^{-1} + 5.9252q^{-2} - 4.8674q^{-3}) \cdot T_{S2} \quad (5)$$

The chosen input order for the FIR model of the deviations in Z-direction is $n_{b,S1} = 10$ and $n_{b,S2} = 10$, the model equation representation is omitted here. Based on the fact, that the order of n_b is limited to 10, the fit quality would improve even more, for higher orders of n_b. Since the number of considered past inputs is influencing the number of total modeling parameters, the variable n_b has to be limited to shorten the amount of data and therefore time needed for training of the model.

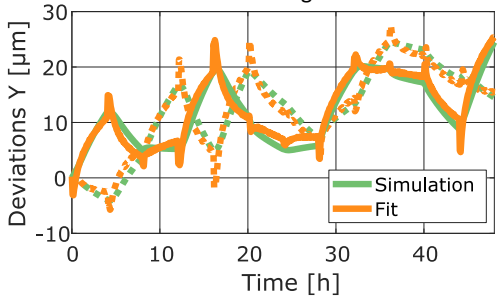

Figure 7. Simulated deviations and estimation for Y-direction using dynamic FIR method, $n_{b,S1} = 2$ and $n_{b,S2} = 4$, for (dashed lines) model training and (solid lines) model validation.

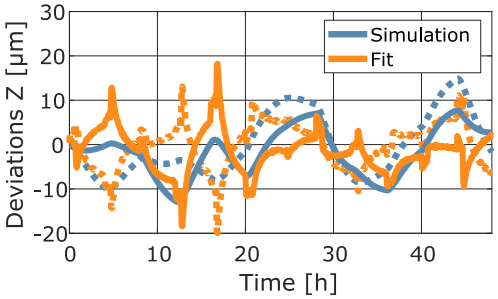

Figure 8. Simulated deviations and estimation for Z-direction using dynamic FIR method, $n_{b,S1} = 10$ and $n_{b,S2} = 10$, for (dashed lines) model training and (solid lines) model validation.

The resulting model estimation for the training and the validation data sets are depicted in Figure 7. and Figure 8. The estimation quality in Y-direction is satisfactory, both in the training as well as in the validation data set. The fit shows peaks at instances where the heat load drastically changes.

The model estimation for the deviations in Z-direction show an increased quality compared to the static model, see Figure 6. It can be seen, that the goodness of fit decreases from the training to the validation data set and that in both cases distinct peaks after load changes appear. Additionally, certain dynamics are not captured by the FIR model.

3.3. ARX Modelling

The ARX model considers past and present system inputs as well as past system outputs to compute the prediction for the current system output. According to Equation (3) a SISO system can be described as follows:

$$E[k] = -a_1 \cdot E[k-1] - \cdots - a_{n_a} \cdot E[k-n_a] + b_0 \cdot u[k] + b_1 \cdot u[k-1] + \cdots + b_{n_b} \cdot u[k-n_b] + e[k] \quad (6)$$

Since the relative TCP deviation can in an industrial application not be measured in the same frequency as the used sample rate of 5 minutes not the real deviations but the predicted ones are fed back into Equation (6) So past predictions are used in combinations with temperature measurements to predict the current deviations.

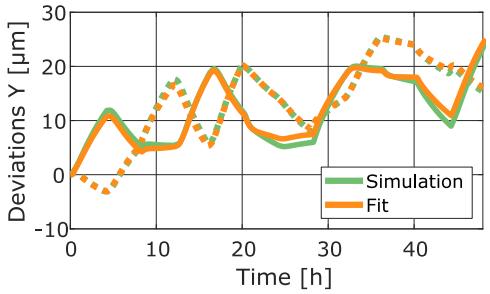

Figure 9. Simulated deviations and estimation for Y-direction using dynamic ARX method, $n_a = 1$, $n_{b,S1} = 2$ and $n_{b,S1} = 4$, for (dashed lines) model training and (solid lines) model validation.

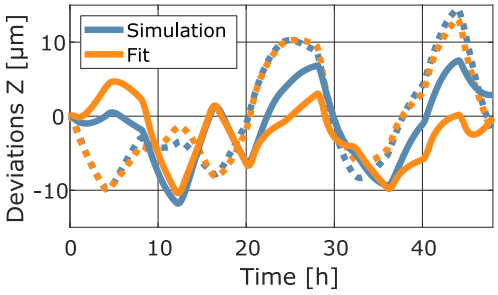

Figure 10. Simulated deviations and estimation for Z-direction using dynamic ARX method, $n_a = 1$, $n_{b,S1} = 10$ and $n_{b,S1} = 10$, for (dashed lines) model training and (solid lines) model validation.

To model the Y- and Z-deviations with an ARX model an order for the considered past outputs (n_a) is necessary. For the sake of simplicity and practical reasons, an order $n_a = 1$ is chosen. The optimal input order for the deviations in Y-directions are the same as for the FIR model, $n_{b,S1} = 2$ and $n_{b,S1} = 4$. Therefore the resulting ARX model equation is as follows:

$$E_Y = -0.0106 - 0.9395q^{-1} \cdot E_Y + (0.9658 - 0.7359q^{-1}) \cdot T_{S1} + (0.0990 + 0.0376q^{-1} - 0.0610q^{-2} - 0.1236q^{-3}) \cdot T_{S2} \quad (7)$$

The chosen input order for the ARX model of the deviations in Z-direction is the same as for the FIR model, $n_{b,S1} = 10$ and $n_{b,S2} = 10$, the model equation representation is omitted here. Same as before, the order of n_b is limited to 10 and therefore the fit quality would improve even more, for higher orders of n_b. Since the number of considered past inputs is influencing the number of total modeling parameters, the variable n_b has to be limited to shorten the amount of data and therefore time needed for training of the model.

The corresponding fits for the training and the validation data sets are depicted in Figure 9 for the Y-deviations and in Figure **10** for the Z-deviations. The fits for both directions in the training data set are nearly perfect. The prediction for the validation data sets are also very satisfactory for both directions.

3.4. Comparison

For the purpose of a quantitative comparison of the prediction quality of the three models, a certain metric is necessary. A literature study performed by Botchkarev [7] showed, that in the field of regression analysis no distinct performance metric is used. Since every measure of the prediction error has its benefits and disadvantages this thesis utilizes the most commonly used prediction metrics and certain additional quality indicators that have a relation to the actual quality of the manufactured workpieces. The used indicators are, Root Mean Square Error (E_{RMS}), Symmetric Mean Absolute Percentage Error (E_{SMAP}), peak to peak improvement (E_{PV}) and the 99th Percentile (P99). Blaser et al. [8] describe these quality indicators in detail.

Since an evaluation of the training data is biased, only the validation data is used for this evaluation. Table 2 shows the results of this analysis. It can be seen, that the ARX model outperforms the other models in all categories. It can also be seen, that the Static and the FIR model both perform similar and that no real improvement is achieved by using only past and present temperature inputs. Only in combination with past predictions, the full potential can be tapped.

Table 2. Quality indicators for the different prediction models for the validation load case. The smaller the value the better the fit.

	Y			Z		
	Static	FIR	ARX	Static	FIR	ARX
E_{RMS} [µm]	2.3	1.6	1.0	4.3	4.5	3.5
E_{SMAP} [%]	9.1	6.9	4.3	48.4	49.8	41.9
E_{PV} [%]	39.4	41.8	13.0	101.8	160.0	62.3
P99 [µm]	5.1	4.1	2.0	10.8	13.2	7.4

References

[1] Tangirala, A. K., 2017, Principles of System Identification: Theory and Practice, IEEE Control Systems, 37/2:181–184.

[2] Ljung, L., 1987, Ljung L System Identification Theory for User, *PTR Prentice Hall Upper Saddle River NJ*. pp. 475–476.

[3] Mayr, J., Blaser, P., Ryser, A., Hernandez-Becerro, P., 2018, An adaptive self-learning compensation approach for thermal errors on 5-axis machine tools handling an arbitrary set of sample rates, CIRP Annals, 67/1:551–554.

[4] Yang, H., Ni, J., 2003, Dynamic Modeling for Machine Tool Thermal Error Compensation, Journal of Manufacturing Science and Engineering, 125/2:245.

[5] MORe Simulations, 2019, www.more-simulations.ch.

[6] Rissanen, J., 1983, A Universal Prior for Integers and Estimation by Minimum Description Length, The Annals of Statistics, 11/2:416–431.

[7] Botchkarev, A., 2018, Performance Metrics (Error Measures) in Machine Learning Regression, Forecasting and Prognostics: Properties and Typology, pp. 1–37.

[8] Blaser, P., Mayr, J., Wegener, K., 2019, Long-Term Thermal Compensation of 5-Axis Machine Tools Due To Thermal Adaptive Learning Control, MM Science Journal.

Special Interest Group Meeting on Thermal Issues
Laboratory for Machine Tools and Production Engineering (WZL) of
RWTH Aachen, Germany, February 2020
www.euspen.eu

Enhancement of vertical turning lathe accuracy by minimising thermal errors depending on rotary table activity and workpiece clamping diameter

Martin Mareš[1], Otakar Horejš[1]

[1] *Czech Technical University in Prague, Research center of Manufacturing Technology, Prague, Czech Republic*

m.mares@rcmt.cvut.cz

Abstract
Thermally induced errors are dominant sources of inaccuracy and are often the most difficult types of errors to reduce today. Software compensation of thermally induced displacements at the TCP is a widely employed technique to reduce these errors due to its cost-effectiveness and minimal demands for additional gauges. Compensation models for machine tool thermal errors were successfully applied on various kinds of machine tool structure and implemented directly into their control systems. The aim of this research is to evaluate an enhancement of vertical turning lathe accuracy by minimising of thermal errors. Thermal errors caused by rotary table speed are nonlinear and a dependency on the workpiece clamping diameter has to be taken into account. Calibration of a reliable compensation model is a real challenge resulting in demands of a dependable verification approach. Techniques using international standard testing and manufacturing of testing workpiece were considered in the research for verifying a practical applicability of the compensation model.

Thermal error, Accuracy, Compensation, Finishing cutting conditions

1. Introduction

The heat generated by moving axes and machining processes creates thermal gradients, resulting in the thermal elongation and bending of machine tool (MT) elements, which substantially deteriorate MT accuracy. Thermal errors cannot be sufficiently reduced by design concepts and/or by temperature control without significant additional costs. On the contrary, indirect (software) compensation of thermal errors at the tool centre point (TCP) is one of the most widely employed reduction techniques due to its cost-effectiveness and ease of application.

Ordinarily, approximation models are based on measured auxiliary variables [1] (temperatures, spindle speed, etc.) used to calculate the resulting thermally induced displacements at the TCP. Many strategies were investigated to establish the models, e.g. multiple linear regressions (MLR) [2], artificial neural networks [3], transfer functions (TF) [4], etc. (for more detail see also [5]).

Although real-time software compensation approaches for thermal errors exist, these compensation approaches have a number of serious drawbacks. In the work [6] a promising approach to thermal error minimisation of spindle unit is introduced but the model was verified within calibration conditions resulting in a small value added compared to MLR simple modelling approaches; an interesting application of thermal error reduction is presented in [7] providing a solution only for thermo-mechanically steady states of tested device; a sophisticated apparatus used for MT surrounding impact simulation is topic of research [8] considering a limited conditions of real MT working cycles though.

An approach to thermal error modelling of a rotary table activity of a vertical turning lathe is proposed in this research. The compensation model based on TFs was directly implemented into MT control system and internal information (temperatures measured close to heat sources) were used as model inputs. A nonlinear MT thermal behaviour during turning operations was observed and workpiece clamping diameter had to be considered as additional model input parameter. The approach practical verification according to international standards ISO 230-3 [9] (using displacement probes) and using testing workpiece manufactured within finishing cutting conditions were considered to prove compensation model industrial applicability. A comparison of the applied compensation method outcomes with original (uncompensated) state of the machine is presented.

2. Modelling of thermo-mechanical behaviour

The chosen compensation strategy is based on TFs; a dynamic method with a physical basis. The difference form (suitable for programing languages e.g. Python) of the TF in the time domain is introduced in eq. (1),

$$y(k) = \frac{u(k-n)a_n + \cdots + u(k-1)a_1 + u(k)a_0}{b_0} - \frac{y(k-m)b_m + \cdots + y(k-1)b_1}{b_0}, \quad (1)$$

where u is the TF input vector, y is the output vector, k-n (k-m) signifies the n-multiple (m-multiple) delay in sampling frequency. Linear parametric models of ARX (autoregressive with external input) or OE (output error) identifying structures were used to set TF calibration coefficients a_n and b_m [10].

2.1. Experimental set-up

All of the experiments were performed on a vertical turning lathe with a maximal clamping diameter of 3,000 mm and maximal rotary table speed of 200 rpm. The MT is composed as multifunctional and is capable of two full-bodied technologies: turning and milling. The milling operations are not considered in the article.

Eddy current sensors (PR6423) firmly clasped in a thermal stable frame are employed for noncontact sensing of displacements between the TCP position and the rotary table (regular position of a workpiece). Other information (rotary table bearing temperature $T_{bearings}$, column temperature T_{column} and rotary table speed) are taken directly from the MT control system. Thermal stable frame assembled from carbon fibre bars was fixed in headstock tool holder as depicted in Figure 1. The frame is divided into two arms of the same length 1,500 mm. Both arms carry connectors for noncontact displacement sensors. Displacement sensors measured thermal displacement of the rotary table in three positions (0, 1,500 and 3,000 mm) defined by measuring artefacts. Sensors in 3,000 mm position are doubled (one for each end of the frame arm) to ensure the symmetricity of the rotary table thermal errors.

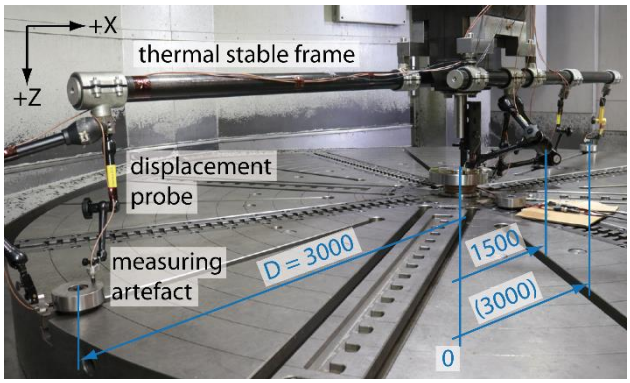

Figure 1. Experimental set-up for calibration measurement

All of the results and conclusions are closely associated with the following experiment conditions: load-free (without a cutting process in calibration part of experiments); testing in one MT axis configuration (with a reference to Positionally-dependant errors given only by thermal stable frame use); deformations in *Z* direction only were taken into account (without any reference to table diameter changes); the compensation model is implemented directly into MT control system and the MT multifunctionality is not considered so far.

2.2. Calibration

The calibration measurement consist of transient behaviour between two thermodynamic equilibria (MT in approximate balance with its surroundings and MT steady state during heat source activity).

Calibration measurement of rotary table thermal behaviour is divided into two cyclically repeated parts. The first part "loading" means 10 min of table rotation on constant rpm. The second part "measuring" means 10 s of measuring thermal deformations in *Z* direction between thermal stable frame and artefacts (see Figure 1). Rotary table thermal behaviour calibration and TF modelling result is shown in Figure 2.

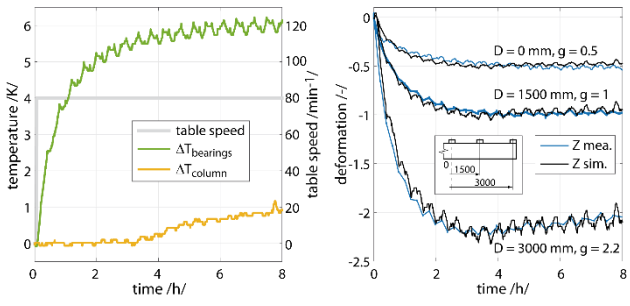

Figure 2. Calibration and modelling of rotary table thermal behaviour

The graph on the left in Figure 2 shows the input into the thermo-mechanical system and the graph on the right shows the measured and simulated outputs. Only heating phase is taken into account. The diameter of 1,500 mm is considered in modelling process (bold blue curve right in Figure 2). Other clamping diameters are solved as magnitude of the calibration curve with good resolution. The approximation of thermal deformations between headstock and rotary table is expressed by eq. (2),

$$z_{sim.} = [(\Delta T_{bearings} - \Delta T_{column}) \cdot \varepsilon_1] \cdot g, \quad (2)$$

where $\Delta T_{bearings}$ is the table bearing temperature difference, ε_1 represents the transfer function approximating thermal errors due to table rotation (for TF calibration coefficients see Table 1) and g represents the gain factor dependant on workpiece clamping diameter (see right part in Figure 2). Temperature behaviour ΔT_{column} is the base temperature difference reflecting to changes in ambient temperature. The influence of the ambient temperature on thermal error is not fully considered due to its modelling difficulties [8] and is scheduled as future work.

Table 1 Coefficients of identified transfer functions

TF	***coefficients***			
ε_1	a_0	a_1	a_2	a_3
	-82.41672	82.41479	0	0
	b_0	b_1	b_2	b_3
	1	-0.64533	0.10375	-0.45835

2.3. Verification

Following experiment has been designed to verify the validity of the compensation model. The verification test consists of rpm spectra with no record of cooling phase.

Figure 3 shows thermo-mechanical system temperature input during verification test and also depicts ambient temperature and table speed behaviours.

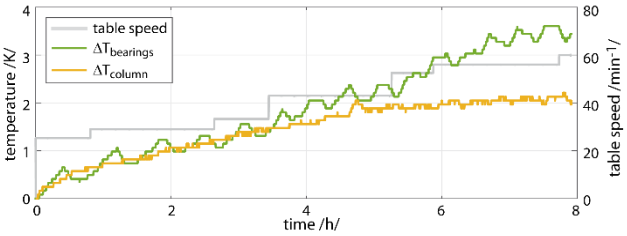

Figure 3. Verification test set-up, conditions and model input behaviours

Figure 4 shows outputs from the thermo-mechanical system as measured (left part in the figure) and simulated (the right part) thermal error during table rotation impact verification test.

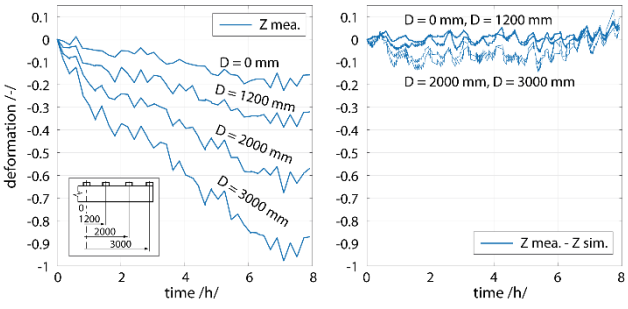

Figure 4. Measured (right; uncompensated state) and simulated (left; after applied compensation) thermal errors during verification test

The conditions of verification test differed from calibration measurement in positions of the artefacts (0, 1,200, 2,000, 3,000 mm). The compensation model was applied offline on measured uncompensated data and MT state after compensation was computed by difference of measured and simulated behaviours. The results in different artefact positions (1,200 and 2,000 mm) were obtained by multiple of linear interpolation of gain factor *g* in the compensation model.

Compared to the uncompensated state, the improvement of the thermo-mechanical state during the rotary table activity was 65% in 0 and 1,200 mm diameters and 84% in 2,000 and 3.000 mm diameters.

The verified compensation model was converted to Step7 code as machine controller Siemens allows for direct implementation. The compensation is executed in a frequency of one per second via an offsets setup on linear axis *Z*.

3. Testing workpiece manufacturing

Another verification test is further introduced due to authentication of a practical applicability of the compensation model: during a real finishing machining; out of the model's calibration range.

The testing workpiece is presented in Figure 5. The workpiece consists of four circular areas 1 (8), 2 (7), 3 (6) and 4 (5) meant for manufacturing and measuring in *Z* direction respectively. The workpiece clamping diameter was 1,200 mm and model gain factor to g = 0.76 had to be adjusted. The workpiece was placed on accurately polished underlies (for potential measurement on CMM machine) and fixed to the rotary table by clamps.

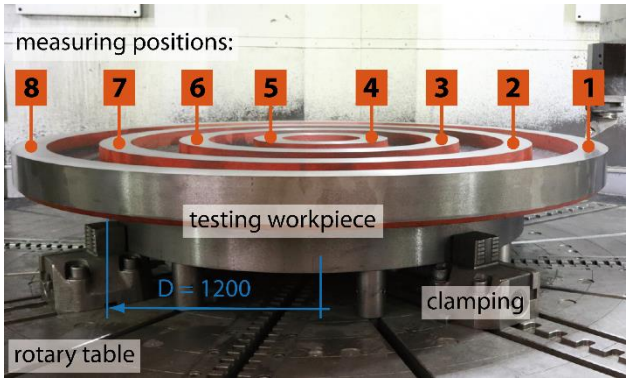

Figure 5. Testing workpiece

The manufacturing process of the testing workpiece during verification test within finishing cutting conditions is depicted left in Figure 6. Measuring principle of manufactured areas is shown right in the same figure.

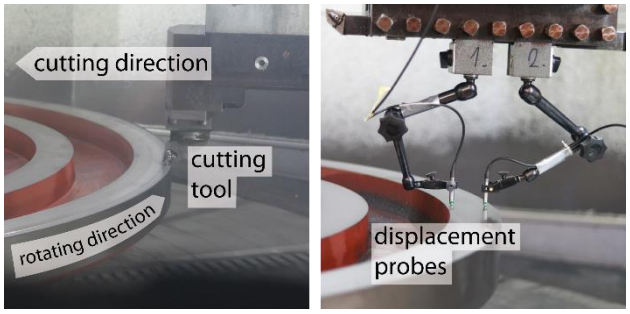

Figure 6. Testing workpiece manufacturing (left) and measuring (right)

The testing workpiece manufacturing process was carried out as fallow. First circular area 1 (8) was manufactured by prescribed finishing cutting conditions (Table 2). Then steady cutting tool waited 1.5 hour between areas 1 (8) and 2 (7). Rotary table was active on constant rpm. Second area 2 (7) was manufactured after the pause and so on until the tool reached the middle of the workpiece and experiment was ended.

Two contact displacement probes were mounted on headstock tool holder to measure the workpiece deformations after MT cooled down. The two points were measured in all measuring positions (1 to 8). Table was repositioned five times (in 45°) and all positions measured for statistical data; evaluation uncertainty of Type A.

Table 2 Cutting parameters

table speed [rpm]	**depth of cut** [mm]	**feed rate** [m·min^{-1}]	**pitch** [mm·rpm^{-1}]
variing (see Fig. 7)	0.2	120	0.15

Two experiments were carried out (with and without thermal error compensation active in MT control system) to evaluate MT accuracy enhancement. The measured model input behaviours and table speed during both tests with cutting process are depicted in Figure 7.

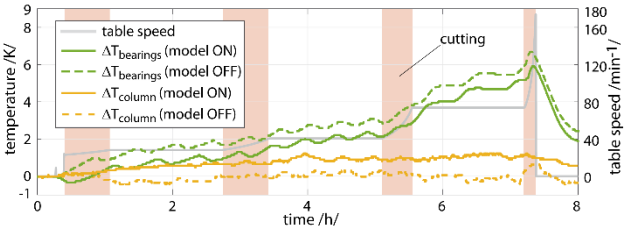

Figure 7. Cutting test set-up, conditions and model input behaviours

From measurements the arithmetical mean of thermal deformations was calculated in all measuring positions. The measured deformations in *Z* direction with active compensation are depicted left in Figure 8. Deformations without compensation are shown right in Figure 8. Since the experiment set-ups are similar both MT thermo-mechanical states are possible to easily compare.

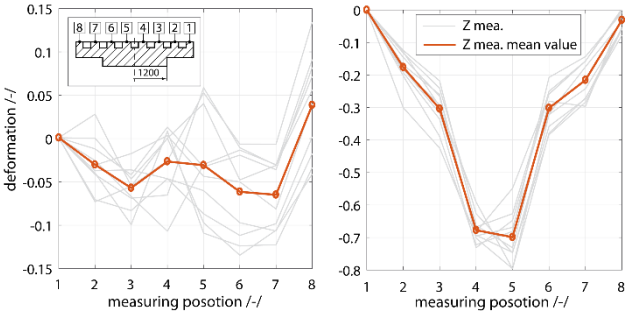

Figure 8. Measured deformations with compensation (left) and without compensation (right) during the finishing cutting tests.

The improvement of the thermo-mechanical state is estimated 7-fold (87%) in the *Z* direction compared to the uncompensated state. Additionally the testing workpiece thermal errors were measured by a precision level and on CMM machine with similar results.

4. Conclusions

The main objective of the scientific investigation presented in this extended abstract is enhancement of MT accuracy by

minimising thermal errors and evaluation of practical applicability of implemented (directly in MT control system) compensation model within finishing cutting conditions. The role of main thermal source, elimination of its influence on MT typical operations, workpiece clamping diameter consideration and minimal increase of the MT costs all represent basic requirements placed on specific compensation methods and TFs seem to be a suitable apparatus.

The tested machine was a vertical turning lathe. Calibration experiments were carried out under specific conditions: no cutting process was involved and were performed along the one MT axes configurations. The developed compensation model approximates undesirable thermal errors caused by the rotary table activity. Compensation was taken into account for linear deformations in *Z* direction and along the whole table diameter (measured with the help of thermal stable frame). The approximation quality of the model based on TFs was compared to uncompensated MT state within finishing cutting conditions with result of 87% of MT thermo-mechanical behaviour improvement.

The follow-up research will focus on MT thermo-mechanical behaviour regarding its multi-functionality (milling operations) and model transferability to other machines of the same construction but different size.

References

[1] Brecher C and Hirsch P, 2004. Compensation of thermo-elastic machine tool deformation based on control internal data. *CIRP Annals – Man. Tech.*, **53**/1, 299−304

[2] Postlethwaite S, Allen J and Ford D, 1998. The use of thermal imaging, temperature and distortion models for machine tool thermal error reduction, *Proc. Inst. Mech. Eng.*, **212**/8, 671−679

[3] Mize C, Ziegert J, 2000. Neural network thermal error compensation of a machining center. *Prec. Eng.*, **24**/4, 338−346

[4] Mareš M, Horejš O and Hornych J, 2017. Modelling of cutting process impact on Machine tool thermal behaviour based on experimental data, *Procedia CIRP*, vol. **58**, 152-157

[5] Mayr J, Jedrzejewski J, Uhlmann E, Donmez M A, Knapp W, Härtig F, Wendt K, Moriwaki T, Shore P, Schmitt R, Brecher C, Würz T and Wegener K, 2012. Thermal issues in machine tools. *CIRP Annals – Man. Tech.*, **61**/2, 771−791

[6] Xiang S., Yao X., Du Z., Yang J., "Dynamic linearization modeling approach for spindle thermal errors of machine tools", Mechatronics, Vol. 53, pp. 215-228, ISSN: 0957-4158, 2018.

[7] Xinyuan W., Enming M., Wei W., Hui L., "Real-time thermal deformation compensation method for active phased array antenna panels", Precision Engineering, Volume **60**, 2019, pp. 104-115

[8] Berger D., Brabandt D., Lanza G. "Conception of a mobile climate simulation chamber for the investigation of the influences of harsh shop floor conditions on in-process measurement systems in machine tools", Measurement, 2015; 74:233–7

[9] International Organization for Standardization, ISO 230-3, "Test Code for Machine Tools - Part 3: Determination of Thermal Effects", Genf, Switzerland, p. 44, 2007

[10] L. Ljung, 2009. System Identification Toolbox 7 User's Guide

FACULTY OF MECHANICAL ENGINEERING CTU IN PRAGUE

Enhancement of vertical turning lathe accuracy by minimising thermal errors depending on rotary table activity and workpiece clamping diameter

Martin Mareš, Otakar Horejš

27.2.2020

www.rcmt.cvut.cz
CZECH TECHNICAL UNIVERSITY IN PRAGUE | FACULTY OF MECHANICAL ENGINEERING
Research Center of Manufacturing Technology | RCMT
Horská 3 | 128 00 Prague 2 | Czech Republic | Phone: +420 221 990 914 | email: info@rcmt.cvut.cz

RCMT

Outline

- **Introduction and motivation**
- **Conditions**
- **Modeling approach**
- **Calibration**
  - No-load conditions
- **Verification**
  - Within finishing conditions
- **Conclusions**

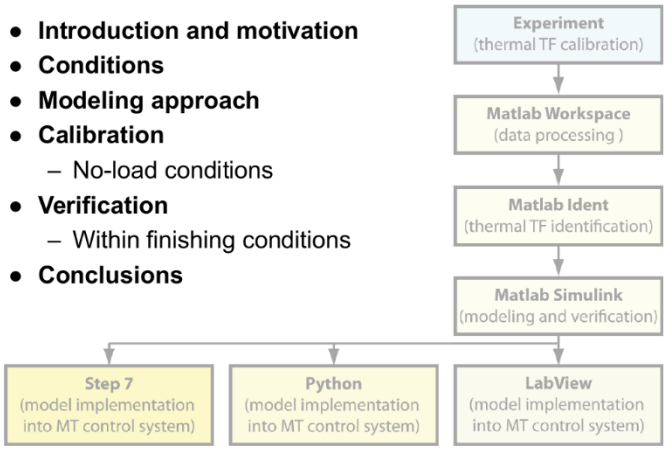

Introduction

- **Internal** and **external** heat sources affect machine tool structure
  - Internal: motors, spindle system and bearings, feed drives, gearbox, ball screw and its nut, cutting process itself, etc.
  - External: MT surrounding.
- Thermal errors are result of heat sources activity during machine tool operation. Those errors affect MT accuracy in negative way (up to 75% [Mayr 2012]).
- Problem solutions:
  - Reconstruction
  - Heat flux control
  - Prediction
  - **Compensation**

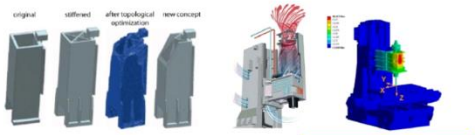

- **Direct** and **indirect** compensation
  - Direct: measuring between the tool and the work-piece
  - **Indirect** uses approximation model

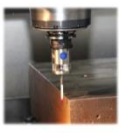

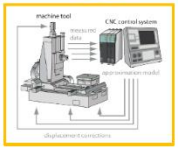

Motivation

- Generally: compress the time of MT moderate heating and increase its accuracy.

Research motivation

- To equip the MT with **thermal error compensation strategy** for real multifunctional industrial applications.

Industrial environment of target machine

Conditions

- Performed on **vertical turning lathe** (with milling option) for large parts (table diameter 3000 mm, max. 200 rpm)
- Activity of dominant thermal sources
  - **Table rotation**
  - **Ambient temperature**
- Compensation ***Z* linear direction**
  - Turning operations
  - Heating phase only
  - No angular deformations
  - *X* direction not considered
- **Workpiece clamping diameter** included
  - Measurement of deformations in table plane using contact probes and measuring artefacts
- Thermal error compensation within **finishing cutting conditions**

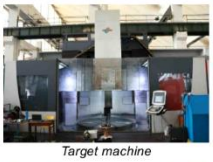

Target machine

Measuring device

Testing within MT multifunctionality

Modelling approach

- **Mathematical apparatus:**
  - **„Thermal" transfer functions**
    - Dynamic method with physical basis [Attia 1981]
    - Minimum of additional gauges [Brecher 2004]
    - Individual solution of each influence participating on thermal error [Tachiya 2011]
- **Modelling approach:**
  - **Partial linearization of the MT thermal issue** (using linear parametric models)
- Model implemented directly into **MT control system** in the form of diagnostic screen

> *"**Mechanical transfer function** generally expresses link between output (response) and input (excitation) of dynamic system in frequency domain"*

> *"Thermal transfer function describes link between temperature measured close to heat source and deformation caused by thermal expansion"*

$$y(t) = \frac{a_1 z^{-1} + a_0 z^{0}}{b_2 z^{-2} + b_1 z^{-1} + b_0 z^{0}} u(t)$$

(output vector; output weight factor; input weight factor; input vector)

differential notation of **2nd order transfer function** with *n*-multiple delay of sampling frequency:

$$y(k) = \frac{u(k-1)a_1 + u(k)a_0 + y(k-2)b_2 + y(k-1)b_1}{b_0}$$

Calibration - experimental setup

- **Inputs into thermomechanical system:**
  - **Two internal key temperatures**
    - Table bearings, column
- **Outputs from thermomechanical system:**
  - **Deformations in *Z* direction**
    - Thermal stable frame with mounted eddy current sensors
    - Positons of four measuring artefacts: **0**, **1500** and 2x **3000** mm
    - **Loading cycle**: 10 min table rotation | 10 s measuring of each artefact

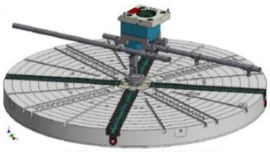

Model of measuring device

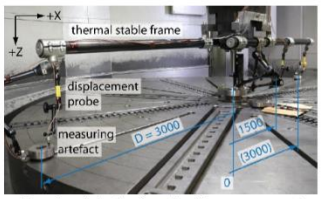

Experimental setup for calibration measurement

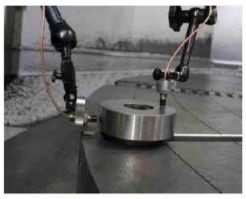

Detail of measuring artefact sensing

Calibration - measuring and results

- One calibration measurement necessary to **TF model training**:
  - Constant table speed 80 rpm (8 h)
- **Model calibrated in clamping diameter 1500 mm** (others are interpolated)
  - Dependency between clamping diameter thermal errors is **not linear**
  - Achieved **90% reduction** of thermal error in all three measured diameters

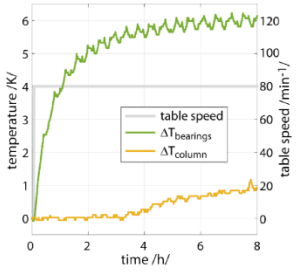

Inputs

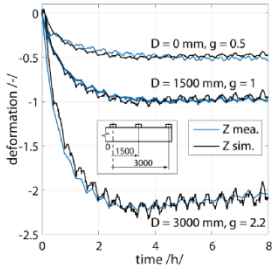

Outputs and simulations

Verification - experimental setup

- **Testing workpiece:**
  - Railway part (approx 500 kg)
  - clamped on diameter **1200 mm**
  - placed on polished underlies
- **Cutting conditions (finishing):**
  - **Depth of cut**: 0.2 mm
  - **Feed rate**: 120 m.min^{-1}
  - **Table speed**: varying
  - **Pitch**: 0.15 mm.rpm^{-1}
  - Loading: 1.5 hour pause with constant rpm after cutting a ring
- **Thermal error measurement:**
  - In the cooled-down state of WP
  - 8 measuring positions
  - 5 table angle positions (in 45°)
  - 2 contact sensors

10 mea. in total

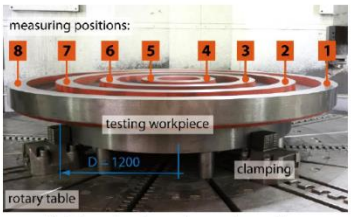

Workpiece clamping and measuring positions

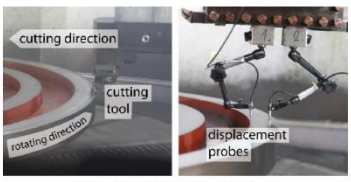

Cutting and measuring procedures

Verification - measuring and results

- **Two experiments:**
  - **Same setup with and without active thermal error compensation model in MT control system**
  - Table speed varying from **30** to **170 rpm**
- Finishing cutting conditions and clamped workpiece have small impact on measured inputs

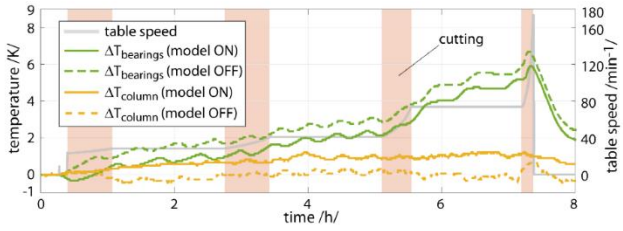

Inputs during both experiments (model ON / model OFF)

Verification - measuring and results

- Achieved **87% reduction** of workpiece thermal error by compensation model application
- Finishing cutting conditions and clamped workpiece have small impact on measured outputs

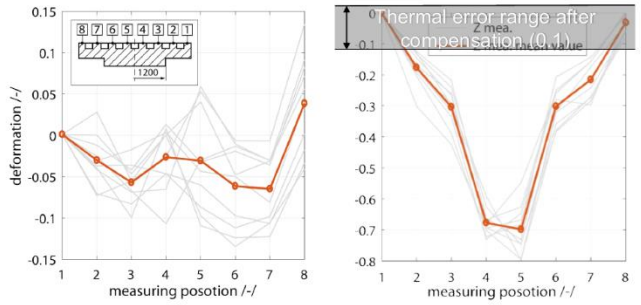

Outputs from model-ON test *Outputs from model-OFF test*

Verification - measuring approach robustness

- **Different cutting test** with thermal error compensation **model switched ON**
- **Three approaches to workpiece measurement:**
  - **Contact probes** (measurement with geometric error of crossbar)
  - **Precision level** (independent measurement provided by MT producer)
  - **3D CMM** (independent measurement provided by external laboratory)

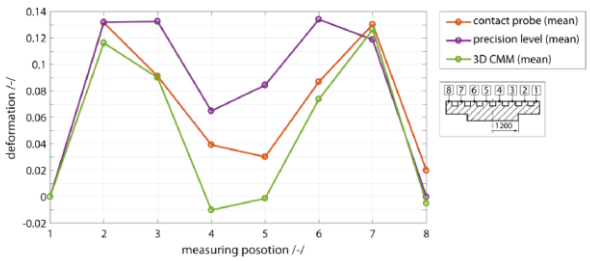

Comparison of three approaches to workpiece thermal error measurement

Conclusions

- Thermal error compensation model of table rotation was developed
- Methodology to measurement thermal error of the table regarding workpiece clamping diameter was introduced
- Model validity was verified during finishing cutting conditions
- Model was implemented directly into MT control system in the form of diagnostic screen
- Model is ready to industrial application

- **Future work**
  - Model extension to MT multifunctionality
  - Model transferability to other machines of the same type but different sizes
  - Model incorporation into machine-learning system for long-term stability according to ideas of Industry 4.0

Diagnostic screen

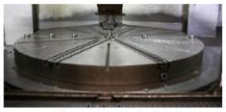

Measuring artefacts

Testing workpiece

Posters

Special Interest Group Meeting on Thermal Issues
Laboratory for Machine Tools and Production Engineering (WZL) of
RWTH Aachen, Germany, February 2020
www.euspen.eu

Measurement and modelling of thermal loads in industrial CT scanner

Marko Katić[1], Nenad Ferdelji[1], Danijel Šestan[1]

[1]*University of Zagreb, Faculty of mechanical engineering and naval architecture*

marko.katic@fsb.hr

Abstract

X-ray computed tomography (XCT) is rapidly becoming the measurement tool of choice in a wide variety of industrial sectors where commonly used measurement techniques aren't optimal, typically when internal features of parts / assemblies need to be inspected. There are several key limiting factors when XCT is used as a metrology tool, such as relatively long measurement time, problems related to measurement of multi-material components, or insufficient energy to penetrate high-density materials while maintaining high resolution. One of the largest issues is the question of traceability of measurement results; due to very large number of influences on measurement uncertainty, it is currently not possible to establish a classical uncertainty budget and declare a priori measurement uncertainty of XCT results.
Influence of temperature on dimensional measurements is well known, and is usually relatively easy either to correct it, or to calculate its influence on the uncertainty of measurement. However, a typical industrial XCT scanner poses additional challenges: having several heat sources in a thermally well-insulated chamber and having a metrology loop in which thermal displacements cause several different errors. In this paper, we discuss one possible approach to this problem which is based, first and foremost, on extensive temperature measurement of the entire XCT metrology loop. These results are then used as ground truth for verification of simulation models, based on Finite Element Analysis (FEA), needed to establish temperature and displacement fields of XCT scanner geometry for the entire range of usable X-ray power levels. Finally, temperature measurements and FEA results are also used for verification of a simplified analytical model which could be useful in robust expression of measurement uncertainty.

Keywords: Accuracy, Dimensional, Measurement, X-ray computed tomography

1. Introduction

Defining thermal influences in an XCT scanner should begin with a systematic approach to measurement of temperature in various parts of XCT metrology loop. In order to acquire reliable results, preliminary investigation was made using a thermal imaging camera while X-ray power was kept at 45 W (Figure 1).

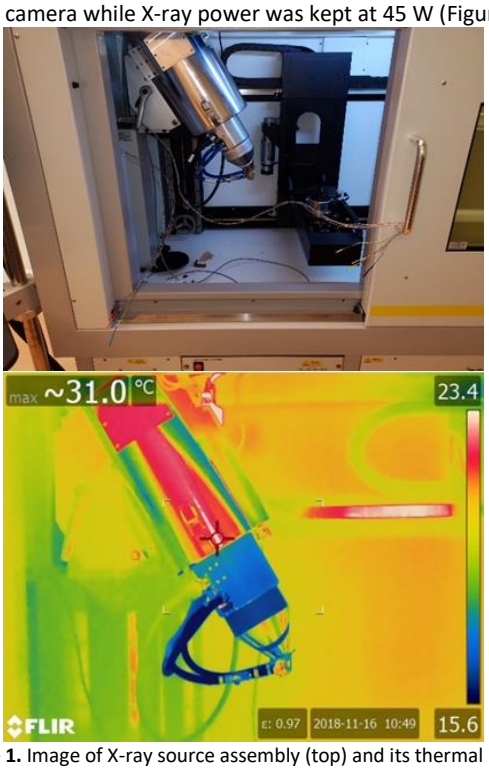

Figure 1. Image of X-ray source assembly (top) and its thermal image (bottom).

While this method couldn't be reliably used to measure absolute temperatures, it did provide valuable insight into existing temperature field distribution. Based on this, eight thermistor probes were traceably calibrated (U = 10 mK, k = 2) and placed at locations within the XCT scanner cabinet shown in Figure 2.

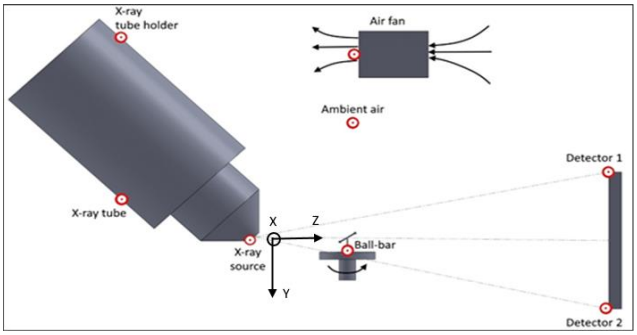

Figure 2. Schematic representation of the XCT scanner and location of installed temperature sensors.

Acquisition of temperature measurement using these sensors, performed over a time period of approx. 2 hours at X-ray power of 45 W, is shown on Figure 3. Measurement results clearly show significant variation of temperature, especially at the X-ray source and X-ray tube assembly. This change of temperature results with thermal expansion of the X-ray source and tube assembly, which in turn changes the position of the X-ray focal spot relative to the measurement object and the X-ray detector. Since these relative positions create the metrology loop, any undetected change has direct consequences on the accuracy and measurement uncertainty of XCT results.

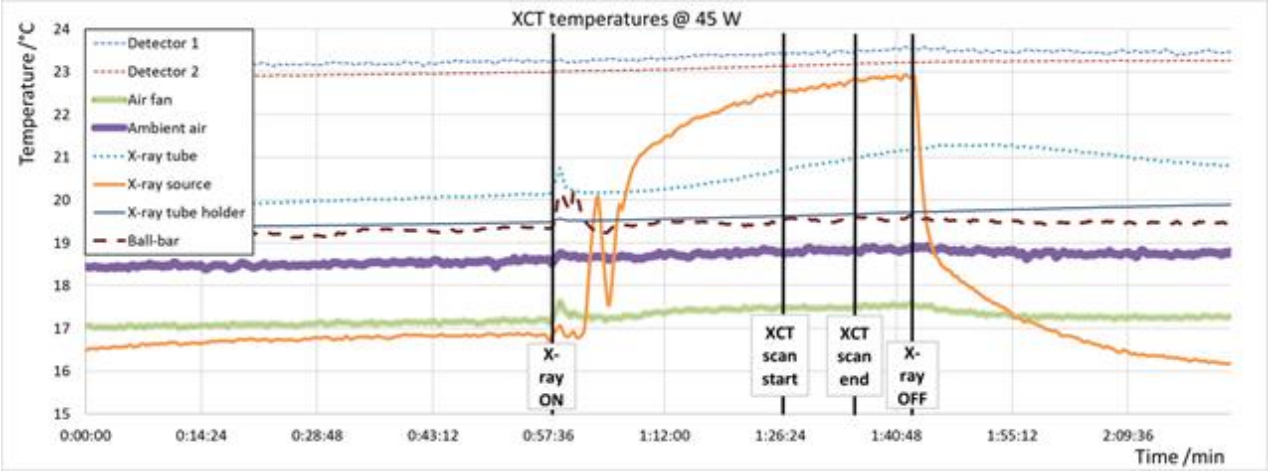

Figure 3. Temperature measurement results for 45 W X-ray power level.

Special Interest Group Meeting on Thermal Issues
Laboratory for Machine Tools and Production Engineering (WZL) of
RWTH Aachen, Germany, February 2020
www.euspen.eu

Multi-phase numerical simulation of coolant flow around the cutting tool

Michael Bräunig[1], Lukáš Topinka[1], Joachim Regel[1], Matthias Putz[1,2]

[1] *Chemnitz University of Technology, Institute for Machine Tools and Production Processes, Professorship Machine Tool Design and Forming Technology, Chemnitz, Germany*
[2] *Fraunhofer Institute for Machine Tools and Forming Technology IWU, Chemnitz, Germany*

michael.braeunig@mb.tu-chemnitz.de

Abstract
The thermal behavior has a significant effect on the manufacturing accuracy. For many machining tasks, the use of cooling lubricant is essential in order to achieve possible cooling and lubricating effect in the cutting zone. Its reduction due to resource-efficient or ecological efforts has an impact on the temperature field in the machining tool, which affects the thermal behavior of the frame structures and can cause machining inaccuracies. This article describes the CFD-model for simulation multi-phase flow of liquid coolant around the cutting tool and the prediction of the temperature field. With experimental investigations, the simulation model is verified and checked for plausibility.

Keywords: CFD-Simulation, thermal investigation, machine tools, tool cooling simulation, multi-phase simulation

1. Introduction

The accuracy of metal cutting machine tools is essential for most of the industrial production. The majority of materials used for machining application are negatively affected by temperature in terms of both tool life and manufacturing accuracy. Coolants are very common in this field but according to an industry survey, at least 50 % of enterprises also use dry machining [1]. Previous studies on effects of air cooling on the tool structure [2,3] shows that the temperature field in the tool with air cooling can be reduced by up to 50% in comparison to machining without any coolant. But for many manufacturing operations are coolant lubricants are still indispensable, as they provide not just a cooling effect in the cutting zone, but also less friction and adhesion between tool and workpiece during cutting operations. Delivery of the liquid coolant into the inner part of tool teeth and the cutting zone can be difficult due to high pressure and high rotational speed of tool as consequence of highspeed machining. Moreover, depending on the tool rotation speed, a significant concentration of fog particles can be evaporated into the environment, which can increase health risks [4] and dangerous for the environment. Therefore, the investigation with focus on their effect and efficiency is necessary.

This work describes the multi-phase simulation model for system consisting of restricted area and machining parts around the cutting zone. This simulation-based investigation was carried out on the rotary milling tool. A numerical model approximates the flow of liquid coolant around the milling tool and makes it possible to evaluate the efficiency of the use of coolant lubricant in order to specific working conditions. Further part concerns with the investigation of heat fluxes through the cutting tool, which is essential to be able to evaluate the cooling effect of the liquid coolants on the cutting tool.

2. The Simulation model

A cutting tool is assembled of many different parts. As the numerical methods for computational fluid dynamics (CFD) are highly demanding on time and computational performance, it is necessary to use area, which is closed to the point of investigation. In this case, only the parts immediately nearby to the cutting zone were chosen and modelled. The 3D CAD model therefore consists of simplified chuck and the four blades cutting tool. The virtual space represents the environment around the tool and its chuck and there is a nozzle for liquid coolant supply. Both the meshing and the calculation were carried out in Ansys Workbench by using CFX.

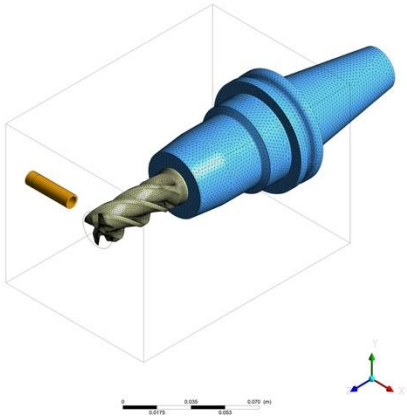

Figure 1. 3D CAD model of the system

For numerical calculation of fluid dynamics, every part of simulation model must be defined as a domain and the connection between them is described as an interface. Both the domains and the interfaces must be set up with its properties, such as Domain Type, Material, Heat transfer, etc., as they describe the interaction and function of the simulation system. This simulation model consists of six domains and 9 interfaces. There are three solid domains representing milling tool, tool chuck and nozzle for coolant supply. Domains for tool and its

chuck are set as rotary with defined rotational speed corresponding to speed used in real experiments. For these two domains is also specified Heat Transfer for option Thermal Energy, which enables further evaluation of cooling effect. Other three domains are then described as Fluid, respectively in multi-phase system representing air and the liquid coolant, with corresponding Surface Tension Coefficient between these two phases. The first *Airvolume* represents the volume space in restricted area of the simulation model. Although it is modelled as a restricted area, it is defined as an open system, so the exchange is enabled with its surrounding environment. Because it is impossible to rotate domain, which is not symmetric and perpendicular to the direction of rotation, there was second *Airvolume 2* developed. This was created as a shape of cylinder, which fills the space of inner part of tool teeth. Third *Airvolume 3* then represents a small space between the cutting tool and tool chuck. The flow of air and coolant in the simulation is turbulent, these Fluid domains are calculated with the shear stress transport (SST) turbulence model. In these domains, the option Total Energy was used for the Heat Transfer. Buoyancy was applied for simulate of the gravitational force causing curving of coolant flow. The schematic built, which shows individual domains and their connections with a 3D model of its real equivalent, is showed in Figure 2.

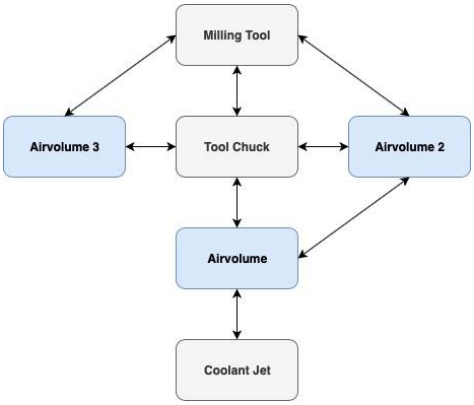

Figure 2. Scheme of domains of the system

3. Evaluation of simulation

To be able to verify the simulation model, the experimental investigations were carried out on a test stand specified particularly for thermal analyses. The tool and the chuck were mounted in a motor spindle. This spindle is fixed on a machine tool table with supporting element. Testing stand has also enclosure shields, so it is possible to isolate working space from its environment and secure better temperature measurement conditions. For recording the coolant flow, there was used a camera with two positions, above the tool and from top to the cutting edges of the tool.

The results of experimental investigation in Figure 3 shows the differences of the liquid coolant flow around the cutting tool for different conditions. Starting with the tool without rotational, a main part of coolant flows around the tool and continues further under curvature caused by gravitational force. There are also other flows, which direction varies by the time. With rotation tool in small rotational speeds, there can be seen change of flow to the field of droplets departing by centrifugal force. With increasing the rotational speed of the tool, the field of droplets changes into the fog of small coolant particles.

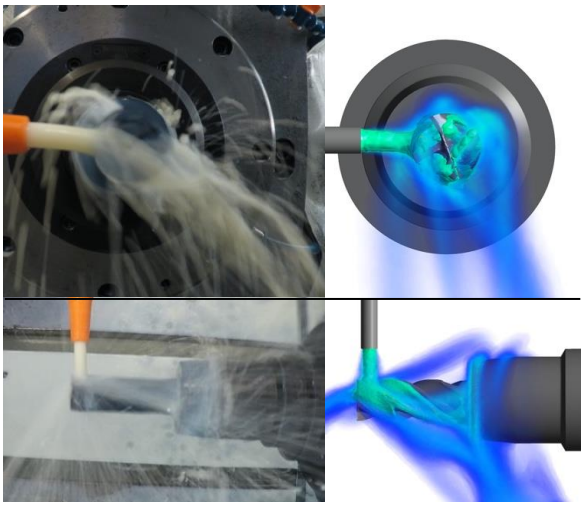

Figure 4. Comparison of real and simulated coolant flow

These instabilities show difficulties of simulation. As it is impossible to predict the direction of some parts of coolant flow after the contact with tool, such as field of droplets, the results of CFD simulation does not fully correspond with the real experiments. Also, the simulation cannot show particles smaller that the dimension of mesh. This can be influenced by changing the dimension of mesh, but it would also rapidly increase calculation time. The point of interest is therefore focused on the main flow. As shows the Figure 4, there can be seen slight inequalities, which can be caused by many reasons, such as small change of physical properties of liquid coolant cause by absorption of air humidity, difference between the surface tension of dry and wet surface or problems with convergency of turbulent models. On the other hand, these slight inequalities should have not an impact on the simulation of cooling effect.

4. Thermal simulation

For the evaluation of heat transfer, it is necessary to define material and thermodynamic properties of every domain. There must also be defined two heat transfer variables. First take its position as the tool chuck is clamped into the spindle. It is provided on the surface of ISO Taper cone with value already found in previous studies. The second important definition is the heat source in this system. There was used a simplified surface of the cutting edges with value corresponding with the induction system, which was carried out in the experimental measurement. The value was therefore set as Heat Flux variable into the simplified surface of cutting edges as shows Figure 5.

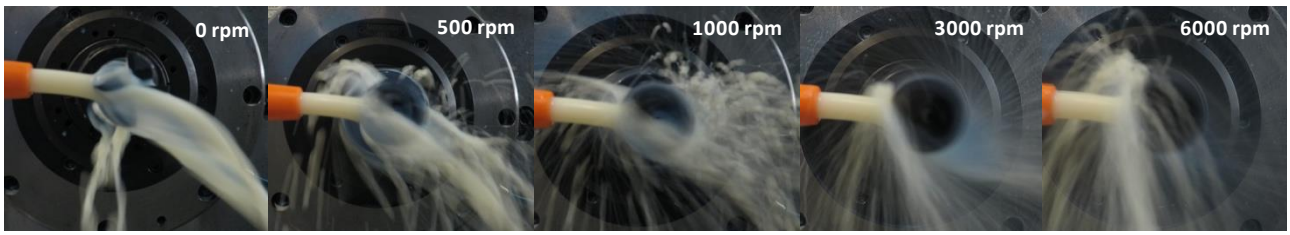

Figure 3. Coolant flow around the cutting tool.

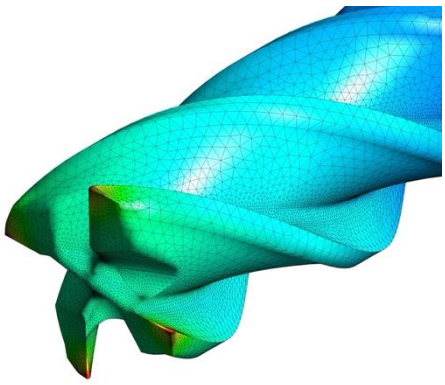

Figure 5. Temperature field of the tool with heat source

For the validation of temperature field through the tool, there was carried out the experiment with the composition of temperature sensors and induction system described in [5]. The temperature results of the simulation coincident with slight differences to the measured values on real milling tool. There are also many factors, which influence calculated temperature field in tool and its chuck. The significant role plays the accuracy of turbulence and flow of the coolant and also the fact, that sensors placed on the surface of cutting tool are not isolated from environment and can therefore measure some inequalities while contact with liquid coolant, which has significantly higher value of *Specific Heat Capacity* than material of the milling tool itself.

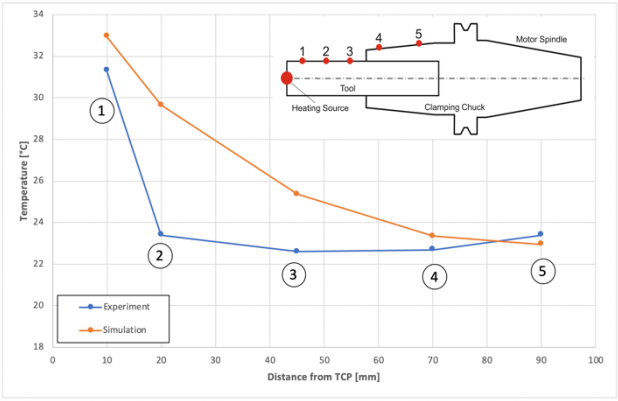

Figure 6. Temperature fields from experiment and simulation at 3000rpm

5. Summary and outlook

Numerical flow simulations provide a better understanding of how the coolant flows around the cutting tool and its effect on the temperature field in the tool. Simulating coolant flow around a rotating tool reveals difficulties caused mostly by turbulence and dispersion of fluid into the environment as a function of rotational speed of the cutting tool. Taking into account the simulation of small particles of liquid spreading into the environment is therefore difficult and increases demands on computational power and accuracy of the simulation itself. However, it is still possible to simulate the temperature field caused by the heating of the cutting surfaces with certain precision and to make the use of coolant more efficient.
There is still a need of research into the fluid flow around the rotating tool and thus refining the existing model, which will allow a better simulation of the fluid flow and thus a better understanding of the cooling of the tools by the use of coolants. Further, it is necessary to assess how much liquid actually reaches the tool and thus contributes indeed to the actual cooling of the tool and not only to cooling the surroundings or the chip removal function. In order to refine the evaluation of the temperature field in the tool, it is also necessary to determine the influence of the isolation of the temperature sensor on the surface of the tool against the liquid with a significantly higher coefficient of thermal capacity compared to the material of the tool itself on the measured values during the experiment.

Acknowledgement

The work is funded by the German Research Foundation – Project-ID 174223256 – TRR 96. The authors thanks for the support.

References

[1] Putz M, Richter C, Regel J and Bräunig M 2018 Industrial consideration of thermal issues in machine tools *Prod. Eng. Res. Devel.* **12** 723–736
[2] Perri G M, Bräunig M, Gironimo G D, Putz M, Tarallo A and Wittstock V 2016 Numerical modelling and analysis of the influence of an air cooling system on a milling machine in virtual environment *Int. J. Adv. Manuf. Technol.* **86** 1853–1864
[3] Putz M, Wittstock V, Semmler U and Bräunig M 2015 Simulation-based thermal investigation of the cutting tool in the environment of single-phase fluxes *Int. J. Adv. Manuf. Technol.* **83** 117-121
[4] Bennett EO, Bennett DL 1987 Minimizing human exposure to chemicals in metal working fluids *Lubr. Eng.* **43** 169–175
[5] Bräunig M, Regel J, Glänzel J, Putz M 2019 Effects of cooling lubricant on the thermal regime in the working space of machine tools *Procedia Manufacturing* **33** 327-334

Special Interest Group Meeting on Thermal Issues
Laboratory for Machine Tools and Production Engineering (WZL) of
RWTH Aachen, Germany, February 2020
www.euspen.eu

Simulation of the thermal behavior of machine tools for efficient machine development and online correction of the Tool Center Point (TCP)-displacement

Stefan Sauerzapf[1], Julia Vettermann[2], Andreas Naumann[3], Jens Saak[2,4], Michael Beitelschmidt[1], Peter Benner[2,4]

[1]*TU Dresden, Institute of Solid Mechanics, Chair of Dynamics and Mechanism Design*
[2]*TU Chemnitz, Faculty of Mathematics, Research Group Mathematics in Industry and Technology*
[3]*TU Chemnitz, Faculty of Mathematics, Research Group Numerical Mathematics (Partial Differential Equations)*
[4]*MPI for Dynamics of Complex Technical Systems Magdeburg, Research Group Computational Methods in Systems and Control Theory*

stefan.sauerzapf@tu-dresden.de

Abstract
Machine tool models play an essential role in the development process and during the whole lifetime of machines. On the one hand, they enable the developer to predict the thermo-elastic behavior of a new machine without the necessity for a prototype. Therefore, time and money can be spared in the development process. On the other hand, model predictive control can be applied to reduce the manufacturing error, induced by the displacement of the tool center point (TCP).
This paper provides a brief overview of the methodology used and developed in the Collaborative Research Center/Transregio 96 (CRC/TR 96) to simulate the thermal behavior of complete machine tools. As an illustration, the newly developed approach is used to simulate the behavior of a simple test model. The different approaches are compared and a short guideline, which method can be used for a given task, will be given.

Thermal Behavior, Simulation, Model Order Reduction (MOR), Finite Element Method (FEM)

1 Introduction

Saving resources is of increasing importance for sustainable production processes. To account for this issue, it is essential to reduce the energy consumption of modern machine tools by smart cooling strategies, further enhanced construction techniques etc., to compensate for an unwanted tool center point (TCP) displacement, before it actually appears. Furthermore, the simulation of the thermal behavior allows model predictive control to reduce the error induced by thermo-elastic deformations, which yield an unwanted tool center point (TCP) displacement.

This paper describes an approach to simulate the thermal behavior of complete machine tools, which is developed and used by projects in the CRC/TR 96.

First, the general methodology will be introduced and the steps to generate a finite element model to calculate the thermal field are described. After that, it is shown, how model order reduction (MOR) can be used to speed up the simulation process. To illustrate the strengths and weaknesses of the different approaches, the thermal field of a simple test model is calculated. These results are compared. To conclude, a short summary of the different approaches will be given and the next development steps are outlined.

2 Modelling of machine tools

The methodology of modelling the machine tool including geometric simplification, the choice of boundary conditions and choosing the right mathematical models, plays a significant role in the calculation of the thermal behavior.

2.1 General Considerations

To model the thermo-elastic behavior of machine tools, two different kinds of coupling have to be taken into account:

- the physical coupling between the heat equation and the equations of elasticity,
- the geometrical coupling between different components that can also move relative to each other (contact problem).

These coupling types must be treated with different mathematical approaches and have their own challenges. For example, the geometrical coupling of the relatively moved parts leads to discontinuous sources in space and time. These sources can be modelled with functions on the part interface, which depend on different temperature fields.

2.2 CAD-Model

The starting point of all simulations is a CAD-Model of the investigated system. The model must contain all the geometric details which are relevant for the simulation. Small features of the geometric model like fillets, bevels or drillings should only be kept in the model, if the behavior at those items is of interest. A simplified geometry can reduce the effort for the next modelling steps significantly. For the given examples, the CAD-Software SolidWorks® was used.

2.3 FE-Model

After generating a sufficiently detailed geometric model of the system, a finite element (FE) model must be created.

Therefor the CAD-Model is imported into the FE-Tool and the simulation domain is discretized into finite elements. The material parameters like specific heat capacity or thermal conductivity, are set for each individual material of all parts of the model.

The boundary conditions take a special role in the modeling of the machine behavior. To calculate the thermal field as accurate as possible, the process heat, the cooling system, the environment interaction, the heat fluxes from the axis drives and the friction losses of the bearings and linear guides have to be taken into account. Modelling of those boundary conditions plays a significant role in the CRC/TR 96. Models for e. g. the dissipative heat of the cutting process or friction losses in linear guides are incorporated into the model. For the presented methodology and workflow, ANSYS Mechanical as an industry-standard computer aided engineering (CAE)-Tool is used to generate the FE-Model.

The equation that describes the thermal field is

$$c\rho\frac{\partial T(t)}{\partial t} - \vec{\nabla}\cdot\left(\lambda\vec{\nabla}T(t)\right) = q(t). \tag{1}$$

and is discretized by using the FE-method.

For simplicity, constant, isotropic, material properties are assumed in this presentation. The material coefficients are the specific heat c, the density ρ and the thermal conductivity λ. T is the temperature at the given material point, q can be any heat source and the variable t signifies the time.

Applying the FE method and using equation (1) leads to the following system equation to calculate the discrete temperature vector $\boldsymbol{T}$ at the FE nodes

$$M\dot{\boldsymbol{T}}(t) + D\boldsymbol{T}(t) = \boldsymbol{q}(t) \tag{2}$$

of one continuous part, with the matrices M (capacity matrix), D (conductivity matrix) and the time dependent load vector $\boldsymbol{q}$.

To model thermal coupling by the exchange of heat between multiple parts, different approaches [8][3][11] can be incorporated into the vector $\boldsymbol{q}$.

The calculation of the transient behavior of machines modeled by the FE-Method can be very time consuming, because a fine discretization, resulting in lots of degrees of freedom (DOF), is needed for a good approximation of the real field. To use model predictive control systems for real time error correction and for parameter and design studies to optimize the machine design during the development, the simulations must be carried out faster, while maintaining the accuracy of the FE-Model.

Model order reduction (MOR) becomes crucial to reduce the simulation time for those models. To build those reduced-order models, by the class of methods addressed in the CRC/ TR96, it is necessary to transform the FE-Model into a so called input-output-model (IO-Model).

2.4 IO-Model

All the data necessary to generate IO-Models are extracted from ANSYS Mechanical, written into an open source, machine-readable description format and processed in specialized software tools and algorithms, developed as part of the research in CRC/ TR96, afterwards.

The formerly described FE-Model is transformed into a model in generalized state space form

$$\begin{aligned} E\dot{\boldsymbol{x}}(t) &= A\boldsymbol{x}(t) + B\boldsymbol{u}(t) \\ \boldsymbol{y}(t) &= C\boldsymbol{x}(t). \end{aligned} \tag{3}$$

The system (3) represents a linear time-invariant (LTI) system with the state $\boldsymbol{x} \in \mathbb{R}^n$, the input $\boldsymbol{u} \in \mathbb{R}^p$ and the output $\boldsymbol{y} \in \mathbb{R}^m$. The matrices $E \in \mathbb{R}^{n\,x\,n}$, $A \in \mathbb{R}^{n\,x\,n}$, $B \in \mathbb{R}^{n\,x\,p}$ and $C \in \mathbb{R}^{m\,x\,n}$ characterize the system. Note that for the here considered thermal simulation of machine tools and their subsystems, the vectors $\boldsymbol{x}$ and $\boldsymbol{y}$ represent the nodal temperatures $\boldsymbol{T}$ and the model output temperatures in points and faces of interest, e.g. at sensor positions and the TCP.

To generate the IO-form of the model from the data extracted from the ANSYS-FE-Model, the open source FE-Toolbox DUNE [6] is used. DUNE provides a modularized software framework, which allows for different mesh structures, different basis functions, including discontinuous functions, several mesh operations, in particular mesh intersections and an interface to sophisticated linear solver libraries like SuiteSparse [7] or PETSc [2] in an exchangeable manner.

For the generation of the IO-system, we implemented the computation of the coefficient matrices in a general way, such that different coupling strategies are easier to extend to newly developed coupling strategies.

2.5 Reduced IO-Model

After the IO-generation, there is the possibility to reduce the high-order IO-Model (3) to a low-dimensional surrogate model that approximates the dynamical behavior of the original model by means of MOR. Several projection-based techniques [1], including balanced truncation, moment matching and the iterative rational Krylov algorithm (IRKA) are implemented in a CRC/TR 96-tailored MOR-tool in MATLAB®.

During this reduction process, projection matrices V and $W \in \mathbb{R}^{n\,x\,r}$ are computed and the reduced system of order $r \ll n$ is obtained by

$$\begin{aligned} W^T EV\dot{\boldsymbol{x}}_r(t) &= W^T AV\boldsymbol{x}_r(t) + W^T B\boldsymbol{u}(t) \\ \boldsymbol{y}_r(t) &= CV\boldsymbol{x}_r(t). \end{aligned} \tag{4}$$

The vectors $\boldsymbol{x}_r$ and $\boldsymbol{y}_r$ denote the state vector and the output vector of the reduced model.

The MOR tool, further, incorporates treatment of inhomogeneous initial conditions, following [4] and allows for the preservation of physical parameters in the surrogate models via adapted MOR-techniques [5].

2.6 Time Integration Step

The different machine tool models are used to calculate the transient temperature field.

To compute the FE-solution, ANSYS and DUNE are used. The IO- and the reduced IO-Models are integrated with the second-order Rosenbrock-2 method [9]. This particular method belongs to the subclass of W-methods, which means we can use a fixed Jacobian over some time steps without the loss of too much accuracy. Furthermore, our experiments showed, that the method also remained stable with the explicit coupling terms.

3 Example Machine Results

The CAD model along with the used boundary conditions and probe positions to illustrate the workflow and to compare the results is shown in Figure 1.

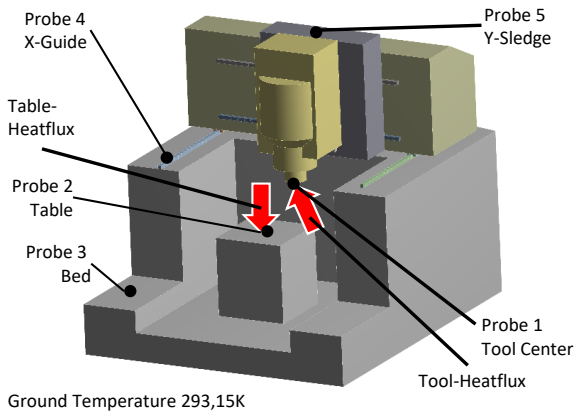

Figure 1. Example Machine and Boundary Conditions

A simplified machine tool, consisting of a machine bed and three sledges is simulated. All parts consist of the same, isotropic material with constant thermal properties. The connection between those components is realized by linear guides, consisting of rails and guide-wagons.

A constant temperature at the ground (293,15K) and two heat flux boundary conditions are applied. No relative movement of the parts is modeled, which means that all parts are fixed.

The model outputs for the reduced model are defined as the average temperatures of the faces that are subject to heat flux boundary conditions.

The coupling between the parts is realized by a simple output coupling using the averaged temperatures on the surfaces in contact.

The described model is used to calculate the thermal field with all four approaches. The reduced model was generated using Balanced Truncation. Figure 2 shows the results of the calculation after a transient simulation of 80 000s (500s steps) real time.

Therefor, the reduced state vector $\boldsymbol{x}_r$ is expanded to obtain an approximate solution $\hat{\boldsymbol{x}}$ for the full model, using the relation $\hat{\boldsymbol{x}}(t) = V\boldsymbol{x}_r(t)$. Note that this approach should be used with care. MOR aims at finding a good approximation of the output $\boldsymbol{y}$, but not necessarily the whole high-dimensional state $\boldsymbol{x}$. Hence, the outputs of the IO-Model should be selected with regard to the desired application of the reduced model.

The solutions of ANSYS, Dune and the IO-Model are nearly identical. As expected, the expanded solution of the reduced model shows differences in areas away from the defined model outputs. To illustrate this statement, Table 1 shows the calculated temperatures at the points marked in Figure 1. The ANSYS solution was used as the benchmark for the calculation of the absolute errors.

Table 1 Probe temperatures and errors in Kelvin

	ANSYS	DUNE	IO	Red-IO
Probe 1	298,729	298,733	298,733	298,582
Δ Probe 1	-	4,00E-03	4,00E-03	1,47E-01
Probe 2	305,621	305,623	305,623	305,623
Δ Probe 2	-	2,00E-03	2,00E-03	2,00E-03
Probe 3	293,162	293,162	293,162	293,419
Δ Probe 3	-	0,00E+00	0,00E+00	2,57E-01
Probe 4	293,324	293,32	293,32	293,334
Δ Probe 4	-	4,00E-03	4,00E-03	1,00E-02
Probe 5	295,661	295,659	295,659	295,657
Δ Probe 5	-	2,00E-03	2,00E-03	4,00E-03

The biggest observed error between the full and reduced model for those representative points is approximately 0,15 K.

The model orders used to calculate those solutions are listed in Table 2. By further increasing the order of the reduced model, a better approximation at the cost of higher simulation times is possible.

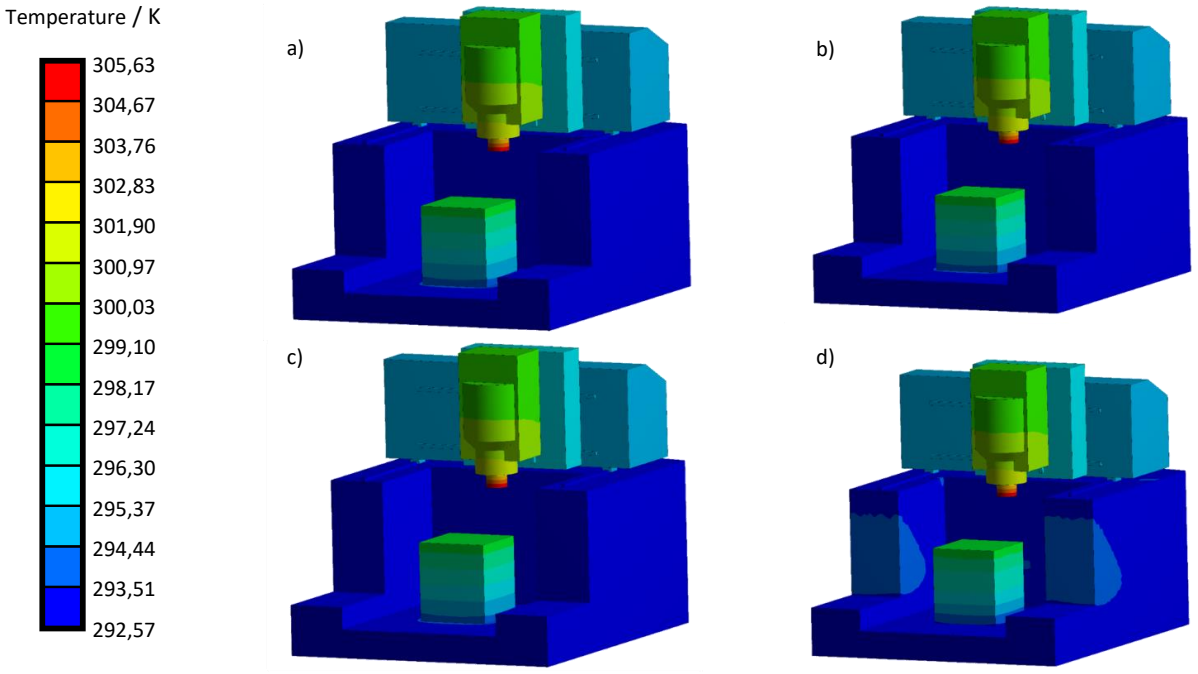

Figure 2. Thermal field of the four different simulation technologies a) ANSYS, b) DUNE, c) IO-Solution and d) Reduced IO-Solution

Table 2: Comparison of model size and simulation times in s

	Tool/ Model	Complete	Model-setup	Integration
Rough – DOFs (Full 45260, Reduced 174)	ANSYS	53,4	7,10	46,30
	DUNE	52,16	31,03	21,13
	IO	27,03	9,15	18,88
	Red-IO	5,91	5,84	0,07
Fine – DOFs (Full 167121, Reduced 183)	ANSYS	193,66	16,94	176,72
	DUNE-FE	224,56	115,23	109,33
	IO	130,09	35,24	94,85
	Red-IO	21,94	21,84	0,1

A comparison of the simulation times for the different approaches shows a remarkable reduction of the computation time by using MOR(Table 2). By reducing the model order of the rough mesh to 0,38 % of the full model, the simulation time to calculate the thermal field can be reduced by 78.14 % with respect to the full IO-Model. The integration step of the reduced model is 270 times faster.

For those Timings, ANSYS 19.2 and DUNE in version 2.4.1 were used. The integration of the Models uses SuiteSparse (5.6.0 - UMFPACK) with the BLAS-Libraries OpenBLAS (0.3.7 for DUNE) and the intel MKL (2019.4.245) together with MTL in svn revision 9592 for the IO-Models. All computations were carried out on a Windows-PC with Intel Core i5-6500 processor.

4 Summary and Outlook

In this paper, a new workflow to calculate the transient behavior of machine tools was introduced. It consists of the usual modeling of a finite element model with subsequent steps to generate a state space (IO-) model and a machine-readable description of the finite element model.

The main advantage in the open format is the exchange with other software tools enabling their features to the standard engineering workflow. Further extensions include problem-tailored time integration methods, which make use of the different time scales between the heat conduction and the relative moving components.

The IO-Model can easily be replaced by a much smaller surrogate model, generated by MOR-techniques, within the same workflow.

The potential for the usage of MOR for different use cases was shown by comparing simulation times and accuracy of the results against the results obtained by using the state of the art FE-tool ANSYS. Significant amounts of computational effort can be spared.

Concerning the ongoing advancement of the modeling techniques and the intended extension to the consideration of uncertain and nonlinear effects in the model, further methods for MOR will be included. Furthermore, the presented workflow will be extended to calculate the deformation of machine tools. This will enable the user to investigate the whole thermo-elastic functional chain of machine tools during machine development and usage.

The shown workflow is wrapped into an ANSYS Mechanical ACT Extension and is used by multiple subprojects of the CRC/TR 96.

Acknowledgement
Funded by the German Research Foundation – Project-ID 174223256 – TRR 96.

References

[1] Antoulas A C, 2005, Approximation of Large-Scale Dynamical Systems, Philadelphia (SIAM Publications)

[2] Balay S, Abhyankar S, Adams M, Brown J, Brune P, Buschelman K Dalcin L, Dener A, Eijkhout V, Gropp W, and others, 2019, PETSc Users Manual

[3] Bastian P, Bude G and Sander O, 2010, Infrastructure for the Coupling of Dune Grids in *Numerical Mathematics and Advanced Applications* 2009, Berlin *(*Springer Berlin Heidelberg*)* 107-114

[4] Beattie C, Gugercin S and Mehrmann V, 2017, Model Reduction for Systems with Inhomogeneous Initial Conditions, *Systems & Control Letters,* Vol. **99**, pp. 99-106

[5] Benner P, Gugercin S and Willcox K, 2015, A Survey of Projection-Based Model Reduction Methods for Parametric Dynamical Systems, *SIAM Review*, Vol. **57**, No. 4, pp. 483–531

[6] Blatt M, Burchardt A, Dedner A, Engwer C, Fahlke J, Flemisch B, Gersbacher C, Gräser C, Gruber F, Grüninger C, Kempf D, Klöfkorn R, Malkmus T, Müthing S, Nolte M, Piatkowski M and Sander O, 2016, „The Distributed and Unified Numerics Environment, Version 2.4," *Archive of Numerical Software,* Vol. 4, pp. 13-29

[7] Davis T A, Hager W W, Duff I S, 2014, SuiteSparse, *URL: faculty.cse.tamu.edu/davis/suitesparse.html*

[8] Engwer C and Müthing S, 2016, Concepts for Flexible Parallel Multi-domain Simulations, Decomposition Methods in Science and Engineering XXII, Springer International Publishing, 187-195

[9] Naumann A, Ruprecht D and Wensch J, 2018, Toward transient finite element simulation of thermal deformation of machine tools in real-time, *Computational Mechanics*

[10] Verwer, J G Spee, E J Blom J G. und Hundsdorfer W, 1999, „A second-order Rosenbrock method applied to photochemical dispersion problems," *SIAM Journal on Scientific Computing,* Vol. 20, pp. 1456-1480

[11] Wohlmut B I, 2000, A mortar finite element method using dual spaces for the Lagrange multiplier*, SIAM Journal on Numerical Analysis*, Vol. **38**, 989-1012

Special Interest Group Meeting on Thermal Issues
Laboratory for Machine Tools and Production Engineering (WZL) of
RWTH Aachen, Germany, February 2020
www.euspen.eu

Spline approximation approach for elastic machine tool structure modelling

P. Dahlem[a], M. Sanders[a], Robert H. Schmitt[a]

[a]*Laboratory for Machine Tools and Production Engineering of RWTH Aachen University, Germany*

Abstract

Uncontrolled environmental conditions often impact manufacturing processes and lead to product quality fluctuations. For machine tools, thermal influences are a major limitation to the volumetric performance. Climate controls for the shop floor, machines or thermally stable structural designs are often economically not feasible, promoting control-based compensation as a possible solution. Since the relationship between disturbing quantities and effects are complex and specific to each machine, appropriate modelling is a critical requirement.

The rigid body model, prevailing in various mathematical formulations [1], is currently a frequently used kinematic model for controller-based compensation of geometric errors and is computationally evaluable on the controller itself. One drawback of this model is that typically the compensation is based on static error tables and the variability of geometric errors is not taken into account. It is therefore the subject of many research activities to consider the variability of geometric errors within extended model approaches or alternatively to record them process parallel [2–4]. In general, the statement can be made that the more information is available on the geometric state of the machine, the less complex models are required. The same applies vice versa. In the context of digitalization, the availability of process-parallel data increases, but still the direct process-parallel recording of the volumetric error is technically unsolved. By recording and knowing the temperature and force distribution on the machine structure, it is possible, for example, to predict the deformation using FEM models, and hence predict the resulting volumetric error. However, this also requires precise information on the geometric structure of the machine and its material composition. The problem that arises is on the one hand the high computational effort that results from the division into finite elements and on the other hand the high initial effort required for the geometry and material modelling. The effort for creating the model is not scalable to different machine types and must be done individually.

Instead of classic FEM the authors pursue a new modeling concept for the elastic structure deformations, which is based on the approximation of typical deformation modes based on Bézier curves. Spline-based deformation modelling is described in various literature as particularly computationally efficient, with only small approximation errors compared to FEM [5–7].
Since this method is not based on basic physical assumptions, it is necessary to specify sensible preforming modes for machine tool structure components based on expert or experimental knowledge. The authors use additional machine tool integrated inclination and interferometric sensors to define actual deformation constraints. Preliminary tests are performed to compile a catalog of deformation modes, of which the best fitting ones are selected.
The spline information is stored in a JSON (JavaScript Object Notation) file, which also contains the machine tool structural loop as well as rough structure component dimensions an positions. The authors call this abstracted physical body model. The foundation on JSON allows for arbitrary enrichment of the dataset with additional keys and objects, so that also static deformation data (geometric errors according to ISO 230-1:2012) can be stored. The authors developed the software VoluSoft which can read and write these files as well as calculate and visualize the machine deformation and the resulting volumetric error at arbitrary machine positions [8]. With this concept the authors try to overcome the drawbacks of FEM-based machine tool structure modelling and develop a solution, which is highly adaptable to different machine tool types even if no detail Information about machine geometry and material is available.

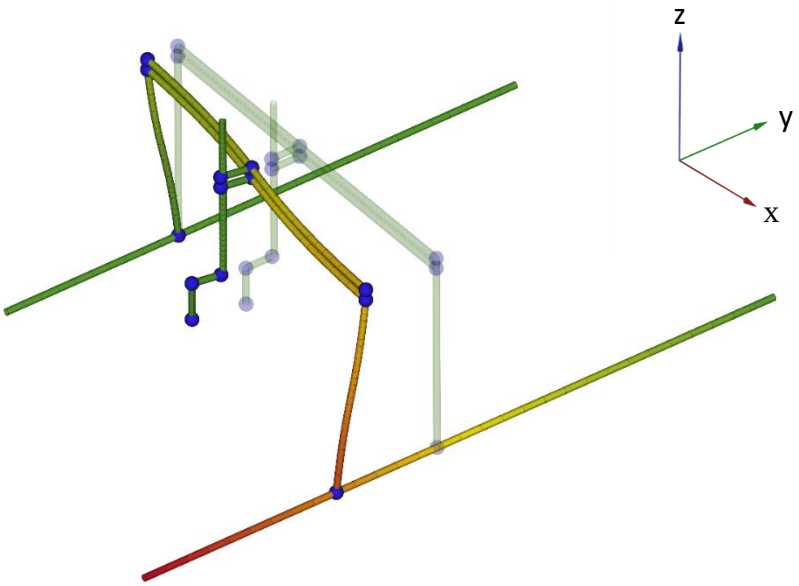

Figure 1 Visualization of a spline-based abstracted physical body model of a FYXZ serial machine tool kinematic. The shown deformation can occur by unsymmetrical deformation of the gantry-axis (Y).

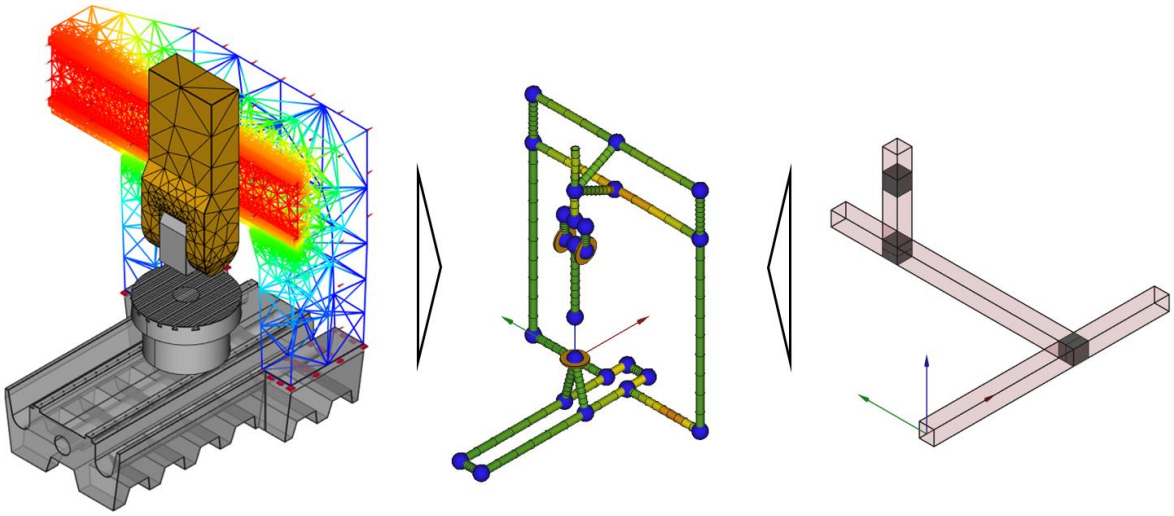

Figure 2 Comparison of FEM-based model (left), rigid-body model for linear axes (right) and spline-based abstracted physical body model (middle) of the exact same machine

References

[1] Lin Y, Shen Y (2003) Modelling of Five-Axis Machine Tool Metrology Models Using the Matrix Summation Approach. The International Journal of Advanced Manufacturing Technology 21(4):243–8.

[2] Benjamin Montavon, Philipp Dahlem, Martin Peterek, Markus Ohlenforst and Robert H. Schmitt (2018) Modelling Machine Tools using Structure Integrated Sensors for Fast Calibration. JMMP 2(1):14.

[3] Baum C, Brecher C, Klatte M, Lee TH, Tzanetos F (2018) Thermally induced volumetric error compensation by means of integral deformation sensors. Procedia CIRP 72:1148–53.

[4] Mayr J, Blaser P, Ryser A, Hernandez-Becerro P (2018) An adaptive self-learning compensation approach for thermal errors on 5-axis machine tools handling an arbitrary set of sample rates. CIRP Annals 67(1):551–4.

[5] Liu Y, Sun L, Liu Y, Cen Z (2011) Multi-scale B-spline method for 2-D elastic problems. Applied Mathematical Modelling 35(8):3685–97.

[6] Höllig K (2003) Finite element methods with B-splines. Society for Industrial and Applied Mathematics (SIAM 3600 Market Street Floor 6 Philadelphia PA 19104), Philadelphia, Pa.

[7] Tönshoff HK, Rehling S, Tracht K (2002) An Alternative Approach to Elasto-Kinematic Modelling of Machine Tool Structures. in Kulianic E, (Ed.). AMST'02 Advanced Manufacturing Systems and Technology: Proceedings of the Sixth International Conference. Springer Vienna. Vienna, s.l., pp. 215–223.

[8] B. Montavon, P. Dahlem, R. H. Schmitt Effektive Analyse von Werkzeugmaschinenkalibierdaten. wt-online.

Special Interest Group Meeting on Thermal Issues
Laboratory for Machine Tools and Production Engineering (WZL) of
RWTH Aachen, Germany, February 2020
www.euspen.eu

Comparison of Thermal Modal Analysis and Proper Orthogonal Decomposition methods for thermal error estimation

Natalia Colinas-Armijo, Beñat Iñigo, Gorka Aguirre

Design and Precision Engineering Group, IDEKO, 20870 Elgoibar, Basque Country, Spain

ncolinas@ideko.es

Abstract
Due to the increasing demand on more accurate products without losing high rates of productivity, the control of thermal induced errors in machine tools is still a relevant issue. To compensate the errors from thermal deformation, the temperature field in the machine needs to be known. In order to reproduce thermal fields, accurate models are needed, but not only that, apart from accurate, models are required to be of low computational effort. To overcome the issue of high time-consuming models, model order reduction techniques have been applied to thermos-elastic models. Moreover, it is necessary to obtain the maximum information as possible from experimental tests. Reduced order models are useful for this too. For all the aforementioned, this work proposes a methodology to evaluate the capabilities and limitations of two model order reduction techniques (thermal modal analysis and proper orthogonal decomposition) and their application to optimal sensor positioning and their robustness considering different load cases and conditions.

Thermal modal analysis, Proper Orthogonal Decomposition

1. Introduction

Controlling errors due to thermal deformations is one of the biggest issues in machine tools due to the demand of more accurate products (straighter tolerances and better quality) and keeping high productivity [1].

In order to predict the thermal induced errors, it arises the need of reproducing the thermal field. To do that, from experimental test it is necessary to acquire the maximum amount of information as possible with the minimum number of inputs. To do that, reducer order models are really useful.

Some works have already been published dealing with model reduction techniques and methods for optimal temperature sensor placement. Koevets et al. [2] proposed a methodology based on comparing the optimal sensor positioning using nodal and modal compensation methods. Benner et al. [3] compared several model order reduction methods to find an optimal sensor positioning. In these works, thermal modal analysis and proper orthogonal decomposition methods are used.

There are several mathematical methods to find the optimum sensor positions for thermo-elastic models. Research on thermal modal analysis has been performed on modelling of machine tools [4], on thermal error compensation on machine tools [5] and other applications [6], since its content on physical meaning helps to characterise well a thermo-elastic system. Proper orthogonal decomposition is a pure mathematical method [7,8] that works well when the conditions are well-known but does not extract all the physical content of the thermo-elastic system.

In this work, a theoretical example of a 2D plate is proposed to compare the reduction methods of thermal modal analysis and proper orthogonal decomposition. The aim of the proposed study is to compare both methods and understand their capabilities and limitations by means of a sensitivity analysis. The objective is to understand in which applications or cases is more suitable each method. This builds a step towards a further analysis on optimal sensor positioning by means of these methods.

2. Thermal modal analysis and Proper Orthogonal Decomposition for thermo-elastic models

The case of study in this work is a square 2D plate fixed in one side, represented in Figure 1. The dimensions of the 2D plate are 250mmx250mm, and two load positions are proposed for evaluation.

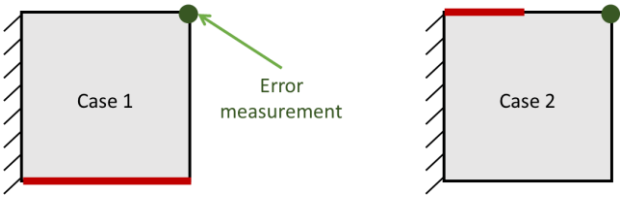

Figure 1. Case study: square 2D plate fixed in one side

The equation for calculating the thermal field may be written as

$$\boldsymbol{C^t}\dot{\boldsymbol{\theta}}(t) + \boldsymbol{K^t}\boldsymbol{\theta}(t) = \boldsymbol{q}(t) \qquad (1)$$

Where $\boldsymbol{C^t}$ is the specific heat or thermal inertia matrix, $\boldsymbol{K^t}$ is the conductivity matrix, $\boldsymbol{q}(t)$ is the thermal load vector and $\boldsymbol{\theta}(t)$ is the temperatures vector. The equation that couples the thermal with the elastic behaviour, when there are not included mechanical loads may be represented as

$$\boldsymbol{K^u}\boldsymbol{u}(t) + \boldsymbol{K^{ut}}\left(\boldsymbol{\theta}(t) - \boldsymbol{\theta_{ref}}\right) = \boldsymbol{0} \qquad (2)$$

where $\boldsymbol{K^u}$ is the stiffness matrix, $\boldsymbol{K^{ut}}$ is the thermoelastic stiffness matrix, $\boldsymbol{u}(t)$ is the displacements vector, $\boldsymbol{\theta}(t)$ is the temperatures vector and $\boldsymbol{\theta_{ref}}$ is the initial temperature vector.

Then the equation for a coupled thermoelastic analysis which results as combination of the Eqs. *(1)* and *(2)*, may be written in matrix form as:

$$\begin{bmatrix} \mathbf{0} & \mathbf{0} \\ \mathbf{0} & \boldsymbol{C^t} \end{bmatrix} \begin{bmatrix} \dot{\boldsymbol{u}}(t) \\ \dot{\boldsymbol{\theta}}(t) \end{bmatrix} + \begin{bmatrix} \boldsymbol{K^u} & \boldsymbol{K^{ut}} \\ \mathbf{0} & \boldsymbol{K^t} \end{bmatrix} \begin{bmatrix} \boldsymbol{u}(t) \\ \boldsymbol{\theta}(t) \end{bmatrix} = \begin{bmatrix} \boldsymbol{K^{ut}\theta_{ref}} \\ \boldsymbol{q} \end{bmatrix} \boldsymbol{z}(t) \quad (3)$$

where $\boldsymbol{C^t}$ is the specific heat or thermal inertia matrix, $\boldsymbol{K^t}$ is the conductivity matrix, $\boldsymbol{K^u}$ is the stiffness matrix, $\boldsymbol{K^{ut}}$ is the thermoelastic stiffness matrix, $\boldsymbol{q}$ is the thermal load vector, $\boldsymbol{u}(t)$ is the displacements vector and $\boldsymbol{\theta}(t)$ is the temperatures vector. Since the quantity of interest are the thermal deformation, the solution results as

$$\boldsymbol{y(t)} = \begin{bmatrix} \boldsymbol{O^u} & \mathbf{0} \\ \mathbf{0} & \boldsymbol{O^t} \end{bmatrix} \begin{bmatrix} \dot{\boldsymbol{u}}(\boldsymbol{t}) \\ \dot{\boldsymbol{\theta}}(\boldsymbol{t}) \end{bmatrix} \quad (4)$$

where $\boldsymbol{O^u}$ and $\boldsymbol{O^t}$ are the matrices that link the temperature and the displacement with the state-space output vector.

Eqs. *(3)* and *(4)* may be re-written in state-space form as follows

$$\begin{cases} \dot{\boldsymbol{x}}(\boldsymbol{t}) = -\boldsymbol{C^{-1}Kx}(\boldsymbol{t}) + \boldsymbol{C^{-1}fz}(\boldsymbol{t}) \\ \boldsymbol{y}(\boldsymbol{t}) = \boldsymbol{Ox}(\boldsymbol{t}) \end{cases} \quad (5)$$

where $\boldsymbol{x}(t)$, $\boldsymbol{z}(t)$ and $\boldsymbol{y}(t)$ are the state vector, the input and the output respectively.

2.1. Thermal modal analysis

The discrete heat equation from Eq. *(3)* may be derived and may be written as

$$\boldsymbol{C^t}\,\frac{d\,\boldsymbol{\theta}(t)}{dt} + \boldsymbol{K^t}\,\boldsymbol{\theta}(t) \;=\; \boldsymbol{q}(t). \quad (6)$$

The system in *Eq. (6)* is a system of *n* first order linear differential equation with constant coefficients. So, the general solution of the system is the sum of the general solution of the homogeneous system plus a particular solution of the whole system.

The homogeneous system is

$$\boldsymbol{C^t}\,\frac{d\,\boldsymbol{\theta}(t)}{dt} + \boldsymbol{K^t}\,\boldsymbol{\theta}(t) \;=\; \mathbf{0} \quad (7)$$

whose solutions are

$$\boldsymbol{\theta}(t) \;=\; \boldsymbol{\Phi}\,e^{-\lambda\,t}, \quad (8)$$

replacing them in the homogeneous system, it results

$$(\boldsymbol{K^t} - \lambda\boldsymbol{C^t})\boldsymbol{\Phi} \;=\; \mathbf{0}. \quad (9)$$

This system is a generalised problem of eigenvalues and eigenvectors. The characteristic equation of this system is $|\boldsymbol{K^t} - \lambda\boldsymbol{C^t}| = \mathbf{0}$. The solution of the characteristic equation gives *n* eigenvalues $\lambda_1, \lambda_2, .., \lambda_n$. The eigenvalues are the inverse of the time constantans of each mode $\tau_1, \tau_2, \ldots, \tau_n$. Replacing the eigenvalues in the system and solving it is obtained a series of eigenvectors $\boldsymbol{\Phi_i}$ associated to them. So, the general equation of the homogeneous system results

$$\boldsymbol{\theta}(t) \;=\; \sum_{i=1}^{n} \boldsymbol{D_i}\,\boldsymbol{\Phi_i}\,e^{-\lambda_i\,t} \quad (10)$$

The particular solution of the whole system depends on the shape of the thermal excitations $\boldsymbol{q}(t)$, and it results

$$\boldsymbol{\theta}(t) \;=\; \boldsymbol{K^{t^{-1}}}\,\boldsymbol{q}(t) \quad (11)$$

thus, the general solution of the system is

$$\boldsymbol{\theta}(t) \;=\; \boldsymbol{K^{t^{-1}}}\,\boldsymbol{q}(t) \;+ \sum_{i=1}^{n} \boldsymbol{D_i}\,\boldsymbol{\Phi_i}\,e^{-\lambda_i\,t} \quad (12)$$

The study of a discrete thermal system can be reduced to the resolution of a classic problem of eigenvalues and eigenvectors as

$$\boldsymbol{K^t}\,\boldsymbol{V_i} \;=\lambda_i\; \boldsymbol{C^t}\,\boldsymbol{\Phi_i} \quad (13)$$

The eigenvectors $\boldsymbol{\Phi_i}$ form a system of *n* lineally independent vectors that constitute a base. The temperature vector $\boldsymbol{\theta}(t)$ can be expressed related to this base with some new coordinates $\boldsymbol{\xi}(t)$, that is

$$\boldsymbol{\theta}(t) \;=\; \textstyle\sum_{i=1}^{n} \boldsymbol{\Phi_i}\boldsymbol{\xi_i}(t) \;=\; \boldsymbol{\Phi}\boldsymbol{\xi}(t). \quad (14)$$

Replacing Eq. *(14)* int the original system of Eq. *(6)* and multiplying by $\boldsymbol{\Phi}^{\mathrm{T}}$

$$\boldsymbol{\Phi^T C^t \Phi}\dot{\boldsymbol{\xi}}(t) \;+ \boldsymbol{\Phi^T K^t}\,\boldsymbol{\Phi}\boldsymbol{\xi}(t) \;= \boldsymbol{\Phi^T}\,\boldsymbol{q}(t), \quad (15)$$

then, if $\boldsymbol{\Phi^T}\,\boldsymbol{q}(t) \;=\; \boldsymbol{\psi}(t)$, Eq. *(15)* may be re-written as

$$\dot{\boldsymbol{\xi}}(t) \;+ \boldsymbol{\lambda}\boldsymbol{\xi}(t) \;= \boldsymbol{\psi}(t), \quad (16)$$

since $\boldsymbol{\Phi^T C^t \Phi} = \mathbf{0}$ and $\boldsymbol{\Phi^T K^t}\,\boldsymbol{\Phi} = \boldsymbol{\lambda}$ due to the orthogonality of the eigenvectors respect to the matrices $\boldsymbol{K^t}$ and $\boldsymbol{C^t}$. As $\boldsymbol{\lambda}$ is a diagonal matrix, immediately it is observed that in Eq. *(16)* there is a system of *n* uncoupled equations with the form

$$\dot{\boldsymbol{\xi}}(t) \;+ \lambda_i\,\boldsymbol{\xi}(t) \;= \boldsymbol{\psi_i}(t). \quad (17)$$

Thus, with $\boldsymbol{\xi}(t)$, denominated natural coordinates, the system of *n* differential equations with *n* variables becomes *n* equations of a single variable.

The eigenvectors $\boldsymbol{\Phi_i}$ are the so-called natural thermal modes, and the methodology employed for uncoupling equations of thermal balance is called Thermal Modal Analysis (TMA).

2.2. Proper Orthogonal Decomposition

Proper Orthogonal Decomposition (POD) method is based on the SVD computation of a matrix that contains various vector results (from simulations or experimental measurements). These vectors are denominated snapshots. Considering the linear dynamical system in Eq. *(5)*, for a fixed input $\boldsymbol{z}(t)$, the state trajectory $\boldsymbol{x}(t)$ at certain instants t_k is measured as

$$\boldsymbol{\chi} = \left[\boldsymbol{x}(t_1)\;\; \boldsymbol{x}(t_2) \ldots\; \boldsymbol{x}\left(t_{n_{snap}}\right)\right] \in \mathbb{R}^{n \times nsnap} \quad (18)$$

being $\boldsymbol{\chi}$ the matrix of snapshots and n_{snap} the number of snapshots, in general $n_{snap} \geq n$. The singular value decomposition of $\boldsymbol{\chi}$ is performed and if the singular values of this matrix fall off rapidly, a low-order k approximation of this system may be computed

$$\boldsymbol{\chi} = \boldsymbol{USV}^* \approx \boldsymbol{U_k S_k V_k}, \quad k \ll n. \quad (19)$$

The eigenvalues of $\boldsymbol{\chi}$ typically decay exponentially for snapshots drawn from the heat equation. The truncation threshold to obtain k is chosen such that the ratio of the energies contained in the bases of the reduced and full models is near 1, that is,

$$\frac{\sum_{i=1}^{k} \lambda_i}{\sum_{i=1}^{n_{snapshots}} \lambda_i} = \frac{\sum_{i=1}^{k} \lambda_i}{trace(\boldsymbol{S})} \approx 1, \quad (20)$$

being λ_i the *i-th* component of the diagonal of the matrix $\boldsymbol{S}$.

Then the model reduction is applied to the state space $\boldsymbol{x}(t)$ as follows

$$\boldsymbol{x}(t) \approx \boldsymbol{S_k}\hat{\boldsymbol{x}}(t) \quad (21)$$

where $\boldsymbol{S_k} \in \mathbb{R}^{n \times k}$ and $\hat{\boldsymbol{x}}(t) \in \mathbb{R}^k$.

The main problem of this method is that the resulting simplification depends on the initial excitation imposed to the system, the obtained singular values are not system invariants. The main advantage arises from the applicability to high-complexity linear and nonlinear systems.

3. Methodology

In this section, a methodology to find the optimum sensor placement for the mathematical methods of thermal modal analysis and proper orthogonal decomposition is proposed. The presented methodology considers physical meaning and practical/operational viability.

3.1. Modes comparison

In order to stablish a reasonable criterion for both methods, the thermal modes of thermal modal analysis are compared with the modes of the base $\boldsymbol{S_k}$ from proper orthogonal decomposition method.

The main difference between the modes from thermal modal analysis $\boldsymbol{\Phi_i}$ and the ones from POD $\boldsymbol{S_{k_i}}$ is the physical meaning or content. In the case of thermal modal analysis, the thermal modes contain information from the physical system and are independent from the thermal load imposed to the system. In the case of POD, the thermal modes depend on the matrix of snapshots $\boldsymbol{\chi}$.

In Figure 2 are shown the first four modes of thermal modal analysis (a) and from POD (b). As it may be observed, the modes shape is completely different. In Figure 2 (b) it is seen that the modes shape of POD depends on the input load.

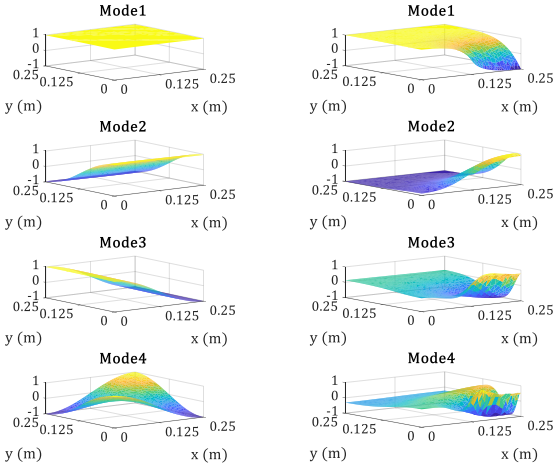

(a) (b)

Figure 2. First four thermal modes from thermal modal analysis (a) and from POD (b).

Figure 3 shows the thermal growth that corresponds to the modes in both cases thermal modal analysis (a) and POD (b). As in the case of the thermal modes the growth behaviour for this case of study for POD Figure 3 (b) depends on the input load location, not like in the thermal modal analysis Figure 3 (b) case that depends on the system.

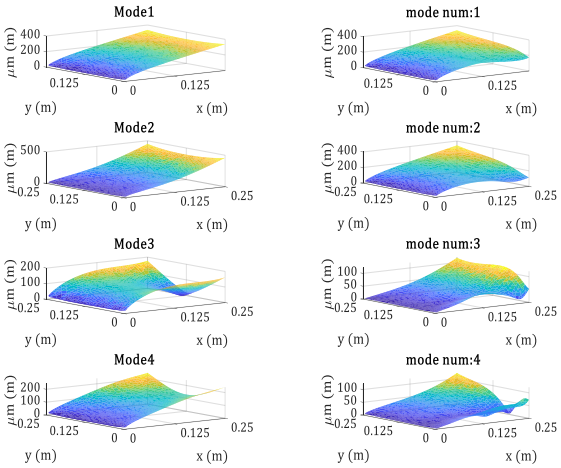

(a) (b)

Figure 3. First four growth modes from thermal modal analysis (a) and from POD (b).

The shape of the thermal modes is going to be used to select the sensor position, in order to optimise the quantity of information acquired.

3.2. Base reduction and number of sensors

The number of relevant modes or order to reduce the base depend on the method. In the case of proper orthogonal decomposition, the reduction is related with the truncation condition in Eq. *(20)*. In the case of thermal modal analysis, the modes are order considering the value of the time constants of each mode τ_i.

3.3. Sensor position selection

Since in real physical systems there exists limitations, (due to shapes, functionalities, …) the first consideration to be made it is to impose limits to the possible sensor locations. To do that, the first step is to divide the body into cells where there could exist the possibility to place the sensors. The sensor location is going to be selected where the maximums or minimums of the most significant modes are located. This would give some physical meaning and content to the problem. Figure 4 shows an example of how the sensor placement pre-selection would be.

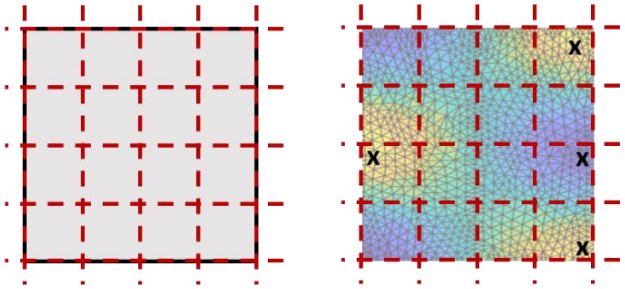

Figure 4. Available positions for sensor location and sensor position location based on absolute maximums of the modes.

For each mode a certain number of absolute maximums is needed, that would mean number of sensors by mode, and the quantity of modes to be used has to be defined or selected. To do so, the information that contains each node and its weight has to be evaluated.

4. Results and analysis

In order to evaluate the capabilities of thermal modal analysis and proper orthogonal decomposition methods, two sensitivity analysis are proposed. The first one is focused on the modal base reduction and the second one with the optimal sensor positioning.

To perform the sensitivity analysis, the load position of case 1 from Figure 1 with a step input is selected to create the base of both methods. From the base obtained with this analysis, several load cases (unit step, sinusoidal) will be evaluated performing variations on amplitudes and frequencies. Moreover, the accuracy of the reduced models when the load position is modified will be evaluated.

In the case of optimal sensor positioning, a comparative analysis of optimal sensor placement will be performed. The objective of this analysis is to understand which method (POD or TMA) is more adequate depending on the case under study.

As a result of the methodology proposed in Section 3, the capabilities and limitations of thermal modal analysis and proper orthogonal decomposition as model order reduction techniques are going to be stated. Furthermore, an evaluation of the capacities and versatility of both methods regarding optimal sensor positioning will be performed.

References

[1] Mayr J et al. 2012 *CIRP Annal.* **61** (2) 771-791.

[2] Koevoets A H, Eggink H J, van der Sanden J, Dekkers J, Ruijl T A M 2007 *13th International Workshop on Thermal Investigation of ICs and Systems (THERMINIC)* 208-213.
[3] Benner P, Herzog R, Lang N, Riedel I and Saak J 2019 *Eng. Optim*. **51** (3) 465–483.
[4] Bueno R, Arzamendi J, Almandoz X 1997 *Integrated Design and Manufacturing in Mechanical Engineering* 307-315.
[5] Zhu J, Ni J, Shih A J 2008 *J. Manuf. Sci. Eng.* **130** 061006-1.
[6] Morishima T, van Ostayen R, van Eijk J, Schmidt Munnig R-H 2015 *Precis. Eng.* **42** 66–72.
[7] Antoulas A C and Sorensen D C 2001 *Int. J. Appl. Math. Comput. Sci.* **11** (5) 1093–1121.
[8] Schilders W, Van der Vorst H and Rommes J 2008 Model order reduction: theory, research aspects and applications.

Special Interest Group Meeting on Thermal Issues
Laboratory for Machine Tools and Production Engineering (WZL) of
RWTH Aachen, Germany, February 2020
www.euspen.eu

Low thermal expansion machine frame designs using lattice structures

Poom Juasiripukdee[1], Ian Maskery[1], Ian Ashcroft[1], Richard Leach[1]

[1]*Faculty of Engineering, University of Notingham, UK*

Poom.juasiripukdee@nottingham.ac.uk

Abstract

The aim of this work is to develop an optimised design for a machine frame, which minimises thermal expansion. The work presents a study of a design concept for a lattice structure with a tailorable coefficient of thermal expansion (CTE). The proposed design is an assembly of two parts: a lattice and a cylinder which fits inside the lattice (Figure 1). The two parts are made of different homogenous materials with different positive CTEs. Nine different models were investigated and their thermal and structural behaviour analysed using a finite element method. The relationship between the size of the cylindrical inner part and the lattice outer part was mapped out to understand their relationship and the effects on the CTE. The simulation showed that for a lattice design, using nylon 12 and ultra-high-molecular-weight polyethylene, the thermal expansion can be reduced from 109×10^{-6} K^{-1} to 12×10^{-6} K^{-1}. An experimental rig was designed to measure the thermal expansion of the model for a range of temperatures. One model has been physically built and the CTE was measured experimentally. The lattices were fabricated using powder bed fusion. The dimensions of the built specimen were measured using X-ray computed tomography. This paper proves that the combination of design optimisation and additive manufacturing can be used to achieve low CTE structures and, therefore, low thermal expansion machine frames at low cost.

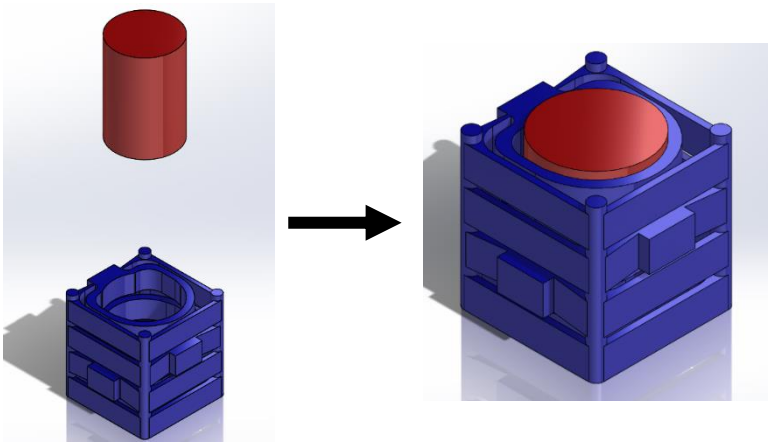

Figure 1. The proposed design.

Coefficient of thermal expansion, lattice structure, metrology frame, finite element analysis, powder bed fusion, additive manufacturing

Special Interest Group Meeting on Thermal Issues
Laboratory for Machine Tools and Production Engineering (WZL) of
RWTH Aachen, Germany, February 2020
www.euspen.eu

Precise length measurement at non-standard temperature

Dmytro Sumin, Rainer Tutsch

TU Braunschweig, Institut für Produktionsmesstechnik
r.tutsch@tu-bs.de

Abstract
Length measurements are to be made at standard temperature 20°C, otherwise errors due to thermal expansion of workpieces and scales will occur. In production environments this cannot always be granted. DIN EN ISO 15530-3 describes a technique to correct the measurement error by referring to a calibrated reference workpiece. We have investigated this approach theoretically and experimentally and present some results.

Measurement, Quality assurance, Thermal error, Workpiece

1 Introduction

Geometric measurements are affected by temperature changes because of the material-specific temperature expansion of workpiece and instrument. For that reason the environmental conditions have to be tightly controlled for precision measurements. In real-world applications, especially in production environments, it is often not possible or economically not affordable to control the environment to the standard temperature of 20°C that is required by the relevant national and international standards. This problem is even more demanding for many developing countries situated in areas with hot climate.

In principle this problem can be solved as far as the temperature distribution is known and a model of the measurement system is available. However, the complexity of a cmm with 3 axes is quite demanding, as 21 degrees of freedom have to be controlled. Only the manufacturer of the cmm has access to the required data. Software modules for correction of thermal errors are available for high-end cmms.

Our measurement strategy is based on DIN EN ISO 15530-3 [1] and can be applied without special mathematical or engineering skills. A single selected workpiece is calibrated and applied as a reference for checking the conformity of all other produced parts of that type. Thermal effects then only affect the geometrical difference between the reference part and the serial part. This difference typically is much smaller than 1mm and only this length difference will change by an index of thermal expansion in the order of 10^{-5} (relative), resulting in an absolute deviation in the order of less than 1µm.

2 Theory

Let l_{20} be the length of a workpiece measured at standard temperature and l the length of that same workpiece measured at some temperature T = 20°C + ΔT. With the coefficient of thermal expansion α we get equation 1:

$$l = l_{20}(1 + \alpha \cdot \Delta T) \qquad (1)$$

In general the workpiece and the scale will have different temperatures so that we can write equation 1 for both of them, identifying them with the index “wp” or “sc”, respectively:

$$l_{sc} = l_{20sc}(1 + \alpha_{sc} \cdot \Delta T_{sc})$$

$$l_{wp} = l_{20wp}(1 + \alpha_{wp} \cdot \Delta T_{wp})$$

This leads to the correction formula:

$$l_{20wp} = l_{wp} \frac{1+\alpha_{sc} \cdot \Delta T_{sc}}{1+\alpha_{wp} \cdot \Delta T_{wp}} \qquad (2)$$

If the temperatures and the coefficients of thermal expansion were precisely known, a correction of the thermal error is possible. Instead of this we refer to the calibrated workpiece with nominally the same geometry, made from the same material (Figure 1) and measured under the same non-standard temperature and end up with the following simple formula:

$$l_{20\,wp} = \frac{l_{20\,rwp} \times l_{wp}}{l_{rwp}}$$

With: l_{20rwp}: known calibration value
l_{rwp}: measured value at temperature T

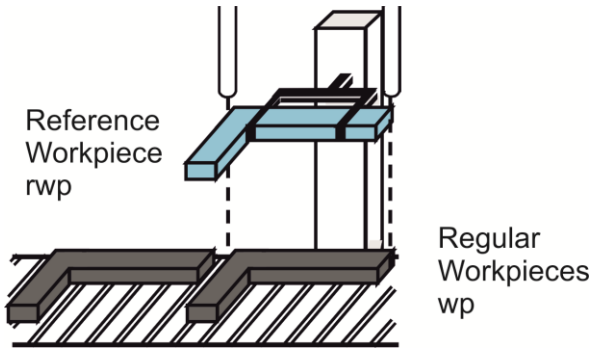

Figure 1. Serial test in production referring to a calibrated reference workpiece rwp

3 Experiments and Simulation Calculations

We tested this approach experimentally with a number of workpieces, ranging from simple end gauges to complex shaped test workpieces (Figure 2). Using a cmm Werth VideoCheck HR without internal temperature compensation for the measurements we varied the room temperature between 16°C and 24°C. In all cases the resulting errors were in the order of only a few µm.

To overcome the limited variation range of the temperature control of the cmm we added an experiment at 40°C, using a precision optoelectronic probe (Heidenhain SP25, Figure 3). Though the error due to thermal expansion in this case was more than 80µm, we were able to correct it to less than 2µm.

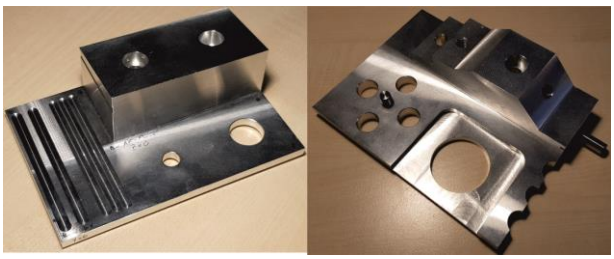

Figure 2. Complex shaped test workpieces used for our experiments

We simulated the temperature distribution resulting from heat exchange between workpiece and surrounding air using the software ANSYS. Workpieces with complex shape show local temperature gradients that lead to inhomogeneous deformation. Because of the similarity of reference and serial workpiece, however, the difference between both will stay small.

An in-depth error analysis according to GUM can be found in [2]. Considering realistic assumptions we estimate the expanded uncertainty of a length measurement of a workpiece with about 100 mm length to 5µm. The analysis of the error budget shows that the main error contributions are the measurements of the actual lengths of workpiece and reference workpiece and variations in material properties in serial production.

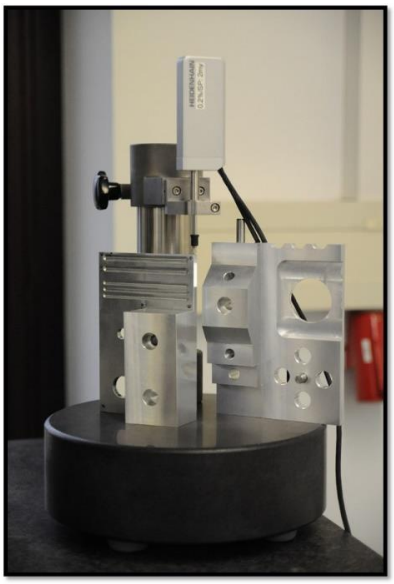

Figure 3. SP25 probe with different workpieces

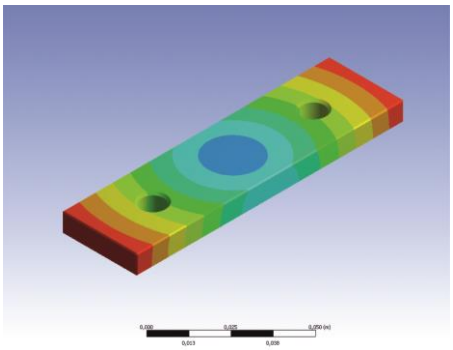

Figure 4. Colour-coded display of the temperature distribution of a workpiece caused by heat exchange with the ambient air

It has to be emphasized that the technique proposed here is limited to homogeneous workpieces. Workpieces made from multi-materials or showing extreme temperature gradients may exhibit large warpage errors that can neither be corrected by our simple approach nor by the more sophisticated correction modules offered by cmm manufacturers

Acknowledgement: The author D. Sumin gratefully acknowledges the funding of his scholarship by The Federal Ministry for Economic Cooperation and Development of Germany and support from Braunschweig International Graduate School of Metrology IGSM.

References

1. N.N.: ISO 15530-3: Geometrical product specifications (GPS) -- Coordinate measuring machines (CMM): Technique for determining the uncertainty of measurement -- Part 3: Use of calibrated workpieces or measurement standards (2011)

2. D. Sumin, R.Tutsch: Precise linear measurements using a calibrated reference workpiece without temperature measurements. Journal of Sensors and Sensor Systems, 7, 609-620, (2018)

Special Interest Group Meeting on Thermal Issues
Laboratory for Machine Tools and Production Engineering (WZL) of
RWTH Aachen, Germany, February 2020
www.euspen.eu

Efficient FE-Modelling of the transient thermo-elastic machine behaviour of 5-axes machine tools

Christian Brecher[1], Stephan Neus[1], Mathias Dehn[1]

[1]*Laboratory for Machine Tools and Production Engineering (WZL) of RWTH Aachen University, Germany*

m.dehn@wzl.rwth-aachen.de

Abstract

The demand for more accurate machine tools is continuously rising. Therefore, thermal error compensation methods need to get more precise under thermo-elastic real time conditions. This paper introduces a simulation model architecture that combines the accuracy of geometric measurements with the adaptability to transient thermal distributions of simulation models. It is shown, how a geometric measurement result can be processed to be fed back into the simulation model to increase its accuracy.

Machine tool, Deformation, Thermo-elastic behaviour, Simulation

1. Introduction

Machine tools like milling and turning machines have become an integral part of the production process. They must cope with continuously rising requirements on workpiece complexity and accuracy. To achieve these requirements, machine tool manufacturers are working on reducing potential machine error sources to a minimum. A major part of the total error is the error resulting from thermal influences, which can have a share of up to 75% on the total error [1]. This high error share is even more concerning, when looking at the trend of small batch sizes to custom fit products to consumer needs [2]. Since machining conditions change more frequently with small batch sizes, the machine is constantly in a transient state. In this transient state, thermal compensation methods are less accurate, which leads to an increase of the thermal machine error. To reduce the error from this transient machine behaviour, this paper introduces an architecture for an FE-model that can simulate the machine distortion and the resulting displacement of the Tool Centre Point (TCP). Furthermore, a procedure is shown how the results of geometric measurements can be fed back into the model to compensate inaccuracies resulting from the model abstraction.

2. Thermal error machine compensation

Machine tool manufacturers take different approaches to compensate thermal machine errors. Besides design measures to control heat flow in and out of the machine structure to homogenize the thermal field in the structure, also Numerical Control (NC) based approaches are well established. Traditionally, this compensation is implemented by measuring the displacement of the TCP in the machining area at one or more positions, for example using an ETVE test according to ISO 230-3 [3]. The measurement results are used to compute a compensation table with which the NC compensates the geometric error [4, 5]. Since geometric machine measurements tend to be either inaccurate or time consuming, current research efforts focus on solving this conflict of objectives. Brecher et. al. were able to develop a measurement procedure that is able to compute axes errors from a dynamic R-Test measurement in under eight minutes [6]. Due to the combination of a short measurement time and accurate measurement results, the dynamic R-Test is used for the geometric measurements in the experiments discussed in this paper. However, all geometric measurements including the dynamic R-Test have in common that they only pose a snapshot of the machine distortion. They are valid for as long as the thermal distribution in the machine structure is nearly constant. For transient machine behaviour the measurement process has to be repeated often, reducing the productivity of the machine.

More recently, there has been a focus on modelling the machine tool deformation. In contrary to a real measurement of the machine geometry, modelling of the machine behaviour, has the benefit that it can be compensated in real time [7, 8]. Turek et. al. created a model which includes the whole machine structure, but in order to integrate it into the machine they needed to simplify the model. This leads to a significant decrease in precision [9].

In order to use the benefit of the accuracy of geometric measurements and the ability to adapt the compensation for a transient heat distribution of the simulation, this paper develops a model architecture to combine the two methods. The resulting theoretical compensation is depicted in Figure 1. The figure shows the displacement of the TCP of a machine tool. In the example, a geometric measurement is conducted at three time points. The TCP displacement at these points is used in a traditional compensation method to compensate the TCP displacement. Since this kind of displacement is not adaptive to the transient machine distortion, the compensation error increases over time. In contrary to this static approach of the traditional machine compensation, the proposed compensation method estimates the TCP displacement between two R-Test measurements using a white box simulation model. The results of the simulation model can be used to compensate the TCP position in between measurements. When the model uncertainty and thus the machine positioning error get too high, the R-Test is repeated. The figure shows how the difference between the actual TCP displacement and the compensation value is much smaller for the proposed method compared to the traditional method, thus decreasing the positioning error.

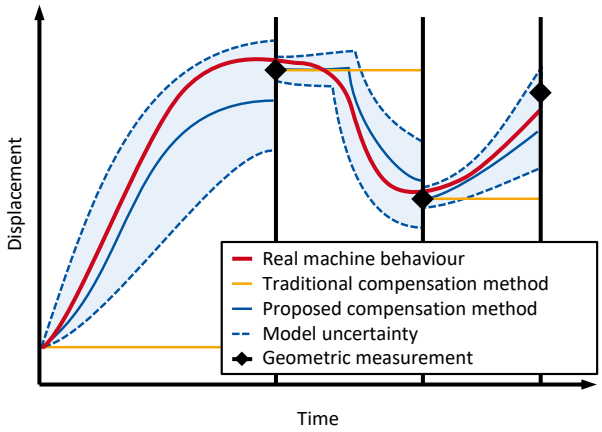

Figure 1. Proposed machine compensation method in comparison to traditional method.

3. Model architecture

The most important requirement for the model architecture is a high computing speed. The computation time needs to be short enough to model in thermal real time, which is considered to be one minute. To achieve a high speed, the simulation will have a high degree of abstraction, which inevitably results in a larger computing error. The model architecture, shown in Figure 2, is designed to cope with this error.

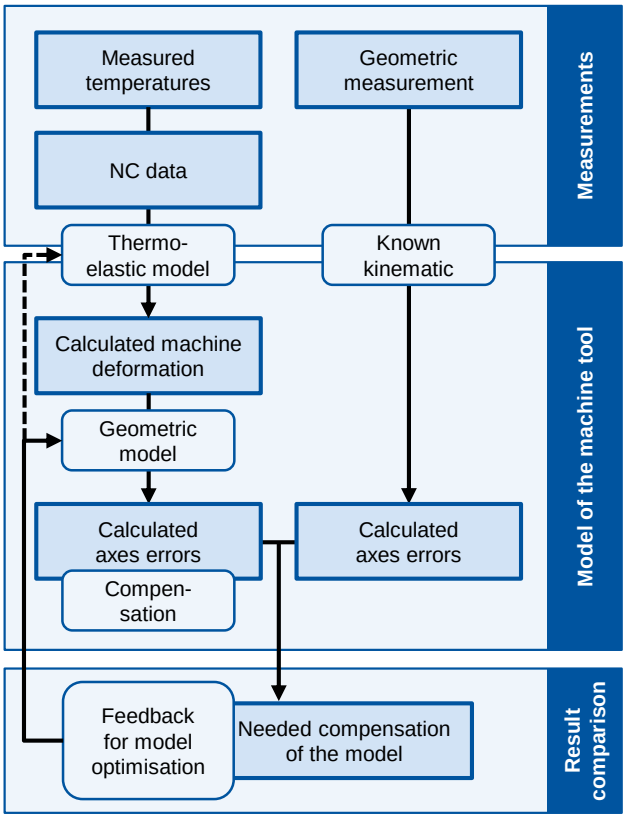

Figure 2. Model architecture for a real time machine compensation with geometric measurement feedback.

The basis for the model are the measurements gathered on the machine. Temperature sensors are placed onto multiple points of the machine structure. Together with the NC data, which provides information for instance about the introduced power, they deliver continuous information about the state of the machine. Next to this continuous data, a dynamic R-Test measurement is conducted in regular intervals and provides accurate "snapshots" about the machine distortion for the point in time of the measurement.

While the individual axes errors can be computed from the geometric measurement directly by a reverse transformation, the temperatures and NC data is fed into a thermo-elastic model of the machine which calculates the machine deformation. The machine deformation is then analysed to give the axes errors which can be used for the compensation of the machine. At this point, the model has two values for axes errors. One of them comes from the geometric measurement and one from the simulation of the machine. The vector between the results is calculated and used to increase the accuracy of the simulation model.

4. Summary and outlook

This paper proposes a model with which it is possible to improve the thermal compensation of machine tools. It is presented how the model combines the existing approaches of geometric machine measurements and white box simulation models. Furthermore, a model architecture is proposed which describes how the method can be integrated into the machine compensation procedure.

In further work, it needs to be explored how precise the model can simulate the machine deformation. Estimating the accuracy of the simulation model can give information about when a geometric measurement needs to be conducted. It should be investigated how the model accuracy develops and how a change of the measurement interval changes the measurement effort and accuracy of the model.

5. Acknowledgment

This IGF Project 'TheKo 5 – Thermo-elasctic error compensation for 5-axis machining centers' (AiF 20377 N) was supported via AiF within the programme for promoting the Industrial Collective Research (IGF) of the German Ministry of Economic Affairs and Energy (BMWi), based on a resolution of the German Parliament.

Gefördert durch:
Bundesministerium für Wirtschaft und Energie
aufgrund eines Beschlusses des Deutschen Bundestages
Forschungsnetzwerk Mittelstand AiF

[1] Mayr J, Jedrzejewski J, Uhlmann E, Donmez M A, Knapp W, Härtig F, Wendt K, Moriwaki T, Shore P, Schmitt R, Brecher C, Würz T and Wegener K 2012 Thermal issues in machine tools *CIRP Annals – Manuf. Tech.* ***61*** 771-791

[2] Wende J and Kiradjiev P 2014 Eine Implementierung von Losgröße 1 nach Industrie-4.0-Prinzipien *Elektrotech. & Informationstech.* **131** 202-206

[3] ISO 230-3: 2007 Test code for machine tools – Part 3: Determination of thermal effects

[4] Siemens 2011 Sinumerik 840D sl / 828D Erweiterungsfuktionen Funktionshandbuch 328

[5] Heidenhain 2007 Genauigkeit ab dem ersten Teil *Klartext* **47** 4-5

[6] Brecher C, Behrens J, Klatte M, Lee T H and Tzanetos F 2018 Measurement and analysis of thermos-elastic deviation of five-axis machine tool using dynamic R-test *8th CIRP Conf. on High Perf. Cutting*

[7] Mayr J 2009 Beurteilung und Kompensation des Temperaturganges von Werkzeugmaschinen *Dissertation ETH Zürich*

[8] Brecher C, Lee T H, Tzanetos F and Zontar D 2019 Hybrid modeling of thermo-elastic behavior of a three-axis machining center using integral deformation sensors *52nd CIRP Conference on Manuf. Sys.* **81** 1301-06

[9] Turek P, Jedrzejewski J and Modrzycki W 2010 Methods of machine tool error compensation *J. Mach. Eng.* **10**

Special Interest Group Meeting on Thermal Issues
Laboratory for Machine Tools and Production Engineering (WZL) of
RWTH Aachen, Germany, February 2020
www.euspen.eu

Research on the impact of the warm-up of multisensor measuring machine on measurement accuracy

Wiktor Harmatys[1], Adam Gąska[1], Piotr Gąska[1], Maciej Gruza[1]

[1]Laboratory of Coordinate Metrology, Cracow University of Technology, al. Jana Pawła II 37, 31-864 Cracow, Poland

wharmatys@mech.pk.edu.pl

Abstract

It will not be an exaggeration to state that nowadays the quality control department is one of the most important sections in modern production facilities. An effective control department can prevent huge financial losses associated with the waste of means of production as well as those resulting from breaching contracts. That explains the high demand for methods and measuring techniques which are characterized by both reliability and accuracy. In terms of geometric quantities measurements the solution which meet those requirements is the Coordinate Measuring Technique (CMT) which over last several decades became one of the most often utilized methods in industrial practice. The main tool of CMT is Coordinate Measuring Machine (CMM). Such machines have been developed and modernized for many years, so the problems of classic CMMs are quite well known and successfully corrected. One of the most significant factors affecting CMM accuracy is temperature. Measuring instruments and especially CMMs are often made of many materials characterized by different coefficients of thermal expansions, which means that appropriate constructions and connections of such elements should be used to avoid excessive stresses and torsions of the machine which cause deterioration of accuracy. The main kinematic elements of devices intended for work in production halls are made of materials such as granite or ceramics which are characterized by a low coefficient of thermal expansion. Such solution allows machines to work in a wide temperature range (15-35 °C) without significant reduction of the quality of measurements. Additionally, temperature compensation is usually used to ensure stable measurement results. In that case correction can be performed for individual kinematic axes and with the use of an additional temperature sensor for the measured part, so the measurement results are referred to standard conditions of 20 °C. Modern market requirements force producers to constantly strive to reduce the costs associated with the production of the product. Such reduction can be implemented in many ways, one of them is minimization of machine downtime and optimization of its worktime. Of course, complete elimination of downtime is impossible even because each measuring machine requires periodic inspections by the service and confirmation of its accuracy, which is usually carried out by external laboratories. During services, the machine is turned off and, as a result, its operating temperature drops, which is why many manufacturers use special programs to warm up the machine before servicing starts. A similar situation related to a decrease in the operating temperature of the machine occurs when system of one or two shifts is used in the plant, when the machine is turned off or not used until the next shift. Researchers from Laboratory of Coordinate Metrology decided to examine whether the problem of using not warm-up machine may cause instability of measurements and whether warming-up measurements should be used before the machine would be used for its primary purposes. Additionally, obtained results allows estimation of the uncertainty of the temperature sensor applied to the machine parts. Experiments were carried out on a Zeiss O'Inspect 442 multisensor measuring machine which is located in a temperature stabilized room T = 20.3 °C ± 0.2 °C. Research started with recording the temperature of the measured part on a stopped machine. The machine was then programmed and stayed turned on for 46 hours of continuous part measurement. The experiments allowed to identify the time needed for the machine to obtain a stable operating temperature as well as its value - Figure 1.

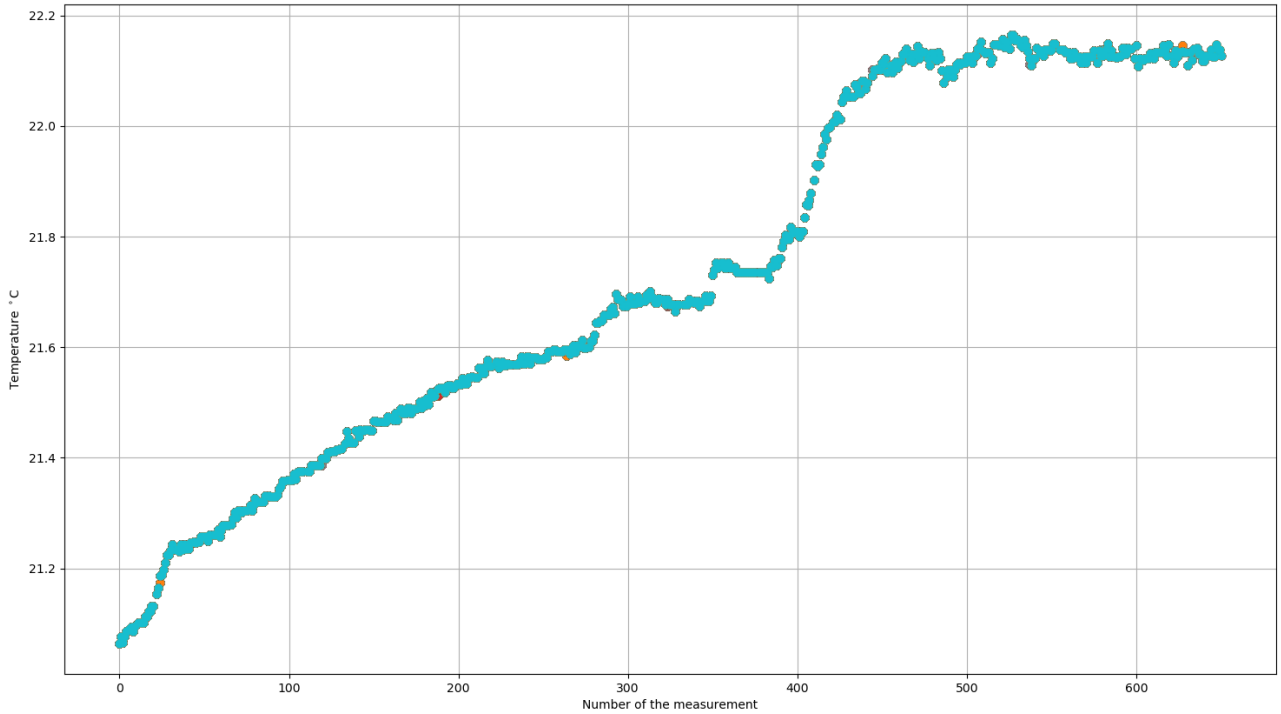

Figure 1. Part temperature changes during 46 hours of measurement.

Additionally, it was checked whether the results collected during temperature stabilization were acceptable and whether they were subjected to additional measurement uncertainty.
The obtained results turned out to be very interesting. The results were divided into two groups: related to machine warming-up process and obtained when the machine had achieved temperature stability. The results show that in the first group where it was expected to observe the non-stability of the measurements, the results in fact do not show an effect associated with the lack of warming-up of the machine, as the first and second group of measurements give comparable results. However, it should be noted that the tests were carried out on a relatively small measuring machine and possible measurement instability associated with measuring the element immediately after turning the machine on is very small and should not affect the results. In the future, the authors plan to repeat the experiment on a machine with a much larger working range.

Metrology, Optical, Temperature, Visual Inspection

info@euspen.eu
www.euspen.eu